frontiers | Research Topics

Survival strategies: cellular responses to stress and damage

Edited by
Aurore Claude-Taupin, Pavel Ivanov, Jing Pu, Jingyue Jia Cassano and Bhawana Bissa

Published in
Frontiers in Cell and Developmental Biology

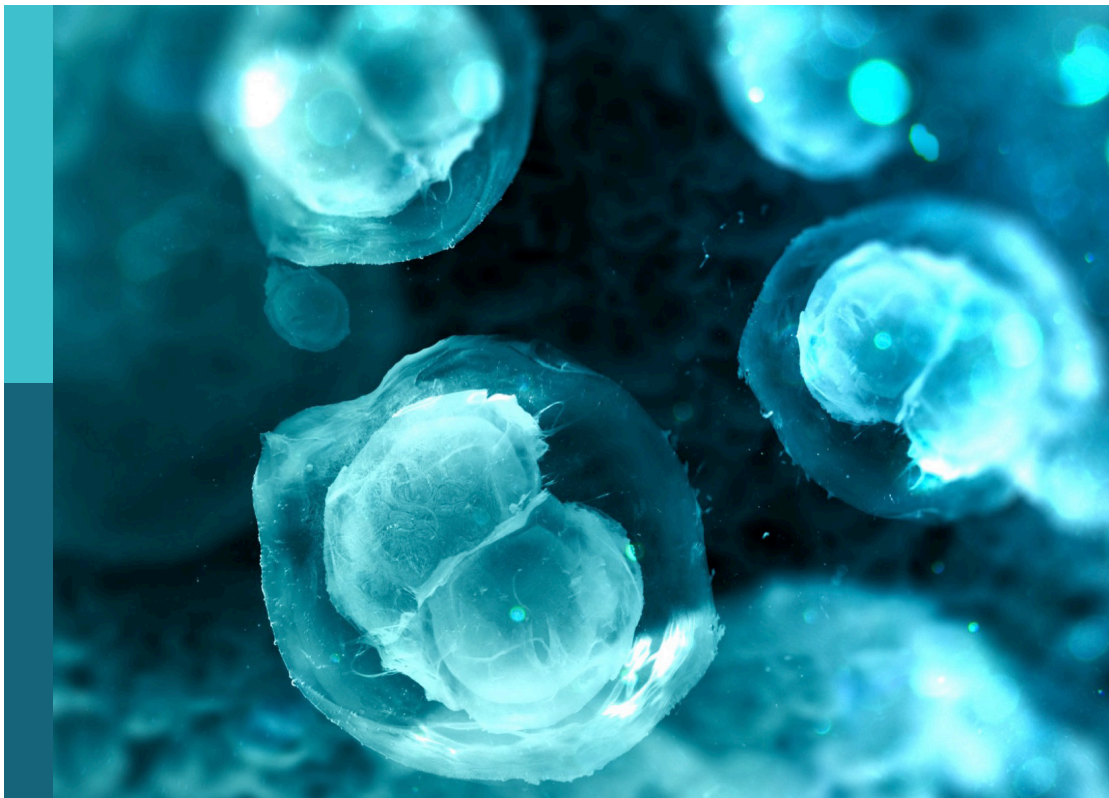

FRONTIERS EBOOK COPYRIGHT STATEMENT

The copyright in the text of individual articles in this ebook is the property of their respective authors or their respective institutions or funders. The copyright in graphics and images within each article may be subject to copyright of other parties. In both cases this is subject to a license granted to Frontiers.

The compilation of articles constituting this ebook is the property of Frontiers.

Each article within this ebook, and the ebook itself, are published under the most recent version of the Creative Commons CC-BY licence. The version current at the date of publication of this ebook is CC-BY 4.0. If the CC-BY licence is updated, the licence granted by Frontiers is automatically updated to the new version.

When exercising any right under the CC-BY licence, Frontiers must be attributed as the original publisher of the article or ebook, as applicable.

Authors have the responsibility of ensuring that any graphics or other materials which are the property of others may be included in the CC-BY licence, but this should be checked before relying on the CC-BY licence to reproduce those materials. Any copyright notices relating to those materials must be complied with.

Copyright and source acknowledgement notices may not be removed and must be displayed in any copy, derivative work or partial copy which includes the elements in question.

All copyright, and all rights therein, are protected by national and international copyright laws. The above represents a summary only. For further information please read Frontiers' Conditions for Website Use and Copyright Statement, and the applicable CC-BY licence.

ISSN 1664-8714
ISBN 978-2-8325-6534-6
DOI 10.3389/978-2-8325-6534-6

Generative AI statement
Any alternative text (Alt text) provided alongside figures in the articles in this ebook has been generated by Frontiers with the support of artificial intelligence and reasonable efforts have been made to ensure accuracy, including review by the authors wherever possible. If you identify any issues, please contact us.

About Frontiers

Frontiers is more than just an open access publisher of scholarly articles: it is a pioneering approach to the world of academia, radically improving the way scholarly research is managed. The grand vision of Frontiers is a world where all people have an equal opportunity to seek, share and generate knowledge. Frontiers provides immediate and permanent online open access to all its publications, but this alone is not enough to realize our grand goals.

Frontiers journal series

The Frontiers journal series is a multi-tier and interdisciplinary set of open-access, online journals, promising a paradigm shift from the current review, selection and dissemination processes in academic publishing. All Frontiers journals are driven by researchers for researchers; therefore, they constitute a service to the scholarly community. At the same time, the *Frontiers journal series* operates on a revolutionary invention, the tiered publishing system, initially addressing specific communities of scholars, and gradually climbing up to broader public understanding, thus serving the interests of the lay society, too.

Dedication to quality

Each Frontiers article is a landmark of the highest quality, thanks to genuinely collaborative interactions between authors and review editors, who include some of the world's best academicians. Research must be certified by peers before entering a stream of knowledge that may eventually reach the public - and shape society; therefore, Frontiers only applies the most rigorous and unbiased reviews. Frontiers revolutionizes research publishing by freely delivering the most outstanding research, evaluated with no bias from both the academic and social point of view. By applying the most advanced information technologies, Frontiers is catapulting scholarly publishing into a new generation.

What are Frontiers Research Topics?

Frontiers Research Topics are very popular trademarks of the *Frontiers journals series*: they are collections of at least ten articles, all centered on a particular subject. With their unique mix of varied contributions from Original Research to Review Articles, Frontiers Research Topics unify the most influential researchers, the latest key findings and historical advances in a hot research area.

Find out more on how to host your own Frontiers Research Topic or contribute to one as an author by contacting the Frontiers editorial office: frontiersin.org/about/contact

Survival strategies: cellular responses to stress and damage

Topic editors

Aurore Claude-Taupin — INSERM U1151 Institut Necker Enfants Malades, France
Pavel Ivanov — Brigham and Women's Hospital, Harvard Medical School, United States
Jing Pu — University of New Mexico, United States
Jingyue Jia Cassano — University of New Mexico, United States
Bhawana Bissa — Central University of Rajasthan, India

Citation

Claude-Taupin, A., Ivanov, P., Pu, J., Jia Cassano, J., Bissa, B., eds. (2025). *Survival strategies: cellular responses to stress and damage*. Lausanne: Frontiers Media SA. doi: 10.3389/978-2-8325-6534-6

Table of contents

frontiers | Frontiers in Cell and Developmental Biology

TYPE Editorial
PUBLISHED 19 June 2025
DOI 10.3389/fcell.2025.1630652

Check for updates

OPEN ACCESS

EDITED AND REVIEWED BY
You-Wen He,
Duke University, United States

*CORRESPONDENCE
Bhawana Bissa,
bhawana.bissa@curaj.ac.in
Aurore Claude-Taupin,
aurore.claude-taupin@inserm.fr

†These authors have contributed equally to this work

RECEIVED 18 May 2025
ACCEPTED 03 June 2025
PUBLISHED 19 June 2025

CITATION
Bissa B, Claude-Taupin A, Ivanov P, Jia J and Pu J (2025) Editorial: Survival strategies: cellular responses to stress and damage. *Front. Cell Dev. Biol.* 13:1630652. doi: 10.3389/fcell.2025.1630652

COPYRIGHT
© 2025 Bissa, Claude-Taupin, Ivanov, Jia and Pu. This is an open-access article distributed under the terms of the Creative Commons Attribution License (CC BY). The use, distribution or reproduction in other forums is permitted, provided the original author(s) and the copyright owner(s) are credited and that the original publication in this journal is cited, in accordance with accepted academic practice. No use, distribution or reproduction is permitted which does not comply with these terms.

Editorial: Survival strategies: cellular responses to stress and damage

Bhawana Bissa[1*†], Aurore Claude-Taupin[2*†], Pavel Ivanov[3], Jingyue Jia[4,5] and Jing Pu[6]

[1]Department of Biochemistry, School of Life Sciences, Central University of Rajasthan, Ajmer, India, [2]Université Paris Cité, INSERM U1151, CNRS U8253, Institut Necker-Enfants Malades, Paris, France, [3]Department of Medicine, Brigham and Women's Hospital and Harvard Medical School, HMS Initiative for RNA Medicine, Boston, MA, United States, [4]Center for Global Health, Department of Internal Medicine, University of New Mexico Health Sciences Center, Albuquerque, NM, United States, [5]Autophagy, Inflammation and Metabolism Center of Biochemical Research Excellence, Albuquerque, NM, United States, [6]Department of Molecular Genetics and Microbiology, University of New Mexico Health Sciences Center, Albuquerque, NM, United States

KEYWORDS

stress granules (SG), autophagy, metabolism, oxidative stress, cell signaling, membrane damage

Editorial on the Research Topic
Survival strategies: cellular responses to stress and damage

Stress and damage in organisms originate at the cellular level and require immediate response to prevent onset of pathological conditions. The ability of cells to effectively counteract stress is vital for the overall health and survival of the organism. The stress that cells encounter varies, including oxidative stress, genotoxic stress, heat shock, nutrient deprivation, hypoxia, exposure to toxic compounds, pathogen invasion, mechanical injury and aging (Fulda et al., 2010). These stress conditions disrupt cellular homeostasis by damaging structural components or impairing critical functions. The ability of cells to offset and withstand stress conditions is primarily mediated by activation of survival pathways such as DNA damage response (DDR), heat shock response (HSR), unfolded protein response (UPR), anti-oxidant response, mitochondrial stress signaling, stress granules (SGs) and autophagy (Yan et al., 2021; Bahar et al., 2016). Beyond these pathways, inter-organellar crosstalk plays a crucial role in mitigating stress conditions (Raimundo, 2014). Furthermore, AMPK and mTOR play essential roles in managing cellular stress by coordinating their actions to restore cellular homeostasis (Hardie, 2015; Saxton and Sabatini, 2017). Depending on the level and type of stress, different pro-survival mechanisms are activated; however if the cell fails to neutralize the stress, various cell death pathways are initiated and eventually lead to disease states such as diabetes, neurodegeneration, cancer, and others (Fulda et al., 2010; Martindale and Holbrook, 2002).

The crosstalk between different survival pathways is important to preserve cellular functions and to repair macromolecular damage. For example, DDR and UPR direct a coordinated response, especially under hypoxic conditions to maintain cell integrity and prevent cell death (Endoplasmic Reticulum Stress and Unfolded Protein Response, 2024). Similarly, HSR can assist UPR to relieve ER stress by enhancing ER export of misfolded proteins (Kim and Gross, 2013). This coordination is essential when UPR is overwhelmed

as in case of ER stress–mediated diabetes (Eizirik et al., 2008). Further, to combat oxidative stress and maintain redox homeostasis, cells utilize robust antioxidant response such as the Nuclear Factor Erythroid 2-Related Factor 2 (Nrf2)/Kelch-like ECH-associated Protein 1 (Keap1) signaling pathway and mitochondrial antioxidant systems to prevent molecular damage (Ma, 2013; Dodson et al., 2019). Various cellular stressors can induce the formation of SGs, which are cytoplasmic biomolecular condensates containing RNA and proteins (Hofmann et al., 2021). SGs can be selectively cleared by autophagy, a process termed granulophagy, to restore cellular homeostasis (Buchan and Parker, 2009). Moreover, autophagy acts as a survival mechanism under nutrient deprivation and helps remove damaged or dysfunctional cellular components to restore metabolic balance (Mizushima and Komatsu, 2011).

Thus, mammalian cells have developed an intricate and robust network of survival pathways that allow adaptation to different stress conditions. Intracellular responses to stress, their regulation and their pathophysiological implications have been extensively studied. This collection is an attempt to bring together recent studies on the stress response mechanisms highlighting different aspects of survival strategies, ranging from strategies of maintaining lysosomal homeostasis to responses to oxidative damage.

The collection includes 5 review articles, 2 original articles and 2 method articles. Wang et al. reviewed the cellular response to lysosomal damage, including alternative secretion pathways and interactions with other organelles from the endolysosomal system, ER and Golgi apparatus. They also explored the contribution of these processes to disease progression. Lysosomal damage responses also involve the conjugation of ATG8 (Autophagy-related protein 8) to single membranes (CASM), as reviewed by Kaur et al. The authors summarized how the decoration of lysosomes with ATG8 promotes downstream effects, such as membrane repair and removal.

Similar to the lysosomal membrane, the nuclear envelope can undergo rupture. In this collection, Di Bona and Bakhoum provided a detailed protocol to study real-time nuclear and micronuclear rupture and repair. They introduce a novel high-resolution fluorescence microscopy-based technique that allows for the induction and imaging of both micronuclear and primary nuclear damage.

In cancer cells, DDR is often dysregulated. Ghai et al. reviewed the roles of Heat Shock Factor 1 (HSF1) in cancer chemoresistance, including through the inhibition of the DDR pathway, thus promoting genomic instability and carcinogenesis. They also highlighted HSF1's role in apoptosis inhibition and autophagy activation, and discussed the therapeutic potential of HSF1 inhibitors to overcome chemoresistance.

As in cancer, autophagy dysregulation has also been implicated in Parkinson's disease. An original study by Limanaqi et al. explored the impact of alpha-synuclein - whose abnormal forms have been linked to Parkinson's disease - on THP1 monocytes and derived macrophages. The authors showed that alpha-synuclein exerted cell- and context-specific effects, including alterations in autophagy, lipid dynamics, and inflammatory pathways, which may help explain the functional impairments of monocytes and macrophages observed in this neurological disorder.

Mitochondrial dysfunction is linked to numerous pathologies. Jiménez-Loygorri et al. described a method to quantitate mitophagy (a selective type of autophagy targeting mitochondria) flux, using the mitoQC reporter and flow cytometry. This approach can be multiplexed with the analysis of other cellular parameters, such as ROS production and cell viability in cultured cells, and has also been validated *ex vivo* in the retina of mitoQC reporter mice.

Sergiev et al. described the role of the mitochondrial protein Mitoregulin in regulating mitochondrial function. They summarized the literature–including sometimes, contradictory findings–on mitoregulin's role in cellular metabolism, particularly in kidney and muscle physiology.

Oxidative stress, characterized by the accumulation of reactive oxygen species (ROS), is another major driver of cellular damage. Liu et al. reviewed how radiotherapy induces skin reactions, notably through oxidative stress, and discussed how antioxidant therapies could help prevent these side effects, thus improving cancer patients' quality of life after radiotherapy. Extending the focus on strategies to protect cells from stress-related damage, Li et al. described a novel method to improve hepatocyte survival upon cryopreservation, using ultrasonic ice seeding technology.

Altogether, this Research Topic gathers original articles, reviews, and methodological papers that explore various aspects of cellular responses to stress and damage, to promote cell survival. We hope it will become a valuable resource for the current and the broader field.

Author contributions

BB: Writing – original draft, Funding acquisition, Conceptualization, Writing – review and editing. AC-T: Writing – original draft, Writing – review and editing, Conceptualization, Funding acquisition. PI: Writing – review and editing, Conceptualization. JJ: Writing – review and editing, Conceptualization, Funding acquisition. JP: Funding acquisition, Conceptualization, Writing – review and editing.

Funding

The author(s) declare that financial support was received for the research and/or publication of this article. BB is supported by SPG/2021/002833 and ICMR (52/27/2020-BIO/BMS) grants. AC-T is funded by Institut National de la Santé et de la Recherche Médicale (INSERM), Centre National de la Recherche Scientifique (CNRS), Université Paris Cité and Agence Nationale de la Recherche (ANR, ANR-24-CE14-0097-01). JJ is supported by grants from NIGMS R35 (R35GM154651) and AIM COBRE (P20GM121176). JP is supported by grant from NIH (NIH/NIGMS R35GM147419).

Acknowledgments

We are grateful to the authors for submitting their valuable work to this Research Topic and thank the reviewers and editorial board for their thoughtful evaluation and support.

Conflict of interest

The authors declare that the research was conducted in the absence of any commercial or financial relationships that could be construed as a potential conflict of interest.

Generative AI statement

The author(s) declare that no Generative AI was used in the creation of this manuscript.

Publisher's note

All claims expressed in this article are solely those of the authors and do not necessarily represent those of their affiliated organizations, or those of the publisher, the editors and the reviewers. Any product that may be evaluated in this article, or claim that may be made by its manufacturer, is not guaranteed or endorsed by the publisher.

References

Bahar, E., Kim, H., and Yoon, H. E. R. (2016). ER stress-mediated signaling: Action potential and Ca(2+) as Key Players. *Int. J. Mol. Sci.* 17, 1558. doi:10.3390/ijms17091558

Buchan, J. R., and Parker, R. (2009). Eukaryotic stress granules: the ins and outs of translation. *Mol. Cell.* 36, 932–941. doi:10.1016/j.molcel.2009.11.020

Dodson, M., de la Vega, M. R., Cholanians, A. B., Schmidlin, C. J., Chapman, E., and Zhang, D. D. (2019). Modulating NRF2 in disease: timing is everything. *Annu. Rev. Pharmacol. Toxicol.* 59, 555–575. doi:10.1146/annurev-pharmtox-010818-021856

Eizirik, D. L., Cardozo, A. K., and Cnop, M. (2008). The role for endoplasmic reticulum stress in diabetes mellitus. *Endocr. Rev.* 29, 42–61. doi:10.1210/er.2007-0015

Endoplasmic Reticulum Stress and Unfolded Protein Response. (2024). *Neurodegener. Dis.* doi:10.3390/ijms21176127

Fulda, S., Gorman, A. M., Hori, O., and Samali, A. (2010). Cellular stress responses: cell survival and cell death. *Int. J. Cell. Biol.* 2010, 214074. doi:10.1155/2010/214074

Hardie, D. G. (2015). AMPK: positive and negative regulation, and its role in whole-body energy homeostasis. *Curr. Opin. Cell. Biol.* 33, 1–7. doi:10.1016/j.ceb.2014.09.004

Hofmann, S., Kedersha, N., Anderson, P., and Ivanov, P. (2021). Molecular mechanisms of stress granule assembly and disassembly. *Biochim. Biophys. Acta Mol. Cell. Res.* 1868, 118876. doi:10.1016/j.bbamcr.2020.118876

Kim, S., and Gross, D. S. (2013). Mediator recruitment to heat shock genes requires dual Hsf1 activation domains and mediator tail subunits Med15 and Med16. *J. Biol. Chem.* 288, 12197–12213. doi:10.1074/jbc.M112.449553

Ma, Q. (2013). Role of Nrf2 in oxidative stress and toxicity. *Annu. Rev. Pharmacol. Toxicol.* 53, 401–426. doi:10.1146/annurev-pharmtox-011112-140320

Martindale, J. L., and Holbrook, N. J. (2002). Cellular response to oxidative stress: signaling for suicide and survival. *J. Cell. Physiol.* 192, 1–15. doi:10.1002/jcp.10119

Mizushima, N., and Komatsu, M. (2011). Autophagy: renovation of cells and tissues. *Cell.* 147, 728–741. doi:10.1016/j.cell.2011.10.026

Raimundo, N. (2014). Mitochondrial pathology: stress signals from the energy factory. *Trends Mol. Med.* 20, 282–292. doi:10.1016/j.molmed.2014.01.005

Saxton, R. A., and Sabatini, D. M. (2017). mTOR signaling in Growth, metabolism, and disease. *Cell.* 168, 960–976. doi:10.1016/j.cell.2017.02.004

Yan, Y., Wang, G., Luo, X., Zhang, P., Peng, S., Cheng, X., et al. (2021). Endoplasmic reticulum stress-related calcium imbalance plays an important role on Zinc oxide nanoparticles-induced failure of neural tube closure during embryogenesis. *Environ. Int.* 152, 106495. doi:10.1016/j.envint.2021.106495

frontiers | Frontiers in Cell and Developmental Biology

TYPE Original Research
PUBLISHED 05 July 2024
DOI 10.3389/fcell.2024.1421360

Check for updates

OPEN ACCESS

EDITED BY
Xianwei Wang,
Xinxiang Medical University, China

REVIEWED BY
Nour S. Erekat,
Jordan University of Science and Technology, Jordan
Carmen Caiazza,
University of Naples Federico II, Italy

*CORRESPONDENCE
Mara Biasin,
mara.biasin@unimi.it
Fiona Limanaqi,
fiona.limanaqi@unimi.it

†These authors have contributed equally to this work

RECEIVED 22 April 2024
ACCEPTED 17 June 2024
PUBLISHED 05 July 2024

CITATION
Limanaqi F, Zecchini S, Ogno P, Artusa V, Fenizia C, Saulle I, Vanetti C, Garziano M, Strizzi S, Trabattoni D, Clerici M and Biasin M (2024), Alpha-synuclein shapes monocyte and macrophage cell biology and functions by bridging alterations of autophagy and inflammatory pathways.
Front. Cell Dev. Biol. 12:1421360.
doi: 10.3389/fcell.2024.1421360

COPYRIGHT
© 2024 Limanaqi, Zecchini, Ogno, Artusa, Fenizia, Saulle, Vanetti, Garziano, Strizzi, Trabattoni, Clerici and Biasin. This is an open-access article distributed under the terms of the Creative Commons Attribution License (CC BY). The use, distribution or reproduction in other forums is permitted, provided the original author(s) and the copyright owner(s) are credited and that the original publication in this journal is cited, in accordance with accepted academic practice. No use, distribution or reproduction is permitted which does not comply with these terms.

Alpha-synuclein shapes monocyte and macrophage cell biology and functions by bridging alterations of autophagy and inflammatory pathways

Fiona Limanaqi[1†*], Silvia Zecchini[1†], Pasquale Ogno[1], Valentina Artusa[2], Claudio Fenizia[2], Irma Saulle[2], Claudia Vanetti[1], Micaela Garziano[2], Sergio Strizzi[1], Daria Trabattoni[1], Mario Clerici[2,3] and Mara Biasin[1*]

[1]Department of Biomedical and Clinical Sciences, University of Milan, Milan, Italy, [2]Department of Pathophysiology and Transplantation, University of Milan, Milan, Italy, [3]IRCCS Fondazione Don Carlo Gnocchi, Milan, Italy

Introduction: Abnormal spreading of alpha-synuclein (αS), a hallmark of Parkinson's disease, is known to promote peripheral inflammation, which occurs in part via functional alterations in monocytes/macrophages. However, underlying intracellular mechanisms remain unclear.

Methods: Herein we investigate the subcellular, molecular, and functional effects of excess αS in human THP-1 monocytic cell line, THP-1-derived macrophages, and at least preliminarily, in primary monocyte-derived macrophages (MDMs). In cells cultured w/wo recombinant αS (1 μM) for 4 h and 24 h, by Confocal microscopy, Western Blot, RT-qPCR, Elisa, and Flow Cytometry we assessed: i) αS internalization; ii) cytokine/chemokine expression/secretion, and C−C motif chemokine receptor 2 (CCR2) levels; iii) autophagy (LC3II/I, LAMP1/LysoTracker, p62, pS6/total S6); and iv) lipid droplets (LDs) accumulation, and cholesterol pathway gene expression. Transwell migration assay was employed to measure THP-1 cell migration/chemotaxis, while FITC-IgG-bead assay was used to analyze phagocytic capacity, and the fate of phagocytosed cargo in THP-1-derived macrophages.

Results: Extracellular αS was internalized by THP-1 cells, THP-1-derived macrophages, and MDMs. In THP1 cells, αS induced a general pro-inflammatory profile and conditioned media from αS-exposed THP-1 cells potently attracted unstimulated cells. However, CCL2 secretion peaked at 4 h αS, consistent with early internalization of its receptor CCR2, while this was blunted at 24 h αS exposure, when CCR2 recycled back to the plasma membrane. Again, 4 h αS-exposed THP-1 cells showed increased spontaneous migration, while 24 h αS-exposed cells showed reduced chemotaxis. This occurred in the absence of cell toxicity and was associated with upregulation of autophagy/lysosomal markers, suggesting a pro-survival/tolerance mechanism against stress-related inflammation. Instead, in THP-1-derived macrophages, αS time-dependently potentiated the intracellular accumulation, and release of pro-inflammatory mediators. This was accompanied by mild toxicity, reduced autophagy-lysosomal markers, defective LDs formation, as well as impaired phagocytosis, and the appearance of stagnant lysosomes engulfed with phagocytosed cargo, suggesting a status of macrophage exhaustion reminiscent of hypophagia.

Discussion: In summary, despite an apparently similar pro-inflammatory phenotype, monocytes and macrophages respond differently to intracellular αS accumulation in terms of cell survival, metabolism, and functions. Our results suggest that in periphery, αS exerts cell- and context-specific biological effects bridging alterations of autophagy, lipid dynamics, and inflammatory pathways.

KEYWORDS

cell survival, cell toxicity, p62, lysosomes, cell migration, chemotaxis, phagocytosis, lipid droplets

1 Introduction

Alpha-synuclein (αS), an intrinsically disordered, and highly dynamic protein which is prone to misfold and aggregate in nerve cells, is now widely recognized as a hallmark of neurodegenerative synucleinopathies including Parkinson's disease (PD) and multiple system atrophy (MSA). While exhaustive evidence has been provided on the pathophysiological roles of αS within nerve and glial cells (Burré et al., 2018; Ryskalin et al., 2018), only scattered reports exist on its biological functions in the periphery. Indeed, αS is ubiquitously expressed in non-neuronal tissues (Hashimoto et al., 1997; Askanas et al., 2000; Baltic et al., 2004; Nakai et al., 2007; Jiménez-Jiménez et al., 2023), including a variety of blood cell types (Pei and Maitta, 2019). In detail, erythrocytes possess exceedingly high concentrations of αS, representing a major source of αS in the periphery (Barbour et al., 2008; Tian et al., 2019). From erythrocytes, αS is released extracellularly to be endocytosed by circulating monocytes, thus concentration-dependently influencing their biology, phenotype, and functions (Liu et al., 2022). This is reminiscent of a "cell-to-cell" spread mechanism that is widely explored in the nervous and enteric systems (Schaeffer et al., 2020). Notably, while endogenous αS in periphery sustains normal innate and adaptive immune responses (Alam et al., 2022), abnormal levels of either exogenous or endogenous αS may promote abnormal immune reactions (Allen Reish and Standaert, 2015; White et al., 2018; Grozdanov et al., 2019; Grozdanov and Danzer, 2020; Limanaqi et al., 2024), including hyper-inflammation and functional alterations in monocytes and macrophages (Klegeris et al., 2008; Gardai et al., 2013; Haenseler et al., 2017; Pellegrini et al., 2022). This is key for the pathobiology of PD, since peripheral monocytes from these patients display a hyper-activated and pro-inflammatory profile (Su et al., 2022) and peripheral monocyte entry in the CNS has been postulated as a key event for αS-induced inflammation and neurodegeneration (Harms et al., 2018). In line with a bidirectional connection between the CNS and peripheral immune system (Natale et al., 2021), evidence in experimental models of PD suggests that neuron-released αS is taken up by macrophages, and in turn, excess/mutant αS is released from monocytes/macrophages and spreads to neurons, contributing to PD-like neuropathology (Moriya et al., 2022). Pathways that have been proposed to be involved in αS internalization either as a free protein, or through extracellular vesicles, include passive diffusion, and direct penetration through the plasma membrane, as well as conventional, and receptor-mediated endocytosis (Haenseler et al., 2017; Brás and Outeiro, 2021; Liu et al., 2022). These considerations suggest that, independently of the source, and spreading mechanisms, αS-induced biological alterations in peripheral cells might promiscuously impinge on the onset/progression of systemic inflammation and neurological diseases. However, the detailed cellular and molecular mechanisms through which αS influences monocyte and macrophage biology remain to be elucidated. αS is suggested to act as an alarmin that activates pro-inflammatory and stress-related pathways through a receptor-mediated mechanism mostly involving TLR4 and TLR2 (Fellner et al., 2013; Kim et al., 2013; Venezia et al., 2021). This notwithstanding, only scattered evidence exists on how intracellular αS, as well as its mobilization dynamics, and functional interactions contribute to shaping monocyte/macrophage biology and functions (Klegeris et al., 2008; Freeman et al., 2013; Gardai et al., 2013; Haenseler et al., 2017).

A key role of the autophagy pathway in governing proteostasis of either endogenous or exogenous αS is documented in several experimental models, including neurons, glia, and recently, T lymphocytes, and induced Pluripotent Stem Cell (iPSC)-derived macrophages (Martinez-Vicente et al., 2008; Colasanti et al., 2014; Haenseler et al., 2017; Ryskalin et al., 2018; Limanaqi et al., 2019; 2021b; Choi et al., 2020; Tang et al., 2021). While autophagy has been implicated in monocyte/macrophage function (Zhang et al., 2012; Germic et al., 2019), scarce evidence exists on whether/how αS affects autophagy in monocytes and macrophages specifically, and its functional consequences. In the light of a high affinity of αS for lipid-rich biological membranes, lipid metabolism also deserves to be investigated as a potential mechanism bridging the effects of αS, biogenesis/maturation of degradative organelles, and inflammatory status in macrophages (Shpilka and Elazar, 2015; Alza et al., 2019; Jarc and Petan, 2020). Based on these premises, herein we investigated the subcellular, molecular, and functional effects of excess αS in human THP-1 monocytic cell line, and THP-1-derived macrophages, and, at least preliminarily in blood-isolated monocyte-derived macrophages (MDMs). Results confirmed that extracellular αS is taken up by THP-1 monocytes, as well as THP-1-derived macrophages, and primary human MDMs. Despite inducing an apparently similar pro-inflammatory phenotype, the effects of excess αS in THP-1 cells, and THP-1-derived macrophages are associated with opposite outcomes on cell survival, and autophagy, along with functional alterations in migration/chemotaxis, and phagocytic capacity, respectively.

2 Materials and methods

2.1 Recombinant protein, cell culture, and treatments

2.1.1 Recombinant protein

Recombinant human αS was purchased from Merck-Sigma (500 ug, S7820). The lyophilized protein was reconstituted in

sterile PBS w/o calcium and magnesium at a final concentration of 1 mg/mL (70 μM) as per manufacturer instructions. 50 uL aliquots were prepared and stored at −20°C. A limulus amebocyte lysate (LAL) chromogenic kit (# HIT302**,** Hycult Biotech) with a minimum detection limit of 0.04 EU/mL was used to measure endotoxin levels before treatment. Endotoxin levels were <0.5 EU/mL and the protein was used at a final dilution of 14 μg/mL (1 μM concentration for 4 or 24 h) based on previous studies (Pellegrini et al., 2022; Limanaqi et al., 2024) and our pilot experiments.

2.1.2 Cell cultures: THP-1 monocytic cell line, and differentiation to THP-1-derived macrophages

THP-1 cells (ATCC TIB-202, human acute monocytic leukemia cell line) were grown in RPM1 supplemented with 10% Fetal Bovine Serum (FBS, EuroClone, Milan, Italy), and 1% penicillin-streptomycin/L-glutamine (EuroClone, Milan, Italy) at 37°C in a humidified 5% CO^2 atmosphere. Cells were maintained in 75 cm suspension flasks and passaged every 3 days when they reached 1 × 10^6/mL concentration. Cells were routinely checked for mycoplasma contamination, and cell viability/count was determined using a Bio-Rad TC20 Automated Cell Counter (Bio-Rad Laboratories).

According to the different methodological assays, THP-1 cells were seeded in either 12-well (4 × 10^5/well, in 1 mL), 24-well (2 × 10^5/well, in 0.5 mL), or 96-well (5 × 10^4/well, in 0.1 mL) suspension plates and cultured in RPMI 1640 with 10% of FBS (EuroClone, Milan, Italy). THP-1 cell medium was then supplemented with αS (1 uM), for 4 or 24 h. At these time-points, cells and supernatants were collected for different analyses and/or further experiments.

As a rough 30%–40% of cells are lost during and after the differentiation process from THP-1 cells to macrophages, for such experiments, THP-1 cells were seeded in excess compared to experiments with their undifferentiated counterpart in order to have a similar final number for both cell types. In detail, THP-1 cells were seeded in adherent 12-well plates (6 × 10^5/well, in 1 mL), 24-well plates (3 × 10^5/well, in 0.5 mL), or 96-well plates (7.5 × 10^4/well, in 0.1 mL) in RPMI 1640 with 10% of FBS (EuroClone, Milan, Italy). For confocal microscopy, cells were seeded in u-Slide 8 Well high ibiTreat: #1.5 polymer coverslip chambers (CAT 80806, Twin Helix, Milan, Italy). Immediately after seeding, cells were treated with 25 ng/mL phorbol myristate acetate (PMA) (Sigma, St. Louis, MO) for 36 h based on previous studies showing that concentration of PMA for stable differentiation ranges from 5 to 100 ng/mL (Park et al., 2007). Cell differentiation was assessed by optical microscope observation (ZOE Fluorescent Cell Imager; Bio-Rad Laboratories). After washing in PBS to remove non-adherent/non-differentiated cells, THP-1-derived macrophages were incubated in fresh RPMI 1640 with 10% FBS for 4 h and then treated with αS (1 uM) for 4 and 24 h. Cells were then collected/fixed for further analyses.

2.1.3 Cell cultures: primary human monocyte-derived macrophages

Thirty mL of whole blood were collected in EDTA-containing vacutainer tubes (Becton Dickinson, Rutherford, NJ) from 3 healthy volunteers. Peripheral blood mononuclear cells (PBMCs) were separated on lymphocyte separation medium (Cedarlane Laboratories, Hornby, ON, Canada) as previously described (Cui et al., 2021). Leukocyte viability was determined using a Bio-Rad TC20 Automated Cell Counter (Bio-Rad Laboratories). The percentage of $CD14^+$ monocytes was determined in PBMCs by Flow cytometry as previously described (Saulle et al., 2021). Accordingly, a PBMC volume containing 2.5 × 10^5 monocytes was seeded in 24-well plates in RPMI 1640 without FBS (EuroClone, Milan, Italy) and cultured for 2 h to isolate monocytes via plastic adherence. After washing in PBS, adherent monocytes were incubated with 100 ng/mL Macrophage Colony-Stimulating Factor (M-CSF, R&D Systems, Minneapolis, MN) in RPMI 1640 with 20% of FBS (EuroClone, Milan, Italy) added each 2 days for 5 days to generate monocyte-derived macrophages (MDMs) as previously described (Saulle et al., 2021). Differentiation was assessed by optical microscope observation (ZOE Fluorescent Cell Imager; Bio-Rad Laboratories). After washing in PBS, MDMs were incubated in fresh RPMI 1640 with 10% FBS, treated with αS for 24 h, and fixed for immunofluorescence.

2.2 Cell viability

THP-1 monocytic cell or PBMCs viability was determined through Trypan Blue exclusion assay and 3-(4,5-dimethylthiazol-2-yl)-2,5-diphenyltetrazolium bromide (MTT) assay. For Trypan Blue assay, 10 μL of cell suspension were mixed and briefly incubated with 10 μL of 0.4% Trypan Blue (Merck-Sigma, Milan, Italy) in 96-well plates. According to the manufacturer protocol, 10 μL of the mix were loaded on chamber slides and counted with the T20 Automated Cell Counter (Bio-Rad Laboratories, Hercules, CA, United States).

MTT was used to assess the viability of both THP-1 monocytic cells, and PMA-differentiated THP-1 macrophages (both untreated and αS-treated at 4 and 24 h) in previously seeded cells (96-well plates) and as previously described (Van Meerloo et al., 2011). Briefly, 30 μL of 3-(4,5-dimethylthiazol-2-yl)-2,5-diphenyltetrazolium bromide (MTT, final concentration 0.5 mg/mL) were added to each well under sterile conditions, and the 96-well plates were incubated for 4 h at 37°C. Supernatants were removed, and dimethyl sulfoxide (100 μL/well) was added. THP-1 cells were transferred into V-shaped 96-well plates and centrifuged to discard the supernatant. Cells were then resuspended in DMSO and transferred into flat 96-well plates. The plates were agitated on a shaker for 10 min and the absorbance of each well was measured at 490 nm with a Bio-Rad automated EIA analyzer (Bio-Rad Laboratories, Hercules, CA, United States). The viability of Control cells (Untreated) was arbitrarily considered as 100%, while the other conditions were expressed as percentage of control.

2.3 RNA extraction and transcriptional analyses through real-time qPCR

For transcriptional analyses, cells were resuspended/collected in RNAzol® (TEL-TEST Inc., Friendswood, TX, United States) and RNA extraction was performed through the phenol-chloroform method, as previously described (Toni et al., 2018; Limanaqi et al., 2022). RNA was quantified by the Nanodrop 2000 Instrument (Thermo Scientific, Waltham, MA, United States). Briefly, 1 μg of RNA was purified from genomic

DNA with RNase-free DNase (RQ1 DNase; Promega) and reverse transcribed into cDNA with Moloney murine leukemia virus reverse transcriptase along with random hexanucleotide primers, oligo dT, and dNTPs (Promega, Fitchburg, WI, United States). cDNA (25 ng) was amplified and quantified by real-time qPCR (CFX96 connect, Bio-Rad, Hercules, CA, United States) through the Universal SYBR® Green Supermix (Bio-Rad, Hercules, CA, United States) in a final reaction mix volume of 10 uL. The following genes were analyzed: *Interleukin-1b (IL-1b), Interleukin-6 (IL-6), Chemokine CC-motif ligand 2 (CCL2), Chemokine CC-motif ligand 4 (CCL4), NOD-, LRR- and pyrin domain-containing protein 3 (NLRP3), Caspase-1 (CASP1), Nuclear Factor kappa B (NF-kB), Triggering Receptor Expressed in Myeloid Cells 1 (TREM1), Triggering Receptor Expressed in Myeloid Cells 1 (TREM2), Signal Transduction and Activator of Transcription 1 (STAT1), Tumor Necrosis Factor alpha (TNF-a), Sequestesome 1 (SQSTM/p62), Microtubule-Associated Protein 1A/1B Light Chain 3B (MAP1LC3B), Lysosomal-Associated Protein 1 (LAMP1), mammalian/mechanistic Target of Rapamycin (mTOR), Soluble N-ethylmaleimide-sensitive factor Attachment Protein 29 (SNAP29), B-cell lymphoma 2 (BCL-2), Bcl-2 Associated X-protein (BAX), Cholesterol 25-Hydroxylase (CH25H), ATP-binding cassette transporter G1 (ABCG1), Caveolin-1 (CAV-1), Liver X Receptor (LXR), X-box Binding Protein 1 (XBP1), Oxy-Sterol-Binding Protein (OSBP), Synuclein-alpha (SNCA), and Glyceraldehyde-3-Phosphate Dehydrogenase (GAPDH)*. All the primers were purchased as already optimized and used at 1x final dilution according to the manufacturer instructions (PrimePCR™ SYBR® Green Assay, Bio-Rad). Reactions were performed according to the following thermal profile: initial denaturation (95°C, 15 min) followed by 40 cycles of 15 s at 95°C (denaturation) and 20 s at 60°C (annealing) and 20 s at 72°C (extension). Negative controls (distilled water, PCR mix non containing cDNA) were included in each run. Results for gene expression analyses were calculated by the $2^{-\Delta\Delta CT}$ equation. Melting curves besides Ct values were analyzed for primer and reaction specificity. Results are presented as the mean N fold (percent) ± SEM of the relative expression units to an internal reference sample and normalized to the *GAPDH* housekeeping gene. Results show the quantifications from $n = 3$ independent experiments.

2.4 Multiplex elisa

The concentration of cytokines/chemokines was assessed in the supernatants of THP-1 cells and THP-1-derived macrophages in the presence/absence of αS by using precast immunoassays formatted on magnetic beads (Bio-Rad Laboratories, Hercules, CA, United States), according to manufacturer's protocol via Luminex 100 technology (Luminex, Austin, TX). The concentrations of following cytokines were assessed: Interleukin-1b, -4 -5, −6, −7, −8, −10 (IL-1b, IL-4, IL-5, IL-6, IL-7, IL-8, IL-10), Granulocyte Colony-Stimulating Factor (G-CSF), Granulocyte-Macrophage Colony-Stimulating Factor (GM-CSF), Interferon Gamma (IFN-g), Monocyte Chemoattractant Protein 1/Chemokine CC-motif Ligand 2 (MCP1/CCL2), Macrophage Inflammatory Protein 1/Chemokine CC-motif Ligand 4 (MIP-1b/CCL4). Results are expressed as pg/mL from n = 3 independent biological replicates.

2.5 Flow cytometry

Detection of cell surface, and intracellular CCR2 was performed as previously described (Fujimura et al., 2015). In detail, after 4 or 24 h of αS incubation, THP-1 cells were harvested, centrifuged, and incubated with mouse anti-CCR2 monoclonal antibody (Beckman Coulter) in V-shaped 96-well plates (2.5×10^5 cells/well/condition) to detect surface antigen for 15 min at RT, protected by light. Then, plates were centrifuged at 1,200 rpm for 8 min at RT to discard the antibody solution. Cells were washed in PBS (Euroclone, Italy), centrifuged again, and fixed in 1% paraformaldehyde (PFA, Sigma-Aldrich, MO, United States). For detection of intracellular antigen, cells were incubated with Intracellular Fixation & Permeabilization Buffer Set (eBioscience™, 88-8824-00) according to the manufacturer protocol, stained with mouse anti-CCR2 and/or anti-NLRP3 monoclonal antibody (Beckman Coulter) for 30 min at RT, and then washed with PBS and resuspended in 1% PFA. Acquisition was performed on a CytoFLEX™ flow cytometer system equipped with CytExpert software (Beckman Coulter), and data were analysed using Kaluza software, version 2.1.1. (Beckman Coulter). For CCR2, results are expressed as % of CCR2-expressing THP-1 cells (gating on total THP-1 cells), and Mean Fluorescence Intensity (MFI) of extra- and intra-cellular CCR2/total CCR2 MFI (gating on CCR2+ THP-1 cells) from n = 3 independent biological replicates. For NLRP3, results show the total MFI of NLRP3 in THP-1 cells from n = 3 independent biological replicates.

2.6 Transwell migration assay

Transwell Inserts (5.0-μm pores, Corning Costar 3,421) were used for migration/chemotaxis assay as previously described (Macanas-Pirard et al., 2017). Briefly, untreated, and αS-treated THP-1 cells (4 and 24 h) were harvested and pelleted by centrifuging at 1,200 rpm for 10 min at RT. Cells were resuspended in fresh RPMI with 5% FBS, counted and seeded on the upper chamber of the 24-well Transwell plate (1.5×10^5/well). The conditioned media (supernatants) recovered from both 4 h and 24 h, CTR untreated and αS-treated THP-1 cells containing 10% FBS, along with different concentrations of cytokines and chemokines previously assessed through Multiplex ELISA, were applied in lower chambers for chemotaxis assay. A condition with RPMI medium with 10% FBS (unconditioned medium) in lower chamber was included as the spontaneous migration control/negative control of chemotaxis. Thus, cells from each experimental condition (Untreated, and αS-treated, 4 and 24 h) were co-cultured with i) RPMI + 10% FBS medium, ii) conditioned medium from untreated THP-1 cells containing RPMI + 10% FBS + low/negligible amount of cytokines/chemokines, and iii) conditioned medium from αS-treated THP-1 cells containing RPMI + 10% FBS enriched in cytokines/chemokines. After 16 h, inserts were removed and migrated cells were i) resuspended and counted thrice with the T20 Automated Cell Counter (Bio-Rad Laboratories, Hercules, CA, United States), and ii) left to settle down and imaged at optical microscope (ZOE Fluorescent Cell

Imager; Bio-Rad Laboratories, Hercules, CA, United States). The number of migrated cells is shown as mean percentage (calculated out of the total cells seeded in the upper chamber) ± SEM (n = 3 biological replicates).

2.7 Western blot

Cells were lysed in ice-cold RIPA lysis buffer supplemented with 2% SDS, and a cocktail of protease and phosphatase inhibitors (cOmplete and PhosSTOP; Roche Applied Science, Mannheim, Germany), sonicated, incubated on ice for 30 min on a platform rotator, and then centrifuged at maximum speed for 30 min at 4°C. Protein concentration from whole cell lysates was determined through BCA protein assay kit (Pierce, United States). 30-to-40 μg proteins per sample were prepared by combining the appropriate volume with 4 ×Reducing Laemmli SDS sample buffer (final 1×, J60015.AC, Thermo-Fisher Scientific) and Milli-Q H_2O. Samples were boiled for 5 min and loaded on 4%-12% Mini-Protean Stain-Free TGX Precast SDS-PAGE gel (4,568,095, Bio-rad, Hercules, CA, United States), which was run at 100 V for 1.5 h. The gel was activated at ChemiDoc MP imaging system (Bio-Rad, Hercules, CA, United States) and proteins were transferred on PVDF membrane through The Trans-Blot Turbo Transfer System TM and Transfer Pack TM (Bio-Rad, Hercules, CA, United States). For αS immunodetection and preservation of protein, membrane was fixed with 0.4% PFA for 30 min at RT as previously described (Stojkovska and Mazzulli, 2021; Limanaqi et al., 2024). The stain-free membrane was imaged at ChemiDoc MP imaging system (Bio-Rad, Hercules, CA, United States) and then blocked in 1×TBS with 5% Bovine Serum Albumin (BSA) for 1 h at RT, washed in TBS-0.1% Tween, and incubated overnight at 4°C with the following antibodies prepared in 2.5% BSA/non-fat dry milk: rabbit anti-alpha-synuclein antibody (1:800, Bioss, United States, BSM-54277R 3H12), rabbit anti-LC3B (1:1000, Cell Signaling, #3868), mouse anti-SQSTM1/p62 (1:1000, Cell Signaling, #88588), rabbit anti-phosphorylated ribosomal protein subunit S6 (pS6, 1:1000, Cell Signaling, #4858), mouse anti-total ribosomal protein subunit S6 (S6, 1:1000 Cell Signaling, #2317), mouse anti-LAMP1 (1:1000, BD Biosciences, AB_398356), and mouse anti-β-actin (1:1000, Merck Sigma, A5316). The day after, the blot was washed 3 × 5 min with 1×TBS-0.1% Tween and incubated for 1 h with HRP-conjugated secondary antibodies goat anti-rabbit (1:5000, STAR208P, Bio-Rad) or goat anti-mouse (1:5000, BD Biosciences, HAF007) in blocking buffer with 2.5% BSA/non-fat dry milk. The blot was washed 3 × 5 min with 1×TBS-0.1% Tween and then incubated for 5 min with Clarity Western ECL substrate and visualized with a ChemiDoc MP imaging system (Bio-Rad, Hercules, CA, United States). For membrane reprobing, a stripping solution (25 mM glycine-HCl, pH 2, supplemented with 1% SDS) was used for approximately 30 min under constant agitation, followed by 3 × 5 min washes in 1×TBS-0.1% Tween and 1 h incubation in blocking solution. Results were analyzed using the Image Lab software (Bio-Rad, Hercules, CA, United States). Quantification was performed through normalization to β-actin. For each experiment, a representative blot is shown, and the graphs show to the mean ± SEM from n = 3 independent experiments.

2.8 Immunofluorescence at confocal microscopy

For immunofluorescence, we followed previously described protocols (Zecchini et al., 2019). Cells cultured in u-Slide chambers and stimulated as described above, were fixed in 4% paraformaldehyde (PFA) for 15 min and permeabilized with 0.1% Triton 100X for 10 min. After brief washing in PBS, cells were incubated in a blocking solution of 5% BSA for 1 h, and then incubated at for 1 h at RT with the following primary antibodies prepared in 1% BSA: rabbit anti-α-syn (1:200, Bioss, United States, BSM-54277R 3H12), mouse anti-SQSTM1(1:1000, Cell Signaling, #88588), rabbit anti LC3B (1:1000, Cell Signaling, #3868), or mouse anti-LAMP1 (1:1000, BD Biosciences, AB_398356). Cells were washed thrice in PBS and incubated with Alexa-Fluor-conjugated secondary antibodies raised against the host species of the primary antibodies, namely Goat anti-mouse Alexa Fluor 488 (Abcam, ab150113) or 647 (Abcam, ab150115), or Goat anti-rabbit Alexa Fluor 488 (Abcam, ab150077) or 647 (Abcam, ab150079), 1: 500 prepared in 1% BSA-PBS (Prodotti Gianni, Milan, Italy). Negative controls were performed by omitting primary antibodies. For F-actin and/or nuclear counterstaining, respectively, Phalloidin (Alexa Fluor™ 647 Cat A22287 or Alexa Fluor™ 594 Cat A12381, Thermo-Fisher Scientific, final concentration 1:100) and/or DAPI (Invitrogen ThermoFisher Scientific, D1306, final concentration 1: 1000) were added to the secondary antibody solution, followed by 3 × 5 min washes in PBS. For LysoTracker-based lysosomal staining, 30 min prior to fixation, cells were incubated with 50 nM LysoTracker® Red DND-99 (Cat L7528, Thermo-Fisher Scientific). For examination of lipid droplets by Oil red O stain (Merck Sigma O0625) together with immunolabelled cellular constituents we used a protocol which was slightly modified form Koopman et al. (Koopman et al., 2001). Briefly, Oil red O was dissolved to a stock solution by adding 500 mg Oil red O to 100 mL isopropanol. Prior to staining, a 36% working solution, containing 12 mL Oil red O stock solution and 8 mL deionised water was prepared and 0.22 uM filtered. After fixation, cells were briefly washed in 60% isopropanol, immersed in the working solution of Oil red O for 30 min, and then rinsed thrice with deionised water. Immune-staining was then performed as routinely. u-Slides were *in situ* mounted by adding Fluoromount medium (F4680, Merck-Sigma, Milan, Italy). Confocal images were acquired on a TCS SP8 System equipped with a DMi8 inverted microscope and a HC PL APO 40×/1.30 Oil CS2 (Leica Microsystems, Wetzlar, Germany) at a resolution of 1024 × 1024 pixels. Image analyses (Integrated density or count of puncta/cells) were performed through ImageJ software (NIH, Bethesda, MD, United States). Quantifications were performed from at least n = 3 microscopy fields per experimental group, and per each independent experiment.

2.9 Phagocytosis assay

THP-1–derived macrophages previously cultured in u-Slide chambers and stimulated as described above were incubated for 2 h with latex beads coated with rabbit IgG–FITC complex (No. 500290, Cayman Chemical, final dilution 1:100) at 37°C in a humidified 5% CO2 atmosphere, according to the manufacturer protocol, and as previously described (Mysore et al., 2021). Beads were added 2 h before the ending of αS incubation. Cells were gently

10.3389/fcell.2024.1421360

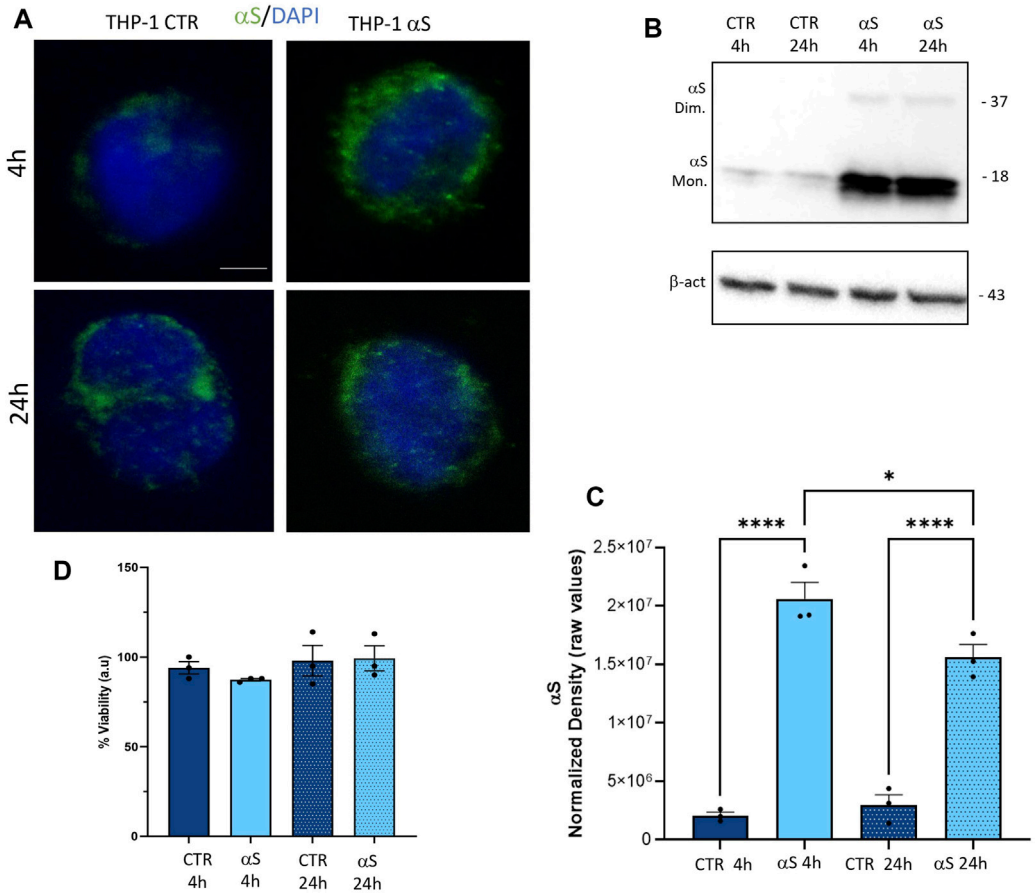

FIGURE 1
THP-1 cells take up exogenous αS in the absence of cell toxicity **(A)**. Representative Immunofluorescence for t αS in control (CTR) and αS-exposed THP-1 cells for 4 h and 24 h. Bars correspond to 5 μm **(B)**. Representative Western blot for αS and β-actin in control (CTR) and αS-exposed THP-1 cells for 4 h and 24 h **(C)**. Quantification of monomeric αS normalized to β-actin. Results are shown as normalized raw values corresponding to mean ± SEM. ***$p < 0.001$; ****$p < 0.0001$ **(D)**. The graph shows results from MTT assay in control (CTR) and αS-exposed THP-1 cells for 4 h and 24 h. Results are shown as arbitrary units (a.u) corresponding to mean ± SEM.

washed twice with pre-warmed Assay buffer prepared in sterile Milli-Q water (No. 500290, Cayman Chemical) to remove non-phagocytosed beads. Cells were then either i) immediately fixed in 4% PFA, or ii) replenished with fresh medium and incubated at 37°C, 5% CO2 for additional 20 h to monitor the intracellular fate of phagocytosed beads/FITC before fixation. In both cases, 30 min prior to fixation, cells were incubated with 50 nM LysoTracker® Red DND-99 (Cat L7528, Thermo-Fisher Scientific). Fixed cells were then stained with Alexa Fluor™ 647 Phalloidin for 30 min (Cat A22287 Thermo-Fisher Scientific, final concentration 1:100), washed twice in PBS and imaged. Confocal images were acquired on a TCS SP8 System equipped with a DMi8 inverted microscope and a HC PL APO 40×/1.30 Oil CS2 (Leica Microsystems, Wetzlar, Germany) at a resolution of 1024 × 1024 pixels. Phagocytosed cargo (FITC), and acidic organelles (LysosoTracker) were quantified and expressed as percentage of cell area/phalloidin, while co-localization of phagocytosed cargo and lysosomes was calculated through the Pearson's R coefficient through the ImageJ software (NIH, Bethesda, MD, United States). Results are expressed as mean ± SEM from n = 3 independent biological replicates.

2.10 Statistical analysis

The GraphPad Prism software package (GraphPad Software, San Diego, CA, United States) was used to generate all the graphs and perform statistical analyses. Data normality was assessed through the Shapiro–Wilk test. The statistical significance was tested through one-way, or two-way ANOVA, followed by the Fisher's LSD post-hoc test. Statistically significant p values are shown in the graphs as *$p < 0.05$, **$p < 0.01$, ***$p < 0.001$, ****$p < 0.0001$. To avoid graphs overcrowding, p values are shown for statistically significant groups only. Results are expressed as mean ± SEM from n = 3 independent experiments/biological replicates.

3 Results

3.1 THP-1 cells take up exogenous αS in the absence of cell toxicity

Both immunofluorescence (Figure 1A), and western-blot analysis (Figure 1B) showed that control THP-1 cells express low constitutive levels of αS (CTR), and they effectively internalize exogenous αS following

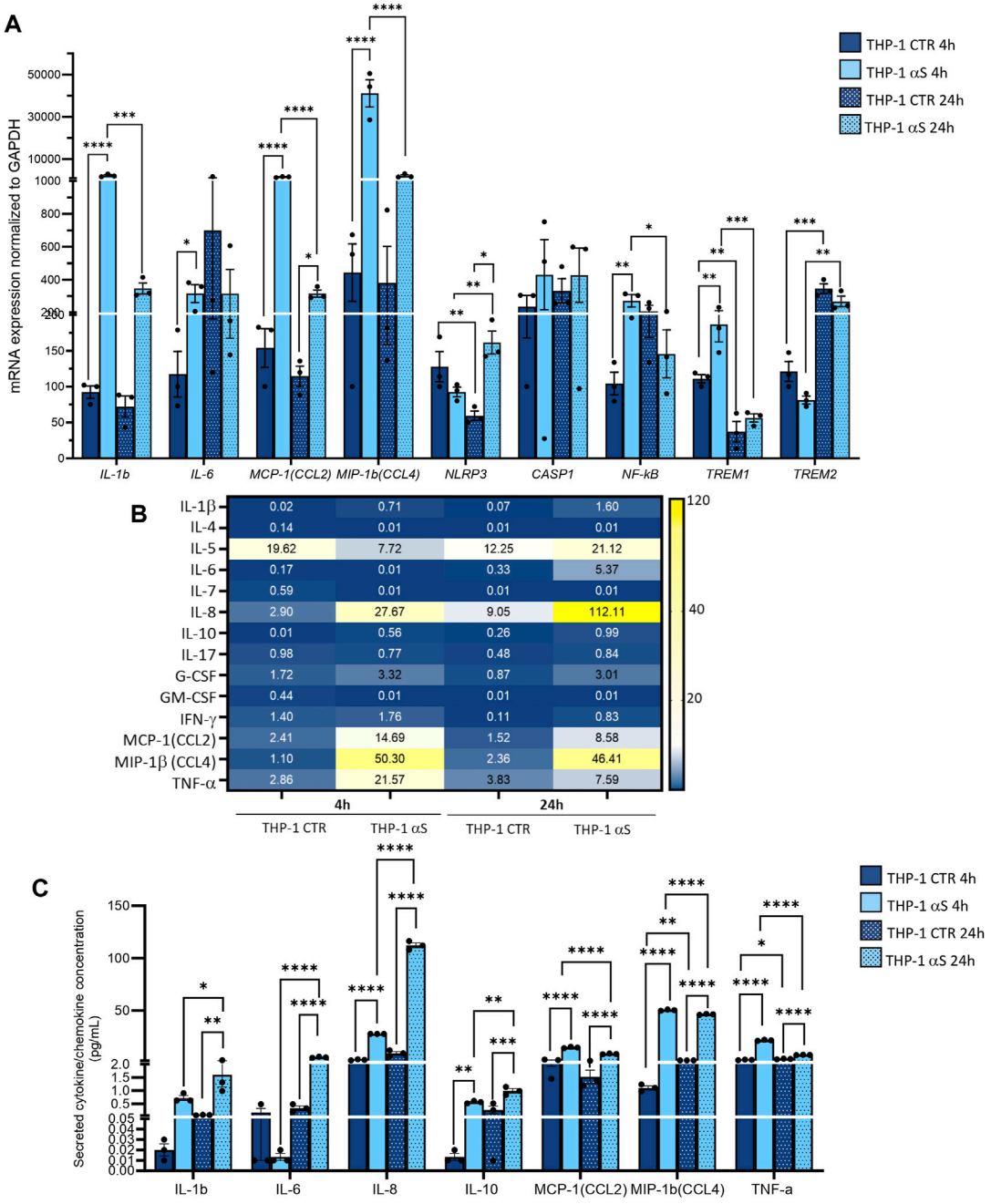

FIGURE 2
Characterization of the inflammatory profile in THP-1 cells. **(A)** Real time RT-qPCR analysis of inflammatory genes in control (CTR) and αS-exposed THP-1 cells (4 h and 24 h). Values were normalized to *GAPDH* and are shown as mean ± SEM. **(B)** Heatmap showing overall mean concentrations (pg/mL) of secreted cytokines/chemokines measured by Multiplex Elisa from the supernatants of CTR, and αS-exposed THP-1 cells (4 h and 24 h). **(C)** Graph showing only statistically significant secreted cytokines/chemokines measured through Multiplex Elisa from the supernatants of CTR, and αS-exposed THP-1 cells (4 h and 24 h). Results are shown as mean ± SEM. *$p < 0.05$; **$p < 0.01$; ***$p < 0.001$; ****$p < 0.0001$.

4 and 24 h exposure. Intracellular exogenous αS detected at 4 and 24 h post-exposure corresponded predominantly to monomeric species, though faint dimers could be observed as well (Figure 1B). Interestingly, the amount of quantified αS at 24 h was moderately, though significantly lower (roughly by 27%) compared to that detected at 4 h (Figure 1C), suggesting that THP-1 cells are able to dilute and probably degrade the intracellular cargo of excess αS. In line with this, 1 μM αS did not cause toxicity in THP-1 cells neither at 4 nor at 24 h (Figure 1D).

3.2 Characterization of αS-induced inflammatory profile in THP-1 cells

Both intracellular mRNA expression and concentrations of secreted cytokines/chemokines were quantified in CTR, and αS-exposed THP-1 cells. αS exposure at either 4 or 24 h produced a general transcriptional upregulation of genes encoding pro-inflammatory cytokines/chemokines/mediators (Figure 2A). However, different profiles were observed at 4 h and 24 h αS

exposure. In detail, the mRNA expression of IL-1β, IL-6, MCP-1/CCL2, MIP-1β/CCL4, NF-kB, and TREM1 was significantly higher in 4 h αS compared with 4 h CTR cells. At 24 h, such an upward trend induced by αS was reproduced for MCP-1/CCL2, MIP-1β/CCL4, and NLRP3 mRNA expression (Figure 2A). Conversely, the expression of IL-1β, MCP-1/CCL2, MIP-1β/CCL4, NF-kB, and TREM1 was significantly reduced, whereas that of TREM2 was upregulated in 24 h compared to 4 h αS-exposed THP-1 cells (Figure 2A). Notably, despite upregulating NLRP3 mRNA expression at 24 h, αS did not affect the intracellular amount of NLRP3 inflammasome, as assessed through flow cytometry (Supplementary Figure S1).

αS exposure at either 4 or 24 h also produced a general increase in the concentration of secreted inflammatory cytokines/chemokines (Figure 2B). In detail, 4 h αS exposure significantly increased IL-8, IL-10, MCP-1/CCL2, MIP-1b/CCL4, and TNF-α compared with 4 h CTR THP-1 cells (Figure 2C). Such an upward trend was observed as well in 24 h αS exposure, as the concentration of secreted IL-1β, IL-6, IL-8, IL-10, MCP-1/CCL2, MIP-1β/CCL4, and TNF-α was significantly increased compared with 24 h CTR. Remarkably, while the concentration of IL-1β, IL-6, IL-8, and IL-10 was higher in 24 h-compared with 4 h-exposed αS, that of MCP-1/CCL2, MIP-1b/CCL4, and TNF-α was instead modestly, but significantly lower in 24 h-compared with 4 h-exposed αS (Figure 2C). These data suggest that αS induces a pro-inflammatory profile in THP-1 cells; however, the uncoupling between mRNA and intracellular/secreted cytokine/chemokines, and mostly, the differences observed between 4 h vs. 24 h αS exposure, suggest the occurrence of compensatory cell mechanisms balancing mRNA transcription, protein translation, turnover, and secretion of specific pro-inflammatory mediators.

We next investigated whether the peculiar inflammatory profile of αS-exposed THP-1 cells is associated with altered extracellular and intracellular dynamics of the MCP-1/CCL2 chemokine receptor CCR2. Initial results on flow cytometry showed that 4 h αS exposure significantly decreases the percentage of total THP-1 cells staining for CCR2 on the cell surface compared with CTR THP-1 4 h monocytes (Supplementary Figure S2A). When gating on CCR2-positive instead of total THP-1 cells, results showed that 4 h αS significantly decreased the mean fluorescence intensity (MFI) ratio of extracellular/total CCR2, meanwhile increasing that of intracellular/total CCR2 (Supplementary Figure S2B). Both analyses showed this effect to be specific to the 4 h αS exposure condition, as no differences were observed between 24 h αS-exposed and 24 h CTR THP-1 cells Supplementary Figure S2A, B). These results suggest that by potentiating CCL2 secretion, αS leads to rapid CCR2 activation followed by receptor internalization and desensitization, which peaks already following brief (4 h) exposure, while prolonged presence of αS (24 h) fosters CCR2 recycling back to the plasma membrane.

3.3 αS time-dependently alters migration and/or chemotaxis

We next assessed whether αS-induced pro-inflammatory profile is associated with functional alterations in THP-1 cells, namely migration and chemotaxis. By combining treated/untreated cells, and unconditioned/conditioned media in a transwell assay model (Figure 3A), we assessed whether i) conditioned media (supernatants) from αS-exposed THP-1 cells (enriched in cytokines/chemokines as previously assessed) attract CTR THP-1 cells, and ii) αS exposure for 4 and 24 h alters THP-1 cells' spontaneous migration and chemotaxis. Results showed that pooled conditioned media (supernatants) from 4 h to 24 h-αS-exposed THP-1 cells potently attract untreated CTR cells cultured for both 4 h and 24 h (Figure 3B, C). In detail, a higher percentage of CTR THP-1 cells migrated in the lower chamber containing conditioned medium (supernatants) collected from αS-exposed cells compared to THP-1 cells that migrated towards both i) the unconditioned medium with FBS, and ii) their own conditioned medium (supernatants that were pooled from 4 h to 24 h CTR THP-1 cells). Instead, increased migration of 4 h αS-exposed compared with CTR THP-1 cells was detected only in the presence of unconditioned medium containing FBS, and supernatant media from THP-1 CTR cells, suggesting spontaneous migration (Figure 3B, C). In the presence of chemokine-rich supernatants from αS-exposed cells, no differences were observed in terms of migrated cells between 4 h αS-exposed and CTR THP-1 cells, suggesting that 4 h αS-overloaded THP-1 cells do not feature increased chemotaxis (Figure 3B, C). Remarkably, migration/chemotaxis of THP-1 cells exposed to αS for 24 h was reduced compared with both 4 h αS-exposed cells, and 24 h CTR THP-1 cells (Figure 3B, C). In fact, a lower percentage of THP-1 cells exposed to αS for 24 h migrated towards their own chemokine-conditioned media compared to both untreated CTR 24 h, and their 4 h αS-exposed counterparts. Collectively, these data suggest that i) the extracellular milieu produced from αS-exposed cells serves as a chemoattractant for untreated monocytic cells, and ii) αS-loaded THP-1 monocytic cells feature altered migration capacity, and chemotaxis, with the effects varying according to the timing of αS exposure.

3.4 αS upregulates autophagy markers in THP-1 cells

To assess whether the effects of αS in THP-1 cells are associated with potential alterations in the autophagy/lysosomal pathway, we examined both mRNA expression (Figure 4A) and protein levels of autophagy-related markers (Figure 4B–F). Early αS exposure (4 h) upregulated mRNA expression of the autophagy adaptor SQSTM1/p62, while 24 h αS exposure significantly upregulated LAMP1 mRNA expression (Figure 4A). While SQSTM1/p62 mRNA expression was lower in 24 h compared to 4 h αS-exposed THP-1 cells, LAMP1 followed an opposite trend (Figure 4A). mTOR expression was increased in 24 h compared to 4 h in both CTR and αS conditions, yet it was not modified by αS exposure compared with CTR at either time-points. Likewise, αS exposure at either time-points did not significantly affect the mRNA expression of MAP1LC3B or SNAP29, which is known to promote autophagosome-lysosome fusion. Western Blot analysis showed that while decreasing overall LC3-II levels (data not shown), αS significantly increased LC3II/I ratio compared to CTR THP-1 cells both at 4 and 24 h, suggesting increased availability of the

10.3389/fcell.2024.1421360

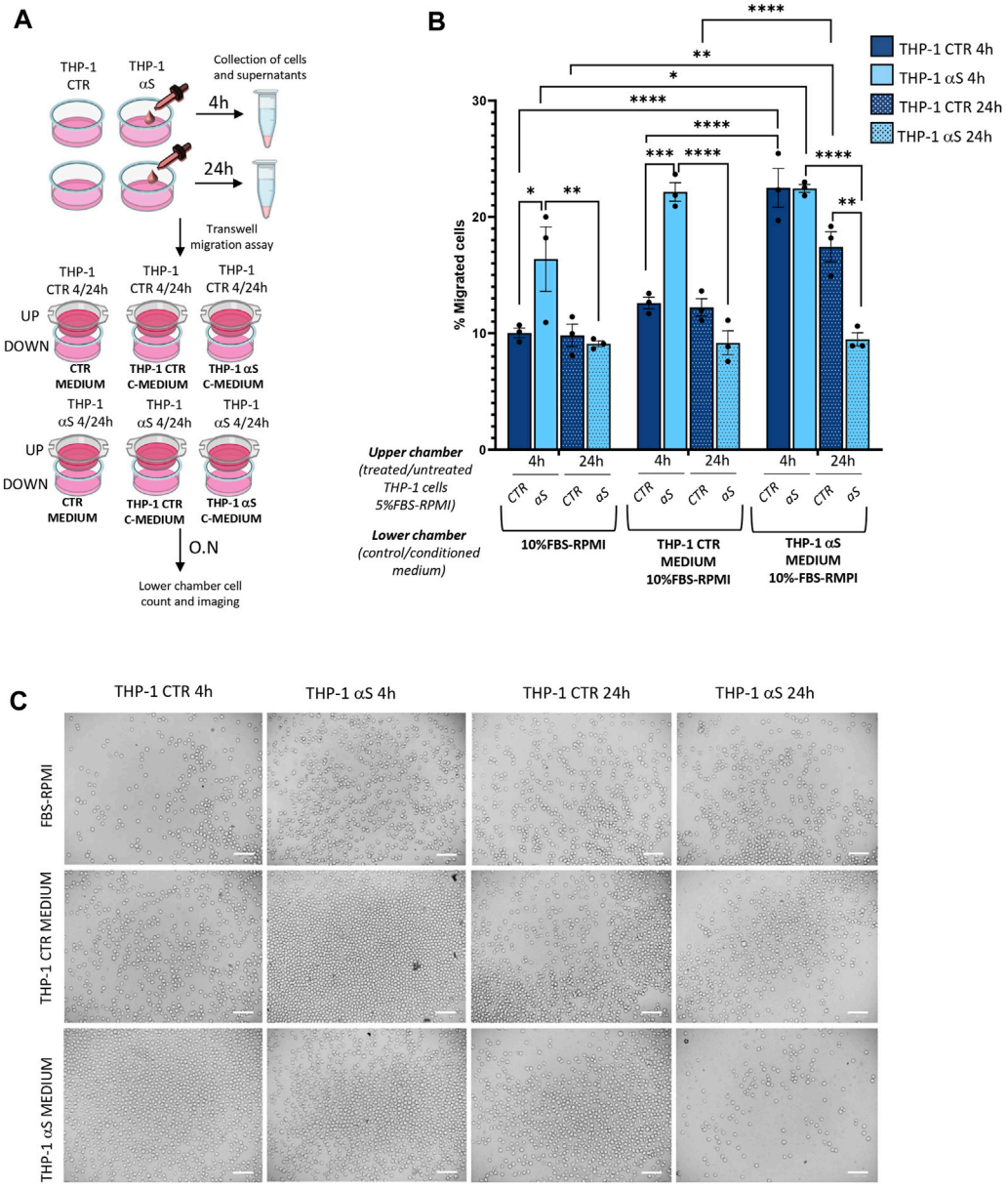

FIGURE 3
αS alters migration/chemotaxis of THP-1 cells. **(A)** Cartoon summarizing the set-up of the transwell assay with the different combinations of untreated (CTR)/αS-exposed cells in the upper chambers, and their unconditioned (CTR medium) or conditioned media/supernatants (C-Medium) in the lower chamber. **(B)** Count of migrated cells in the lower chambers of the transwell assay under different experimental conditions/combinations. Cells were counted through the Trypan Blue exclusion assay and were expressed as percentage (number of migrated cells out of the total number of cells seeded in the upper chamber). Values are shown as mean ± SEM. *$p < 0.05$; **$p < 0.01$; ***$p < 0.001$; ****$p < 0.0001$. **(C)**. Representative microscopy field of the migrated cells from the different experimental conditions/combinations. Bars correspond to 100 μM.

lipidated LC3 isoform for autophagosome formation (Figure 4C). This was parallelled by a decrease in p62 levels at 24 h αS exposure compared to CTR, suggesting effective degradation of p62 protein despite its early transcriptional upregulation (Figure 4D). In fact, while the early upregulation of SQSTM1/p62 mRNA expression induced by 4 h αS suggests an attempt to activate degradation pathways by increasing the availability of the autophagy adaptor protein (Figure 4A), the decrease in p62 protein levels by 24 h αS exposure suggests an effective progression of autophagy (Figure 4D). Supporting this claim, the pS6/total S6 protein ratio, a reliable index of mTOR activity, was significantly reduced by αS exposure at both time points compared with CTR THP-1 cells (Figure 4E). These data also suggest that pS6/S6 ratio is partly uncoupled to mTOR mRNA expression, which was not significantly modified by αS at either time-points. Instead, LAMP1 protein increase occurred at 24 αS exposure (Figure 4F), consistently with the transcriptional upregulation of LAMP1 mRNA by 24 h αS. Altogether, these data suggest that αS, mostly at 24 h exposure, elicits upregulation of autophagy/lysosomal markers, possibly via mTOR inactivation.

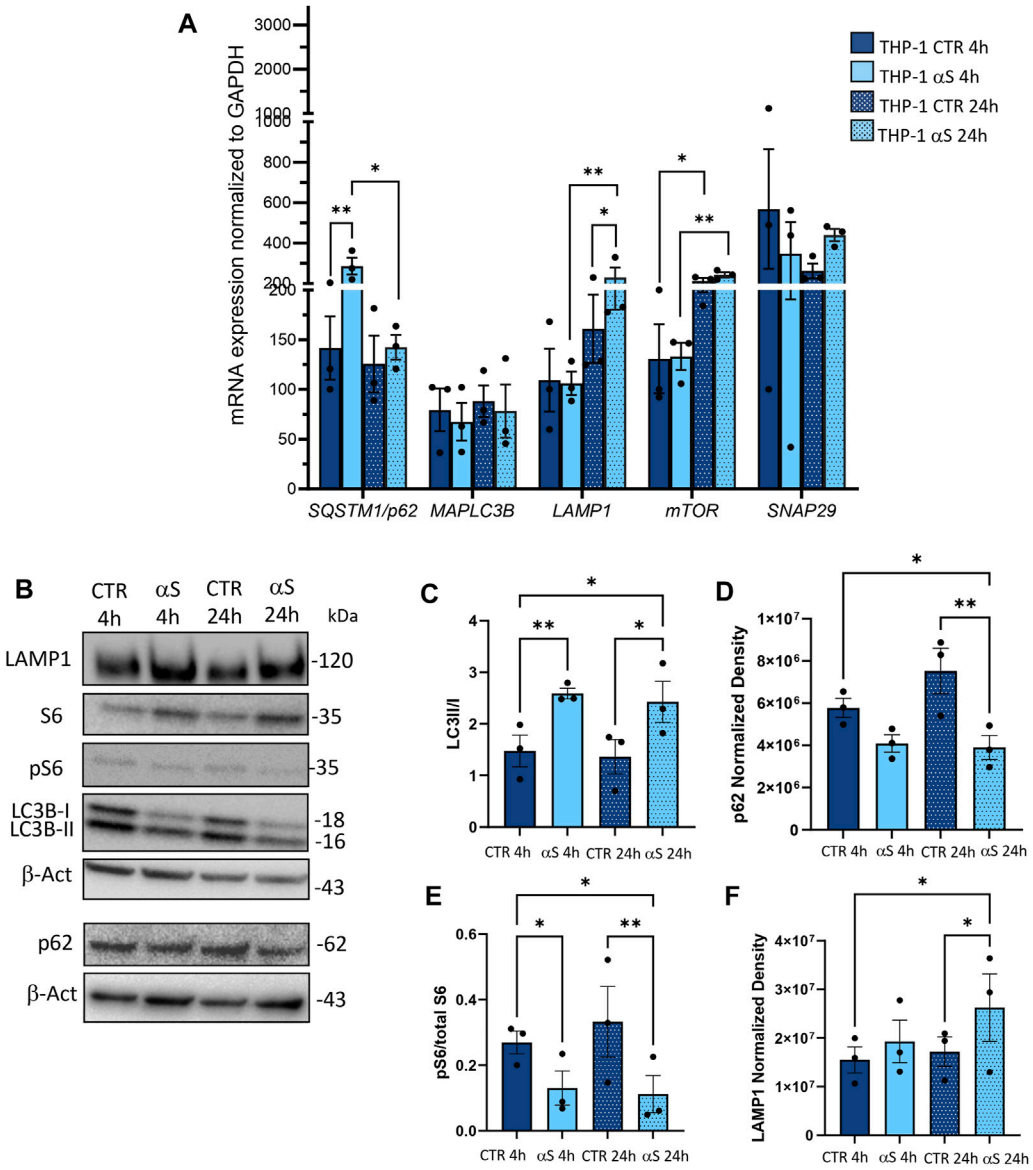

FIGURE 4
αS increases autophagy-lysosomal markers in THP-1 monocytic cells. **(A)** Real time RT-qPCR analysis of autophagy-related genes in control (CTR) and αS-exposed THP-1 cells (4 h and 24 h). Values were normalized to *GAPDH* and are shown as mean ± SEM. **(B)** Representative Western Blot against LC3II, LC3I, pS6, S6, p62, LAMP1 and β-actin in control (CTR) and αS-exposed THP-1 monocytes (4h and 24 h). **(C–F)** Quantification of LC3II/I ratio **(C)**, p62 **(D)**, LAMP1 **(E)**, and pS6/S6 ratio **(F)**. Normalization was performed against β-actin, and results are shown as normalized raw values corresponding to mean ± SEM. *$p < 0.05$; **$p < 0.01$.

3.5 Characterization of αS-induced inflammatory profile and toxicity in THP-1-derived macrophages

Inflammatory profiles of CTR and αS-exposed THP-1-derived-macrophages were characterized similarly to their monocytic counterpart. In detail, mRNA expression of IL-1β, MCP-1/CCL2, MIP-1β/CCL4, STAT1, and TNF-α was significantly higher in 4 h αS compared with 4 h CTR THP-1-derived macrophages (Figure 5A). This upward trend persisted at 24 h αS exposure for IL-1β, MCP-1/CCL2, and MIP-1β/CCL4, along with upregulation of CASP1 mRNA expression (Figure 5A). Instead, IL-6 mRNA expression decreased in 24 h αS-exposed compared with CTR cells (Figure 5A). Again, the mRNA expression of CCL4, CASP1, NF-kB, STAT1, TREM1, and TNF-α was lower in 24 h compared with 4 h αS exposure (Figure 5A).

Contrary to what was observed for monocytic THP-1cells, αS exposure in THP-1-derived macrophages produced a time-related increase in the concentration of secreted inflammatory cytokines/chemokines (Figure 5B, C), except for CCL2 which showed a downward, though non statistically significant trend in 24 h vs. 4 h αS (Figure 5B). Instead, IL-8 concentrations were constantly above the detection limit (Figure 5B). In detail, significant differences between αS and CTR cells were observed for most secreted cytokines/chemokines only at 24h, when αS exposure significantly increased IL-1β, IL-4, IL-6, IL-10, IL-17, G-CSF,

10.3389/fcell.2024.1421360

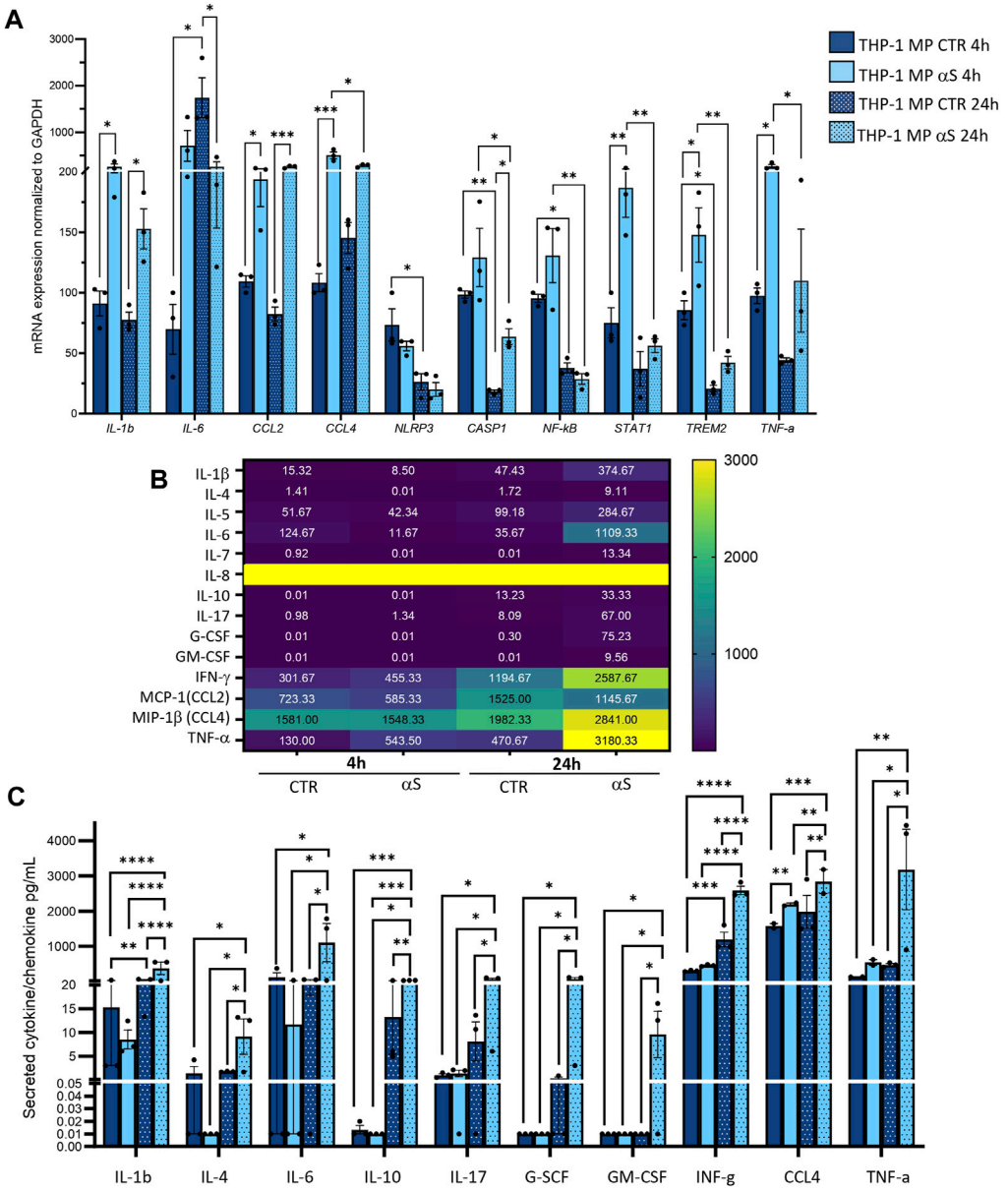

FIGURE 5
Characterization of αS-induced inflammatory phenotype in THP-1-derived macrophages. **(A)** Real time RT-qPCR analysis of inflammatory genes in control (CTR) and αS-exposed THP-1-derived macrophages (MP, 4 h and 24 h). Values were normalized to *GAPDH* and are shown as mean ± SEM. **(B)** Heatmap showing overall mean concentrations (pg/mL) of secreted cytokines/chemokines measured by Multiplex Elisa from the supernatants of CTR, and αS-exposed THP-1-derived macrophages (MP, 4h and 24 h). IL-8 concentrations were constantly above the detection limit. **(C)** Graph showing only statistically significant secreted cytokines/chemokines measured through Multiplex Elisa from the supernatants of CTR, and αS-exposed THP-1-derived macrophages (MP, 4 h and 24 h). Results are shown as mean ± SEM. *$p < 0.05$; **$p < 0.01$; ***$p < 0.001$; ****$p < 0.0001$.

GM-CSF, IFN-γ, MIP-1b/CCL4, and TNF-α compared with CTR THP-1-derived macrophages (Figure 5C). The concentration of these very same cytokines/chemokines was also significantly higher in 24 h αS- compared with 4 h αS-exposed cells. This suggests that several mRNA reductions, including IL-6 expression at 24 h αS-exposed vs. CTR cells, as well as CCL4, and TNF-α expressions at 24 h compared with 4 h αS (Figure 5A), represent a compensatory response to increased cytokine production. Thus, αS potentiates the pro-inflammatory profile in THP-1-derived macrophages, which is magnified at 24 h αS exposure in terms of secreted cytokine/chemokines.

Intracellular staining for IL-1β suggested that the lack of significant effects at 4 h αS in terms of secreted inflammatory mediators is due to the intracellular accumulation of this cytokine which peaks at this time-point (Figure 6A, B). In detail, intracellular IL-1β staining was significantly increased by both 4 h and 24 h αS exposure compared to CTR THP-1-derived macrophages; however, it was significantly lower in 24 h compared with 4 h αS exposure (Figure 6B), a trend which was opposite to that observed for secreted IL-1β (Figure 5C). 24 h αS exposure also led to the appearance of apoptotic/picnotic nuclei (Figure 6A), which, contrary to what was observed in THP-1

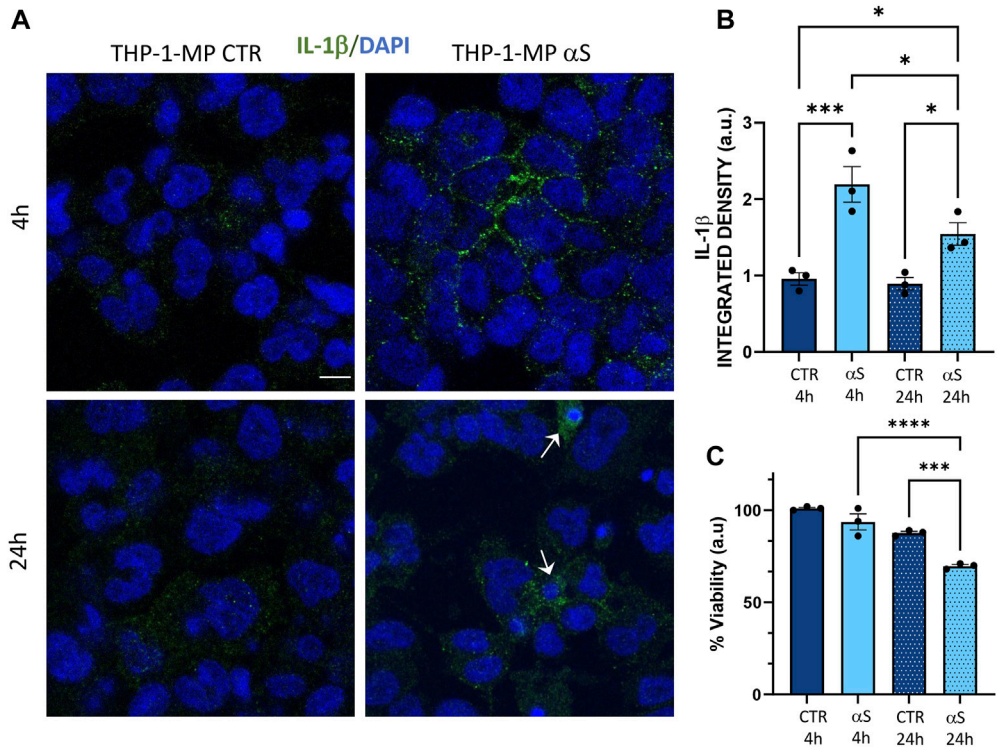

FIGURE 6
αS induces early intracellular accumulation of IL-1β in THP-1-derived macrophages. **(A)** Representative Immunofluorescence against IL-1β in control (CTR) and αS-exposed THP-1-derived macrophages (MP) for 4 h and 24 h. Arrows point at apoptotic/dying cells. Bars correspond to 10 μm. **(B)** Quantification of IL-1β integrated fluorescence density from control (CTR) and αS-exposed THP-1-derived macrophages (MP) for 4h and 24 h. Results are shown as mean ± SEM. *$p < 0.05$; ***$p < 0.001$; **(C)** MTT assay in control (CTR) and αS-exposed THP-1-derived macrophages for 4h and 24 h. Results are shown as arbitrary units (a.u) corresponding to mean ± SEM. ***$p < 0.001$; ****$p < 0.0001$.

monocytic cells, was consistent with a rough 20%-to-30% reduction of cell viability in 24 h αS-exposed compared with CTR THP-1-derived macrophages (Figure 6C). In line with this, a consistent reduction of the mRNA BCL-2/BAX ratio was also detected in 24 h αS-exposed compared with CTR THP-1-derived macrophages (Supplementary Figure S3).

3.6 αS uptake is associated with reduced autophagolysosomal markers in THP-1-derived macrophages

To assess αS internalization and the autophagy/lysosomal dynamics in THP-derived macrophages, we performed a series of immunofluorescence, western blot, and gene expression analyses. Similarly to what was observed in THP-1 monocytic cells, THP-1-derived macrophages effectively internalized exogenous αS (Figure 7A–C), which accumulated predominantly as monomeric species (Figure 7A, B). Two interesting phenomena were observed in THP-1 derived macrophages contrary to THP-1 monocytic cells: i) endogenous αS protein was not detected in THP-1-derived macrophages (Figure 7A, C), suggesting that PMA-induced differentiation goes along with αS downregulation, as confirmed at mRNA level as well (Supplementary Figure S4); and ii) no statistically significant differences were detected in 4 h αS compared with 24 αS THP-1-derived macrophages in terms of intracellular αS amount, despite a tendency to decrease which is probably due to cell death (Figure 7B). This suggests the absence of an effective clearance mechanism to cope with intracellular αS overload in THP-1-derived macrophages, ultimately making them susceptible to αS-induced cell toxicity. Indeed, in THP-1-derived macrophages, exogenous αS staining showed a variously-sized, punctuate pattern reminiscent of protein inclusions that occasionally colocalized with the autophagy adaptor protein and substrate p62 (Figure 7C). Most importantly, αS exposure at 4 h and 24 h led to a significant increase in both p62 staining (Figure 7D), and p62 puncta/cell (Figure 7E), suggesting impaired turnover/clearance of p62.

To gain deeper insights into the effects of αS upon the autophagy-lysosomal pathway, we next examined mRNA and protein expressions of the same autophagy-related mediators that were measured in THP-1 monocytes. Similarly to what observed in THP-1 monocytes, 4 h αS exposure upregulated mRNA expression of the autophagy adaptor SQSTM1/p62 in THP-1-derived macrophages (Figure 8A); however, it significantly decreased mRNA expression of LAMP1, and SNAP29 compared with CTR macrophages (Figure 8A). Downregulation of LAMP1, and a downward trend for SNAP29 persisted at 24 h αS exposure compared with 24 h CTR (Figure 8A). Furthermore, mRNA expression of MAPLC3B, LAMP1, and mTOR was lower in 24 h αS- compared to 4 h αS-exposed THP-1-derived macrophages (Figure 8A). mRNA expression of LAMP1, and mTOR was also

10.3389/fcell.2024.1421360

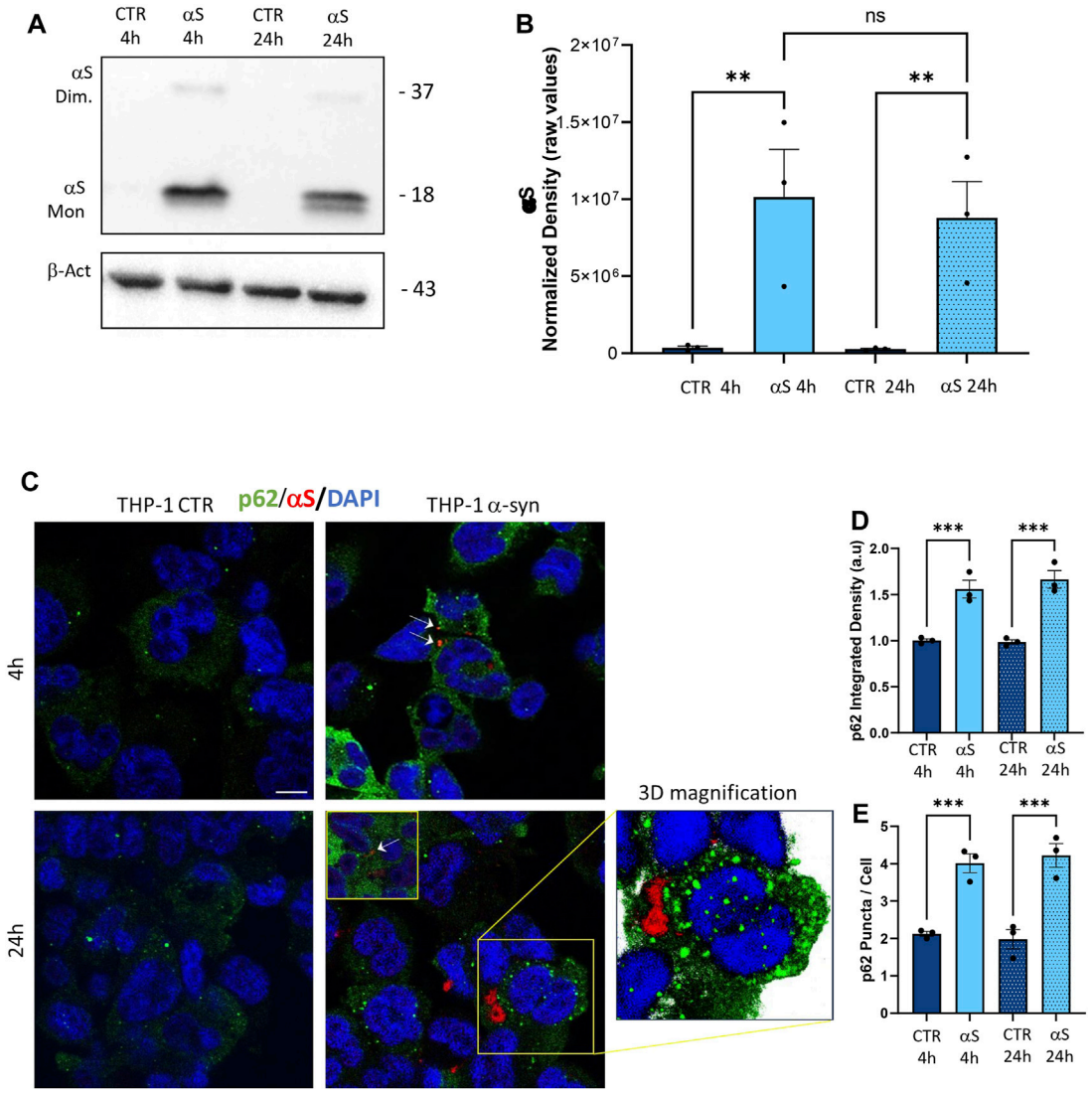

FIGURE 7
The uptake of αS is associated with p62 accumulation in THP-1-derived macrophages. **(A)** Representative Western blot for αS and β-actin in control (CTR) and αS-exposed THP-1-derived macrophages (MP, 4 h and 24 h). **(B)** Quantification of monomeric αS normalized to β-actin. Results are shown as normalized raw values corresponding to mean ± SEM. ***$p < 0.001$; ****$p < 0.0001$. **(C)** Representative Immunofluorescence against αS and p62 in control (CTR) and αS-exposed THP-1 monocytes for 4 h and 24 h. Arrows point at αS-p62 co-localizing puncta. Bars correspond to 10 μm. **(D, E)** Quantification of p62 integrated fluorescence density, and p62 puncta/cell in control (CTR) and αS-exposed THP-1-derived macrophages (MP) at 4 h and 24 h. Results are shown as mean ± SEM. ***$p < 0.001$; ****$p < 0.0001$.

reduced in 24 h vs. 4 h CTR THP-1-derived macrophages, probably due to the progressive metabolic rewiring that takes places following PMA withdrawal in these cells. Western Blot analysis showed that, contrary to what observed in THP-1 monocytic cells, 24 h αS significantly decreased LC3II/I protein ratio (Figure 8C) meanwhile increasing p62 protein compared to CTR THP-1-derived macrophages (Figure 8D). LAMP1 protein time-dependently decreased in both experimental conditions while αS exposure at both 4 h and 24 h consistently reduced LAMP1 protein compared with CTRs (Figure 8E). Timing of PMA withdrawal produced a decrease in both mRNA expression of mTOR, and pS6/totalS6 protein ratio (24 h vs. 4 h), while αS exposure itself did not significantly alter pS6/totalS6 ratio at either time points, despite an upward trend being observed at 24 h compared with CTR THP-1 derived macrophages (Figure 8F). In line with the early reduction of LAMP1 by αS, LysoTracker staining was also decreased in 4 h αS-exposed compared to CTR THP-1-derived macrophages (Figure 9A, B). Again, exogenous internalized αS, while producing an evident qualitative decrease in LAMP1 staining, moderately co-localized with F-actin but not with LAMP1 in THP-1-derived macrophages (Figure 9C). These data suggest that, opposite to what observed in THP-1 monocytes, αS reduces autophagy/lysosomal markers in THP-1-derived macrophages via mTOR-independent mechanisms potentially including impaired LC3 lipidation/autophagosome maturation, autophagosome-lysosome fusion, impaired lysosomal efficacy, and aberrant interaction with cytoskeleton proteins, which eventually occludes the clearance of p62 and αS.

10.3389/fcell.2024.1421360

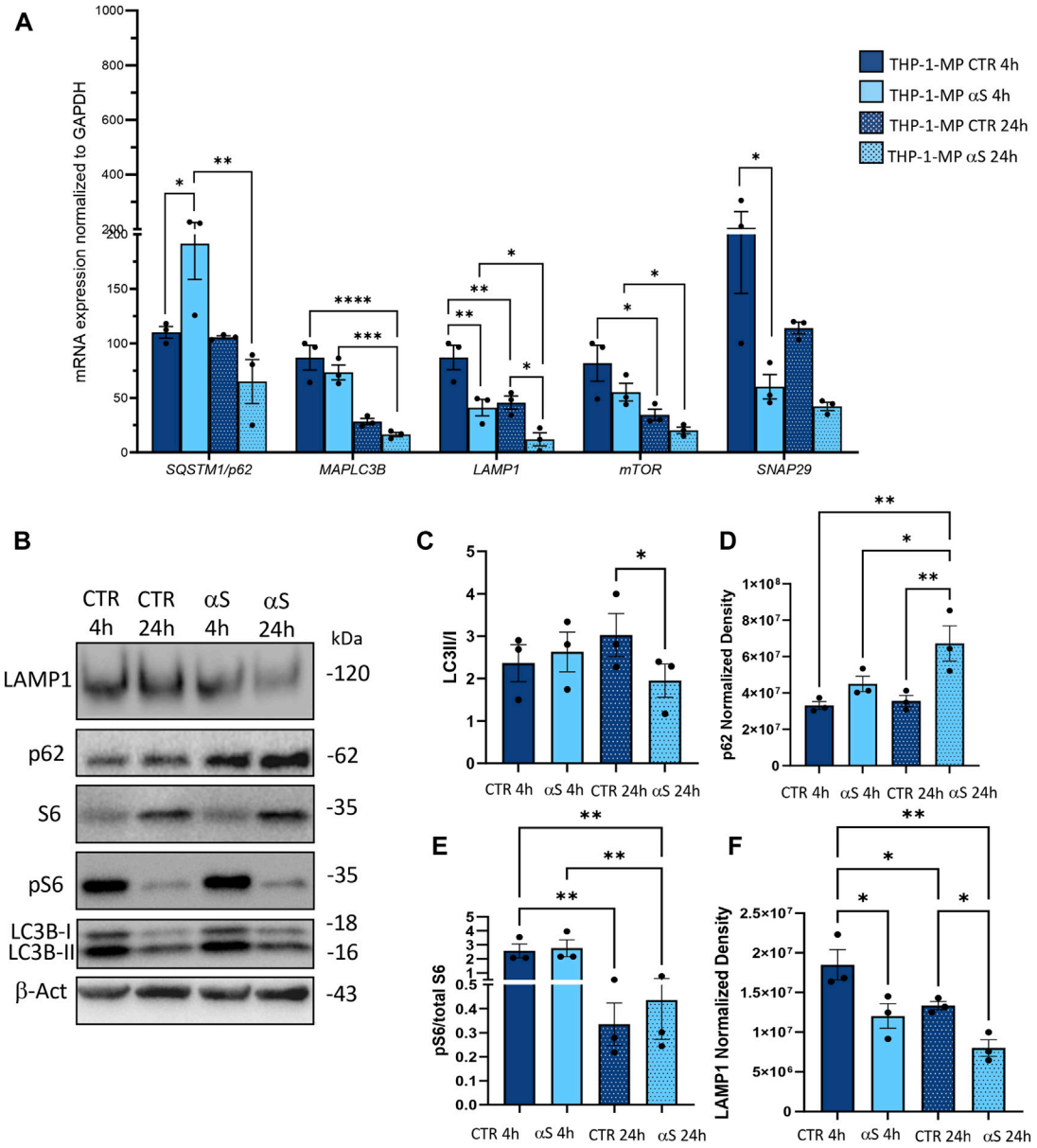

FIGURE 8
αS impairs autophagy-lysosomal markers in THP-1-derived macrophages. **(A)** Real time RT-qPCR analysis of autophagy-related genes in control (CTR) and αS-exposed THP-1-derived macrophages (4 h and 24 h). Values were normalized to *GAPDH* and are shown as mean ± SEM. *$p < 0.05$; **$p < 0.01$; ***$p < 0.001$; ****$p < 0.0001$. **(B)** Representative Western Blot against LC3II, LC3I, pS6, S6, p62, LAMP1 and β-actin in control (CTR) and αS-exposed THP-1-derived macrophages (MP, 4 h and 24 h). **(C–F)** Quantification of LC3II/I **(C)**, p62 **(D)**, LAMP1 **(E)**, and pS6/S6 **(F)**. Normalization was performed against β-actin, and results are shown as normalized raw values corresponding to mean ± SEM. *$p < 0.05$; **$p < 0.01$.

Preliminary results on primary human monocyte-derived macrophages (MDMs) showed that αS is internalized by such cells where it appeared as cytosolic puncta Figure 10). Even if still low, constitutive expression of αS with a prominent nuclear localization was also detected within such cells (Figure 10A), contrary to THP-1-derived macrophages. In primary human MDMs, 24 h αS exposure produced a qualitative decrease in LAMP1 immunostaining meanwhile fostering cytoskeleton rearrangements resulting in a hyper-branched cell morphology, reminiscent of reactive macrophages. Again, in human MDMs, αS co-localized with F-actin clusters but not LAMP1 (Figure 10C).

3.7 αS-induced alterations of autophagy in THP-1-derived macrophages are associated with impaired lipid droplets and altered expression of cholesterol genes

As alterations in intracellular lipid metabolism are associated with both macrophage inflammation and defects in degradative organelles, we next assessed if αS-induced reduction of autophagy-lysosomal markers associates with altered lipid dynamics in THP-1-derived macrophages. Results were unexpected, showing that αS consistently reduces lipid droplets' (LDs) accumulation, as assessed

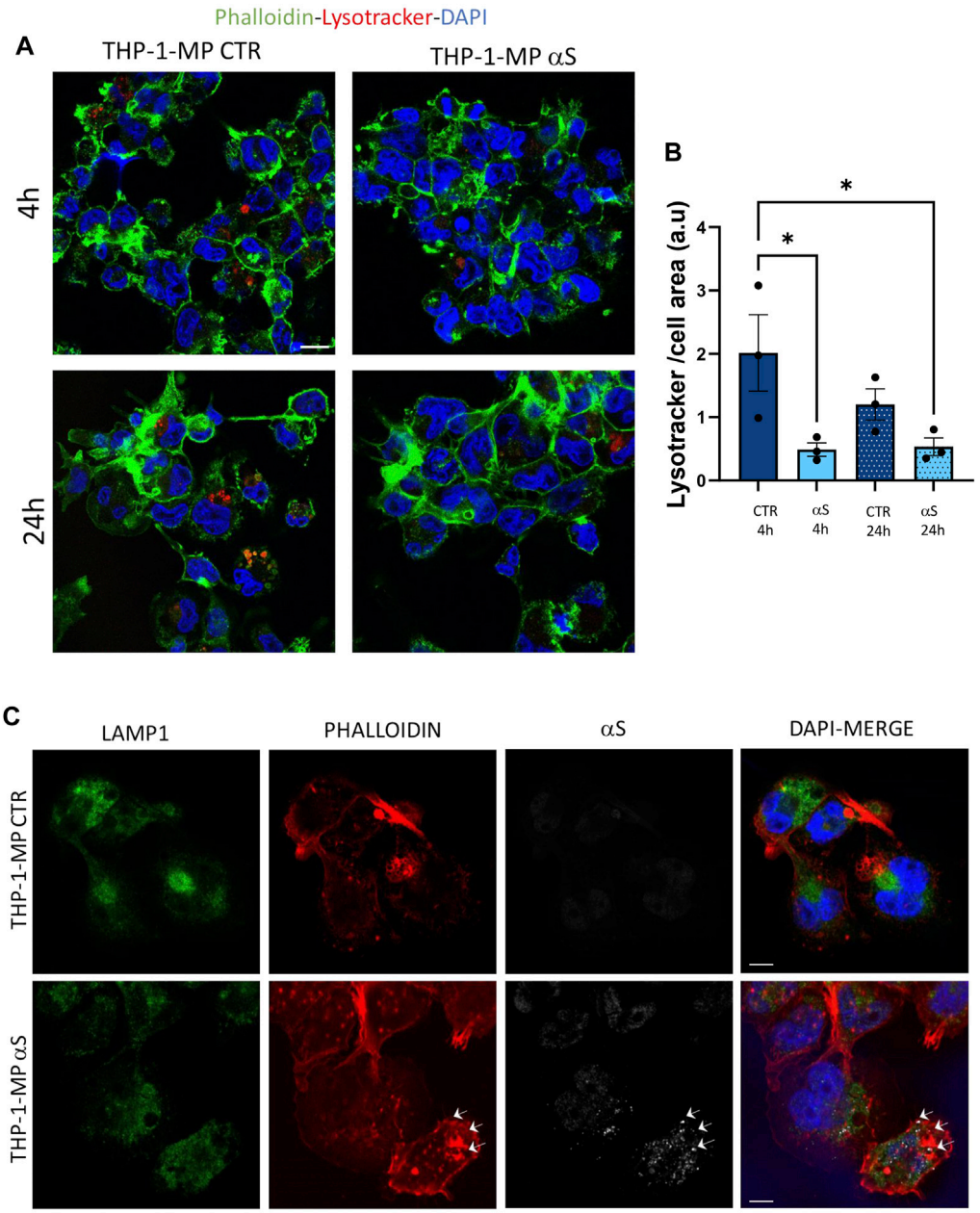

FIGURE 9
αS reduces lysosomal staining and co-localizes with F-actin in THP-1-derived macrophages. **(A)** Representative image of immunofluorescence staining with LysoTracker and F-actin (phalloidin) in control (CTR) and αS-exposed THP-1-derived macrophages (4 h and 24 h). **(B)** LysoTracker quantification in control (CTR) and αS-exposed THP-1-derived macrophages (4 h and 24 h). Values are shown as mean ± SEM. *$p < 0.05$. **(C)** Representative image of combined immunofluorescence for αS, LAMP1, and F-actin (phalloidin) in control (CTR) and αS-exposed THP-1-derived macrophages (4 h and 24 h). Arrows point at αS-phalloidin co-localization. Bars correspond to 10 μM.

through Oil-Red-O staining, in THP-1-derived macrophages (Figures 11A, B). LDs' reduction was mostly evident in cells containing high levels of exogenous αS, including αS-filled cells undergoing cell death (Figure 11A). Combined immunofluorescence analysis for Oil-Red-stained LDs, LC3B, and LAMP1 (Figure 11C) showed that 24 h αS-exposure reduces the colocalization of LC3B and LAMP1 (Figure 11D), as well as the colocalization of LDs and LC3B (Figure 11E), and that of LDs, LCB, and LAMP1 (Figure 11F). These effects were associated with the modulation of cholesterol pathway genes' expression, namely downregulation of the cholesterol efflux gene ABCG1 in 4 h αS-exposed cells, and upregulation of CAV-1, LXR, and XBP1 in 24 h αS-exposed compared with CTR THP-1-derived macrophages (Supplementary Figure S5). Instead, OSBP mRNA expression showed an upward, though not statistically significant trend following 4 h and 24 h αS exposure compared with respective CTR THP-1-derived macrophages (Supplementary Figure S5). Collectively, these data suggest that αS-induced alterations in lipid metabolism, including LDs formation and cholesterol pathway, might in turn contribute to impairing autophagy/

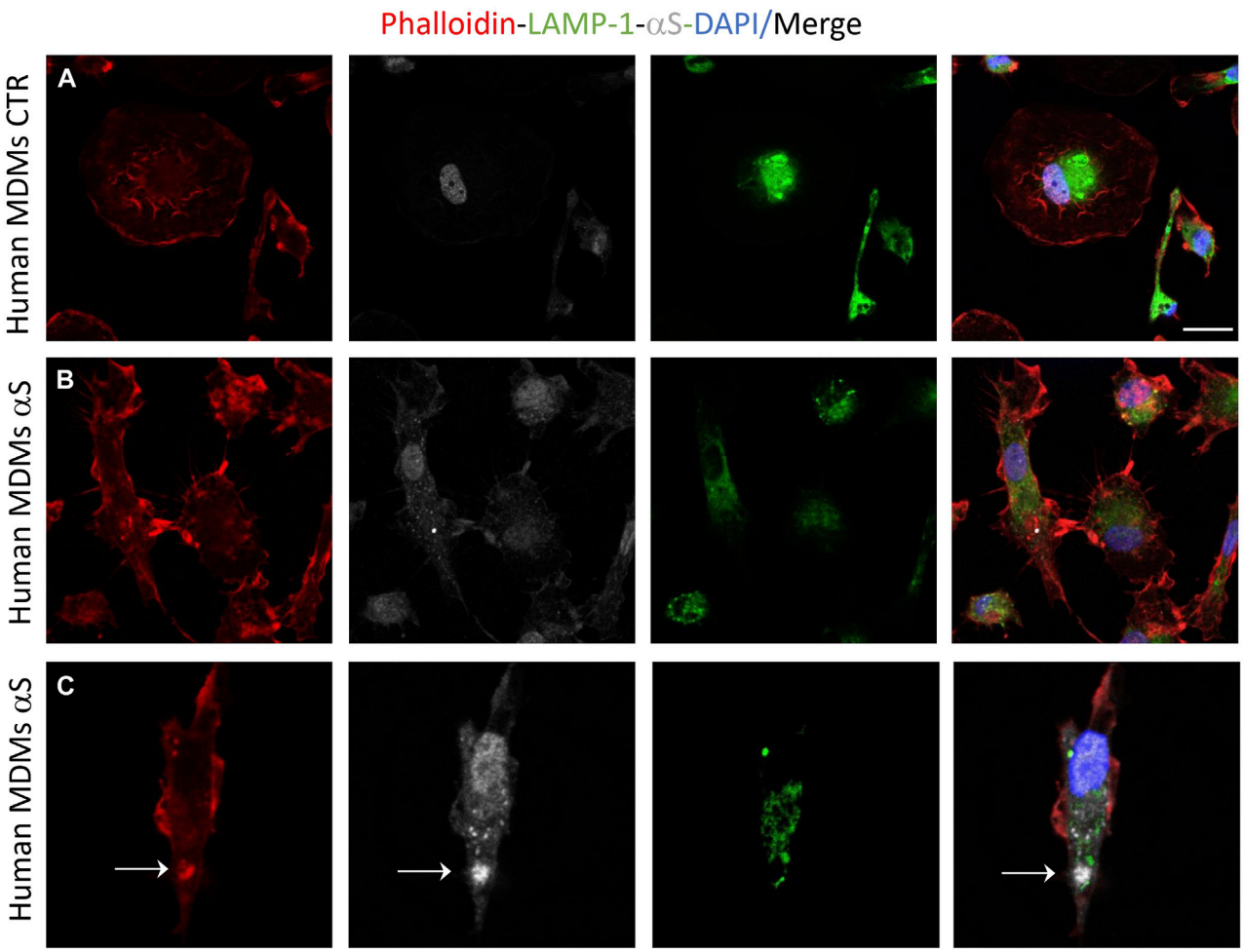

FIGURE 10
Human monocyte-derived macrophages (MDMs) take-up exogenous αS. Representative image of combined immunofluorescence for αS, LAMP1, and F-actin (phalloidin) in control (CTR, **A**) and αS-exposed, human MDMs (24 h, **B**,**C**).

lysosomal system via defective autophagosome, lysosome, and/or autolysosome formation/maturation.

3.8 αS impairs phagocytosis and the clearance of phagocytosed cargo in THP-1-derived macrophages

Finally, we assessed whether αS functionally alters THP-derived macrophages by measuring their phagocytic capacity and the intracellular fate of phagocytosed cargo. In line with previous evidence in both microglia and primary human macrophages (Gardai et al., 2013; Haenseler et al., 2017), our results showed that αS reduces the phagocytic capacity of THP-1-derived macrophages (Figure 12A, B). In fact, following 2 h incubation with FITC-IgG latex beads, 4 h αS-exposed THP-1-derived macrophages showed a two-fold reduction of FITC signal corresponding to phagocytosed beads (Figure 12A, B). At such a time-point, only occasional colocalization of beads and LysoTracker-marked lysosomes was detected in both αS-exposed and CTR cells, without significant differences (Figure 12A, C). Remarkably, following beads washout and culturing of cells for additional 20 h, FITC signal was almost completely absent in CTR-THP-1-derived macrophages, suggesting effective processing/dimming of FITC dye in acidic organelles (Figure 12A–C). Instead, the same amount of initially phagocytosed beads (FITC signal) was still present in αS-exposed THP-1-derived macrophages even after additional 20 h culturing following beads washout (Figure 12A, B). Such FITC-stained phagocytosed cargo markedly filled the LysoTracker-stained organelles, resulting in a co-localization pattern reminiscent of engulfed/stagnant lysosomes (Figure 12A, C). These data suggest that αS impairs phagocytosis and lysosomal processing of phagocytosed cargo. Combined staining for F-actin, αS, and LAMP1 showed the occasional presence of extracellular material which clustered near/around the phagocytic-like protrusions of CTR THP-1-derived macrophages (Figure 12D). In 24 h αS-exposed THP-1 derived macrophages, several αS-filled dying/dead cells were instead observed, which clustered near aberrantly appearing

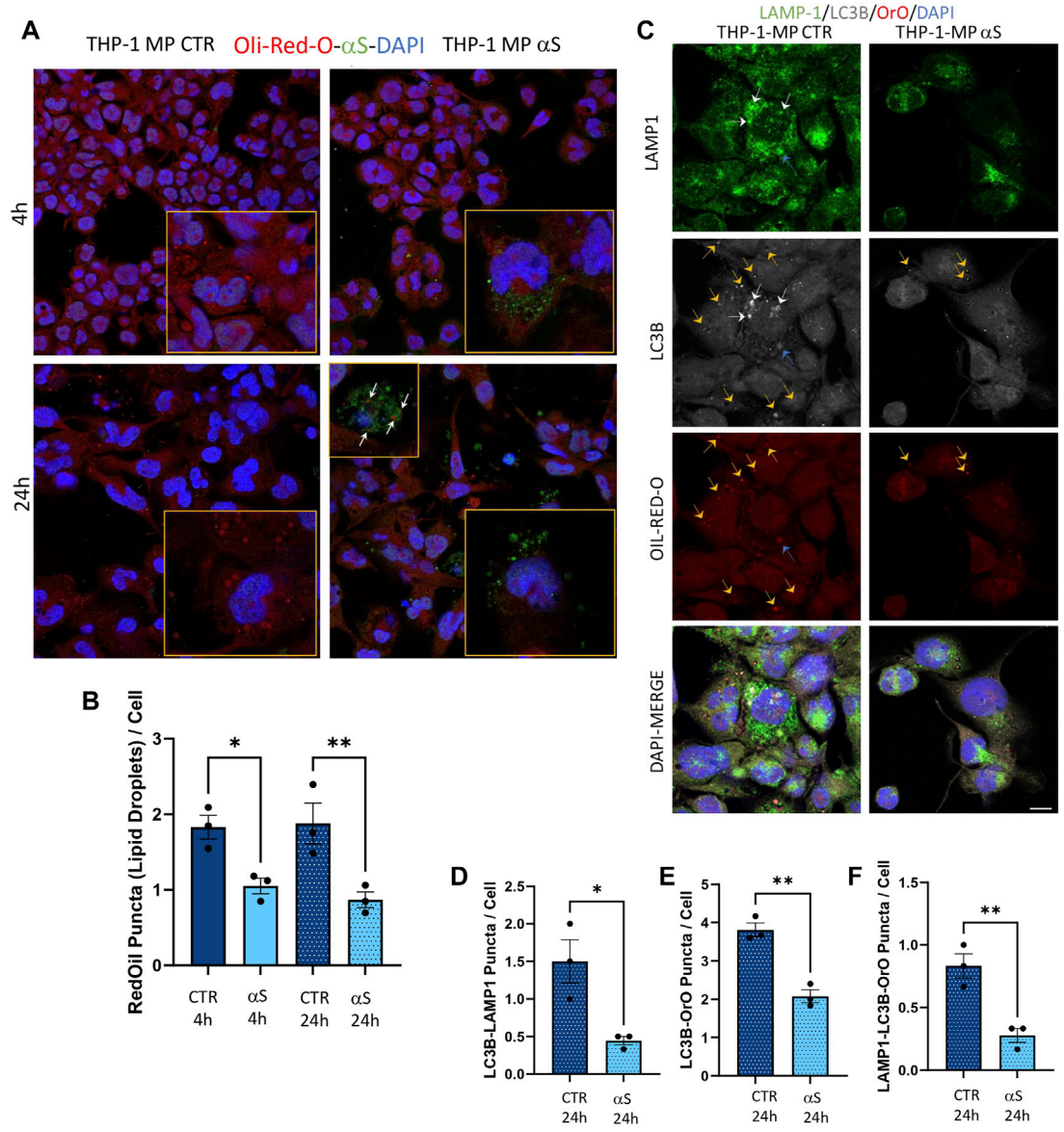

FIGURE 11
αS-induced autophagy perturbation in THP-1-derived macrophages is associated with altered lipid homeostasis. **(A)** Representative immunofluorescence of combined staining with Oil-Red-O (OrO) and αS in control (CTR) and αS-exposed THP-1-derived macrophages (4 h and 24 h). Arrows point at αS-OrO co-localization. Bars correspond to 10 μM. **(B)** Oil-Red-O puncta (lipid droplet) quantification in control (CTR) and αS-exposed THP-1-derived macrophages (4 h and 24 h). Values are shown as mean ± SEM. *$p < 0.05$, **$p < 0.01$. **(C)** Representative immunofluorescence of combined staining with Oil-Red-O, LC3B, LAMP1 in control (CTR) and αS-exposed THP-1-derived macrophages (MP, 24 h). White arrows point at LC3B-LAMP1 co-localization. Yellow arrows point at LC3B-Oil-red-O co-localization. Blue arrows point at LC3B-Oil-red-O-LAMP1 co-localization. Bars correspond to 10 μM. D-F. Quantification of LC3B-LAMP1 **(D)**, LC3B-Oil-red-O **(E)**, and LC3B-Oil-red-O-LAMP1 co-localizing puncta **(F)** in control (CTR) and αS-exposed THP-1-derived macrophages (MP, 24 h). Values are shown as mean ± SEM. *$p < 0.05$, **$p < 0.01$.

phagocytic-like protrusions of THP-1-derived macrophages, reminiscent of impaired efferocytosis (Figure 12D).

4 Discussion

In the present study we add to previous evidence that extracellular αS is effectively internalized by THP-1 monocytes, and THP-1-derived macrophages (Figures 1, 7) (Haenseler et al., 2017; Liu et al., 2022; Moriya et al., 2022), to show how this produces consistent, though different biological and functional effects in the two cell types. Indeed, different time-related intracellular αS dynamics were observed between the two cell types, which were in turn associated with diverse effects upon cell viability, inflammatory profile, and markers of the autophagy-lysosomal pathway. Firstly, in THP-1 monocytic cells, a decrease in intracellular αS amount was detected at 24 h compared with 4 h exposure. Coupled with the lack of toxic effects induced by excess αS (1 μM) at 4 h or 24 h, these data suggest that THP-1 cells well-tolerate αS overload, probably by diluting and/or degrading the

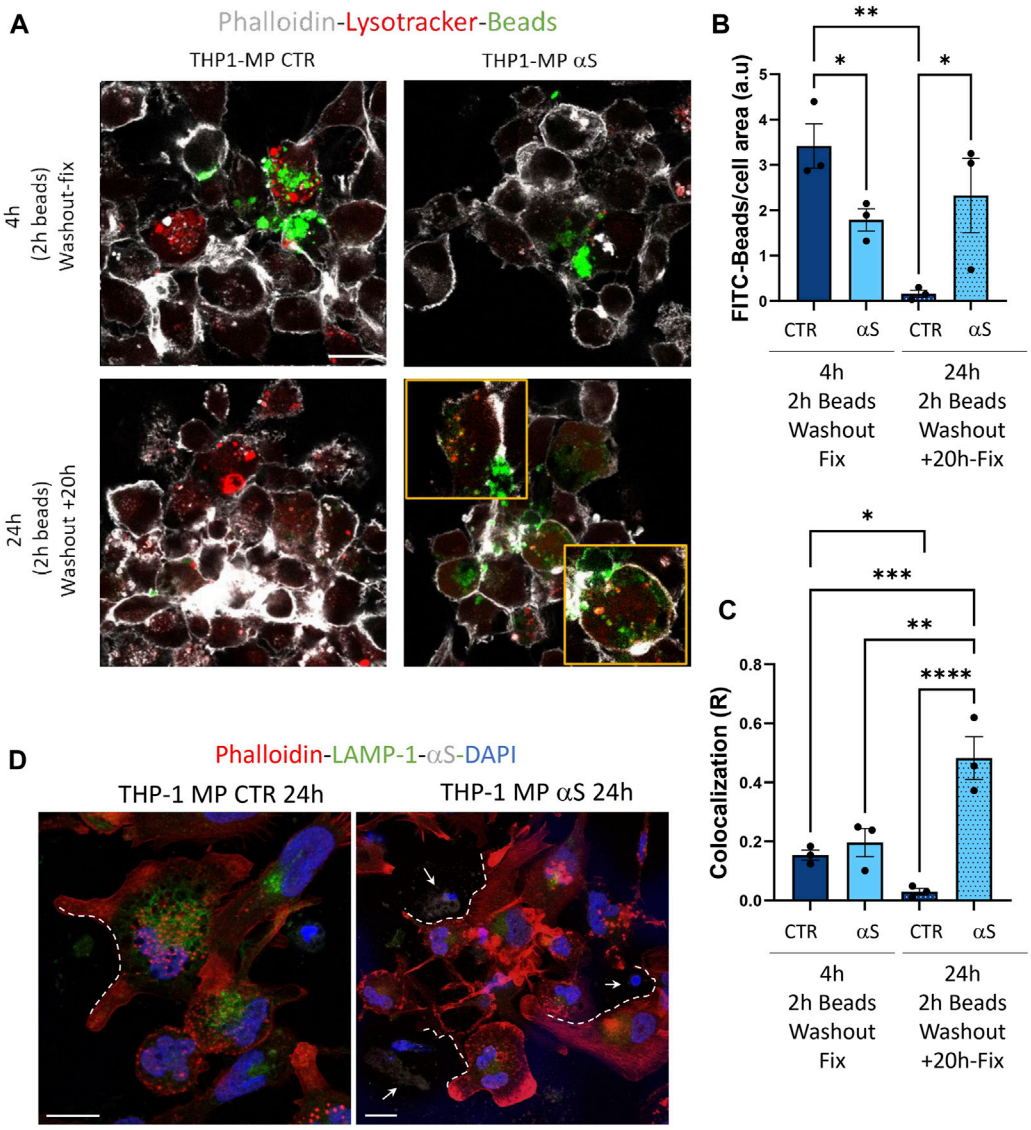

FIGURE 12
αS impairs phagocytosis and lysosomal processing of phagocytosed cargo in THP-1-derived macrophages. **(A)** Representative immunofluorescence of control (CTR) and αS-exposed THP-1-derived macrophages (4 h) immediately after 2 h incubation with FITC-latex beads (4 h, Washout fix) and following an additional 20 h culturing after beads washout (24 h, Washout + 20 h). Cells were stained with LysoTracker and Phalloidin. Bars correspond to 10 μM. **(B, C)**. Quantification of FITC-beads **(B)** and LysoTracker-FITC R colocalization **(C)** in control (CTR) and αS-exposed THP-1-derived macrophages in the two experimental conditions (4 h, Washout fix, and 24 h, Washout + 20 h). Values are shown as mean ± SEM. *$p < 0.05$, **$p < 0.01$, ***$p < 0.001$. ****$p < 0.0001$. **(D)** Combined immunofluorescence for αS, LAMP1, and F-actin (phalloidin) in control (CTR) and αS-exposed THP1-derived macrophages (MP, 24 h). White dashed lines indicate phagocytic-like protrusions, and arrows point at αS-filled dead cells. Bars correspond to 10 μM.

cargo of internalized protein (Figure 1A–D). Such an effect was not observed in THP-1-derived macrophages (Figure 7B), which were instead intoxicated by prolonged αS exposure (24 h, Figure 6, Supplementary Figure S3). These data are in line with the results of a recent study (Haenseler et al., 2017). Again, in both cell-types, excess αS induced an apparently similar pro-inflammatory profile by potentiating the gene transcription and secretion of various cytokines and chemokines. In detail, in THP-1 monocytes, upregulation of most secreted cytokines/chemokines occurred already after short αS exposure (4 h) (Figure 2). Indeed, the conditioned medium from αS-THP-1 monocytes potently attracted unstimulated cells (Figure 3). Confirming previous evidence, our data suggest that intracellular αS accumulation induces a pro-inflammatory extracellular milieu which serves as a chemoattractant for circulating monocytes (Klegeris et al., 2008; Allen Reish and Standaert, 2015; White et al., 2018; Grozdanov et al., 2019; Liu et al., 2022; Pellegrini et al., 2022; Su et al., 2022). Remarkably, such a pro-inflammatory scenario was not reproduced for all cytokines/chemokines at 24 h of αS exposure (Figure 2C). In detail, the concentrations of MCP-1/CCL2, MIP-1b/CCL4, and TNF-α were lower in 24 h-compared with 4 h-exposed αS. Similar different effects of 4 h vs. 24 h αS exposure were observed for the extra- and intracellular dynamics of the CCL2 receptor (CCR2) in THP-1 monocytes (Supplementary Figure S2). In fact, 4 h

αS exposure readily decreased cell surface CCR2 while increasing intracellular/total CCR2 ratio compared with CTR, suggesting rapid monocytic activation and receptor internalization which follows up ligand binding. However, no further differences were observed at prolonged αS exposure (24 h) vs. either 24 h CTR or 24 αS-exposed cells, suggesting that CCR2 recycling back to the plasma membrane takes place at such a time-point (Supplementary Figure S2). As CCR2 dynamics involve a delicate balance between agonist-dependent CCR2 sensitivity, and constitutive chemokine scavenging activity of the receptor (Volpe et al., 2012; Shroka et al., 2023), it is likely that prolonged αS exposure triggers a compensatory cellular mechanism which contributes to reducing CCR2 responsiveness and/or CCL2 levels. Unveiling the molecular bases of such a compensatory mechanism, as documented, for instance, for TLR signalling via a feedback mechanism operated by SOCS3 and SHP phosphatases (Kubo et al., 2003), goes beyond the aim of the present study; however it deserves to be addressed by future studies. In our hands, CCR2 dynamics appeared unrelated to CCL2-dependent chemotaxis, as αS-exposed THP-1 cells displayed unaltered, and reduced chemotaxis at 4 h and 24 h, respectively (Figure 3). Interestingly, αS-exposed cells also showed a time-dependent alteration in their spontaneous (FBS-driven) migration capacity (Figure 3), suggesting that intracellular αS levels influence the mobility of monocytic cells in response to growth factors beyond cytokines/chemokines, which deserves further investigation as well.

Contrary to what was observed for the monocytic THP-1 cells, αS exposure in THP-1-derived macrophages produced a time-related intracellular accumulation (4 h), and subsequent (24 h) secretion of inflammatory cytokines/chemokines (IL-1β, IL-4, IL-6, IL-10, IL-17, G-CSF, GM-CSF, IFN-γ, MIP-1b/CCL4, and TNF-α) (Figures 5, 6). Such an effect included a marked upregulation of cytokines which were not altered by αS in the THP-1 monocytic counterpart, namely G-CSF, GM-CSF, and IFN-γ. Remarkably, our results suggest that autophagy might represent a major cellular mechanism underpinning the different effects of αS within monocytes and macrophages. In fact, the effects of αS were associated with induction of autophagy-lysosomal markers in THP-1 monocytic cells (Figure 4) and their suppression in THP-1-derived macrophages (Figures 7–10). In detail, the stimulating effects of αS upon the autophagy/lysosomal markers were mostly evident at 24 h exposure, when increased LC3II/I ratio was parallelled by a decrease in p62 protein, and the mTOR activity index pS6/total S6 protein ratio, along with an increase in LAMP1 at both mRNA and protein levels (Figure 4). These findings suggest that THP-1 monocytes respond to excess αS by reducing mTOR activity, to promote upregulation of autophagolysosome markers, and degradation of autophagy substrates. This might explain why reduced levels of internalized αS were detected at 24 vs. 4 h exposure, and why THP-1 monocytes well tolerate αS overload. Although the cytoplasmic cleanup function of autophagy is generally anti-inflammatory in most cell types, autophagy upregulation has been implicated in monocytes' activation during the early stages of pathological events, and preventing the induction of autophagy in monocytes hinders their survival, differentiation and cytokine production (Zhang et al., 2012; Germic et al., 2019; Chen et al., 2023). Thus, autophagy activation following αS internalization in THP-1 monocytes may occur as a pro-survival/tolerance mechanism coping with stress-related inflammation, which in turn, is functionally associated with blunted CCL2 secretion and reduced chemotaxis. However, further studies employing pharmacological modulators or genetic manipulation of autophagy are needed to confirm such results, and to explore whether/how autophagy interferes with CCL2 release and CCR2 dynamics.

Notably, in THP-1-derived macrophages, 24 h αS significantly decreased LC3II/I ratio while increasing p62 protein, which went along with decreased LAMP1 levels detected already at 4 h of αS exposure both at protein and mRNA level (Figure 8). Supporting αS-induced lysosomal dysfunction, LysoTracker staining was also consistently decreased (Figure 9). However, the index of mTOR activity, namely the pS6/total S6 ratio was not significantly affected by αS exposure (Figure 8), suggesting that αS downregulates autophagy-lysosomal markers through an mTOR-independent mechanism. These results suggest that αS-loaded macrophages fail to overcome the detrimental effects of αS, with autophagy impairment potentially bridging reduced cell survival, and excess activation of pro-inflammatory pathways. Our data are in line with previous evidence that αS induces impairment of autophagy pathway and/or lysosome rupture in a variety of cell types, including microglia and macrophages (Freeman et al., 2013; Tu et al., 2021). Herein, we also detected significant αS-induced modulations of SQSTM1/p62, and LAMP1 mRNA expressions in both cell types, which suggests also a transcriptional, probably epigenetic effect on such targets. Importantly, in THP-1-derived macrophages, αS also produced an early downregulation of the autophagosome-lysosome fusion marker SNAP29 (Figure 8A), in line with both previous studies (Tang et al., 2021), and our data showing reduced co-localization of LC3 and LAMP-1 (Figure 11C, D). Again, in both THP-1-derived macrophages, and MDMs, we constantly detected a co-localization of αS and F-actin (Figures 9, 10), which deserves further investigations on the possible role of αS on cytoskeleton dynamics.

In our hands, the effects of αS in THP-1-derived macrophages were associated with reduced intracellular accumulation of LDs (Figure 11). This finding was unexpected at first glance, as excess LDs accumulation has been previously associated with both macrophage hyper-inflammation, and autophagy impairment (Rosas-Ballina et al., 2020). Reduced LDs might be due to increased lipophagy, impaired LD biogenesis, or excess lipid/cholesterol efflux (Robichaud et al., 2021). However, autophagy/lysosome-dependent lipolysis is unlikely to be our case, as αS itself reduced autophagolysosomal markers (LC3B and LAMP1, LysoTracker), as well as their co-localization with LDs (Figure 11). Again, mRNA expression of the cholesterol pathway genes CAV-1, CH25H, and LXR showed a downwards trend in 4 h αS-exposed vs. CTR THP-1-macrophages, with the cholesterol efflux/transporter gene ABCG1A being significantly decreased; contrariwise, most genes except for ABCG1A (namely, CAV-1, LXR, and XBP1) were significantly upregulated by 24 h αS exposure (Supplementary Figure S5). A consistent reduction of LDs was observed already at 4 h αS exposure and persisted at 24 h, which suggests that upregulation of specific cholesterol pathway genes detected at 24 h αS might represent a compensatory response to protein reductions. This mechanism seems inversely specular to what observed herein for pro-inflammatory genes and related encoded proteins. A plausible explanation to LDs impairment by αS stems from evidence showing that αS interacts with lipids on biological membranes to promote lipids extraction, or even lowering of cholesterol, an

essential constituent of LDs (Emanuele et al., 2016; Alza et al., 2019; Lazarevic et al., 2022). Studies on the biological role of LDs showed that these organelles act as sinks that sequester various oxidized/toxic lipids and proteins to limit their availability for participation in signaling pathways that may cause cell damage and inflammation (Jarc and Petan, 2020). Again, a recent stream of evidence converges in that LDs, through their flow from-and-to the endoplasmic reticulum, are an essential source for autophagosome biogenesis and normal progression of autophagy (Shpilka and Elazar, 2015). Thus, while altering the integrity of biological membranes, αS might also impinge on the biogenesis of LDs, which might in turn fuel cell toxicity, inflammation, and impaired autophagy in macrophages. A recent study (Haenseler et al., 2017) showed that αS depletes intracellular cholesterol by promoting excess cholesterol efflux in iPSC-derived macrophages. This was in turn associated with impaired phagocytic capacity, which is in line with our results (Figure 12) and those documented in peritoneal macrophages (Gardai et al., 2013). Though in our hands αS early decreased the mRNA expression of the cholesterol transporter ABCG1A, we did not directly verify if impaired LDs are due to altered cholesterol efflux. However, herein we document that, besides impairing phagocytosis in THP-1-derived macrophages, αS compromises lysosomal processing of phagocytosed cargo probably by altering their acidification (Figure 12). In summary, our data suggest that αS bridges impaired lipid metabolism, defective autophagy/lysosomal system, and excess inflammation to alter macrophage biology by producing a status of macrophage exhaustion reminiscent of hypophagia.

Finally, it is worth of mentioning that, although low, endogenous αS was detectable in THP-1 monocytes (Figure 1) and it was abolished in THP-1-derived macrophages (Figure 7A, C; Supplementary Figure S4) but not in M-CSF-differentiated MDMs (Figure 10), suggesting that αS downregulation occurs downstream of PMA treatment. This is probably related to the different biological roles of αS and PMA on shared molecular targets, such as protein kinase C (PKC), and PKC-dependent regulation of vesicle trafficking, as documented in various biological contexts (Kim et al., 2010; Huang et al., 2018).

In summary, our findings suggest that monocytes and macrophages respond differently to intracellular αS accumulation in terms of cell survival, metabolism, and functions, which deserves to be further investigated for its implications in the pathobiology of inflammation and synucleinopathies such as PD. However, we wish to point out that our study is not devoid of limitations. First, undifferentiated THP-1 monocytes are immortalized, actively dividing cells, and as such, they own a different inherent metabolic profile compared with their differentiated counterpart. Second, our findings are mostly descriptive and observational, as we did not employ specific pharmacologic/genetic modulators of autophagy/lysosomal pathway to confirm that the effects of αS are indeed specifically related to stimulation or suppression of autophagy. This is important since autophagy substrates, including p62 and αS itself, are also degraded by the proteasome (Limanaqi et al., 2020; 2021a). Further studies on primary cells, and the use of combined administration with various autophagy modulators will be seminal to further clarify the biological role of αS in monocytes and macrophages in health and disease, which is currently under investigation in our lab.

Data availability statement

The original contributions presented in the study are included in the article/Supplementary Material, further inquiries can be directed to the corresponding authors.

Ethics statement

The studies involving humans were approved by Approval for the use of human PBMCs was granted by the Ethics Committee of University of Milan (2022/No 14). The studies were conducted in accordance with the local legislation and institutional requirements. The participants provided their written informed consent to participate in this study.

Author contributions

FL: Conceptualization, Data curation, Formal Analysis, Investigation, Methodology, Software, Writing–original draft. SZ: Formal Analysis, Investigation, Methodology, Writing–review and editing. PO: Investigation, Writing–review and editing. VA: Investigation, Methodology, Writing–review and editing. CF: Formal Analysis, Methodology, Visualization, Writing–review and editing. IS: Investigation, Methodology, Visualization, Writing–review and editing. CV: Investigation, Writing–review and editing. MG: Writing–review and editing. SS: Investigation, Writing–review and editing. DT: Funding acquisition, Validation, Visualization, Writing–review and editing. MC: Funding acquisition, Validation, Visualization, Writing–review and editing. MB: Conceptualization, Funding acquisition, Investigation, Supervision, Validation, Visualization, Writing–review and editing.

Funding

The author(s) declare financial support was received for the research, authorship, and/or publication of this article. The present research was partially supported by Fondazione Romeo ed Enrica Invernizzi, Unione Europea–Next Generation EU PRIN 2022-PNRR-P2022ALFEK, and by the University of Milan through the APC initiative.

Acknowledgments

The authors acknowledge support from the University of Milan through the APC initiative.

Conflict of interest

The authors declare that the research was conducted in the absence of any commercial or financial relationships that could be construed as a potential conflict of interest.

The author(s) declared that they were an editorial board member of Frontiers, at the time of submission. This had no impact on the peer review process and the final decision.

Publisher's note

All claims expressed in this article are solely those of the authors and do not necessarily represent those of their affiliated organizations, or those of the publisher, the editors and the reviewers. Any product that may be evaluated in this article, or claim that may be made by its manufacturer, is not guaranteed or endorsed by the publisher.

Supplementary material

The Supplementary Material for this article can be found online at: https://www.frontiersin.org/articles/10.3389/fcell.2024.1421360/full#supplementary-material

References

Alam, M. M., Yang, D., Li, X.-Q., Liu, J., Back, T. C., Trivett, A., et al. (2022). Alpha synuclein, the culprit in Parkinson disease, is required for normal immune function. *Cell Rep.* 38, 110090. doi:10.1016/j.celrep.2021.110090

Allen Reish, H. E., and Standaert, D. G. (2015). Role of α-synuclein in inducing innate and adaptive immunity in Parkinson disease. *J. Parkinson's Dis.* 5, 1–19. doi:10.3233/JPD-140491

Alza, N. P., Iglesias González, P. A., Conde, M. A., Uranga, R. M., and Salvador, G. A. (2019). Lipids at the crossroad of α-synuclein function and dysfunction: biological and pathological implications. *Front. Cell. Neurosci.* 13, 175. doi:10.3389/fncel.2019.00175

Askanas, V., Engel, W. K., Alvarez, R. B., McFerrin, J., and Broccolini, A. (2000). Novel immunolocalization of alpha-synuclein in human muscle of inclusion-body myositis, regenerating and necrotic muscle fibers, and at neuromuscular junctions. *J. Neuropathol. Exp. Neurol.* 59, 592–598. doi:10.1093/jnen/59.7.592

Baltic, S., Perovic, M., Mladenovic, A., Raicevic, N., Ruzdijic, S., Rakic, L., et al. (2004). Alpha-synuclein is expressed in different tissues during human fetal development. *JMN* 22, 199–204. doi:10.1385/JMN:22:3:199

Barbour, R., Kling, K., Anderson, J. P., Banducci, K., Cole, T., Diep, L., et al. (2008). Red blood cells are the major source of alpha-synuclein in blood. *Neurodegener. Dis.* 5, 55–59. doi:10.1159/000112832

Brás, I. C., and Outeiro, T. F. (2021). Alpha-synuclein: mechanisms of release and pathology progression in synucleinopathies. *Cells* 10, 375. doi:10.3390/cells10020375

Burré, J., Sharma, M., and Südhof, T. C. (2018). Cell biology and pathophysiology of α-synuclein. *Cold Spring Harb. Perspect. Med.* 8, a024091. doi:10.1101/cshperspect.a024091

Chen, D., Zhang, C., Luo, J., Deng, H., Yang, J., Chen, S., et al. (2023). Activated autophagy of innate immune cells during the early stages of major trauma. *Front. Immunol.* 13, 1090358. doi:10.3389/fimmu.2022.1090358

Choi, I., Zhang, Y., Seegobin, S. P., Pruvost, M., Wang, Q., Purtell, K., et al. (2020). Microglia clear neuron-released α-synuclein via selective autophagy and prevent neurodegeneration. *Nat. Commun.* 11, 1386. doi:10.1038/s41467-020-15119-w

Colasanti, T., Vomero, M., Alessandri, C., Barbati, C., Maselli, A., Camperio, C., et al. (2014). Role of alpha-synuclein in autophagy modulation of primary human T lymphocytes. *Cell Death Dis.* 5, e1265. doi:10.1038/cddis.2014.211

Cui, C., Schoenfelt, K. Q., Becker, K. M., and Becker, L. (2021). Isolation of polymorphonuclear neutrophils and monocytes from a single sample of human peripheral blood. *Star. Protoc.* 2, 100845. doi:10.1016/j.xpro.2021.100845

Emanuele, M., Esposito, A., Camerini, S., Antonucci, F., Ferrara, S., Seghezza, S., et al. (2016). Exogenous alpha-synuclein alters pre- and post-synaptic activity by fragmenting lipid rafts. *EBioMedicine* 7, 191–204. doi:10.1016/j.ebiom.2016.03.038

Fellner, L., Irschick, R., Schanda, K., Reindl, M., Klimaschewski, L., Poewe, W., et al. (2013). Toll-like receptor 4 is required for α-synuclein dependent activation of microglia and astroglia. *Glia* 61, 349–360. doi:10.1002/glia.22437

Freeman, D., Cedillos, R., Choyke, S., Lukic, Z., McGuire, K., Marvin, S., et al. (2013). Alpha-synuclein induces lysosomal rupture and cathepsin dependent reactive oxygen species following endocytosis. *PLoS ONE* 8, e62143. doi:10.1371/journal.pone.0062143

Fujimura, N., Xu, B., Dalman, J., Deng, H., Aoyama, K., and Dalman, R. L. (2015). CCR2 inhibition sequesters multiple subsets of leukocytes in the bone marrow. *Sci. Rep.* 5, 11664. doi:10.1038/srep11664

Gardai, S. J., Mao, W., Schüle, B., Babcock, M., Schoebel, S., Lorenzana, C., et al. (2013). Elevated alpha-synuclein impairs innate immune cell function and provides a potential peripheral biomarker for Parkinson's disease. *PLoS ONE* 8, e71634. doi:10.1371/journal.pone.0071634

Germic, N., Frangez, Z., Yousefi, S., and Simon, H.-U. (2019). Regulation of the innate immune system by autophagy: monocytes, macrophages, dendritic cells and antigen presentation. *Cell Death Differ.* 26, 715–727. doi:10.1038/s41418-019-0297-6

Grozdanov, V., Bousset, L., Hoffmeister, M., Bliederhaeuser, C., Meier, C., Madiona, K., et al. (2019). Increased immune activation by pathologic α-synuclein in Parkinson's disease. *Ann. Neurology* 86, 593–606. doi:10.1002/ana.25557

Grozdanov, V., and Danzer, K. M. (2020). Intracellular alpha-synuclein and immune cell function. *Front. Cell Dev. Biol.* 8, 562692. doi:10.3389/fcell.2020.562692

Haenseler, W., Zambon, F., Lee, H., Vowles, J., Rinaldi, F., Duggal, G., et al. (2017). Excess α-synuclein compromises phagocytosis in iPSC-derived macrophages. *Sci. Rep.* 7, 9003. doi:10.1038/s41598-017-09362-3

Harms, A. S., Thome, A. D., Yan, Z., Schonhoff, A. M., Williams, G. P., Li, X., et al. (2018). Peripheral monocyte entry is required for alpha-Synuclein induced inflammation and Neurodegeneration in a model of Parkinson disease. *Exp. Neurol.* 300, 179–187. doi:10.1016/j.expneurol.2017.11.010

Hashimoto, M., Yoshimoto, M., Sisk, A., Hsu, L. J., Sundsmo, M., Kittel, A., et al. (1997). NACP, a synaptic protein involved in alzheimer's disease, is differentially regulated during megakaryocyte differentiation. *Biochem. Biophysical Res. Commun.* 237, 611–616. doi:10.1006/bbrc.1997.6978

Jarc, E., and Petan, T. (2020). A twist of FATe: lipid droplets and inflammatory lipid mediators. *Biochimie* 169, 69–87. doi:10.1016/j.biochi.2019.11.016

Jiménez-Jiménez, F. J., Alonso-Navarro, H., García-Martín, E., Santos-García, D., Martínez-Valbuena, I., and Agúndez, J. A. G. (2023). Alpha-synuclein in peripheral tissues as a possible marker for neurological diseases and other medical conditions. *Biomolecules* 13, 1263. doi:10.3390/biom13081263

Kim, C., Ho, D.-H., Suk, J.-E., You, S., Michael, S., Kang, J., et al. (2013). Neuron-released oligomeric α-synuclein is an endogenous agonist of TLR2 for paracrine activation of microglia. *Nat. Commun.* 4, 1562. doi:10.1038/ncomms2534

Klegeris, A., Pelech, S., Giasson, B. I., Maguire, J., Zhang, H., McGeer, E. G., et al. (2008). Alpha-synuclein activates stress signaling protein kinases in THP-1 cells and microglia. *Neurobiol. Aging* 29, 739–752. doi:10.1016/j.neurobiolaging.2006.11.013

Koopman, R., Schaart, G., and Hesselink, M. K. (2001). Optimisation of oil red O staining permits combination with immunofluorescence and automated quantification of lipids. *Histochem Cell Biol.* 116, 63–68. doi:10.1007/s004180100297

Kubo, M., Hanada, T., and Yoshimura, A. (2003). Suppressors of cytokine signaling and immunity. *Nat. Immunol.* 4, 1169–1176. doi:10.1038/ni1012

Lazarevic, V., Yang, Y., Paslawski, W., and Svenningsson, P. (2022). α-Synuclein induced cholesterol lowering increases tonic and reduces depolarization-evoked synaptic vesicle recycling and glutamate release. *npj Park. Dis.* 8, 71. doi:10.1038/s41531-022-00334-7

Limanaqi, F., Biagioni, F., Busceti, C. L., Ryskalin, L., Polzella, M., Frati, A., et al. (2019). Phytochemicals bridging autophagy induction and alpha-synuclein degradation in parkinsonism. *IJMS* 20, 3274. doi:10.3390/ijms20133274

Limanaqi, F., Biagioni, F., Gambardella, S., Familiari, P., Frati, A., and Fornai, F. (2020). Promiscuous roles of autophagy and proteasome in neurodegenerative proteinopathies. *IJMS* 21, 3028. doi:10.3390/ijms21083028

Limanaqi, F., Biagioni, F., Salvetti, A., Puglisi-Allegra, S., Lenzi, P., and Fornai, F. (2021a). Morphology, clearing efficacy, and mTOR dependency of the organelle autophagoproteasome. *Eur. J. Histochem* 65, 3220. doi:10.4081/ejh.2021.3220

Limanaqi, F., Busceti, C. L., Celli, R., Biagioni, F., and Fornai, F. (2021b). Autophagy as a gateway for the effects of methamphetamine: from neurotransmitter release and synaptic plasticity to psychiatric and neurodegenerative disorders. *Prog. Neurobiol.* 204, 102112. doi:10.1016/j.pneurobio.2021.102112

Limanaqi, F., Zecchini, S., Dino, B., Strizzi, S., Cappelletti, G., Utyro, O., et al. (2022). Dopamine reduces SARS-CoV-2 replication *in vitro* through downregulation of D2 receptors and upregulation of type-I interferons. *Cells* 11, 1691. doi:10.3390/cells11101691

Limanaqi, F., Zecchini, S., Saulle, I., Strizzi, S., Vanetti, C., Garziano, M., et al. (2024). Alpha-synuclein dynamics bridge Type-I Interferon response and SARS-CoV-2 replication in peripheral cells. *Biol. Res.* 57, 2. doi:10.1186/s40659-023-00482-x

Liu, Z., Chan, R. B., Cai, Z., Liu, X., Wu, Y., Yu, Z., et al. (2022). α-Synuclein-containing erythrocytic extracellular vesicles: essential contributors to hyperactivation of monocytes in Parkinson's disease. *J. Neuroinflammation* 19, 53. doi:10.1186/s12974-022-02413-1

Macanas-Pirard, P., Quezada, T., Navarrete, L., Broekhuizen, R., Leisewitz, A., Nervi, B., et al. (2017). The CCL2/CCR2 Axis affects transmigration and proliferation but not resistance to chemotherapy of acute myeloid leukemia cells. *PLoS ONE* 12, e0168888. doi:10.1371/journal.pone.0168888

Martinez-Vicente, M., Talloczy, Z., Kaushik, S., Massey, A. C., Mazzulli, J., Mosharov, E. V., et al. (2008). Dopamine-modified α-synuclein blocks chaperone-mediated autophagy. *J. Clin. Invest.*, JCI32806. doi:10.1172/JCI32806

Moriya, S., Hanazono, M., Fukuhara, T., Iwase, K., Hattori, N., and Takiguchi, M. (2022). A53T mutant α-synuclein fibrils formed in macrophage are spread to neurons. *Cell. Mol. Life Sci.* 79, 234. doi:10.1007/s00018-022-04263-9

Mysore, V., Cullere, X., Mears, J., Rosetti, F., Okubo, K., Liew, P. X., et al. (2021). FcγR engagement reprograms neutrophils into antigen cross-presenting cells that elicit acquired anti-tumor immunity. *Nat. Commun.* 12, 4791. doi:10.1038/s41467-021-24591-x

Nakai, M., Fujita, M., Waragai, M., Sugama, S., Wei, J., Akatsu, H., et al. (2007). Expression of alpha-synuclein, a presynaptic protein implicated in Parkinson's disease, in erythropoietic lineage. *Biochem. Biophysical Res. Commun.* 358, 104–110. doi:10.1016/j.bbrc.2007.04.108

Natale, G., Limanaqi, F., Busceti, C. L., Mastroiacovo, F., Nicoletti, F., Puglisi-Allegra, S., et al. (2021). Glymphatic system as a gateway to connect neurodegeneration from periphery to CNS. *Front. Neurosci.* 15, 639140. doi:10.3389/fnins.2021.639140

Park, E. K., Jung, H. S., Yang, H. I., Yoo, M. C., Kim, C., and Kim, K. S. (2007). Optimized THP-1 differentiation is required for the detection of responses to weak stimuli. *Inflamm. Res.* 56, 45–50. doi:10.1007/s00011-007-6115-5

Pei, Y., and Maitta, R. W. (2019). Alpha synuclein in hematopoiesis and immunity. *Heliyon* 5, e02590. doi:10.1016/j.heliyon.2019.e02590

Pellegrini, C., D'Antongiovanni, V., Miraglia, F., Rota, L., Benvenuti, L., Di Salvo, C., et al. (2022). Enteric α-synuclein impairs intestinal epithelial barrier through caspase-1-inflammasome signaling in Parkinson's disease before brain pathology. *npj Park. Dis.* 8, 9. doi:10.1038/s41531-021-00263-x

Robichaud, S., Fairman, G., Vijithakumar, V., Mak, E., Cook, D. P., Pelletier, A. R., et al. (2021). Identification of novel lipid droplet factors that regulate lipophagy and cholesterol efflux in macrophage foam cells. *Autophagy* 17, 3671–3689. doi:10.1080/15548627.2021.1886839

Rosas-Ballina, M., Guan, X. L., Schmidt, A., and Bumann, D. (2020). Classical activation of macrophages leads to lipid droplet formation without *de novo* fatty acid synthesis. *Front. Immunol.* 11, 131. doi:10.3389/fimmu.2020.00131

Ryskalin, L., Busceti, C. L., Limanaqi, F., Biagioni, F., Gambardella, S., and Fornai, F. (2018). A focus on the beneficial effects of alpha synuclein and a Re-appraisal of synucleinopathies. *CPPS* 19, 598–611. doi:10.2174/1389203718666171117110028

Saulle, I., Marventano, I., Saresella, M., Vanetti, C., Garziano, M., Fenizia, C., et al. (2021). ERAPs reduce *in vitro* HIV infection by activating innate immune response. *J. Immunol.* 206, 1609–1617. doi:10.4049/jimmunol.2000991

Schaeffer, E., Kluge, A., Böttner, M., Zunke, F., Cossais, F., Berg, D., et al. (2020). Alpha synuclein connects the gut-brain Axis in Parkinson's disease patients – a view on clinical aspects, cellular pathology and analytical methodology. *Front. Cell Dev. Biol.* 8, 573696. doi:10.3389/fcell.2020.573696

Shpilka, T., and Elazar, Z. (2015). Lipid droplets regulate autophagosome biogenesis. *Autophagy* 11, 2130–2131. doi:10.1080/15548627.2015.1093719

Shroka, T. M., Kufareva, I., Salanga, C. L., and Handel, T. M. (2023). The dual-function chemokine receptor CCR2 drives migration and chemokine scavenging through distinct mechanisms. *Sci. Signal.* 16, eabo4314. doi:10.1126/scisignal.abo4314

Stojkovska, I., and Mazzulli, J. R. (2021). Detection of pathological alpha-synuclein aggregates in human iPSC-derived neurons and tissue. *Star. Protoc.* 2, 100372. doi:10.1016/j.xpro.2021.100372

Su, Y., Shi, C., Wang, T., Liu, C., Yang, J., Zhang, S., et al. (2022). Dysregulation of peripheral monocytes and pro-inflammation of alpha-synuclein in Parkinson's disease. *J. Neurol.* 269, 6386–6394. doi:10.1007/s00415-022-11258-w

Tang, Q., Gao, P., Arzberger, T., Höllerhage, M., Herms, J., Höglinger, G., et al. (2021). Alpha-Synuclein defects autophagy by impairing SNAP29-mediated autophagosome-lysosome fusion. *Cell Death Dis.* 12, 854. doi:10.1038/s41419-021-04138-0

Tian, C., Liu, G., Gao, L., Soltys, D., Pan, C., Stewart, T., et al. (2019). Erythrocytic α-Synuclein as a potential biomarker for Parkinson's disease. *Transl. Neurodegener.* 8, 15. doi:10.1186/s40035-019-0155-y

Toni, L. S., Garcia, A. M., Jeffrey, D. A., Jiang, X., Stauffer, B. L., Miyamoto, S. D., et al. (2018). Optimization of phenol-chloroform RNA extraction. *MethodsX* 5, 599–608. doi:10.1016/j.mex.2018.05.011

Tu, H., Yuan, B., Hou, X., Zhang, X., Pei, C., Ma, Y., et al. (2021). α-synuclein suppresses microglial autophagy and promotes neurodegeneration in a mouse model of Parkinson's disease. *Aging Cell* 20, e13522. doi:10.1111/acel.13522

Van Meerloo, J., Kaspers, G. J. L., and Cloos, J. (2011). "Cell sensitivity assays: the MTT assay," in *Cancer cell culture*. Editor I. A. Cree (Totowa, NJ: Humana Press), 237–245. doi:10.1007/978-1-61779-080-5_20

Venezia, S., Kaufmann, W. A., Wenning, G. K., and Stefanova, N. (2021). Toll-like receptor 4 deficiency facilitates α-synuclein propagation and neurodegeneration in a mouse model of prodromal Parkinson's disease. *Park. Relat. Disord.* 91, 59–65. doi:10.1016/j.parkreldis.2021.09.007

Volpe, S., Cameroni, E., Moepps, B., Thelen, S., Apuzzo, T., and Thelen, M. (2012). CCR2 acts as scavenger for CCL2 during monocyte chemotaxis. *PLoS ONE* 7, e37208. doi:10.1371/journal.pone.0037208

White, A. J., Wijeyekoon, R. S., Scott, K. M., Gunawardana, N. P., Hayat, S., Solim, I. H., et al. (2018). The peripheral inflammatory response to alpha-synuclein and endotoxin in Parkinson's disease. *Front. Neurol.* 9, 946. doi:10.3389/fneur.2018.00946

Zecchini, S., Giovarelli, M., Perrotta, C., Morisi, F., Touvier, T., Di Renzo, I., et al. (2019). Autophagy controls neonatal myogenesis by regulating the GH-IGF1 system through a NFE2L2-and DDIT3-mediated mechanism. *Autophagy* 15, 58–77. doi:10.1080/15548627.2018.1507439

Zhang, Y., Morgan, M. J., Chen, K., Choksi, S., and Liu, Z. (2012). Induction of autophagy is essential for monocyte-macrophage differentiation. *Blood* 119, 2895–2905. doi:10.1182/blood-2011-08-372383

frontiers | Frontiers in Cell and Developmental Biology

TYPE Methods
PUBLISHED 11 September 2024
DOI 10.3389/fcell.2024.1460061

Check for updates

OPEN ACCESS

EDITED BY
Aurore Claude-Taupin,
INSERM U1151 Institut Necker Enfants Malades, France

REVIEWED BY
Thomas Anthony Ryan,
Syganture Discovery Ltd., United Kingdom
Shirisha Nagotu,
Indian Institute of Technology Guwahati, India

*CORRESPONDENCE
Patricia Boya,
patricia.boya@unifr.ch

RECEIVED 05 July 2024
ACCEPTED 02 September 2024
PUBLISHED 11 September 2024

CITATION
Jiménez-Loygorri JI, Jiménez-García C, Viedma-Poyatos Á and Boya P (2024) Fast and quantitative mitophagy assessment by flow cytometry using the *mito*-QC reporter. *Front. Cell Dev. Biol.* 12:1460061. doi: 10.3389/fcell.2024.1460061

COPYRIGHT
© 2024 Jiménez-Loygorri, Jiménez-García, Viedma-Poyatos and Boya. This is an open-access article distributed under the terms of the Creative Commons Attribution License (CC BY). The use, distribution or reproduction in other forums is permitted, provided the original author(s) and the copyright owner(s) are credited and that the original publication in this journal is cited, in accordance with accepted academic practice. No use, distribution or reproduction is permitted which does not comply with these terms.

Fast and quantitative mitophagy assessment by flow cytometry using the *mito*-QC reporter

Juan Ignacio Jiménez-Loygorri[1], Carlos Jiménez-García[2], Álvaro Viedma-Poyatos[1] and Patricia Boya[1,2]*

[1]Department of Cellular and Molecular Biology, Centro de Investigaciones Biológicas Margarita Salas, CSIC, Madrid, Spain, [2]Department of Neuroscience and Movement Science, Faculty of Science and Medicine, University of Fribourg, Fribourg, Switzerland

Mitochondrial quality control is finely tuned by mitophagy, the selective degradation of mitochondria through autophagy, and mitochondrial biogenesis. Removal of damaged mitochondria is essential to preserve cellular bioenergetics and prevent detrimental events such as sustained mitoROS production, pro-apoptotic cytochrome c release or mtDNA leakage. The array of tools available to study mitophagy is very limited but in constant development. Almost a decade ago, we developed a method to assess mitophagy flux using MitoTracker Deep Red in combination with lysosomal inhibitors. Now, using the novel tandem-fluorescence reporter *mito*-QC (mCherry-GFP-FIS1$^{101–152}$) that allows to differentiate between healthy mitochondria (mCherry^{+}GFP^{+}) and mitolysosomes (mCherry^{+}GFP^{-}), we have developed a robust and quantitative method to assess mitophagy by flow cytometry. This approach has been validated in ARPE-19 cells using PINK1/Parkin-dependent (CCCP) and PINK1/Parkin-independent (DFP) positive controls and complementary techniques. Furthermore, we show that the *mito*-QC reporter can be multiplexed, especially if using spectral flow cytometry, to simultaneously study other cellular parameters such as viability or ROS production. Using this technique, we evaluated and characterized two prospective mitophagy inducers and further dissected their mechanism of action. Finally, using *mito*-QC reporter mice, we developed a protocol to measure mitophagy levels in the retina *ex vivo*. This novel methodology will propel mitophagy research forward and accelerate the discovery of novel mitophagy modulators.

KEYWORDS

FACS, mitochondria, autophagy, retina, SI, Fisetin, phenanthroline

Introduction

Mitophagy is a subtype of selective autophagy that leads to the degradation and recycling of whole mitochondria. It can be further subdivided in two main pathways: PINK1/Parkin-dependent or receptor-mediated mitophagy. PINK1/Parkin-dependent mitophagy is traditionally triggered by loss of mitochondrial membrane potential

Abbreviations: ΔΨm, Mitochondrial membrane potential; AMD, Age-related macular degeneration; BNIP3, BCL2/adenovirus E1B 19 kDa protein-interacting protein 3; BNIP3L/NIX, BCL2/adenovirus E1B 19 kDa protein-interacting protein 3-like; CCCP, Carbonyl cyanide m-chlorophenyl hydrazone; DFP, Deferiprone; FIS1, Mitochondrial fission 1 protein; GFP, Green fluorescent protein; HIF-1α, Hypoxia-inducible factor 1-alpha; MFI, Mean fluorescence intensity; PINK1, PTEN-induced kinase 1; OMM, Outer mitochondrial membrane; ROS, Reactive oxygen species; RPE, Retinal pigment epithelium; SI, Sodium iodate.

(ΔΨm) (Narendra et al., 2010). The PINK1 kinase is recruited to the outer mitochondrial membrane (OMM) where, in homeostatic conditions, is translocated through the intermembrane space, processed by the peptidase MPP and sent back to the cytosol for degradation via proteasome (Hasson et al., 2013). Mitochondrial depolarization (loss of ΔΨm) uncouples PINK1 translocation, and it accumulates in the OMM. PINK1 then phosphorylates basally-ubiquitinated OMM proteins at Ubiquitin^{Ser65} and the analogous residue of Parkin, an E3 ligase that will further poly-ubiquitinate OMM proteins (Narendra et al., 2008). These events lead to a positive feedback loop that amplifies the targeting signals for mitophagy. Adaptor proteins with a ubiquitin-binding domain, such as CALCOCO2/NDP52, OPTN or SQSTM1/p62 (Lazarou et al., 2015), will recognize ubiquitinated proteins and recruit autophagy initiation machinery (Nguyen et al., 2016).

Receptor-mediated mitophagy is ubiquitin-independent and can also be triggered by hypoxia or developmental cues (Esteban-Martinez et al., 2017a). It is mediated by adaptor proteins that contain both a mitochondria-targeting sequence (MTS) and a LC3-interacting domain (LIR), namely BNIP3, BNIP3L/NIX, FUNDC1 or FKBP8 (Teresak et al., 2022). In recent years, it has been identified that other mechanisms such as cardiolipin externalization or changes in OMM lipid composition can also lead to direct recognition by LC3 (Teresak et al., 2022). Nonetheless, all pathways lead to mitochondria being engulfed into an autophagosome, which will later fuse with a lysosome to ensure degradation of its cargo.

Our lab has previously described a method to assess mitophagic degradation by flow cytometry using MitoTracker DeepRed (Mauro-Lizcano et al., 2015; Esteban-Martinez et al., 2017b). Even though it has been widely used and enables analysis of mitophagy flux, it still has some limitations. For example, a simultaneous induction of mitochondrial biogenesis might mask small but robust increases on mitophagy and use of lysosomal inhibitors is required (Esteban-Martinez et al., 2017b). The development of tandem fluorescent reporters has changed the way we analyze autophagy, as it allows us to monitor effective degradation inside acidic lysosomes using a combination of pH-sensitive (GFP, Keima) and pH-insensitive (mCherry) fluorescent proteins fused to a targeting sequence. Different mitophagy reporters such as MitoTimer, mtKeima or *mito*-QC have been developed, the latter also allowing fixation for downstream immunocytochemistry analysis (Jiménez-Loygorri et al., 2023; Jimenez-Loygorri and Boya, 2024).

The *mito*-QC reporter consists of a fusion protein containing mCherry-GFP-FIS1$^{101-152}$, that targets the OMM. In steady-state conditions, both mCherry and GFP fluoresce in the membrane of healthy mitochondria (Figure 1A) (McWilliams et al., 2018). Upon delivery of mitochondria to the lysosomes for degradation, acidic pH quenches GFP and mitolysosomes can be identified as mCherry-only puncta (Figure 1A). We have previously described the use of *mito*-QC to assess mitophagy levels by confocal immunofluorescence (Rosignol et al., 2020; Figueiredo-Pereira et al., 2023; Jimenez-Loygorri and Boya, 2024), however this procedure is time- and resource-consuming. In the present manuscript, we describe a medium-throughput protocol to assess simultaneously mitophagy and mitochondrial mass by flow cytometry *in vitro* and in *ex vivo* retinal cultures and highlight the possibility of performing more complex assays and targeted screens by multiplexing with additional fluorescent probes.

Materials and methods

Herein, we present an optimized traditional and spectral flow cytometry protocol that provides sensitive simultaneous readouts of mitophagy and mitochondrial mass using tandem fluorescent reporters like *mito*-QC. This assay can be performed *in vitro* or using organotypic *ex vivo* culture and may be multiplexed to analyze other parameters such as reactive oxygen species (ROS) production or viability.

Cell lines

ARPE-19 cells (Dunn et al., 1996) stably expressing the *mito*-QC reporter were generated by retroviral transfection in the laboratory of Dr. Ian G. Ganley as previously described (Montava-Garriga et al., 2020) and maintained in DMEM: F-12 medium (Gibco, 41966029, 21765037) supplemented with 15% FBS (Merck, F7524), 2 mM L-glutamine (Gibco, 25030081), and 1 U/mL Pen/Strep antibiotics (Gibco, 15140122) in a humidified incubator at 37°C, 5% CO_2. To ensure stable expression of the reporter, selection was performed by adding 800 ug/mL Hygromycin B (Gibco, 10453982) after every passage.

Seeding and treatments

For flow cytometry or immunofluorescence experiments, 5-6 × 10^4 cells per well were seeded in a 24-well plate the day before the experiment and left to adhere overnight. For western blot analysis, 3 × 10^5 cells were seeded in a 6-well plate and left to adhere overnight. Treatments were added for the indicated timepoints at the following concentrations: 25 μM CCCP (Carbonyl cyanide m-chlorophenyl hydrazone; 25 mM stock in DMSO; Merck, C2759), 1 mM DFP (Deferiprone; 125 mM stock in sterile H_2O; Merck, 379409), 10 μM Fisetin (10 mM stock in EtOH; Merck, F4043), 50 μM Phenanthroline (50 mM stock in DMSO; Merck, 131377), 20 mM SI (Sodium iodate; 333 mM fresh stock in DMEM; Merck, S4007), 750 μM H_2O_2 (30% stock in DMEM; Fluka, 95300).

Cell sample preparation

1. Medium containing floating dead cells was collected in a standard plastic flow cytometry tube.
2. Cells were washed with 500 μL of sterile PBS 1X to remove FBS residue and PBS was also collected.
3. 150 μL of 0.05% Trypsin (Gibco, 11500636) was added per well and cells were incubated for 5′ in an incubator at 37°C and 5% CO_2. Verify that cells have detached from the bottom of the well using a brightfield microscope.
4. 500 μL of FBS-containing complete medium were added to each well to inactivate Trypsin.

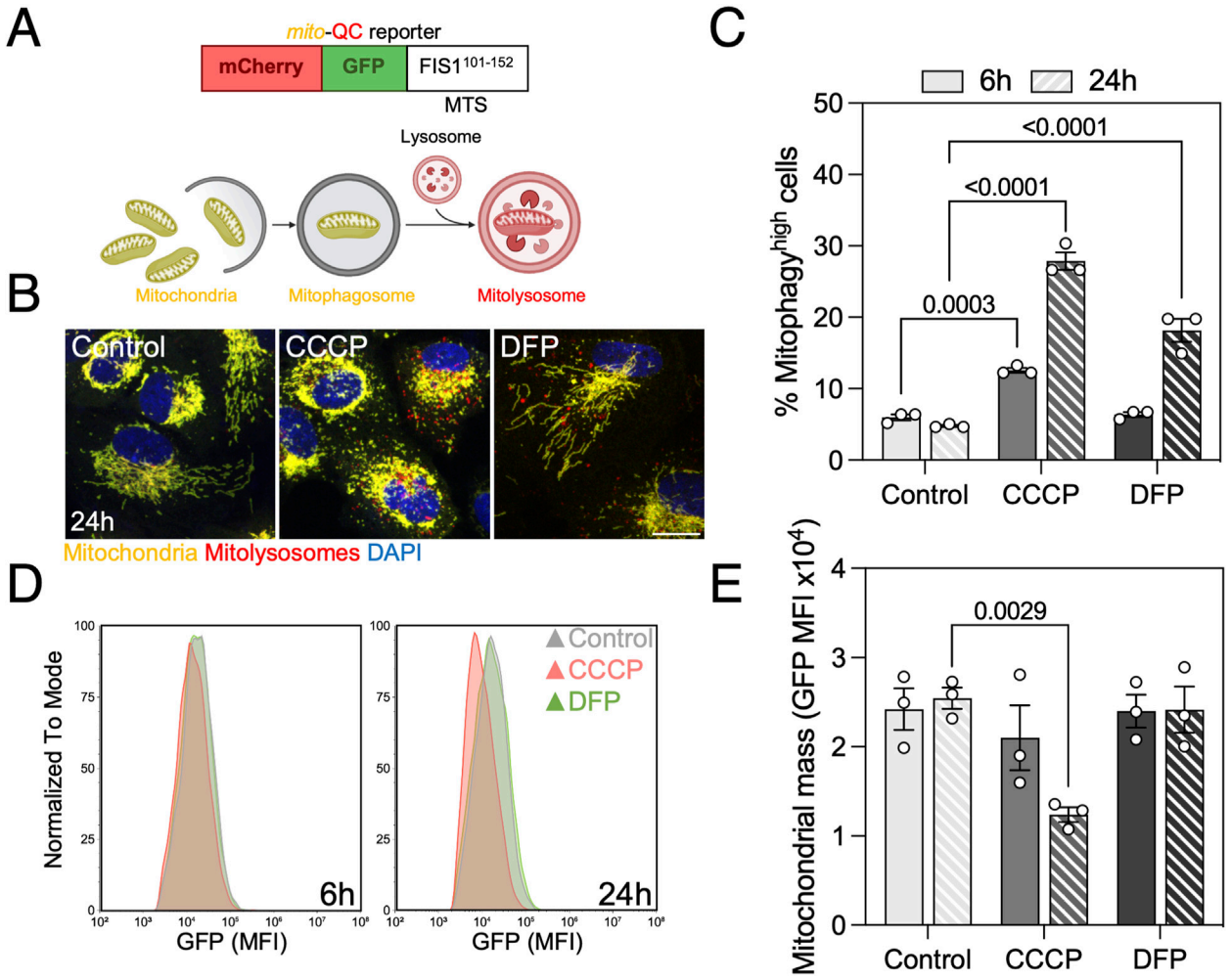

FIGURE 1
Mitophagy assessment in ARPE-19 cells by traditional flow cytometry using the *mito*-QC reporter. **(A)** Basis of the *mito*-QC reporter, whereby mitochondria are tagged with the chimeric protein mCherry-GFP-FIS1$_{101–152}$. Upon mitophagy induction, mitochondria will be delivered to the lysosome where acidic pH will quench GFP and mitolysosomes will be identified as mCherry-only puncta. **(B)** ARPE-19 cells stably expressing the *mito*-QC reporter treated with 25 μM CCCP or 1 mM DFP for the indicated timepoints. **(C)** Quantification of % of mitophagy^{high} population as defined in Supplementary Figure S1. **(D)** Representative histogram of FITC-GFP mean fluorescence intensity (MFI), equivalent to mitochondrial mass, in cells from **(C)**. **(E)** Quantification of mitochondrial mass as shown in **(D)**. Scale bar, 15 μm. All data are expressed as the mean ± s.e.m. Dots represent independent experiments. *P* values were calculated using two-way ANOVA with Dunnett's *post hoc* test. Diagrams were created using BioRender.

5. Cells were collected in the flow cytometry tube and pelleted by centrifugation at 1,000 *g* for 5′.
6. Supernatant was discarded and 100–200 μL of complete medium was added to each tube. For selected experiments, cells were incubated with 1 nM MitoTracker Deep Red (Invitrogen, M22426), 1 μM MitoSOX Red (Invitrogen, M36008), for 30′ min or 1:2,000 ViaDye Red (Cytek, R7-60008), CellROX Deep Red 5 μM (Invitrogen, C10433) for 15′ at 37°C and 5% CO_2.
7. Samples were resuspended by gentle shaking and, if necessary, 50 μL of 5X DAPI (4′,6-diamidino-2-phenylindole; Merck, D9542) were added to each tube, reaching a final concentration of 1 μg/mL, for viable population selection. If required, e.g. working with UV-autofluorescent compounds, there are far red-emitting nuclear dyes available such as TO-PRO-3 (Thermo Fisher, T3605).
8. Tubes were kept in ice until flow cytometry analysis.

Retina dissection and *ex vivo* culture

C57BL/6J mice expressing the *mito*-QC reporter ubiquitously were generated and provided by Dr. Ian G. Ganley (McWilliams et al., 2018). Organotypic *ex vivo* retina culture was performed as previously described (Gomez-Sintes et al., 2017). Briefly, mice were sacrificed by cervical dislocation and both eyes were enucleated using curved forceps. Using Vannas scissors, a circular incision was made along the limbus and both cornea and lens were removed using fine forceps. The optic nerve was sectioned and the neuroretina was isolated by gently pulling from the RPE/choroid-containing eyecup. Retinas were cultured in flotation in a 24-well plate and maintained in DMEM supplemented with 1 μM Insulin (Merck, I2643), 2 mM L-Glutamine, 100 U/mL penicillin and 0.1 mg/mL streptomycin. Treatments were added for the indicated timepoints at the following concentrations: 25 μM

CCCP (25 mM stock in DMSO), 1 mM DFP (125 mM stock in sterile H_2O).

Ex vivo retina sample preparation

1. Similarly, medium containing floating dead cells was collected in a standard plastic flow cytometry tube.
2. Whole retinas were washed with 500 µL of sterile PBS 1X to remove medium residue and PBS was also collected.
3. 300 µL of 5 mg/mL Trypsin in HBSS (Gibco, 14170-088) was added per well and retinas were incubated for 5–10′ in an incubator at 37°C and 5% CO_2.
4. 900 µL of 10% FBS in HBSS were added to each well to inactivate Trypsin and retinas were dissociated by gentle pipetting using a p1000 tip (10–20 times).
5. Single cell suspension was collected in the flow cytometry tube and pelleted by centrifugation at 1,000 *g* for 5′.
6. Supernatant was discarded and 200 µL of complete medium was added to each tube.
7. Samples were resuspended by gentle shaking and 50 µL of 5X DAPI was added to each tube, reaching a final concentration of 1 µg/mL, for viable population selection.
8. Tubes were kept in ice until flow cytometry analysis.

Conventional flow cytometer setup and gating

Using a CytoFLEX S V4-B2-Y4-R3 Flow Cytometer (Beckman Coulter), at least 10,000 events were acquired using mCherry-PI (610/20), FITC-GFP (525/40), PB450-DAPI (450/45) and APC (660/10) emission filters. Gating of the viable cell population was performed as shown in Supplementary Figures S1, S3. Control cells were used to set the threshold of mitophagy^{high} population defined by a mCherry/GFP ratio of ~5%. The percentage of DAPI$^-$ cells, mitophagy^{high} cells, FITC-GFP MFI and APC MFI were exported for downstream analysis performed using CytExpert v1.2 (Beckman Coulter).

Spectral flow cytometer setup and gating

Using a Cytek Aurora equipped with five lasers (Cytek Biosciences), at least 10,000 events were acquired. Similarly, control cells were used to set the threshold of mitophagy^{high} population defined by a mCherry/GFP ratio of ~5%. Wild-type, control cells and unstained cells were used to set the gates and spectra for every probe (Supplementary Figure S5). Analysis was performed using SpectroFlo (Cytek Biosciences) for raw data unmixing and downstream analysis was performed using Flowjo v10.10 (BD Biosciences).

Immunofluorescence

ARPE-19 were seeded on glass coverslips, treated as indicated and fixed using 3.7% PFA containing 175 mM HEPES (Gibco, 15630) at pH 7.0 for 15 min. Cells were incubated with 1 µg/mL DAPI in PBS pH 7.0 for 15 min, washed 3 times with PBS pH 7.0 and mounted using or ProLong Diamond (Thermo Fisher, P36961). Images were captured with a 0.5-µm z-step using a Leica TCS SP8 confocal microscope equipped with a × 63 immersion objective.

Protein isolation, quantification and western blot

Adherent cells were scraped in cold RIPA lysis buffer (Merck, R0278) supplemented with protease and phosphatase inhibitors. Protein concentration was determined using the Pierce BCA Protein Assay (Thermo Fisher, 23225) following the manufacturer's instructions. Total protein extract (15–30 µg) was supplemented with 4X Laemmli loading buffer (Bio-Rad, 1610747) and resolved using Any kD Criterion TGX Precast Stain-free gels (Bio-Rad, 5678124). Proteins were transferred to 0.2 µm PVDF membranes using a TransBlot Turbo Transfer System (Bio-Rad) and total protein was quantified using Ponceau S staining (Merck, 78376). Membranes were blocked with 5% non-fat milk in TBS-T (0.5% Tween-20 (Bio-Rad, 1706531) in PBS) for 1 h. Membranes were then incubated overnight at 4°C in primary antibodies diluted 1:1,000 (Supplementary Table S1) in 5% BSA in TBS, and subsequently for 1 h at room temperature in secondary antibodies diluted 1:2,000 in TBS-T (Supplementary Table S1). Membranes were developed using Pierce ECL Western Blotting substrate (Thermo Fisher, 32106) or Amersham ECL Prime (Cytiva, 10308449) and x-ray film (AGFA) using a CURIX 60 Processor (AGFA).

Statistical analysis

Data shown in figures represents the mean ± s.e.m. of at least three independent experiments with biological replicates. Differences between groups were assessed using Student's *t*-test (two groups), one-way or two-way ANOVA (more than two groups) with appropriate *post hoc* tests. A *P*-value under 0.05 was considered statistically significant and exact, corrected *P*-values are shown. Raw data management was done in Microsoft Excel and statistical analyses were performed using GraphPad Prism 10.0 software.

Results

Mito-QC reporter provides sensitive detection of mitophagy and mitochondrial mass *in vitro* and *ex vivo*

The ARPE-19 cell line originated from the retinal pigment epithelium of a healthy adult donor, and underwent spontaneous immortalization (Dunn et al., 1996). ARPE-19 cells stably expressing the *mito*-QC reporter were used for all experiments (Montava-Garriga et al., 2020) and mitophagy levels were defined as the population of cells with an increased mCherry/GFP ratio (Supplementary Figure S1).

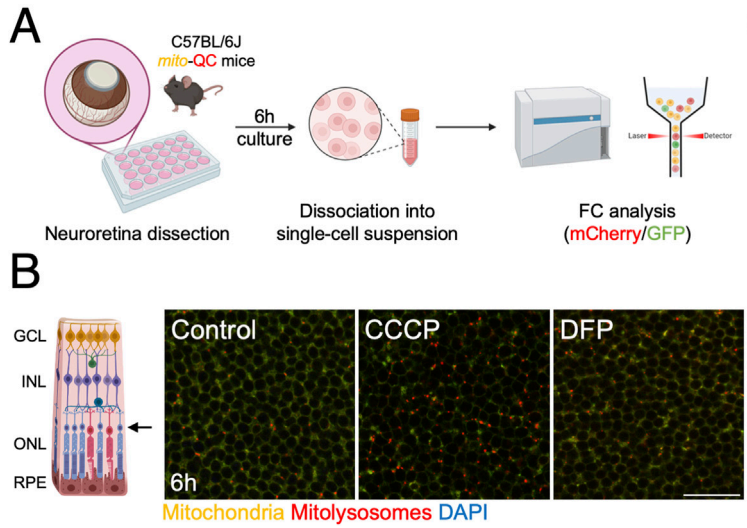

FIGURE 2
Mitophagy assessment in organotypic *ex vivo* retina culture. **(A)** Neuroretinas from C57BL/6J mice expressing the *mito*-QC reporter were dissected and cultured *ex vivo* for 6 h in defined medium in the present of 25 μM CCCP or 1 mM DFP. Samples were dissociated into a single-cell suspension and analyzed by FC. **(B)** Representative images of the photoreceptor-containing outer nuclear layer (ONL). **(C)** Quantification of the % of mitophagy^{high} cells in neuroretina *ex vivo* culture as defined in Supplementary Figure S3. Scale bar, 25 μm. All data are expressed as the mean ± s.e.m. Dots represent individual mice. *P* values were calculated using one-way ANOVA with Dunnet's *post hoc* test. Diagrams were created using BioRender.

We treated *Park2*-expressing ARPE-19 cells with CCCP and DFP to validate the sensitivity of the reporter when analyzed by flow cytometry. CCCP is a protonophore that disrupts ΔΨm by uncoupling the proton gradient, and is traditionally used as an inducer of PINK1/Parkin-mediated mitophagy (Narendra et al., 2008). DFP is an iron chelator that inhibits HIF-prolyl hydroxylases (PHDs), leading to HIF-1α stabilization, hypoxia-like response and upregulation of downstream mitophagy regulators such as *BNIP3* or *BNIP3L*/NIX that engage in receptor-mediated mitophagy (Allen et al., 2013). Both compounds induced mitophagy at the 24 h timepoint, but only CCCP induced a significant increase after 6 h (Figures 1B, C).

Simultaneously, this reporter allows for quantification of mitochondrial mass defined by the mean fluorescence intensity (MFI) of its GFP component. CCCP significantly decreased cytosolic mitochondrial mass at both timepoints, but no changes were observed with DFP (Figures 1D, E). These results point to either a possible compensation by mitochondrial biogenesis to maintain homeostasis during receptor-mediated mitophagy or, since this pathway requires transcriptional activity to increase BNIP3 and BNIP3L/NIX levels, that mitochondrial mass decrease will be observed at a later timepoint. In parallel, we performed a comparative analysis using spectral flow cytometry and obtained similar results regarding mitophagy levels (Supplementary Figure S2A) and mitochondrial mass (Supplementary Figure S2B) after mitophagy induction with CCCP and DFP, indicating that *mito*-QC can also be measured using this novel technology.

In addition, we also analyzed mitophagy in organotypic *ex vivo* retina culture from *mito*-QC mice (Figure 2A; Supplementary Figure S3). Replicating our findings *in vitro*, CCCP was able to induce mitophagy after 6 h of treatment but DFP was not (Figures 2B, C). The *mito*-QC reporter can therefore be used as a medium-throughput readout to assess mitophagy and mitochondrial mass *in vitro* and *ex vivo*.

Fisetin and phenanthroline induce mitophagy but no mitochondrial biogenesis

To further validate the use of the *mito*-QC reporter, we tested two compounds that we had previously found to significantly increase mitophagy using MitoTracker DeepRed flux assay: Fisetin and Phenanthroline (Mauro-Lizcano et al., 2015). Both compounds induced a robust mitophagy increase at 6 h that was exacerbated by 24 h (Figure 3A). With a similar kinetic to CCCP, both compounds significantly reduced mitochondrial mass at both timepoints analyzed suggesting no concomitant activation of mitochondrial biogenesis (Figure 3B). To further dissect the mechanism of action of these mitophagy inducers, we performed immunoblotting against the mediators of iron depletion-induced mitophagy and observed that Phenanthroline increased the protein levels of HIF-1α and its downstream targets, the mitophagy receptors BNIP3 and BNIP3L/NIX (Figure 3C). Fisetin decreased BNIP3L/NIX levels at the 24 h timepoint, but this observation might rather be representative of acute mitophagy as BNIP3L/NIX is a resident protein at the OMM (Wilhelm et al., 2022). We also evaluated PINK1 stabilization, phospho-Ubiquitin^{Ser65} and ubiquitin adaptor (OPTN, SQSTM1/p62, CALCOCO2/NDP52) levels but observed no differences with Fisetin nor Phenanthroline treatment (Figure 3D), indicating that their activity is PINK1/Parkin-independent.

Mitophagy is impaired in an *in vitro* model of retinal degeneration

We previously described high mitophagy levels in the neuroretina and RPE (McWilliams et al., 2019; Jimenez-Loygorri et al., 2024). Sodium iodate (SI) is commonly used as a

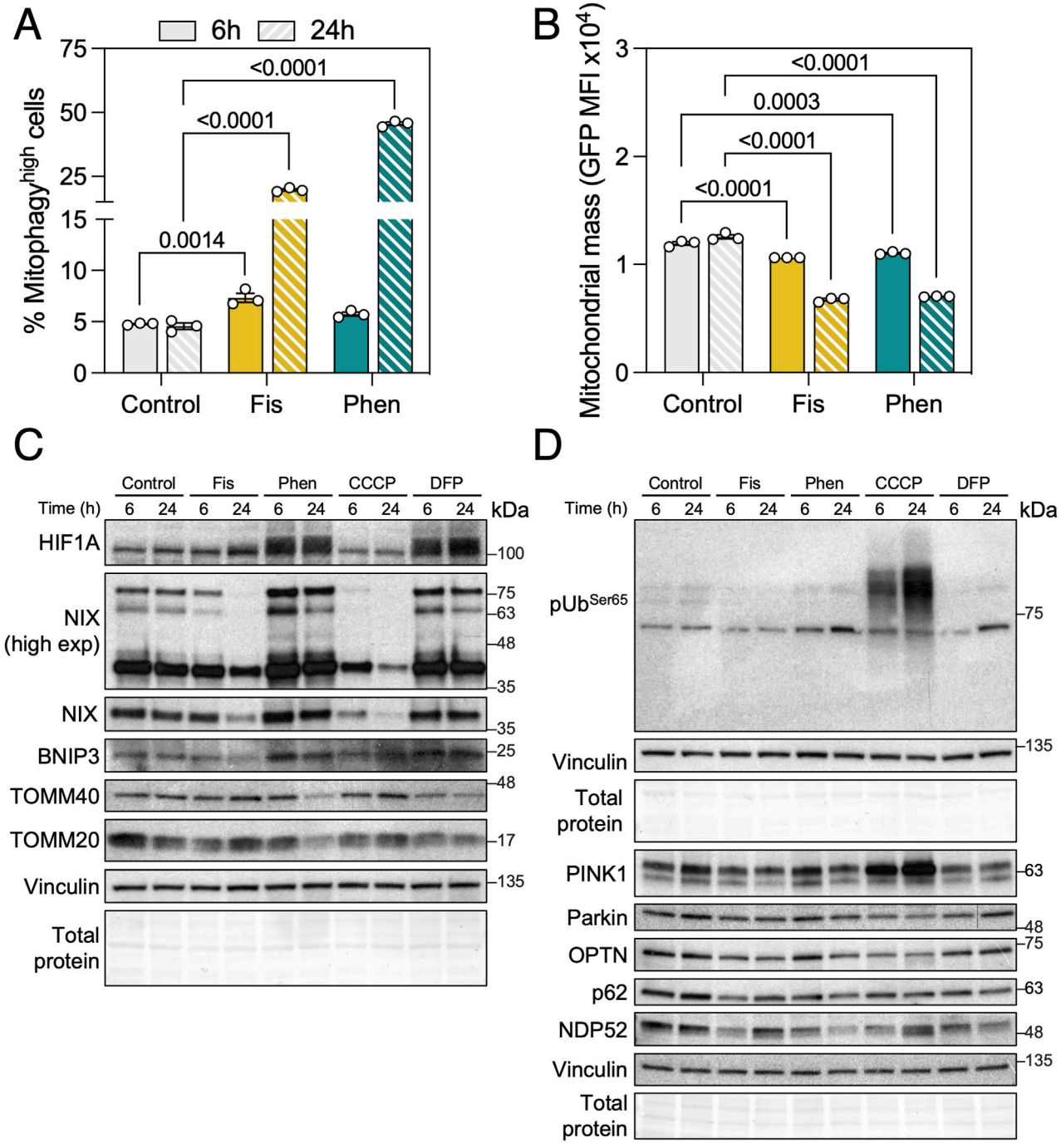

FIGURE 3
Phenanthroline and Fisetin are potent mitophagy inducers. **(A)** ARPE-19 *mito*-QC cells were treated with 10 μM Fisetin (Fis) or 50 μM Phenanthroline (Phen) for the indicated timepoints, quantification of % of mitophagy^{high} population is shown. **(B)** Quantification of mitochondrial mass (GFP MFI). **(C)** Immunoblotting against proteins involved in receptor-mediated mitophagy (HIF-1α, BNIP3L/NIX, BNIP3) and mitochondrial markers (TOMM20, TOMM40). Vinculin was used as a loading control. **(D)** Immunoblotting against proteins involved in PINK1/Parkin-dependent mitophagy (phospho-Ubiquitin^{Ser65}, PINK1, Parkin, OPTN, SQSTM1/p62, NDP52). Vinculin was used as a loading control. All data are expressed as the mean ± s.e.m. Dots represent independent experiments. *P* values were calculated using two-way ANOVA with Dunnett's *post hoc* test.

pharmacological model of age-related macular degeneration (AMD), both *in vitro* and *in vivo* (Chowers et al., 2017). Even though AMD has been historically linked to mitochondrial dysfunction (Fisher and Ferrington, 2018) and impaired autophagy (Kaarniranta et al., 2023), evidence on the role of mitophagy in AMD progression is scarcer (Jiménez-Loygorri et al., 2023). Using *mito*-QC analysis by flow cytometry we observed that treatment with SI for 24 h slightly increased mitophagy levels (Figure 4A) concomitant with a moderate but significant increase in mitochondrial mass (Figure 4B). Traditional

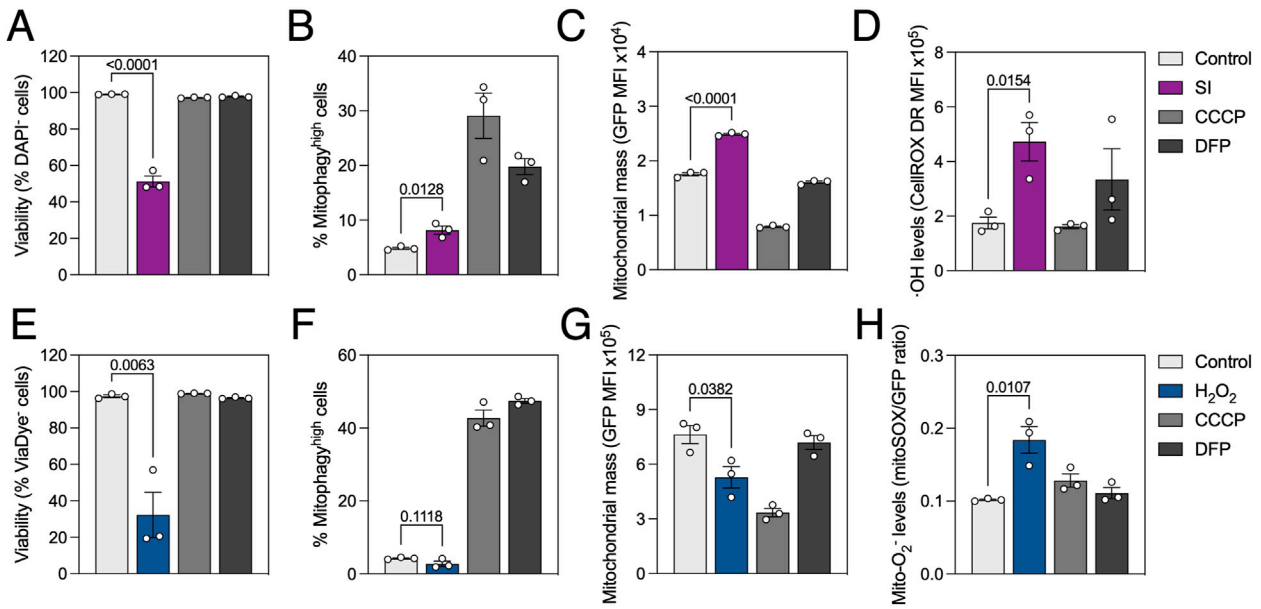

FIGURE 4
Oxidative stress reduces cell viability, differentially modulates mitophagy and stimulates ROS production. ARPE-19 *mito*-QC cells were treated with 20 mM sodium iodate (SI) or 750 μM H_2O_2 for 24 h. **(A)** Simultaneous measurement of viability by nuclear exclusion assay using DAPI in SI-treated cells. Viable population does not incorporate the dye and are identified as $DAPI^-$. **(B)** Quantification of % of $mitophagy^{high}$ population in SI-treated cells. **(C)** Quantification of mitochondrial mass (GFP MFI) in SI-treated cells. **(D)** Simultaneous measurement of reactive oxygen species (ROS) using CellROX Deep Red dye in SI-treated cells. **(E)** Simultaneous measurement of viability using ViaDye Red in H_2O_2-treated cells. Viable population does not incorporate the dye and are identified as $ViaDye^-$. **(F)** Quantification of % of $mitophagy^{high}$ population in H_2O_2-treated cells. **(G)** Quantification of mitochondrial mass (GFP MFI) in H_2O_2-treated cells. **(H)** Simultaneous measurement of mitochondrial ROS using MitoSOX Red dye in H_2O_2-treated cells. All data are expressed as the mean ± s.e.m. Dots represent independent experiments. *P* values were calculated using one-way ANOVA with Dunnet's *post hoc* test.

flow cytometers additionally equipped with violet and red lasers allow for multiplexing with additional dyes. We combined *mito*-QC readout with DAPI (λ_{ex} = 350 nm; λ_{em} = 465 nm), for nuclear exclusion viability assessment, and CellROX Deep Red (λ_{ex} = 644 nm; λ_{em} = 665 nm), a fluorogenic probe with high sensitivity for OH radical detection. SI decreased cell viability to ~70% (Figure 4C) and stimulated ROS production (Figure 4D), in line with previously published data (Chan et al., 2019).

Taking advantage of spectral flow cytometry which can detect the whole emission spectrum under different excitation lasers and dissect the contribution of every fluorophore, we also combined *mito*-QC with traditional red-emitting fluorescent probes. Treatment with H_2O_2 significantly decreased viability to ~40%, measured using ViaDye Red (λ_{ex} = 615 nm; λ_{em} = 740 nm) which binds to intracellular proteins when the plasma membrane is compromised (Figure 4E). While no changes were observed regarding mitophagy levels (Figure 4F), mitochondrial mass was decreased in H_2O_2-treated cells (Figure 4G). These observations were concurrent with increased mitochondrial O_2^- production, measured using MitoSOX Red dye (λ_{ex} = 396 nm; λ_{em} = 610 nm; Figure 4H). Markedly, all results were replicated in wild-type ARPE-19 cells using the same dyes (Supplementary Figures S4A, C) and MitoTracker Deep Red (λ_{ex} = 644 nm; λ_{em} = 665 nm) as a surrogate to measure mitochondrial mass (Supplementary Figure S4B). Spectral unmixing overcomes partial spectrum overlap and allows for simultaneous measurement of *mito*-QC and probes with similar fluorescence profiles.

Discussion

In the present manuscript we provide a standardized protocol to assess mitophagy in cells and *ex vivo* dissociated tissue using the tandem fluorescent *mito*-QC reporter via flow cytometry. Our results with *mito*-QC validate the ability of CCCP and Fisetin to stimulate mitophagy flux, as previously reported by our group using the MitoTracker Deep Red approach (Esteban-Martinez et al., 2017b), and now show that Phenanthroline also induces mitophagy in ARPE-19 cells. Finally, we highlight the possibility of simultaneously measuring other mitochondrial or intracellular parameters using additional probes and conventional or spectral flow cytometry. We also report that mitophagy is impaired in cell type-relevant oxidative stress models (SI, H_2O_2). Furthermore, the use of *mito*-QC bypasses the need for lysosomal degradation inhibitors (Mauro-Lizcano et al., 2015) and the putative confounding effects of drug or ROS interaction MitoTracker dye (Xiao et al., 2016).

The analysis of *mito*-QC by flow cytometry has been crucial for key findings such as the metabolic readaptation following iron chelation (Long et al., 2022) or to understand the interplay between BNIP3L/NIX-mediated mitophagy and pexophagy (Wilhelm et al., 2022). While protocols to measure mitophagy by flow cytometry using mt-Keima are readily available (Um et al., 2018; Winsor et al., 2020), this is, to our knowledge, the first protocol focused on the next-generation fixable *mito*-QC reporter. Compared to mt-Keima, the possibility of fixing *mito*-QC opens the possibility

of implementing, for example, flow cytometry immunophenotyping strategies to assess mitophagy in specific cell subsets within a heterogenous sample. A novel tandem reporter called SRAI (Signal-Retaining Autophagy Indicator) composed of a pH-insensitive CFP variant (TOLLES) and a highly pH-sensitive YFP variant (YPet) has recently been developed and utilized to measure both mitophagy (Katayama et al., 2020) and ER-phagy (Jimenez-Moreno et al., 2023) *in vitro* or using viral vector delivery *in vivo*. There are also published guidelines on how to measure mitochondrial turnover using MitoTimer (Hernandez et al., 2013), but interpretation of data using MitoTimer should be cautious as it does not directly report mitochondria degradation within lysosomes (Gottlieb and Stotland, 2015).

While previous reports have raised concerns regarding the evaluation of PINK1/Parkin-dependent mitophagy using the *mito*-QC reporter (Liu et al., 2021), our results show that CCCP induced detectable levels of mitophagy as early as 6 h in ARPE-19 *mito*-QC cells. Similarly, we have previously reported an increase in $mCherry^{+}GFP^{-}$ mitolysosomes in response to Antimycin + Olygomycin (AO), another classical inducer of the PINK1/Parkin-dependent mitophagy pathway (Rosignol et al., 2020).

Phenanthroline is a metal ion chelator commonly used as a ligand in the chemical industry (Park et al., 2012). It had previously been suggested that phenanthroline induces severe DNM1L/DRP1-dependent mitochondrial fragmentation that leads to mitophagy (Park et al., 2012). We have now further characterized its mechanism of action showing that phenanthroline induces HIF-1α stabilization and transcription of downstream mitophagy receptors BNIP3L/NIX and BNIP3. Interestingly, in our previous work we found that phenanthroline was not able to induce mitophagy in neuroblastoma-derived SH-SY5Y cells (Mauro-Lizcano et al., 2015) but a 10-fold increase was observed in ARPE-19 cells, indicating that its effect might be cell type-dependent. Phenanthroline has also been proposed as a pro-survival agent against apoptosis (Maitra et al., 2021) and parthanatos-mediated cell death (Chiu et al., 2012).

Fisetin is a natural flavonoid that acts as a potent SIRT1 NAD^{+}-dependent histone deacetylase activator (Jang et al., 2012). The NAD^{+}/NADH ratio is affected by mitochondrial function, and *vice versa* (Lautrup et al., 2024). Fisetin has been described to increase the NAD^{+}/NADH ratio and induce mitophagy (Jang et al., 2012), through a mechanism that was dependent on the ubiquitin adaptor SQSTM1/p62 (Molagoda et al., 2021). Despite a robust increase in mitophagy in SH-SY5Y (Mauro-Lizcano et al., 2015) and ARPE-19 cells, we did not observe any changes in traditional PINK1/Parkin-dependent or receptor-mediated mitophagy effectors. The mechanism of action of Fisetin remains to be elucidated, but it has shown neuroprotective effects in models of neuroinflammation involving NLRP3 inflammasome activation (Molagoda et al., 2021; Ding et al., 2022). Both compounds showed no signs of cytotoxicity *in vitro* and warrant further exploration in diseases involving impaired mitophagy.

Previous evidence in the literature was suggestive of impaired autophagy in the SI model of AMD-associated geographic atrophy (Chan et al., 2019). In the present manuscript we indeed observed a slight increase in mitophagy but also a concomitant accumulation of mitochondria in the viable population of cells challenged with SI, replicating our previous findings using *mito*-QC immunofluorescence (Jimenez-Loygorri et al., 2024). Primary RPE cultures from patients with AMD similarly display marked mitochondrial dysfunction (Ferrington et al., 2017) as well as autophagy defects (Ye et al., 2016) that could be a result of dysfunctional mitophagy. Boosting mitophagy could therefore be a novel potential therapeutic strategy in the prevention and/or treatment of AMD.

Finally, we also performed a comparison between widely available standard flow cytometry and spectral cytometry, exploring its added value. Polychromatic flow cytometry or standard flow cytometry is based on the principle one detector, one fluorochrome thanks to a series of dichroic filters. So, only a portion of the emitting signal can be collected. Spectral flow cytometry can collect the full fluorescence spectrum of every cell allowing the separation and differentiation among their spectral signatures, allowing more elaborate, multiplexed assays. This is possible thanks to the spectral unmixing algorithm which identifies the spectral signature of every fluorochrome plus the autofluorescence of the cells and resolves the complete spectra of every cell based on these parameters, allowing to differentiate the contribution of each fluorochrome in a certain wavelength (Robinson, 2022). Using this methodology, we were able to combine *mito*-QC analysis with green- and red-emitting intracellular probes that present partial spectral overlap with GFP and mCherry (Supplementary Figure S5).

Mitophagy analysis by flow cytometry, using *mito*-QC or similar reporters, therefore represents an update to previously used methodology, reducing time, cost and resources when compared to traditional microscopy analysis. Herein we provide a standardized protocol for *mito*-QC analysis using traditional and spectral flow cytometry, multiplexing with an array of intracellular probes and insight on mitophagy regulation using two inducers and models of oxidative stress.

Summary blurb

mito-QC reporter analysis by flow cytometry is a reliable and semi-high throughput method to measure mitophagy *in vitro* and *ex vivo*.

Data availability statement

The raw data supporting the conclusions of this article will be made available by the authors, without undue reservation.

Ethics statement

Ethical approval was not required for the studies on humans in accordance with the local legislation and institutional requirements because only commercially available established cell lines were used. The animal study was approved by Margarita Salas Center for Biological Research Bioethics Comitee and Comunidad de Madrid (PROEX 154.3/21). The study was conducted in accordance with the local legislation and institutional requirements.

Author contributions

JJ-L: Conceptualization, Data curation, Formal Analysis, Investigation, Methodology, Validation, Visualization, Writing–original draft, Writing–review and editing. CJ-G: Formal Analysis, Investigation, Methodology, Visualization, Writing–original draft, Writing–review and editing. ÁV-P: Formal Analysis, Investigation, Writing–review and editing. PB: Conceptualization, Funding acquisition, Project administration, Resources, Supervision, Writing–review and editing.

Funding

The author(s) declare that financial support was received for the research, authorship, and/or publication of this article. Research in the PB lab is supported by grants 310030_215271 Swiss National Science Foundation (SNSF) and PID2021-126864NB I00 from MCIN, Spain. JJ-L holds a FPI fellowship from MCIN (PRE2019-088222). CJ-G is supported by the University of Fribourg.

Acknowledgments

We thank Ian Ganley for generating and providing the *mito*-QC reporter mice and *mito*-QC ARPE-19 cell lines; the animal facility (Angélica Horrillo, María Tijero) at the CIB Margarita Salas; the flow cytometry facility at the CIB Margarita Salas and University of Fribourg (Patricia Yagüe and Sarah Cattin, respectively); Beatriz Villarejo-Zori for advice on *ex vivo* experiments and all members of the Autophagy Lab for thoughtful discussions and support.

Conflict of interest

The authors declare that the research was conducted in the absence of any commercial or financial relationships that could be construed as a potential conflict of interest.

Publisher's note

All claims expressed in this article are solely those of the authors and do not necessarily represent those of their affiliated organizations, or those of the publisher, the editors and the reviewers. Any product that may be evaluated in this article, or claim that may be made by its manufacturer, is not guaranteed or endorsed by the publisher.

Supplementary material

The Supplementary Material for this article can be found online at: https://www.frontiersin.org/articles/10.3389/fcell.2024.1460061/full#supplementary-material

References

Allen, G. F., Toth, R., James, J., and Ganley, I. G. (2013). Loss of iron triggers PINK1/Parkin-independent mitophagy. *EMBO Rep.* 14 (12), 1127–1135. doi:10.1038/embor.2013.168

Chan, C. M., Huang, D. Y., Sekar, P., Hsu, S. H., and Lin, W. W. (2019). Reactive oxygen species-dependent mitochondrial dynamics and autophagy confer protective effects in retinal pigment epithelial cells against sodium iodate-induced cell death. *J. Biomed. Sci.* 26 (1), 40. doi:10.1186/s12929-019-0531-z

Chiu, S. C., Huang, S. Y., Tsai, Y. C., Chen, S. P., Pang, C. Y., Lien, C. F., et al. (2012). Poly (ADP-ribose) polymerase plays an important role in intermittent hypoxia-induced cell death in rat cerebellar granule cells. *J. Biomed. Sci.* 19 (1), 29. doi:10.1186/1423-0127-19-29

Chowers, G., Cohen, M., Marks-Ohana, D., Stika, S., Eijzenberg, A., Banin, E., et al. (2017). Course of sodium iodate-induced retinal degeneration in albino and pigmented mice. *Invest Ophthalmol. Vis. Sci.* 58 (4), 2239–2249. doi:10.1167/iovs.16-21255

Ding, H., Li, Y., Chen, S., Wen, Y., Zhang, S., Luo, E., et al. (2022). Fisetin ameliorates cognitive impairment by activating mitophagy and suppressing neuroinflammation in rats with sepsis-associated encephalopathy. *CNS Neurosci. Ther.* 28 (2), 247–258. doi:10.1111/cns.13765

Dunn, K. C., Aotaki-Keen, A. E., Putkey, F. R., and Hjelmeland, L. M. (1996). ARPE-19, a human retinal pigment epithelial cell line with differentiated properties. *Exp. Eye Res.* 62 (2), 155–169. doi:10.1006/exer.1996.0020

Esteban-Martinez, L., Sierra-Filardi, E., McGreal, R. S., Salazar-Roa, M., Marino, G., Seco, E., et al. (2017a). Programmed mitophagy is essential for the glycolytic switch during cell differentiation. *EMBO J.* 36 (12), 1688–1706. doi:10.15252/embj.201695916

Esteban-Martinez, L., Villarejo-Zori, B., and Boya, P. (2017b). Cytofluorometric assessment of mitophagic flux in mammalian cells and tissues. *Methods Enzymol.* 588, 209–217. doi:10.1016/bs.mie.2016.09.081

Ferrington, D. A., Ebeling, M. C., Kapphahn, R. J., Terluk, M. R., Fisher, C. R., Polanco, J. R., et al. (2017). Altered bioenergetics and enhanced resistance to oxidative stress in human retinal pigment epithelial cells from donors with age-related macular degeneration. *Redox Biol.* 13, 255–265. doi:10.1016/j.redox.2017.05.015

Figueiredo-Pereira, C., Villarejo-Zori, B., Cipriano, P. C., Tavares, D., Ramírez-Pardo, I., Boya, P., et al. (2023). Carbon monoxide stimulates both mitophagy and mitochondrial biogenesis to mediate protection against oxidative stress in astrocytes. *Mol. Neurobiol.* 60 (2), 851–863. doi:10.1007/s12035-022-03108-7

Fisher, C. R., and Ferrington, D. A. (2018). Perspective on AMD pathobiology: a bioenergetic crisis in the RPE. *Invest Ophthalmol. Vis. Sci.* 59 (4), AMD41–AMD47. doi:10.1167/iovs.18-24289

Gomez-Sintes, R., Villarejo-Zori, B., Serrano-Puebla, A., Esteban-Martinez, L., Sierra-Filardi, E., Ramirez-Pardo, I., et al. (2017). Standard assays for the study of autophagy in the *ex vivo* retina. *Cells* 6 (4), 37. doi:10.3390/cells6040037

Gottlieb, R. A., and Stotland, A. (2015). MitoTimer: a novel protein for monitoring mitochondrial turnover in the heart. *J. Mol. Med. Berl.* 93 (3), 271–278. doi:10.1007/s00109-014-1230-6

Hasson, S. A., Kane, L. A., Yamano, K., Huang, C. H., Sliter, D. A., Buehler, E., et al. (2013). High-content genome-wide RNAi screens identify regulators of parkin upstream of mitophagy. *Nature* 504 (7479), 291–295. doi:10.1038/nature12748

Hernandez, G., Thornton, C., Stotland, A., Lui, D., Sin, J., Ramil, J., et al. (2013). MitoTimer: a novel tool for monitoring mitochondrial turnover. *Autophagy* 9 (11), 1852–1861. doi:10.4161/auto.26501

Jang, S. Y., Kang, H. T., and Hwang, E. S. (2012). Nicotinamide-induced mitophagy: event mediated by high NAD+/NADH ratio and SIRT1 protein activation. *J. Biol. Chem.* 287 (23), 19304–19314. doi:10.1074/jbc.M112.363747

Jiménez-Loygorri, J. I., Benítez-Fernández, R., Viedma-Poyatos, Á., Zapata-Muñoz, J., Villarejo-Zori, B., Gómez-Sintes, R., et al. (2023). Mitophagy in the retina: viewing mitochondrial homeostasis through a new lens. *Prog. Retin Eye Res.* 96, 101205. doi:10.1016/j.preteyeres.2023.101205

Jimenez-Loygorri, J. I., and Boya, P. (2024). Aging STINGs: mitophagy at the crossroads of neuroinflammation. *Autophagy* 20 (7), 1684–1686. doi:10.1080/15548627.2024.2322421

Jimenez-Loygorri, J. I., Viedma-Poyatos, A., Gomez-Sintes, R., and Boya, P. (2024). Urolithin A promotes p62-dependent lysophagy to prevent acute retinal neurodegeneration. *Mol. Neurodegener.* 19 (1), 49. doi:10.1186/s13024-024-00739-3

Jimenez-Moreno, N., Salomo-Coll, C., Murphy, L. C., and Wilkinson, S. (2023). Signal-retaining autophagy indicator as a quantitative imaging method for ER-phagy. *Cells* 12 (8), 1134. doi:10.3390/cells12081134

Kaarniranta, K., Blasiak, J., Liton, P., Boulton, M., Klionsky, D. J., and Sinha, D. (2023). Autophagy in age-related macular degeneration. *Autophagy* 19 (2), 388–400. doi:10.1080/15548627.2022.2069437

Katayama, H., Hama, H., Nagasawa, K., Kurokawa, H., Sugiyama, M., Ando, R., et al. (2020). Visualizing and modulating mitophagy for therapeutic studies of neurodegeneration. *Cell* 181 (5), 1176–1187. doi:10.1016/j.cell.2020.04.025

Lautrup, S., Hou, Y., Fang, E. F., and Bohr, V. A. (2024). Roles of NAD(+) in health and aging. *Cold Spring Harb. Perspect. Med.* 14 (1), a041193. doi:10.1101/cshperspect.a041193

Lazarou, M., Sliter, D. A., Kane, L. A., Sarraf, S. A., Wang, C., Burman, J. L., et al. (2015). The ubiquitin kinase PINK1 recruits autophagy receptors to induce mitophagy. *Nature* 524 (7565), 309–314. doi:10.1038/nature14893

Liu, Y. T., Sliter, D. A., Shammas, M. K., Huang, X., Wang, C., Calvelli, H., et al. (2021). Mt-Keima detects PINK1-PRKN mitophagy *in vivo* with greater sensitivity than mito-QC. *Autophagy* 17 (11), 3753–3762. doi:10.1080/15548627.2021.1896924

Long, M., Sanchez-Martinez, A., Longo, M., Suomi, F., Stenlund, H., Johansson, A. I., et al. (2022). DGAT1 activity synchronises with mitophagy to protect cells from metabolic rewiring by iron depletion. *EMBO J.* 41 (10), e109390. doi:10.15252/embj.2021109390

Maitra, S., Sornjai, W., Smith, D. R., and Vincent, B. (2021). Phenanthroline impairs βAPP processing and expression, increases p53 protein levels and induces cell cycle arrest in human neuroblastoma cells. *Brain Res. Bull.* 170, 29–38. doi:10.1016/j.brainresbull.2021.02.001

Mauro-Lizcano, M., Esteban-Martinez, L., Seco, E., Serrano-Puebla, A., Garcia-Ledo, L., Figueiredo-Pereira, C., et al. (2015). New method to assess mitophagy flux by flow cytometry. *Autophagy* 11 (5), 833–843. doi:10.1080/15548627.2015.1034403

McWilliams, T. G., Prescott, A. R., Montava-Garriga, L., Ball, G., Singh, F., Barini, E., et al. (2018). Basal mitophagy occurs independently of PINK1 in mouse tissues of high metabolic demand. *Cell Metab.* 27 (2), 439–449. doi:10.1016/j.cmet.2017.12.008

McWilliams, T. G., Prescott, A. R., Villarejo-Zori, B., Ball, G., Boya, P., and Ganley, I. G. (2019). A comparative map of macroautophagy and mitophagy in the vertebrate eye. *Autophagy* 15 (7), 1296–1308. doi:10.1080/15548627.2019.1580509

Molagoda, I. M. N., Athapaththu, A., Choi, Y. H., Park, C., Jin, C. Y., Kang, C. H., et al. (2021). Fisetin inhibits NLRP3 inflammasome by suppressing TLR4/MD2-mediated mitochondrial ROS production. *Antioxidants (Basel)* 10 (8), 1215. doi:10.3390/antiox10081215

Montava-Garriga, L., Singh, F., Ball, G., and Ganley, I. G. (2020). Semi-automated quantitation of mitophagy in cells and tissues. *Mech. Ageing Dev.* 185, 111196. doi:10.1016/j.mad.2019.111196

Narendra, D., Tanaka, A., Suen, D. F., and Youle, R. J. (2008). Parkin is recruited selectively to impaired mitochondria and promotes their autophagy. *J. Cell Biol.* 183 (5), 795–803. doi:10.1083/jcb.200809125

Narendra, D. P., Jin, S. M., Tanaka, A., Suen, D. F., Gautier, C. A., Shen, J., et al. (2010). PINK1 is selectively stabilized on impaired mitochondria to activate Parkin. *PLoS Biol.* 8 (1), e1000298. doi:10.1371/journal.pbio.1000298

Nguyen, T. N., Padman, B. S., and Lazarou, M. (2016). Deciphering the molecular signals of PINK1/parkin mitophagy. *Trends Cell Biol.* 26 (10), 733–744. doi:10.1016/j.tcb.2016.05.008

Park, S. J., Shin, J. H., Kim, E. S., Jo, Y. K., Kim, J. H., Hwang, J. J., et al. (2012). Mitochondrial fragmentation caused by phenanthroline promotes mitophagy. *FEBS Lett.* 586 (24), 4303–4310. doi:10.1016/j.febslet.2012.10.035

Robinson, J. P. (2022). Flow cytometry: past and future. *Biotechniques* 72 (4), 159–169. doi:10.2144/btn-2022-0005

Rosignol, I., Villarejo-Zori, B., Teresak, P., Sierra-Filardi, E., Pereiro, X., Rodriguez-Muela, N., et al. (2020). The mito-QC reporter for quantitative mitophagy assessment in primary retinal ganglion cells and experimental glaucoma models. *Int. J. Mol. Sci.* 21 (5), 1882. doi:10.3390/ijms21051882

Teresak, P., Lapao, A., Subic, N., Boya, P., Elazar, Z., and Simonsen, A. (2022). Regulation of PRKN-independent mitophagy. *Autophagy* 18 (1), 24–39. doi:10.1080/15548627.2021.1888244

Um, J. H., Kim, Y. Y., Finkel, T., and Yun, J. (2018). Sensitive measurement of mitophagy by flow cytometry using the pH-dependent fluorescent reporter mt-keima. *J. Vis. Exp.* 138, 58099. doi:10.3791/58099

Wilhelm, L. P., Zapata-Muñoz, J., Villarejo-Zori, B., Pellegrin, S., Freire, C. M., Toye, A. M., et al. (2022). BNIP3L/NIX regulates both mitophagy and pexophagy. *Embo J.* 41 (24), e111115. doi:10.15252/embj.2022111115

Winsor, N. J., Killackey, S. A., Philpott, D. J., and Girardin, S. E. (2020). An optimized procedure for quantitative analysis of mitophagy with the mtKeima system using flow cytometry. *Biotechniques* 69 (4), 249–256. doi:10.2144/btn-2020-0071

Xiao, B., Deng, X., Zhou, W., and Tan, E. K. (2016). Flow cytometry-based assessment of mitophagy using MitoTracker. *Front. Cell Neurosci.* 10, 76. doi:10.3389/fncel.2016.00076

Ye, F., Kaneko, H., Hayashi, Y., Takayama, K., Hwang, S. J., Nishizawa, Y., et al. (2016). Malondialdehyde induces autophagy dysfunction and VEGF secretion in the retinal pigment epithelium in age-related macular degeneration. *Free Radic. Biol. Med.* 94, 121–134. doi:10.1016/j.freeradbiomed.2016.02.027

frontiers | Frontiers in Cell and Developmental Biology

TYPE Methods
PUBLISHED 18 September 2024
DOI 10.3389/fcell.2024.1475095

Check for updates

OPEN ACCESS

EDITED BY
Jingyue Jia Cassano,
University of New Mexico, United States

REVIEWED BY
Kohta Ikegami,
Cincinnati Children's Hospital Medical Center, United States
Fulong Wang,
Southeast University, China

*CORRESPONDENCE
Melody Di Bona,
mela1989@gmail.com

RECEIVED 02 August 2024
ACCEPTED 05 September 2024
PUBLISHED 18 September 2024

CITATION
Di Bona M and Bakhoum SF (2024) A new microscopy pipeline for studying the initial stages of nuclear and micronuclear rupture and repair.
Front. Cell Dev. Biol. 12:1475095.
doi: 10.3389/fcell.2024.1475095

COPYRIGHT
© 2024 Di Bona and Bakhoum. This is an open-access article distributed under the terms of the Creative Commons Attribution License (CC BY). The use, distribution or reproduction in other forums is permitted, provided the original author(s) and the copyright owner(s) are credited and that the original publication in this journal is cited, in accordance with accepted academic practice. No use, distribution or reproduction is permitted which does not comply with these terms.

A new microscopy pipeline for studying the initial stages of nuclear and micronuclear rupture and repair

Melody Di Bona[1,2]* and Samuel F. Bakhoum[1,2]

[1]Radiation Oncology, Memorial Sloan Kettering Cancer Center, New York, NY, United States, [2]Human Oncology and Pathogenesis Program, Memorial Sloan Kettering Cancer Center, New York, NY, United States

Nuclear envelope repair is a fundamental cellular response to stress, especially for cells experiencing frequent nuclear ruptures, such as cancer cells. Moreover, for chromosomally unstable cancer cells, characterized by the presence of micronuclei, the irreversible rupture of these structures constitutes a fundamental step toward cancer progression and therapy resistance. For these reasons, the study of nuclear envelope rupture and repair is of paramount importance. Nonetheless, due to the constraint imposed by the stochastic nature of rupture events, a precise characterization of the initial stage of nuclear repair remains elusive. In this study, we overcame this limitation by developing a new imaging pipeline that deterministically induces rupture while simultaneously imaging fluorescently tagged repair proteins. We provide a detailed step-by-step protocol to implement this method on any confocal microscope and applied it to study the major nuclear repair protein, barrier-to-autointegration factor (BAF). As a proof of principle, we demonstrated two different downstream analysis methods and showed how BAF is differentially recruited at sites of primary and micronuclear rupture. Additionally, we applied this method to study the recruitment at primary nuclei of the inner nuclear membrane protein LEM-domain 2 (LEMD2) and Charged Multivesicular Protein 7 (CHMP7), the scaffolding protein of the endosomal sorting complex required for transport III (ESCRT-III) membrane remodeling complex. The CHMP7-LEMD2 binding is the fundamental step allowing the recruitment of ESCRT-III, which represents the other major nuclear repair mechanism. This demonstrates the method's applicability for investigating protein dynamics at sites of nuclear and micronuclear envelope rupture and paves the way to more time-resolved studies of nuclear envelope repair.

KEYWORDS

high-resolution microscopy, micronuclear rupture, nuclear envelope rupture, nuclear envelope repair, real-time protein recruitment analysis, spatiotemporal protein recruitment analysis, micronuclear repair impairment

1 Introduction

Nuclear envelope rupture at primary nuclei is a recurring event in cells undergoing shear or confinement stress (Maciejowski and Hatch, 2020), and as such, repair mechanisms have evolved to restore nuclear compartmentalization, fundamental for cell survival (Denais et al., 2016a; Halfmann et al., 2019). This is especially true in cancer (Denais et al., 2016b;

Vargas et al., 2012), where mechanisms of nuclear envelope repair such as barrier-to-autointegration factor (BAF) (Halfmann and Roux, 2021) and the membrane remodeling complex ESCRT-III (Raab et al., 2016; Olmos et al., 2015) can influence patient prognosis (Li et al., 2018; Sears and Roux, 2020). Moreover, most aggressive human tumors are characterized by chromosomal instability (Bakhoum and Cantley, 2018), a hallmark of cancer often associated with poor prognosis, distant metastasis, and therapy resistance (Al-Rawi et al., 2024; Ippolito et al., 2021; Chen et al., 2024). Chromosomally unstable cells harbor aberrant structures called micronuclei. Micronuclei experience rupture far more frequently than primary nuclei. Moreover, micronuclear rupture is generally irreversible (Hatch et al., 2013; Vietri et al., 2020), suggesting a wide dysregulation of repair mechanisms (Martin et al., 2024). Thus, micronuclear collapse represents a milestone in cancer progression and aggressiveness (Di Bona and Bakhoum, 2024).

For these reasons, both primary nuclei and micronuclei have been the subject of numerous studies seeking to elucidate the dynamics of protein recruitment in the context of membrane repair and DNA sensing (Vietri et al., 2020; Martin et al., 2024; Willan et al., 2019; Tang et al., 2022; Mohr et al., 2021; Mackenzie et al., 2017). To date, such investigations have primarily employed spatially resolved techniques such as confocal and high-resolution microscopy. However, when the temporal dimension is integrated, both temporal and spatial resolutions are compromised. The stochastic nature of the rupture event necessitates prolonged live-cell imaging experiments, introducing challenges in balancing imaging file size and mitigating phototoxicity, while maintaining adequate temporal resolution (Ettinger and Wittmann, 2014). Moreover, the extended measurement duration imposes a constraint to the achievable spatial resolution as it necessitates to account for both cellular and intracellular movements (Liu et al., 2018). Finally, this approach is inherently inefficient as the molecular events occurring post-rupture generally take place within a time window shorter than the interval between consecutive frames.

In this study, we introduce a novel high-resolution fluorescence microscopy-based technique that addresses these challenges by enabling timely and precise recording of protein recruitment at the specific site of rupture. To this end, we devised a pipeline that induces rupture in both micronuclei and primary nuclei by exposing the nuclear envelope to a high-intensity 405-nm laser (Halfmann et al., 2019; Denais et al., 2016b; Raab et al., 2016; Kono et al., 2022; Penfield et al., 2018) while imaging. This pipeline allows for the recording of a fluorescence time-lapse with temporal resolution adjustable down to seconds, depending on the timescale of the event being studied. First, we characterized the best parameters for inducing both primary and micronuclear envelope rupture, identified with loss of compartmentalization through a fluorescent protein fused with a nuclear localization sequence (NLS-RFP) (Mackenzie et al., 2017; Hatch and Hetzer, 2016), while minimizing bleaching and phototoxicity. After validating the effective rupture of micronuclei via recruitment of the DNA sensing cyclic GMP-AMP synthase (cGAS) (Mackenzie et al., 2017), we applied this pipeline to study the recruitment of the nuclear envelope repair protein BAF at the site of micronuclear and primary nuclear rupture. Moreover, we demonstrated its applicability to study sequential protein recruitment, using as a proof of principle the recruitment of the ESCRT-III complex scaffold protein, CHMP7, through its interaction with the inner nuclear membrane protein LEMD2 (Gu et al., 2017).

We present a point-by-point protocol that can be applied to any confocal microscope or any microscope with a bleaching/FRAP module, followed by two different analysis applications, one with the open-source software ImageJ (Rasband, W.S., ImageJ, U.S. National Institutes of Health, https://imagej.nih.gov) and one with the 3D rendering software Imaris (Oxford Instruments).

2 Materials and equipment

- Adherent cells (we used HeLa wild-type, gift from the Cheeseman lab, Massachusetts Institute of Technology, purchasable from the ATCC)
- Lentiviral vectors or viral preparations for fluorescent protein expression (see Table 1)
- DMEM + high glucose + pen/strep + sodium pyruvate (MSKCC core facilities)
- Fetal bovine serum (Fisher Scientific, MT35015CV)
- Phosphate-buffered saline (MSKCC core facilities)
- Trypsin-EDTA (Fisher Scientific, 25-300-120)
- Blasticidin 10 mg/mL (InvivoGen, ant-bl-1)
- Puromycin 10 mg/mL (InvivoGen, ant-pr-1)
- Ibidi 8-well chambers (ibiTreat 90 u-slide, 80826-90, Ibidi)
- Live Cell Imaging solution (A59688DJ, Invitrogen)
- Hoechst 33342 (62249, Thermo Fisher)
- Optical fluorescence microscope with a minimum resolution of 250 nm. We recommend the use of a confocal microscope; the wide-field system could work if coupled with an FRAP/bleaching module. The microscope should be equipped with a temperature- and humidity-controlled chamber for live cell imaging. Here, we used an inverted Zeiss LSM880 (Carl Zeiss Microscopy GmbH, Germany) equipped with an Airyscan detector (gain 850, digital gain 1) in the super-resolution mode. For image acquisition, we suggest using an objective with an optical magnification of at least ×60, oil or water immersion. In this study, we used a ×63 oil immersion Plan-Apochromat 63×/1.4 Oil DIC M27.
- For image processing, we suggest using deconvolution or other noise reduction algorithms with the microscope built-in software. Here, we processed the images using Airyscan processing in Zeiss ZEN black software using default parameters. For further image analysis, we show possible applications with the open-source software ImageJ (Rasband, W.S., ImageJ, U.S. National Institutes of Health, https://imagej.nih.gov) and the 3D reconstruction software Imaris (Oxford Instruments).
- For statistical analysis and graphical representation, we used the software GraphPad Prism 9 (https://www.graphpad.com/). Sketches were made using BioRender App (https://app.biorender.com; with publication license). Figures were prepared using Adobe Illustrator Software (Adobe).

TABLE 1 Lentiviral vectors for fluorescent protein expression.

Plasmid name	Protein of interest	Antibiotic selection	Origin	Catalog number
pVLX_puro-mCherry-NLS-TagRFP	NLS-RFP	Puromycin	Hatch lab	NA
cGAS-GFP	cGAS fused to EGFP	Puromycin	Maciejowski Lab	NA
EGFP-BAF	BAF fused to EGFP	Blasticidin	Addgene	101772
pGenLenti-CHMP7GFP	CHMP7-GFP	Puromycin	Insert from pMGF182,Addgene	plasmid #97006
pGenLenti-LEMD2mCherry	LEMD2-mCherry	Blasticidin	Insert from pMGF196,Addgene	Plasmid #97005

3 Methods

3.1 Generating cell lines

3.1.1 Timing: at least 1 month before the experiment

Generate stable cell lines, rather than rely on transient transfection, expressing the proteins of interest fused with a fluorescent protein. Here, we used lentiviral vectors to generate stable HeLa cells expressing the proteins of interest. To produce the lentiviral vectors, we co-transfected the parental cell line HEK293 (ATCC, CRL-3216) with packaging vectors and the vector of interest listed in Table 1. We used Lipofectamine 2000 (Thermo Fisher Scientific 11668019), following the manufacturers' instructions. We then collected the supernatant containing the lentiviral particles after 48 h and used it to transduce HeLa cells. For HeLa cell infection, we plated 200,000 cells resuspended in 1 mL of fresh media, together with 6 µL of polybrene (Santa Cruz Biotechnologies sc-134220) and 1 mL of virus suspension in a 6 well-plate. Cells were left to adhere with the virus for 24 h before changing the medium. Appropriate antibiotic selection was added after 48 h of infection. For double protein expression, we proceeded sequentially. We suggest sorting cells for fluorescent protein expression using fluorescence-activated cell sorting in addition to antibiotic selection. Selection of clones is recommended to ensure consistency.

3.2 Culturing cell lines

3.2.1 Timing: 10 days before the experiment

Thaw the cell line expressing the chosen fluorescent protein/s at least 10 days before the experiment, and culture in DMEM high glucose supplemented with 10% FBS and with the appropriate antibiotic (5–20 µg/mL puromycin or blasticidin) and seed them in an appropriate container (1×10^6 cells in a 10-cm dish). Passage the cells every 3–4 days for HeLa, or adjust depending on the cell line doubling time.

3.2.2 Timing: the day before the experiment

Wash the cells with PBS, trypsinize them, and seed them at a density of $0.5–15 \times 10^5$ cells in each of the four central wells of an 8-well ibidi chamber, for a maximum volume of 350 µL per well. Fill the border wells of the chamber with PBS to prevent evaporation of the media.

3.2.2.1 STOP point

It is possible to plate the cells at a lower concentration and use them up to 3 days after plating them.

3.3 Staining adherent cells (optional, for DNA visualization)

3.3.1 Timing: 1–2 h before the experiment

Wash away the media from the wells of the ibidi chamber, wash once with PBS, and incubate the cells for 15 min in a 37°C incubator containing a sterile solution of 2.5 µg/mL Hoechst 33342 dissolved in live cell imaging solution. When the incubation time is over, wash thoroughly 4x with live cell imaging and then replace with fresh live cell imaging solution.

Optional: if treatments are needed, depending on the duration of the treatment, change the media on the cells with the appropriate drug dissolved in the live cell imaging solution. If the treatment needs to be washed out, perform it before staining the cells.

3.4 Image acquisition

3.4.1 Timing: 1 h before starting the experiment

Optional: perform any treatment longer than 1 h or that needs to be washed out, before setting the ibidi chamber in the microscope. For shorter treatments, we suggest changing the media with the live cell imaging solution mixed with the drug of interest from the ibidi well when the chamber is already in the incubation chamber of the microscope. This will minimize the time spent to allow the cells to settle.

1. Place the ibidi with the live cell imaging solution on the microscope, in the temperature-controlled chamber. Let the cells sit for at least 1 h to bring the glass and the oil of the objective, to temperature and to minimize temperature-driven objective and sample drift.
2. Set the optical configuration of the microscope, and turn on the appropriate lasers (intensity will depend on the fluorescent protein expression, but needs to be kept constant among conditions). We used a 488-nm laser line to image GFP-tagged proteins and a 561-nm laser line to image RFP- or mCherry-tagged proteins, both at 1.5% power. When imaging nucleic acid through Hoechst staining, we used a 0.7% power 405-nm laser line.

We used a pixel size of 30 nm, 512 × 512 pixels per image (13.5 μm × 13.5 μm). The regular imaging acquisition speed was 0.85 μs, with a scan time of 521 ms. We acquired one Z-slice every 500 nm for a total Z-stack of 3 μm for the primary nucleus and a Z-stack comprising the whole micronucleus (depending on micronuclear size). For the time lapse measurement, we acquired one Z-stack every 30 s, but depending on the speed of acquisition and on the expected time of the event under study, this time can be decreased to 10 s.

For the rupture, we selected a region of interest (ROI) of 12 × 18 pixels in a peripheral region of the micronucleus or primary nucleus and used a pixel dwell time (the time the laser is spending on each pixel) of 32.77 μs After the first frame of regular imaging, we bleached the ROI with a 405-nm laser at 95% and 100 iterations on the ROI before resuming regular imaging.

3.4.2 Starting the experiment

3. Find the focus of the microscope on the adherent cells by using the oculars and an epifluorescence lamp or a built-in autofocus system.

3.4.2.1 Optional: run a rupture test (requires NLS-RFP expression or other rupture marker)

4. Choose a cell with a good NLS-RFP expression and an intact micronucleus.
5. Define the Z-stack: choose the first and last plane of the series needed to be imaged. We suggest choosing a Z-stack that comprises the whole micronucleus.
6. Choose an ROI that is situated on the nuclear periphery or on the micronucleus. In systems allowing bleaching of a specific z-position, choose the central plane of the Z-stack as the bleaching plane. This will account for the intrinsic mobility of the micronucleus and ensure that the rupture site will be in focus during the entire measurement.
7. As a starting condition, use 100 iterations of the laser with a 32.77 μs pixel dwell time for bleaching. In experimental systems in which these bleaching conditions are not ensuring 100% rupture, the pixel dwell time or iterations can be increased until complete rupture is achieved.
8. Acquire the measurement, stopping after three frames after rupture. For frame sizes and intervals, refer to step 2. Assess the integrity of the micronucleus through NLS-RFP visualization (Supplementary Figure S2). Another possibility, although not tested here, is to measure the presence of NES-GFP.
9. Repeat steps 4–8 for five times, using a different cell each time.
10. If any of the micronuclei did not rupture, increase the pixel dwell time or the iterations, and repeat steps 4–8 for five times. Increase the conditions until all of the micronuclei rupture.

3.4.2.2 Run a pilot measurement

11. Choose a cell with a good expression of the fluorescent protein under examination. For micronuclei studies, choose a cell with an intact micronucleus that is preferably not above the primary nucleus to maximize the precision of focus and imaging.
12. Define the Z-stack: choose the first and last plane of the series that needs to be imaged. We suggest choosing a Z-stack that comprises the whole micronucleus, while for primary nuclei imaging, we suggest a Z-stack of approximately 2–2.5 μm total.
13. Choose an ROI that is situated on the nuclear periphery or on the micronucleus. If your system allows it, choose a different Z-position for the bleaching and pick the central plane of the Z-stack (see step 6).
14. Start the measurement by acquiring as a starting point a time-lapse every 30 s.
15. If you notice that the protein of interest is already present in the first frame after rupture, then scale down the sampling time accordingly.

3.4.2.3 Run the experiment

16. Repeat the steps 11–14 using the sampling time found in step 15, on a different cell. We recommend using different cells for different measurements to avoid the possibility that protein recruitment at one cellular site might affect recruitment time at a second site.
17. Start the measurement acquiring the time-lapse with the sampling time chosen previously. We recommend to not exceed a length of 1 h for the measurements to avoid bleaching, phototoxicity, and sample drifting.
18. Save the measurement file.
19. Optional: process the raw data (e.g., Airyscan processing, denoising, and deconvolution) and save the processed version.

3.4.2.4 STOP point

20. Proceed with image analysis.

3.5 Analysis with Fiji

Once the live-cell measurements have been acquired, processed (in our case through the Airyscan processing function in Zeiss built-in software ZEN), and saved in native format (.czi), it is possible to proceed with the analysis. As an application example, we quantified the time of post-rupture recruitment for each protein of interest (POI) using the free image analysis software ImageJ, downloadable at (https://fiji.sc/). To enable the drag and drop option and the possibility to open microscope native formats in ImageJ, the BioFormats Importer plugin needs to be installed (downloadable through ImageJ-Plugins-BioFormats). A Z-projection using the maximum intensity is recommended (Image-Stacks-Z projects), but other Z-projection modes might be preferred by the user (e.g., mean intensity), depending on the application. Once a Z-projected file is generated, we recommend adjusting brightness and contrast (Image-Adjust-Brightness/Contrast) for each channel using the Auto function. At this point, the POI intensity can be manually calculated. We recommend selecting a round ROI (using the button "Oval selection") on the background, on the POI at the beginning of the experiment, and on the POI after rupture. From this ROI, fluorescence intensity information is extracted. After confirming that the box of "Mean gray intensity" under the measurements settings is checked (Analyze-Set measurement), clicking Measure (Analyze-Measure) will return the mean intensity value of Background, POI at the beginning of the experiment, and POI at the selected frames after rupture.

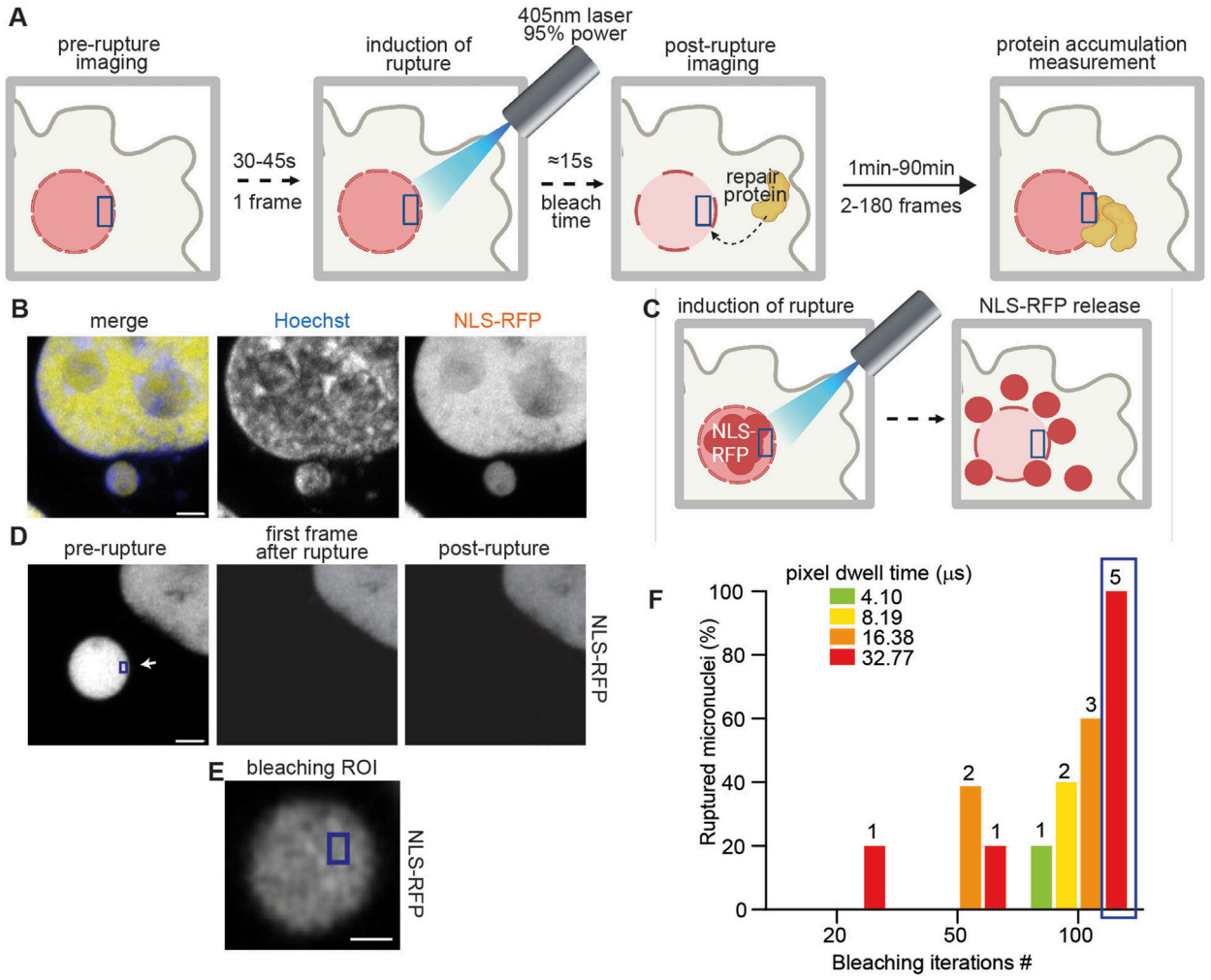

FIGURE 1
Laser-induced micronuclear rupture. **(A)** Schematic representation of the method workflow. An ROI is selected in the micronucleus or primary nucleus that, after the first frame of imaging, is exposed to a 405-nm laser at 95% power for 15 s. Imaging is then performed for the chosen time to record the behavior of repair proteins at the site of rupture. **(B)** Representative images of HeLa cells expressing NLS-RFP (yellow) and stained with Hoechst (blue). Scale bar = 2 µm **(C)** Schematic representation of NLS-RFP release in the cytosol after laser-induced rupture. **(D)** Representative images of a micronucleus in HeLa cells expressing NLS-RFP pre and post laser-induced rupture. Scale bar = 2 µm. The ROI used for bleaching (blue) is indicated with the white arrow. **(E)** Representative image of an ROI (blue) on a micronucleus in HeLa cells expressing NLS-RFP. Scale bar = 0.5 µm. **(F)** Graphical representation of micronuclear rupture efficiency after bleaching the ROI as in **(E)** using the indicated pixel dwell times and number of iterations. The number of ruptured micronuclei is indicated on the columns, and the total micronuclei probed for each measurement was 5. The blue box highlights the optimal conditions (enabling virtual 100% micronuclear rupture) that we chose for further bleaching.

The post-rupture frame in which the POI appears at least 10 times brighter than the first frame (after background subtraction) is identified as the recruitment time. The precise time information is obtained from the raw data (Image-Show Info) and can then be used for further analysis or graphical representation.

3.6 Analysis with Imaris

As a second application example, we quantified the change of POI amount (volume of protein) over time after the rupture occurs. To do so, we used the 3D rendering software Imaris (we recommend using the 8.4 version or above). First, we converted the microscopy file in the native Imaris format. After opening it in "Slice View," we created a "New Surface" corresponding to the POI.

To create the surface, we used an ROI that comprises the site of rupture for all the time frames. Then, we chose the channel corresponding to the POI, and, after smoothing using a surface detail of 0.0318 µm, we selected an automatic threshold. We then finalized the surface generation using the "track surface" option to allow for graphing the volume of the POI over time. After checking that the surface (i.e., the 3D-rendered POI) was correctly recognized on all the frames, we joined the tracks and the identified POI in one single surface tracked along the whole measurement ("edit Track" and "edit Surfaces"). We then selected the "Statistics" tab and generated a graph of the POI volume (other valuable measurement possibilities are area, volume overlap between different surfaces, or sphericity) over time. We finally exported these data in .csv files for further analysis or graphical representation.

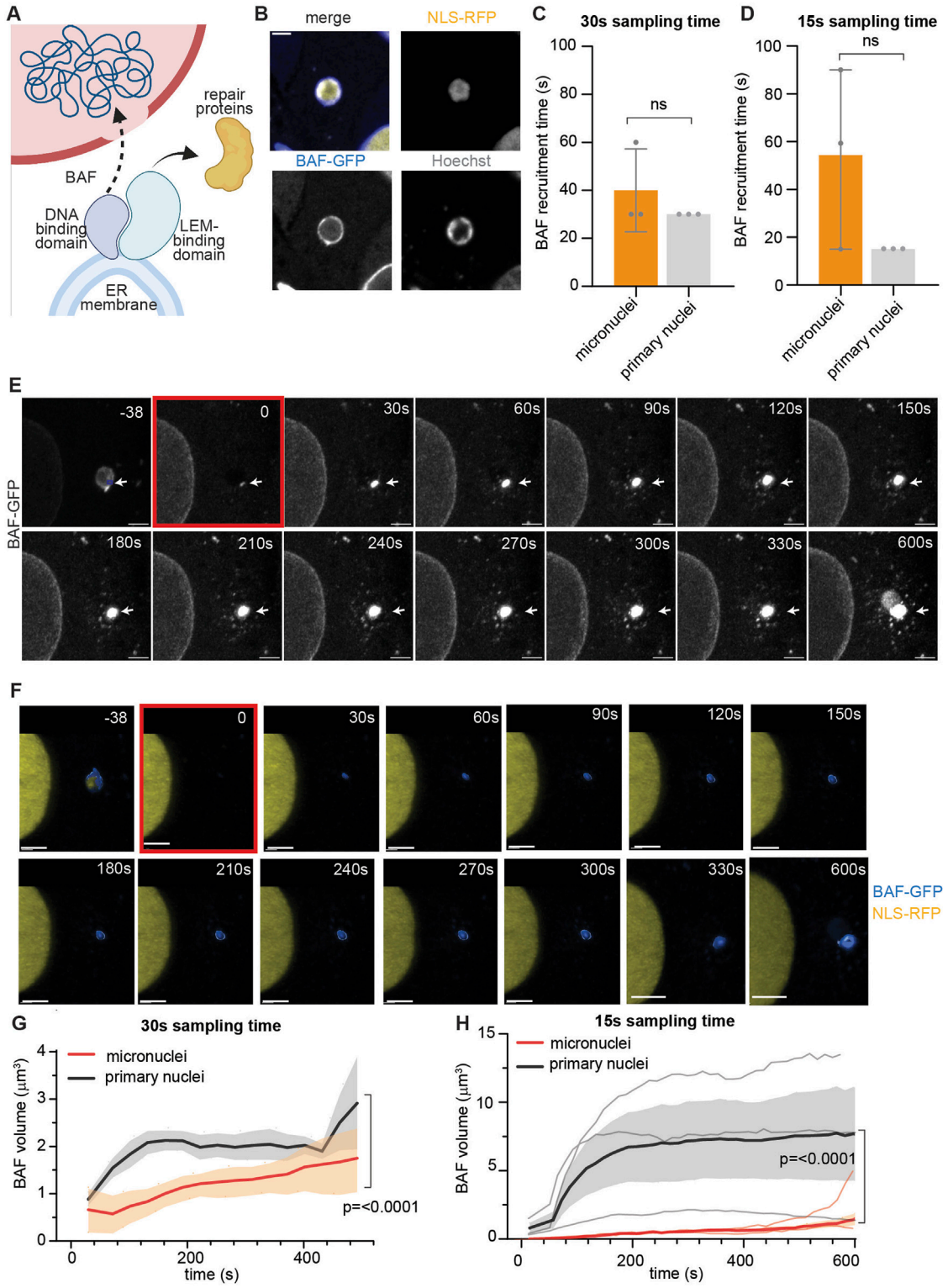

FIGURE 2
Barrier-to-autointegration factor post-rupture recruitment is impaired at micronuclei. **(A)** Schematic representation of the role of BAF (blue) in nuclear repair. At the site of rupture, BAF is recruited to the exposed chromatin by its DNA-binding domain. This enables repair both by directly bringing the ER membrane to the rupture site to plug the hole and by recruiting other repair proteins through the LEM-binding domain. **(B)** Representative images of HeLa cells expressing NLS-RFP (yellow), BAF-GFP (blue), and stained for Hoechst (gray). Scale bar = 2 µm. **(C)** Calculated BAF arrival time at the rupture site of micronuclei and primary nuclei using a 30 s sampling time. **(D)** Calculated BAF arrival time at the rupture site of micronuclei and primary nuclei using a 15 s sampling time. **(B, C)** For three biological replicates, mean ± standard deviation is plotted. Statistical significance is calculated using unpaired student's t-test. **(E)** Representative maximum intensity Z-projections of BAF-GFP recruitment at the site of micronuclear rupture. The rupture location is indicated with a white arrow throughout the measurement, while the ROI used for bleaching (blue) is indicated only in the initial frame. In the last frame of the measurement (600 s), the micronucleus shape is visible in the BAF-GFP channel, indicating BAF recruitment to the whole micronucleus.
(*Continued*)

FIGURE 2 (Continued)
Scale bar = 2 μm. **(F)** Three-dimensional reconstruction of the images shown in **(D)** (overlayed to the fluorescent original image in the background) of HeLa cells expressing BAF-GFP (blue) and NLS-RFP (yellow). The frame in which rupture is induced is highlighted in red. Scale bar = 6 μm. **(G)** Representation of the variation in time of BAF volume in primary nuclei (black) versus micronuclei (red) calculated as in **(E, F)** from measurements taken using a 30-s interval. We ruptured primary nuclei and micronuclei in different cells to avoid proteins being recruited at the same time at two different sites. Nonetheless, the conditions used to rupture primary and micronuclei are the same. Mean ± SEM of three biological replicates, statistical significance was calculated using the Mann–Whitney test, and *p*-value is indicated. **(H)** Representation of the variation in time of BAF volume in primary nuclei (black) versus micronuclei (red), calculated as in **(E, F)** from measurements taken using a 15-s interval. We ruptured primary nuclei and micronuclei in different cells, to avoid proteins being recruited at the same time at two different sites. Nonetheless, the conditions used to rupture primary and micronuclei are the same. Mean ± SEM of three biological replicates, statistical significance was calculated using the Mann–Whitney test, and *p*-value is indicated. Individual curves are overlapped in gray (primary nuclei) and orange (micronuclei).

4 Results

4.1 Nuclear and micronuclear rupture

Recognizing the need to understand nuclear envelope rupture and repair dynamics with high temporal resolution, we aimed to overcome the existing limitations posed by the inherent stochasticity of rupture and the lack of real-time visualization techniques with appropriate temporal resolution. Our goal was to develop a method that enables the study of protein recruitment at the rupture site during the critical initial minutes following rupture.

To this aim, we optimized a microscopy pipeline that, by harnessing the ability to induce nuclear envelope rupture with a 405-nm laser (Denais et al., 2016b; Raab et al., 2016; Kono et al., 2022; Penfield et al., 2018), removes the stochastic variable and allows for proper time resolution in the moments immediately following this event (Figure 1A).

First, we sought to understand the optimal parameters to induce virtually 100% rupture events, while minimizing the exposure time to the 95% 405-nm laser light used to induce rupture. To discriminate between micronuclei ruptured or intact, we used HeLa cells expressing NLS-RFP, which is released into the cytoplasm upon loss of compartmentalization (Figures 1B–D; Supplementary Figure S1A). As a further validation, we used HeLa cells expressing NLS-RFP and cGAS-GFP, a DNA-recognizing protein that is rapidly recruited in bright foci at the site of primary or micronuclear rupture (Mackenzie et al., 2017; Agustinus et al., 2023) (Supplementary Figures S1B–D) We opted to maintain a consistent ROI size of 360 nm × 540 nm across all measurements (Figure 1E), as this was the minimum size that accommodated even the smallest observed micronuclei (data not shown). Thus, we characterized the probability of rupture while changing the pixel dwell time and the iterations on the ROI of the 405-nm laser. For the following applications, we used the minimum values that induced rupture in all of the attempts made. In our experimental system, these conditions were a pixel dwell time of 32.77 μs and 100 iterations (refer to Step 2 for the acquisition parameters) (Figure 1F).

4.2 BAF recruitment at the site of micronuclei and primary nuclei rupture

Next, we used our pipeline to study the recruitment of the primary repair protein BAF at the site of nuclear envelope rupture (Halfmann et al., 2019; Halfmann and Roux, 2021; Young et al., 2020) (Figure 2A). After generating HeLa cells expressing NLS-RFP and the fusion protein BAF-GFP, we used them to visualize BAF dynamics after inducing nuclear rupture (Figure 2B).

Given the irreversibility of the rupture occurring at micronuclei, we wondered whether there was any difference in BAF recruitment at the primary nucleus or at the micronuclear site. To investigate this, we used ImageJ to calculate the timing of BAF recruitment following primary and micronuclear rupture—specifically the velocity of BAF arrival at the rupture site. Figures 2C, D illustrate the impact of reducing the sampling time. We showed that decreasing the sampling time from 30 to 15 s allowed us to capture a more pronounced difference, although not statistically significant, in BAF recruitment time between micronuclei and primary nuclei. This difference was mostly lost using the 30 s sampling time, proving the importance of high temporal resolution in investigating fast processes such as nuclear envelope repair.

We then asked if the extent of BAF recruitment was different at the site of primary or micronuclear rupture. To answer this, we used the software Imaris for 3D volumetric reconstruction (Figures 2E, F; Supplementary Figure S2) and quantified the changes in the volume of BAF after inducing rupture. As shown in Figures 2G, H, the amount of BAF recruited at the primary nuclei is greater than at sites of micronuclear rupture.

4.3 CHMP7 recruitment at primary nuclear envelope rupture through LEMD2

Recognizing the critical role of protein recruitment in the early stages of nuclear envelope repair, we sought to further investigate these processes at primary nuclei with our pipeline. To this aim, we focused on the sequential recruitment of LEM Domain-2 (LEMD2) and charged multivesicular protein 7 (CHMP7) at the site of primary nuclear envelope rupture (Figure 3A). LEMD2-mediated recruitment of the ESCRT-III membrane remodeling complex scaffolding protein, CHMP7, is a crucial step for primary nuclei envelope repair in which it allows for the subsequent nucleation and function of the ESCRT-III complex, which repairs the nuclear envelope (Raab et al., 2016; Gu et al., 2017; von Appen et al., 2020; Thaller et al., 2019). After generating HeLa cells stably expressing CHMP7-GFP and LEMD2-mCherry (Figure 3B), we applied our laser-induced rupture pipeline and studied the behavior of the two proteins after primary nuclei envelope rupture. Despite the variability in CHMP7 arrival time, our method was able to confirm that the recruitment of CHMP7 is secondary to the appearance of LEMD2, as reported in literature (Gu et al., 2017; von Appen et al., 2020; Thaller et al., 2019) (Figure 3C).

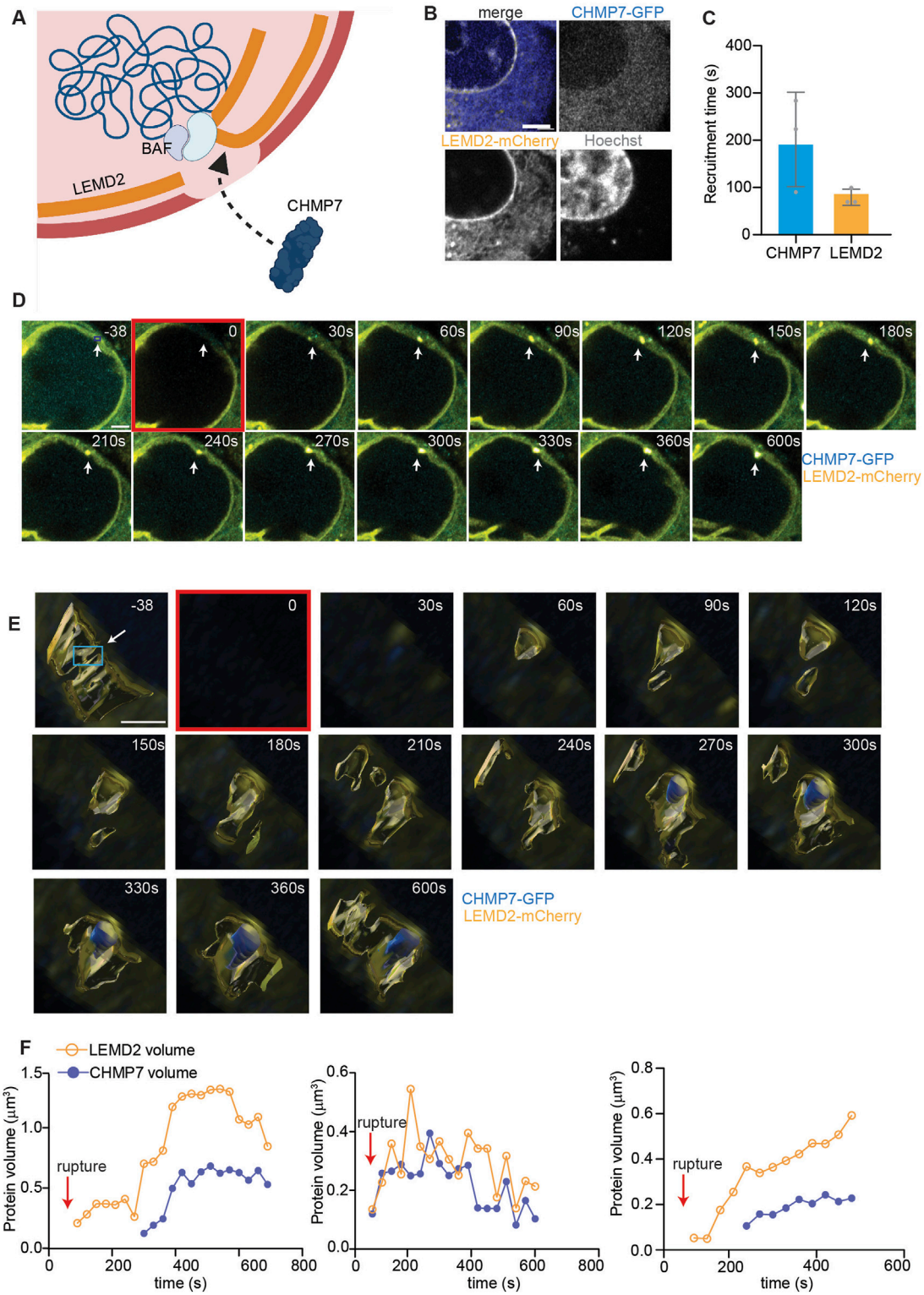

FIGURE 3
CHMP7 recruitment at sites of primary nuclei rupture shadows LEMD2 dynamics. **(A)** Schematic representation of LEMD2-CHMP7 recruitment at the site of primary nuclei rupture. LEMD2, an inner nuclear membrane protein, is recruited at the rupture site by the BAF LEM-binding domain. CHMP7, a cytosolic protein associated to the endoplasmic reticulum, is recruited at the rupture site through its interaction with LEMD2. **(B)** Representative images of HeLa cells expressing LEMD2-mCherry (yellow), CHMP7-GFP (blue), and stained for Hoechst (gray). Scale bar = 2 µm. **(C)** Calculated arrival time at the rupture site of CHMP7 and LEMD2, showing how the latter is recruited first. Mean ± standard deviation of three biological replicates is plotted. **(D)** Representative maximum intensity Z-projection of HeLa cells expressing CHMP7-GFP (blue) and LEMD2-mCherry (yellow) in which rupture has been induced on primary nuclei. Scale bar = 2 µm. The rupture location is indicated with a white arrow throughout the measurement, while the ROI used for bleaching (blue box) is indicated only in the initial frame. **(E)** Three-dimensional reconstruction of an ROI of 5 µm × 5 µm encompassing the rupture site of images shown in **(D)** of HeLa cells expressing CHMP7-GFP (blue) and LEMD2-mCherry (yellow). The frame in which rupture is induced is highlighted in
(*Continued*)

FIGURE 3 (Continued)
red. Scale bar = 2 μm. In the initial frame, we indicated the ROI used for bleaching with a white arrow and a blue box. **(F)** Individual curves showing the trend in CHMP7 (blue) and LEMD2 (yellow) volume after primary nuclear rupture, calculated from images as in **(D, E)**. We reconstructed only a narrow region around the rupture location, and we measured and plotted only CHMP7 and LEMD2 independent volumes and not their co-localization. Each graph represents an independent experiment conducted using the same rupture settings, and the rupture event is indicated with the red arrow.

Then, we asked if a correlation existed between LEMD2 quantity and CHMP7 recruitment extent. Using 3D volume reconstruction, we indeed showed that the trend in CHMP7 volume changes is mirroring LEMD2 quantity variation (Figures 3D–F).

4.4 Pitfalls and limitations

Our microscopy pipeline is limited to single-cell studies and cannot be applied to population studies. Moreover, the recruitment of repair proteins at small and localized laser-induced ruptures might not fully represent physiological processes, as different repair mechanisms are usually deployed to address ruptures of different sizes (Halfmann et al., 2019; Young et al., 2020). In addition, we deem the application of these methods to cells in suspension more challenging, due to the problems in focusing and imaging inherently motile cells. Moreover, the overexpression of some envelope proteins such as lamins or, as happened in our experiments, cGAS, might influence the probability of rupture. We thus recommend running a rupture test first, and if the rupture rate is lower than 98%, to recalibrate the iterations or speed of bleaching. Similarly, the laser intensity and pixel size used for imaging may need to be adjusted depending on the expressed proteins and their fluorescent tags. While this should not affect the functionality of the laser-induced rupture step, it is necessary to ensure that the bleaching pixel dwell time and the ROI area remain consistent across different microscopes and experimental conditions.

5 Discussion

We developed and optimized a new fluorescence microscopy-based pipeline to study nuclear envelope rupture and the consequent recruitment of repair proteins. Our method efficiently induces rupture in both primary nuclei and micronuclei and distinguishes between the sequence and extent of protein recruitment. By integrating high-resolution microscopy with the established laser-induced rupture, (Halfmann et al., 2019; Denais et al., 2016b; Raab et al., 2016; Kono et al., 2022; Penfield et al., 2018) we achieve precise, controlled rupture both spatially and temporally. This approach enables us to capture protein behavior immediately following the rupture event at the specific location, offering new insights into the dynamics of nuclear repair processes.

As a paradigm for repair processes, we studied the post-rupture dynamics of the first-responder repair protein, BAF. We identified the time and the extent of BAF recruitment at the site of rupture, showing how BAF dynamics evolves over time. By decreasing the sampling time, we observed an increased gap in the BAF recruitment time between primary nuclei and micronuclei. Although this difference is not statistically significant, the clustering of BAF recruitment times for primary nuclei at the shortest sampled value (i.e., the first frame post-rupture) suggests that further reducing the interval between frames might reveal a significantly faster recruitment of BAF at primary nuclei envelope rupture sites compared to micronuclei.

Furthermore, by comparing BAF quantities in primary nuclei and micronuclei, we demonstrated that post-rupture BAF recruitment is diminished in the latter. This reduction is time-dependent and likely specific to the narrow window immediately following rupture. Trends in our data and previous literature (Halfmann et al., 2019; Young et al., 2020) suggest that BAF recruitment eventually reaches the same plateau in both micronuclei and primary nuclei. This early reduction in BAF recruitment might explain the inefficient repair often observed in micronuclei, along with p62-mediated ESCRT-III degradation induced by mitochondrial ROS (Martin et al., 2024; Di Bona et al., 2024).

Finally, we applied the method to study the sequential recruitment of proteins during nuclear envelope damage. In this instance, we used the inner nuclear membrane protein LEMD2 and the ESCRT-III scaffolding protein CHMP7. We showed that LEMD2 is the first to localize at the site of nuclear envelope rupture, followed by CHMP7 at a second stage. This is in agreement with the nuclear repair theories that identify BAF as the initial responder and recruiter of LEM-domain proteins like LEMD2, which then facilitates the subsequent recruitment of CHMP7 and ESCRT-III (Halfmann and Roux, 2021; Gu et al., 2017; Young et al., 2020). Additionally, we found that the quantity of CHMP7 is closely related to the amount of LEMD2, as evidenced by the trends in the volume-over-time curves for these proteins. In this case, we focused solely on the primary nucleus since an additional non-canonical LEMD2-CHMP7 binding that might bias the results has been described at micronuclei (Di Bona et al., 2024).

This method can be used to characterize treatments and inhibitors that might affect nuclear envelope repair proteins, by comparing their mobility or quantity. Similarly, we envisage this method to also be applicable in studying the dynamics of DNA-sensing cytoplasmic proteins, such as cGAS, and to test its separation of function mutant (i.e., DNA binding vs. cyclase). Finally, we believe this technique could provide a platform for testing the effects of various treatments on the probability of rupture. For example, it can be used to assess the propensity of micronuclei or primary nuclei to rupture after shorter laser exposure under conditions affecting lipid stability. In fact, users could replicate the experiments we performed to characterize the method (Figure 1F) and calculate the probability of rupture by varying parameters such as the velocity of bleaching, under control or treated conditions.

In conclusion, our work presents a new pipeline, easily implementable on any confocal microscope, for precisely

studying protein behavior immediately after nuclear envelope rupture. This method allowed us to shed light on the crucial but poorly characterized process of micronuclear repair. Moreover, by demonstrating the method's applicability in studying the sequential recruitment of proteins, we have paved the way for extensive research on primary and micronuclei envelope rupture and repair. This will enhance our understanding of the mechanisms underlying micronuclear irreversible collapse and potentially offer ways to reverse it, with significant implications for the treatment of chromosomally unstable tumors.

Data availability statement

The original contributions presented in the study are included in the article/Supplementary Material; further inquiries can be directed to the corresponding author.

Author contributions

MD: conceptualization, data curation, formal analysis, investigation, methodology, project administration, resources, validation, visualization, writing–original draft, and writing–review and editing. SB: funding acquisition and writing–review and editing.

Funding

The authors declare that financial support was received for the research, authorship, and/or publication of this article. MD is supported by an American-Italian Cancer Foundation Post-Doctoral Research Fellowship. For SB, we acknowledge NIH DP5OD026395, NCI P50CA247749, R01CA256188-01, the Congressionally Directed Medical Research Program, Burroughs Wellcome Fund, Josie Robertson Foundation, and Mark Foundation for Cancer Research.

Acknowledgments

The authors thank members of the Bakhoum Lab and Dr. Pablo Guasp Baratech at Memorial Sloan Kettering Cancer Center for useful discussions and feedbacks. The authors thank staff at the MSKCC molecular cytology core facilities and media preparation.

Conflict of interest

SB owns equity in, receives compensation from, serves as a consultant to, and serves on the scientific advisory board and board of directors of Volastra Therapeutics and serves on the scientific advisory board of Meliora Therapeutics.

The remaining author declares that the research was conducted in the absence of any commercial or financial relationships that could be construed as a potential conflict of interest.

Publisher's note

All claims expressed in this article are solely those of the authors and do not necessarily represent those of their affiliated organizations, or those of the publisher, the editors, and the reviewers. Any product that may be evaluated in this article, or claim that may be made by its manufacturer, is not guaranteed or endorsed by the publisher.

Supplementary material

The Supplementary Material for this article can be found online at: https://www.frontiersin.org/articles/10.3389/fcell.2024.1475095/full#supplementary-material

SUPPLEMENTARY FIGURE S1
Assessing micronuclei effective rupture. **(A)** Representative images of micronuclei in HeLa cells expressing NLS-RFP to which laser rupture has been applied. (Top) Micronucleus bleached, but still intact. Despite bleaching, the micronucleus is discernible in the NLS-RFP channel by increasing the contrast. (Bottom) Representative image of an effectively ruptured micronucleus. In this case, despite increasing the contrast, the micronucleus is not visible in the NLS-RFP channel, denoting effective rupture. The ROI used for bleaching (blue box) is indicated by the white arrow in the left image. Yellow arrowheads indicate the location of the micronucleus. Scale bars = 2 μm. **(B)** Schematic representation of cGAS recruitment at ruptured micronuclei. **(C)** Representative images of micronuclei in HeLa cells expressing NLS-RFP to which laser rupture has been applied. Given the slower dynamics of cGAS recruitment, we used 1 min interval between frames. (Top) Micronucleus bleached, but intact, pre and post-rupture, showing NLS-RFP (yellow) and without cGAS recruitment (blue). (Bottom) Ruptured micronucleus, characterized by loss of NLS-RFP (yellow) and by cGAS-GFP recruitment (blue). The ROI used for bleaching (blue box) is indicated by the white arrow in the left image. Yellow arrowheads indicate the location of the micronucleus. Scale bars = 2 μm. **(D)** Identification of cGAS-GFP recruitment at N = 18 micronuclei classified as ruptured or intact using the presence of NLS-RFP, validating the occurrence of the rupture event.

SUPPLEMENTARY FIGURE S2
BAF recruitment at primary nuclei. **(A)** Representative maximum intensity Z-projection of BAF-GFP recruitment at the site of primary nuclei rupture. The rupture location is indicated with a white arrow throughout the measurement, while the ROI used for bleaching (blue) is indicated only in the initial frame. Scale bar = 2 μm. **(B)** 3D reconstruction of the images shown in **(A)** (overlayed to the fluorescent original image in the background) of HeLa cells expressing BAF-GFP (blue) and NLS-RFP (yellow). The frame in which rupture is induced is highlighted in red. Scale bar = 2 μm.

SUPPLEMENTARY MOVIE S1
Representative time-lapse of BAF recruitment to the site of primary nuclear rupture. The movie is generated through ImageJ using 2 frames per second after a maximum intensity Z-projection.

SUPPLEMENTARY MOVIE S2
Representative time-lapse of BAF recruitment to the site of micronuclear rupture. The movie is generated through ImageJ, using 2 frames per second after a maximum intensity Z-projection.

References

Agustinus, A. S., Al-Rawi, D., Dameracharla, B., Raviram, R., Jones, B., Stransky, S., et al. (2023). Epigenetic dysregulation from chromosomal transit in micronuclei. *Nature* 619 (7968), 176–183. doi:10.1038/s41586-023-06084-7

Al-Rawi, D. H., Lettera, E., Li, J., DiBona, M., and Bakhoum, S. F. (2024). Targeting chromosomal instability in patients with cancer. *Nat. Rev. Clin. Oncol.* 21, 645–659. doi:10.1038/s41571-024-00923-w

Bakhoum, S. F., and Cantley, L. C. (2018). The multifaceted role of chromosomal instability in cancer and its microenvironment. *Cell* 174 (6), 1347–1360. doi:10.1016/j.cell.2018.08.027

Chen, X., Agustinus, A. S., Li, J., DiBona, M., and Bakhoum, S. F. (2024). Chromosomal instability as a driver of cancer progression. *Nat. Rev. Genet.* doi:10.1038/s41576-024-00761-7

Denais, C. M., Gilbert, R. M., Isermann, P., McGregor, A. L., Te Lindert, M., Weigelin, B., et al. (2016b). Nuclear envelope rupture and repair during cancer cell migration. *Science* 352 (6283), 353–358. doi:10.1126/science.aad7297

Denais, C. M., Gilbert, R. M., Isermann, P., Mcgregor, A. L., Weigelin, B., Davidson, P. M., et al. (2016a). Nuclear envelope rupture and repair during cancer cell migration. *Science* 352 (6283), 353–358. doi:10.1126/science.aad7297

Di Bona, M., and Bakhoum, S. F. (2024). Micronuclei and cancer. *Cancer Discov.* 14 (2), 214–226. doi:10.1158/2159-8290.CD-23-1073

Di Bona, M., Chen, Y., Agustinus, A. S., Mazzagatti, A., Duran, M. A., Deyell, M., et al. (2024). Micronuclear collapse from oxidative damage. *Science* 385 (6712), eadj8691. doi:10.1126/science.adj8691

Ettinger, A., and Wittmann, T. (2014). Fluorescence live cell imaging. *Methods Cell Biol.* 123, 77–94. doi:10.1016/B978-0-12-420138-5.00005-7

Gu, M., LaJoie, D., Chen, O. S., von Appen, A., Ladinsky, M. S., Redd, M. J., et al. (2017). LEM2 recruits CHMP7 for ESCRT-mediated nuclear envelope closure in fission yeast and human cells. *Proc. Natl. Acad. Sci. U. S. A.* 114 (11), E2166–E75. doi:10.1073/pnas.1613916114

Halfmann, C. T., and Roux, K. J. (2021). Barrier-to-autointegration factor: a first responder for repair of nuclear ruptures. *Cell Cycle* 20 (7), 647–660. doi:10.1080/15384101.2021.1892320

Halfmann, C. T., Sears, R. M., Katiyar, A., Busselman, B. W., Aman, L. K., Zhang, Q., et al. (2019). Repair of nuclear ruptures requires barrier-to-autointegration factor. *J. Cell Biol.* 218 (7), 2136–2149. doi:10.1083/jcb.201901116

Hatch, E. M., Fischer, A. H., Deerinck, T. J., and Hetzer, M. W. (2013). Catastrophic nuclear envelope collapse in cancer cell micronuclei. *Cell* 154 (1), 47–60. doi:10.1016/j.cell.2013.06.007

Hatch, E. M., and Hetzer, M. W. (2016). Nuclear envelope rupture is induced by actin-based nucleus confinement. *J. Cell Biol.* 215 (1), 27–36. doi:10.1083/jcb.201603053

Ippolito, M. R., Martis, V., Martin, S., Tijhuis, A. E., Hong, C., Wardenaar, R., et al. (2021). Gene copy-number changes and chromosomal instability induced by aneuploidy confer resistance to chemotherapy. *Dev. Cell* 56 (17), 2440–2454.e6. doi:10.1016/j.devcel.2021.07.006

Kono, Y., Adam, S. A., Sato, Y., Reddy, K. L., Zheng, Y., Medalia, O., et al. (2022). Nucleoplasmic lamin C rapidly accumulates at sites of nuclear envelope rupture with BAF and cGAS. *J. Cell Biol.* 221 (12), e202201024. doi:10.1083/jcb.202201024

Li, J., Hu, B., Fang, L., Gao, Y., Shi, S., He, H., et al. (2018). Barrier-to-autointegration factor 1: a novel biomarker for gastric cancer. *Oncol. Lett.* 16 (5), 6488–6494. doi:10.3892/ol.2018.9432

Liu, T. L., Upadhyayula, S., Milkie, D. E., Singh, V., Wang, K., Swinburne, I. A., et al. (2018). Observing the cell in its native state: imaging subcellular dynamics in multicellular organisms. *Science* 360 (6386), eaaq1392. doi:10.1126/science.aaq1392

Maciejowski, J., and Hatch, E. M. (2020). Nuclear membrane rupture and its consequences. *Annu. Rev. Cell Dev. Biol.* 36, 85–114. doi:10.1146/annurev-cellbio-020520-120627

Mackenzie, K. J., Carroll, P., Martin, C. A., Murina, O., Fluteau, A., Simpson, D. J., et al. (2017). cGAS surveillance of micronuclei links genome instability to innate immunity. *Nature* 548 (7668), 461–465. doi:10.1038/nature23449

Martin, S., Scorzoni, S., Cordone, S., Mazzagatti, A., Beznoussenko, G. V., Gunn, A. L., et al. (2024). A p62-dependent rheostat dictates micronuclei catastrophe and chromosome rearrangements. *Science.* 385 (6712), eadj7446. doi:10.1126/science.adj7446

Mohr, L., Toufektchan, E., von Morgen, P., Chu, K., Kapoor, A., and Maciejowski, J. (2021). ER-directed TREX1 limits cGAS activation at micronuclei. *Mol. Cell* 81 (4), 724–738.e9. doi:10.1016/j.molcel.2020.12.037

Olmos, Y., Hodgson, L., Mantell, J., Verkade, P., and Carlton, J. G. (2015). ESCRT-III controls nuclear envelope reformation. *Nature* 522 (7555), 236–239. doi:10.1038/nature14503

Penfield, L., Wysolmerski, B., Mauro, M., Farhadifar, R., Martinez, M. A., Biggs, R., et al. (2018). Dynein pulling forces counteract lamin-mediated nuclear stability during nuclear envelope repair. *Mol. Biol. Cell* 29 (7), 852–868. doi:10.1091/mbc.E17-06-0374

Raab, M., Gentili, M., De Belly, H., Thiam, H. R., Vargas, P., Jimenez, A. J., et al. (2016). ESCRT III repairs nuclear envelope ruptures during cell migration to limit DNA damage and cell death. *Science* 352 (6283), 359–362. doi:10.1126/science.aad7611

Sears, R. M., and Roux, K. J. (2020). Diverse cellular functions of barrier-to-autointegration factor and its roles in disease. *J. Cell Sci.* 133 (16), jcs246546. doi:10.1242/jcs.246546

Tang, S., Stokasimov, E., Cui, Y., and Pellman, D. (2022). Breakage of cytoplasmic chromosomes by pathological DNA base excision repair. *Nature* 606 (7916), 930–936. doi:10.1038/s41586-022-04767-1

Thaller, D. J., Allegretti, M., Borah, S., Ronchi, P., Beck, M., and Lusk, C. P. (2019). An ESCRT-LEM protein surveillance system is poised to directly monitor the nuclear envelope and nuclear transport system. *Elife* 8, e45284. doi:10.7554/eLife.45284

Vargas, J. D., Hatch, E. M., Anderson, D. J., and Hetzer, M. W. (2012). Transient nuclear envelope rupturing during interphase in human cancer cells. *Nucleus* 3 (1), 88–100. doi:10.4161/nucl.18954

Vietri, M., Schultz, S. W., Bellanger, A., Jones, C. M., Petersen, L. I., Raiborg, C., et al. (2020). Unrestrained ESCRT-III drives micronuclear catastrophe and chromosome fragmentation. *Nat. Cell Biol.* 22 (7), 856–867. doi:10.1038/s41556-020-0537-5

von Appen, A., LaJoie, D., Johnson, I. E., Trnka, M. J., Pick, S. M., Burlingame, A. L., et al. (2020). LEM2 phase separation promotes ESCRT-mediated nuclear envelope reformation. *Nature* 582 (7810), 115–118. doi:10.1038/s41586-020-2232-x

Willan, J., Cleasby, A. J., Flores-Rodriguez, N., Stefani, F., Rinaldo, C., Pisciottani, A., et al. (2019). ESCRT-III is necessary for the integrity of the nuclear envelope in micronuclei but is aberrant at ruptured micronuclear envelopes generating damage. *Oncogenesis* 8 (5), 29. doi:10.1038/s41389-019-0136-0

Young, A. M., Gunn, A. L., and Hatch, E. M. (2020). BAF facilitates interphase nuclear membrane repair through recruitment of nuclear transmembrane proteins. *Mol. Biol. Cell* 31 (15), 1551–1560. doi:10.1091/mbc.E20-01-0009

frontiers | Frontiers in Cell and Developmental Biology

TYPE Review
PUBLISHED 09 October 2024
DOI 10.3389/fcell.2024.1480571

Check for updates

OPEN ACCESS

EDITED BY
Bhawana Bissa,
Central University of Rajasthan, India

REVIEWED BY
Denis Firsanov,
University of Rochester, United States
Qinghua Zeng,
Southern Research Institute, United States
Fengsheng Li,
PLA Rocket Force Characteristic Medical Center, China
Ningbo Liu,
Tianjin Medical University, China

*CORRESPONDENCE
Ying Xin,
xiny@jlu.edu.cn
Xin Jiang,
jiangx@jlu.edu.cn

†These authors have contributed equally to this work

RECEIVED 14 August 2024
ACCEPTED 24 September 2024
PUBLISHED 09 October 2024

CITATION
Liu C, Wei J, Wang X, Zhao Q, Lv J, Tan Z, Xin Y and Jiang X (2024) Radiation-induced skin reactions: oxidative damage mechanism and antioxidant protection.
Front. Cell Dev. Biol. 12:1480571.
doi: 10.3389/fcell.2024.1480571

COPYRIGHT
© 2024 Liu, Wei, Wang, Zhao, Lv, Tan, Xin and Jiang. This is an open-access article distributed under the terms of the Creative Commons Attribution License (CC BY). The use, distribution or reproduction in other forums is permitted, provided the original author(s) and the copyright owner(s) are credited and that the original publication in this journal is cited, in accordance with accepted academic practice. No use, distribution or reproduction is permitted which does not comply with these terms.

Radiation-induced skin reactions: oxidative damage mechanism and antioxidant protection

Chuchu Liu[1,2,3†], Jinlong Wei[1,2,3†], Xuanzhong Wang[1,2,3], Qin Zhao[1,2,3], Jincai Lv[1,2,3], Zining Tan[4], Ying Xin[4*] and Xin Jiang[1,2,3*]

[1]Jilin Provincial Key Laboratory of Radiation Oncology and Therapy, The First Hospital of Jilin University and College of Basic Medical Science, Jilin University, Changchun, China, [2]Department of Radiation Oncology, The First Hospital of Jilin University, Changchun, China, [3]NHC Key Laboratory of Radiobiology, School of Public Health of Jilin University, Changchun, China, [4]Key Laboratory of Pathobiology, Ministry of Education and College of Basic Medical Science, Jilin University, Changchun, China

According to official statistics, cancer remains the main reason of death and over 50% of patients with cancer receive radiotherapy. However, adverse consequences after radiation exposure like radiation-induced skin reactions (RISR) have negative or even fatal impact on patients' quality of life (QoL). In this review we summarize the mechanisms and managements of RISRs, a process that involve a variety of extracellular and intracellular signals, among which oxidative stress (OS) are now commonly believed to be the initial part of the occurrence of all types of RISRs. As for the management of RISRs, traditional treatments have been widely used but without satisfying outcomes while some promising therapeutic strategies related to OS still need further researches. In the context we discuss how OS leads to the happening of RISRs of different types, hoping it can shed some light on the exploration of new countermeasures.

KEYWORDS

radiation-induced skin reactions, mechanism, oxidative stress, treatment, antioxidant

1 Introduction

Radiotherapy is widely used in clinic as the main means of controlling malignant tumors (Chandra et al., 2021). However, while the tumors are under effective control, the surrounding normal tissues and organs may be damaged to varying degrees due to the influence of radiation. Radiation-induced skin reactions (RISRs) is one of the main complications caused by radiation (Wei et al., 2019a). It usually occurs in the thin and wrinkled parts of the skin such as neck, armpit and groin. Radiation directly damages not only the skin but also its deep tissue cells, causing dryness, loss of elasticity, pigmentation, soft tissue fibrosis, capillary dilatation, and radiation dermatitis in irradiated areas (Yang et al., 2020), which often has a great impact on the course of radiotherapy, thus affecting the treatment effect of patients. Long-term sequelae will affect the QoL of patients (Bray et al., 2016).

RISRs can be divided into acute RISRs and chronic RISRs according to the onset time. Acute RISRs are caused by one or multiple large doses of external radiation in a short period of time, including acute erythema and desquamation (Yang et al., 2020; Hegedus et al., 2017). Chronic RISRs are delayed adverse reactions that typically takes months to years to develop after exposure to ionizing radiation. Chronic RISRs include chronic ulcers, fibrosis,

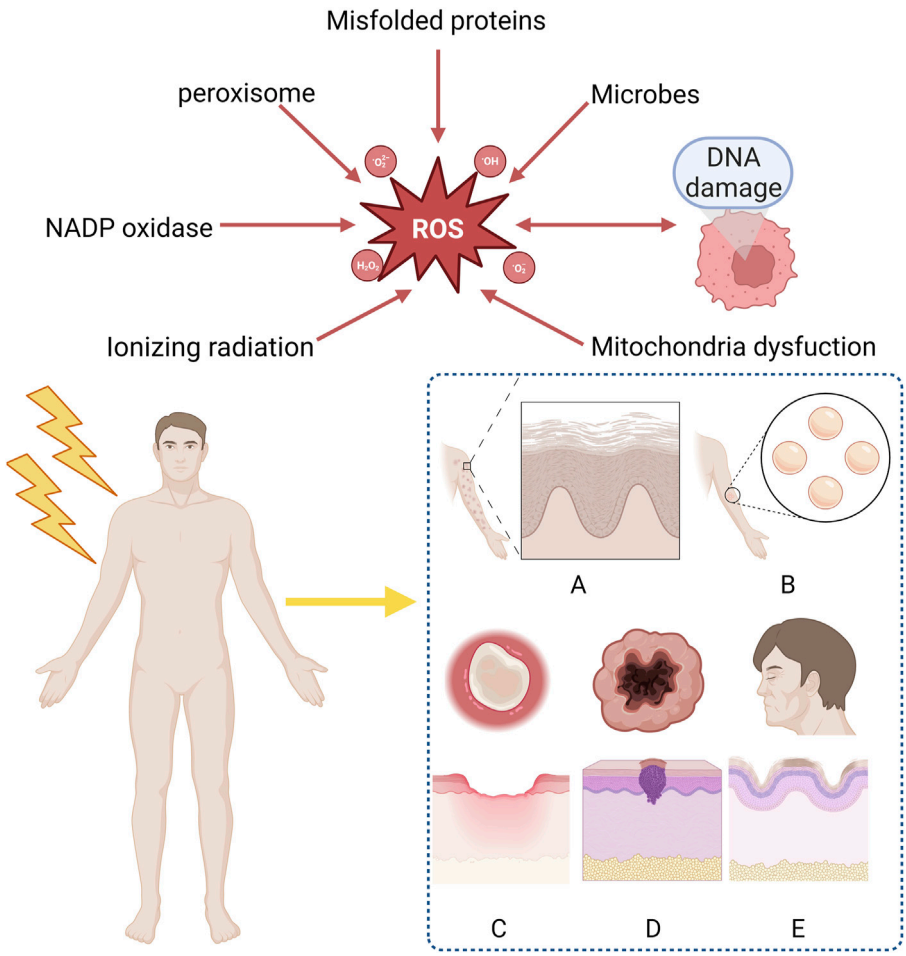

FIGURE 1
Clinical manifestation of radiation-induced skin reactions and sources of ROS. ROS mainly derive form ionizing radiation, mitochondria dysfunction, DNA damage, microbes, misfolded proteins, peroxisome, NADP oxidase and are considered as the reason why RISRs occur. Acute RISRs include acute erythema and bluster while chronic RISRs include chronic ulcers, fibrosis, skin aging and carcinogenesis. (RISRs: Radiation-induced skin reactions; ROS: Reactive oxygen species; NADP: Nicotinamide-adenine dinucleotide phosphate).

telangiectasia and skin carcinogenesis (Martin et al., 2016). This review aims at summarizing the oxidative stress mechanisms related to RISRs in order to search for potential targets of antioxidant treatments (Figure 1).

2 Oxidative stress mechanism

Oxidative damage is the major causes of RISR (Xue et al., 2021). OS is a situation when steady-state reactive oxygen species (ROS) concentration is transiently or chronically enhanced, disturbing cellular metabolism and its regulation and damaging cellular constituents (Lushchak, 2011). It is highly associated with the inflammation response (Mittal et al., 2014). ROS/RNS (reactive nitrogen species) includes superoxide, nitrogen oxide, hydrogen peroxide, hydroxyl radicals, peroxynitrite, etc. Based on the different types of RISRs, we analyzed the mechanisms of radiation-induced skin damage, fibrosis, skin carcinogenesis and skin aging respectively in the following paragraphs (Figure 1).

2.1 Radiation-induced skin damage

Radiation-induced skin damage, also known as acute forms of radiation dermatitis, occur within days to weeks, usually arise within 90 days. The most frequent symptoms are primary transient erythema, generalized erythema, skin dryness, hair loss, hyperpigmentation, dry desquamation, skin scaling and flaking and moist desquamation (Hegedus et al., 2017). From the molecular biology perspective, radiation causes skin injury by directly or indirectly damaging DNA and cellular structure. In other words, radiation-induced skin damage is the consequence of direct tissue injury in conjunction with local inflammatory reactions, including reduction and impairment of functional stem cells, endothelial cell changes, release of inflammatory factors, epidermal cell apoptosis and necrosis. IR can directly interact with DNA or indirectly through radiolysis of water. Exposure of DNA to IR can cause many different types of damage, and these damages can be roughly divided into DNA base damages, DNA single strand breaks (SSBs), and DNA double strand breaks (DSBs), with DSBs being considered the most dangerous type (Melia and

Parsons, 2023). Even more tricky is that DNA damages caused by IR often does not occur singly, but rather generate clustered/complex DNA damage (CDD), containing two or more DNA lesions within one or two helical turns of the DNA. CDD is composed of various types of DNA damage, among which DSBs are the simplest form of CDD site (Wilkinson et al., 2023). Electron transfer or singlet molecular oxygen produced by radiation targets DNA base guanine, giving rise to 8-hydroxydeoxyguanosine (8-OHdG), a ubiquitous maker of OS, in the strand DNA (Ichihashi et al., 2003). After irradiation, the number of hydrogen molecule and hydroxyl (free radical) molecule in cells increases, causing the two-thirds of radiation-induced DNA damage (Sanche, 2009). The 2 hydroxyl molecules will recombine and form hydrogen peroxide, which is highly unstable, and then the hydrogen peroxide readily combines in the cell to form organic hydrogen peroxides molecule, which is stable. At this point, the radiation damage is "fixed" to the cells, resulting in the loss of an essential enzyme in the cell which could lead to cell death or a future mutation of the cell (Brown and Rzucidlo, 2011). Basically the extensive production of ROS and their fixation behavior on cells are the initial parts of almost all kinds of RISRs, gradually damaging human skin as time goes by.

When irradiated, the early inflammatory response mainly manifests as the increase of pro-inflammatory cytokines (IL-1, IL-3, IL-5, IL-6, tumor necrosis factor TNF-α) and chemokines (IL-8) (Wei et al., 2018). These factors can activate neutrophils and produce ROS, thus lead to the damage of skin tissue and protective barriers. TNF-a, IL-6, and IL-1 are involved in the inflammatory response. When combined with receptors respectively, they can activate NK-κB through varies of ways and upregulate COX2, which eventually increase the number of ROS (Cheki et al., 2018). COX-2 can mediate the excessive production of arachidonic acids (such as prostaglandins and thromboxanes). When the levels of these AAs increase, tissues can become inflamed within hours and may last for weeks, occurring in various organs and tissues including the skin, such as the lungs, bones, and joints. Under normal physiological conditions, COX-2 is almost non-existent in most tissues of the body and only appears locally under inflammatory stimulation. Overexpression may lead to radiation resistance. Based on the above points, nonsteroidal anti-inflammatory drugs (NSAIDs) targeting COX-2 have good clinical potential for treating RISRs (Laube et al., 2016; Laube et al., 2013). The increasing ROS will result in genetical changes, DNA damage and mitochondria dysfunction (Yahyapour et al., 2018). Mitochondrial dysfunction typically included impaired respiratory chain function, structural abnormalities, depletion of cell ATP pool, disrupted cellular signaling and increased mitochondria-derived ROS (mtROS) generation (Dong et al., 2023). These mtROS will in turn induce OS and mitochondrial dysfunction. Besides, mitochondrial membrane integrity might be damaged during this process, releasing mitochondrial ligands or damage-associated molecular patterns (DAMPs), exacerbating the situation (Dela Cruz and Kang, 2018; Marchi et al., 2023). TGF-β also plays important role in radiation-induced skin damage, it has the function of wound healing, proliferation, differentiation of multiple cell types and synthesis of extracellular matrix proteins in inflammatory response of normal tissue. In the process of RISRs, TGF-β and platelet-derived growth factor (PDGF) can regulate fibroblast activity and promote the production of extracellular matrix proteins (Bentzen, 2006; Pohlers et al., 2009). Combined with its receptor, TGF-β upregulate the expression of miRNA-21, thus inhibit the superoxide dismutase 2 (SOD2), an important factor that eliminates ROS (Farhood et al., 2019) (Figure 2).

In conclusion, ionizing radiation induces the production and aggregation of ROS, leading to cell apoptosis or necrosis, thereby activating immune cells to produce a large number of inflammatory factors. When bound with corresponding receptors, these inflammatory factors activate the NF-κB pathway thus upregulating COX expression and ultimately produce more ROS, further leading to DNA damage and mitochondrial dysfunction. These signals and pathways stated above will not just function in the happening of radiation-induced skin damage as different types of RISRs are more like phased manifestations at different time points rather than individual reactions. As we know, when irradiation lasts for a period of time, acute RISRs would develop into chronic RISRs with radiation-induced skin fibrosis (RIF) being the most representative of which. In the next part, we will illustrate the mechanism of RIF.

2.2 Radiation-induced skin fibrosis

Radiation-induced skin fibrosis refers to a harmful chronic disease that appears weeks to years after radiation (Straub et al., 2015). When long-term ionizing radiation exposure causes damage to collagen fibers in the dermis of the skin, hardening of the skin and mucous membranes, RIF happens. It is a multicellular process involving the interaction of various cellular systems in skin tissue (Rodemann and Bamberg, 1995). The release of ROS, microvascular injury, recruitment of inflammatory cells, and activation of myofibroblasts all take part in the process of RIF (Wang et al., 2020), among which ROS play a significant role mainly through two pathways.

One way is through a positive feedback regulation mechanism with TGF-β. When skin tissue is irradiated, monocytes, macrophages, fibroblasts, keratinocytes and many other cells will release IL-1, which will eventually increase the level of ROS in cells. ROS can activate TGF-β signal. The activated TGF-β then stimulates the Smad signaling cascade reaction, which in turn promotes ROS production by upregulating the transcription of NOX4 of NADPH, thereby a positive feedback regulation mechanism has been established between ROS and TGF-β (Richter et al., 2015; Derynck and Zhang, 2003). Ionizing radiation induces the demethylation of CpG dinucleotides in exon 1 of the Zrt-and Irt-like protein 9 (ZIP9), then recruit the transcription factor Sp 1 to promote ZIP9 expression. Overexpression of ZIP9 activates the TGF- β/Smad signaling pathway and proceed the development of RIFs (Qiu et al., 2020). Besides, human stromal cell-derived factor-1 α (SDF-1α) used to be thought as a key chemokine in the happening of diabetic nephropathy, but recently Zhang et al. found that it is also involved in radiation-induced skin damage and fibrosis as well (Cao et al., 2019). Briefly speaking, the SDF-1α/CXCR4 axis can promote the pro-fibrotic TGF-β/Smad signaling through PI3K-MAPK signaling cascade in human keratinocyte HaCaT cells and skin fibroblast WS1 cells, thus lead to skin fibrosis (Zhang et al., 2013). The other is through the disturbance of epigenetic

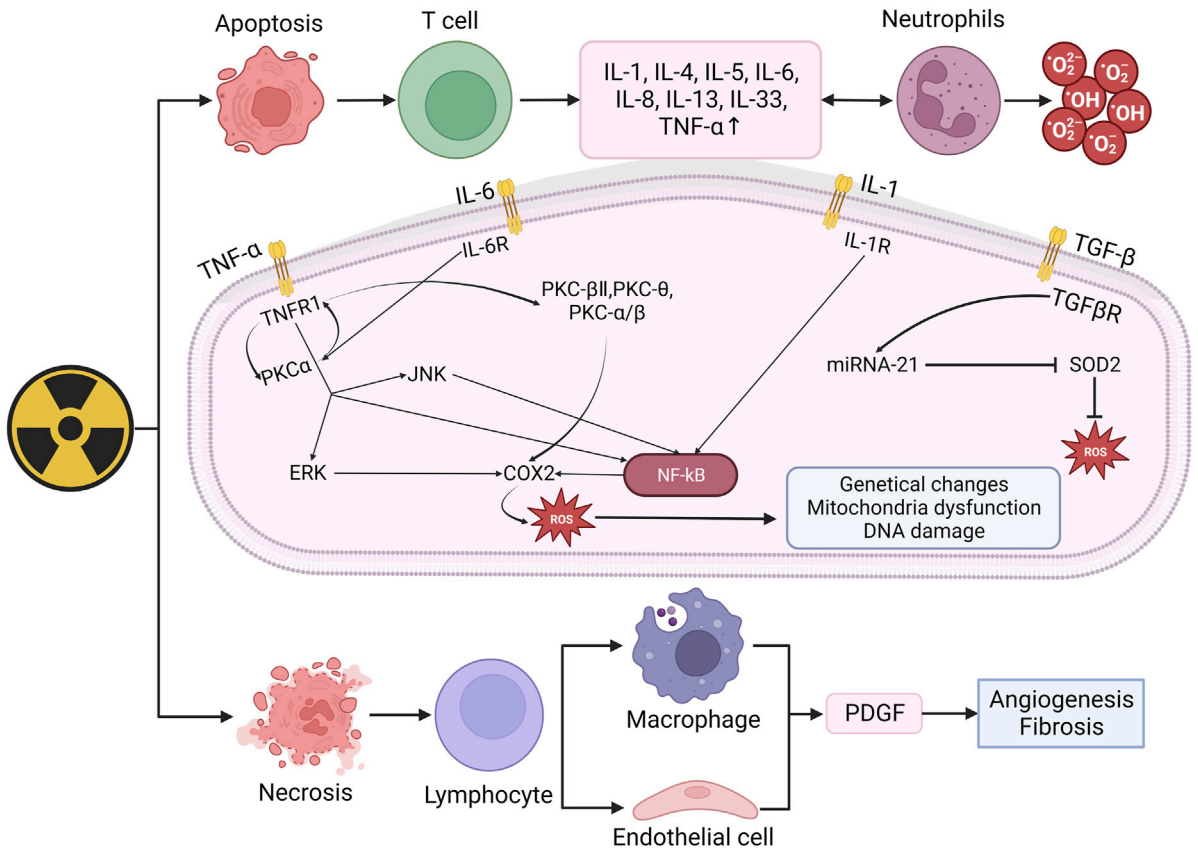

FIGURE 2
Mechanism of radiation-induced skin damage and OS. Radiation leads to apoptosis and necrosis and then upregulate the expression of IL-1, IL-4, IL-5, IL-6, IL-8, TNF-α. When combined with receptors respectively, these factors can activated NK-κB and eventually increase ROS. The increasing ROS may result in genetical changes, DNA damage and mitochondira dysfunction, thus lead to skin damage. (IL: Interleukin; TNF-α: Tumor necrosis factor: TGF-β, Transforming growth factor beta; PKC: Protein kinase C; ERK: Extracellular regulated protein kinases; JNK: c-Jun N-terminal kinase; NF-kB: Nuclear factor kB; SOD2: Superoxide dismutase 2; PDGF: Platelet-derived growth factor).

modification. As stated above, when irradiated, the mitochondrial ROS will increase and change concentration of epigenetic metabolites, leading to modifications of the cellular epigenome (Yamamori et al., 2017) (Figure 3A).

Wnt/β-catenin is another classical profibrotic pathway. Inhibition of this pathway has been found to attenuate radiation-induced skin fibrosis through inhibiting the transformation of epithelial and endothelial cells into myofibroblasts (Lee et al., 2020). Microvascular injury may also be responsible for the occurrence of RIFs. After irradiation, the subendothelial Extracellular matrix (ECM) component is exposed to platelets, which promotes excessive secretion of von Willebrand factor (vWF), tissue factor and platelet activation factor (PAF), while reducing the production of NO, prostacyclin and transmembrane glycoprotein thrombomodulin (TM) and its fibrinolytic activity. These changes eventually trigger an antifibrinolytic-coagulation cascade effect, causing coagulation and vascular occlusion, accelerating the process of RIF (Soloviev et al., 2003) (Figure 3B).

In short, ionizing radiation-induced overexpression of ZIP9 activated the TGF-β/Smad signaling and upregulates NOX, thus leading to extensive production of ROS. These overproduced ROS then activates collagen genes resulting the occurrence of skin fibrosis. Besides, IR can activate platelet and fibroblast through Wnt/β-catenin and TGF-β, causing vascular occlusion and fibrosis. Based on what've been discussed above, it is not hard for us to find that OS and TGF-β play the plays a dominant role in the occurrence and development of RIF, leaving us the curiosity to go deeply into the potential of antioxidants and TGF-β targeted drugs in management of RISRs.

2.3 Radiation-induced skin carcinogenesis

Ultraviolet (UV) radiation contributes to the development of skin carcinogenesis through direct and indirect DNA damage, production of reactive oxygen species and local immunomodulation (Thompson and Kim, 2020). Cellular injury resulting from excessive ROS generation represents a consequence of interference with cellular membranes, proteins and DNA, changing the overall biological activities. As a result of these actions, oxidative products with mutagenic properties are formed, initiating the process of carcinogenesis within epidermal cells (Allegra et al., 2020; Ciążyńska et al., 2021). ROS are able to modify several pathways that are activated in tumors, including the activating protein-1 pathway, epidermal growth factor receptor, NF-κB, mitogen-activated protein kinase/extracellular signal-

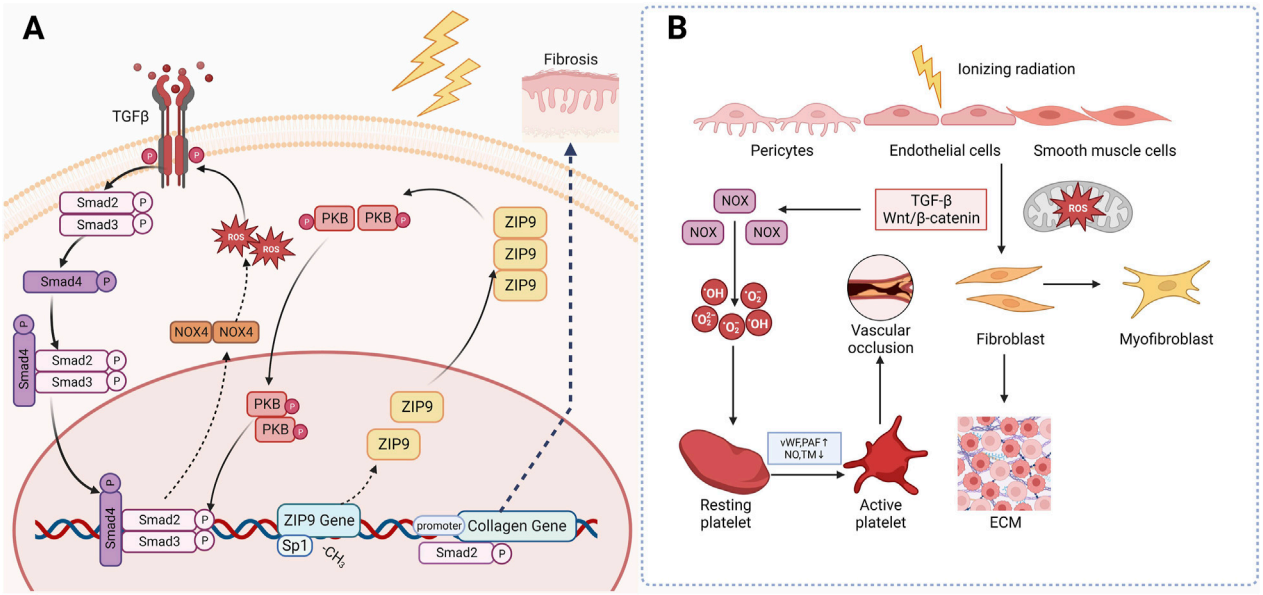

FIGURE 3
Mechanism of radiation-induced skin fibrosis and OS. **(A)**: Ionizing radiation induces the expression of ZIP9 and overexpression of ZIP9 activates the TGF- β/Smad signaling pathway and proceed the development of RIFs. **(B)**: Wnt/β-catenin is another classical profibrotic pathway that can induce the transformation of epithelial and endothelial cells into myofibroblasts. (TGF-β: Transforming growth factor beta; NOX4: NADPH oxidase 4; PKB: Protein Kinase B; ZIP9: Zrt-and Irt-like protein 9; vWF: Von Willebrand factor; PAF: Platelet activation factor; TM: Thrombomodulin).

regulated kinase (MAPK/ERK), and p38 MAPK (Hammouda et al., 2020; van Hogerlinden et al., 1999; Loercher et al., 2004).

After irradiation, mutations accumulated in NOD-like receptor thermal protein domain associated protein1 (NLRP1) gene cause changes in the structures of domains, resulting in the formation of oligomers of NLRP1 and the activation of inflammasomes (Ciazynska et al., 2020), which can promote the production of caspase1, thus upregulating the expression of IL-1β and IL-18. These NLRP1-dependent production of IL-1β and IL-18 may contribute to the process of skin carcinogenesis (Ciazynska et al., 2020; King et al., 2019). It is also suspected that NLRP1 may involve in radiation-induced skin carcinogenesis by inhibiting the caspase-2/9-mediated apoptotic pathway (Zhai et al., 2017). Recently, NLPR3 has also been found to be a new approach to skin carcinogenesis (Wei et al., 2019b).

Radiation aryl hydrocarbon receptor (AHR) signaling is also responsible to radiation-induced skin carcinogenesis. AHR accelerates the process of RISRs as a sensitizer for it increases after irradiation and expression of mRNA and protein of both cytochrome P450 1A1 and cytochrome P450 1B1 in the epidermis are enhanced, upregulating the bioactivation of environmental pollutants, thereby making human skin more susceptible to radiation-induced skin cancers or dermatitis (Katiyar et al., 2000). The global genome repair (GGR) and apoptosis in epidermal keratinocytes (KC) are repressed (Pollet et al., 2018) after exposure to UV and sensitivity of cells to PAH-mediated DNA adduct formation increase (Nair et al., 2009), ultimately contributes to skin photo carcinogenesis. Octinoxate, an inhibitor of cytochrome 1A1 (CYP1A1) and cytochrome 1B1 (CYP1B1), can elevate CYP1A1 and CYP1B1 mRNA levels in mouse and thus modulate AHR signaling, indicating that it might exhibit protective effect on human skin. Topical application of BDDI (E/Z-2-benzylidene-5,6-dimethoxy-3,3-dimethylindan-1-one), a type of AHR antagonist, can significantly reduce the UVB-induced expression of carcinogenic genes (Tigges et al., 2014). Beta HPVs are another risk factors of skin carcinogenesis since it can promote proliferation and circumvent cellular stresses via the E6 and E7 oncoproteins when being irradiated (Tommasino, 2019) (Figure 4).

Carcinogenesis is a complicated process that involves multiple factors, pathways and so on. In this context, we briefly summarize the mechanism related to HPV infection and NLRP3 inflammasome. Although the frequency of radiation-induced skin carcinogenesis is not that high as other types of RISRs, its negative impact on patient survival and QoL is profound and significant, which is worthy of our attention. Unfortunately, due to its rarity and the complexity of its mechanisms, there are not many existing research results, further explorations still need to be done.

2.4 Radiation-induced skin aging

Aging is a natural intrinsic process associated with the loss of fibrous tissue, slower cell turnover and reduction in immune system competence. Many factors contribute to akin aging, among which the most significant one is ultraviolet radiation. Skin aging events are initiated and often propagated by oxidation events though invisible to naked eyes (D'Arino et al., 2023; Kammeyer and Luiten, 2015). The effects of skin damage caused by UV radiation produce injuries that are mainly invisible to the naked eye (Silva Acosta et al., 2021). Both intrinsic (proliferative exhaustion and telomere shortening)

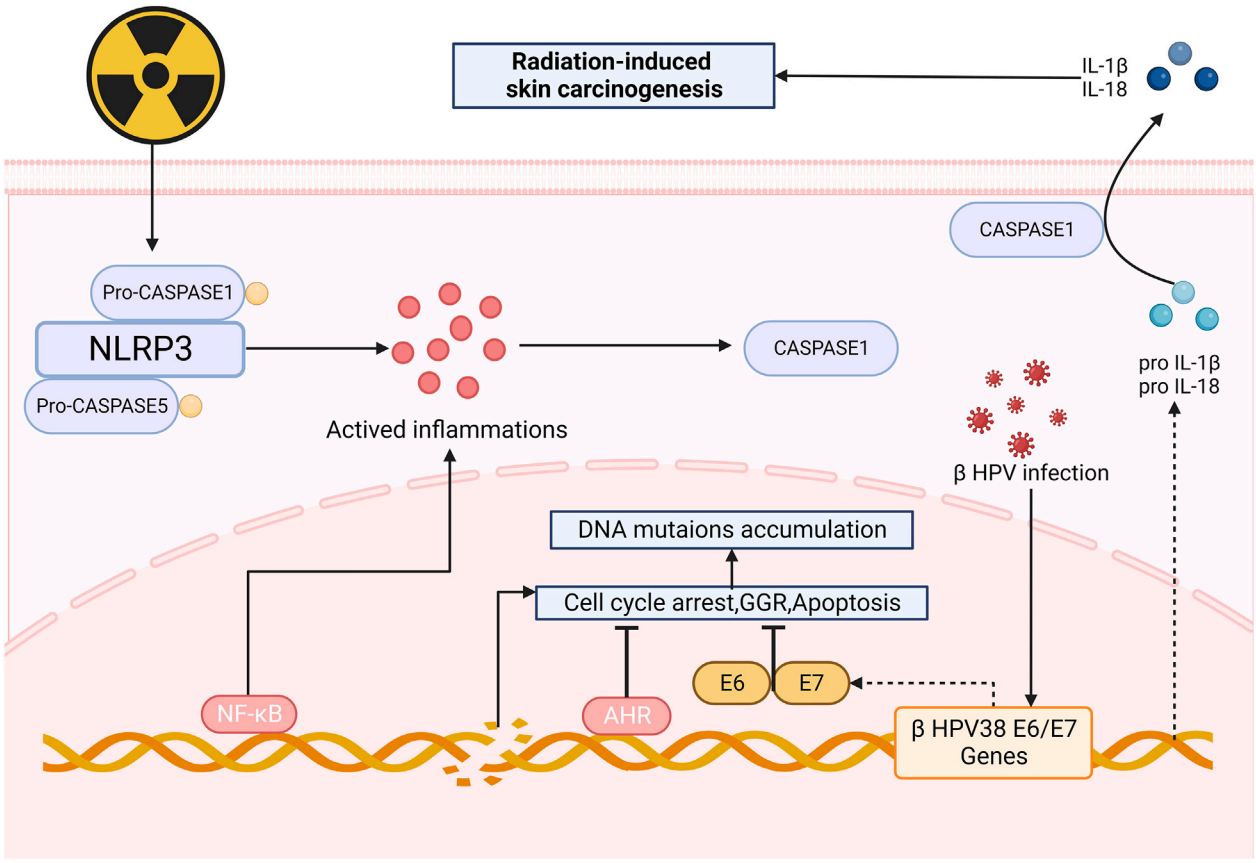

FIGURE 4
Mechanism of radiation-induced skin carcinogenesis and OS. After irradiation, the formation of oligomers of NLRP1 and the activation of inflammasomes can promote the production of caspase1, upregulating the expression of IL-1β and IL-18, thus leading to skin carcinogenesis. AHR and HPVs also take part in skin carcinogenesis, serving as facilitators. (NLRP3: Nucleotide-binding domain and leucine-rich-repeatcontaining family pyrin 3; AHR: radiation aryl hydrocarbon receptor; IL-1β: Interleukin-1β; GGR: Global genome repair).

and extrinsic stresses as well as the activation of oncogenes can lead to cellular senescence (Lee et al., 2021). How do extrinsic stresses cause skin ageing? One of the core mechanisms mediating skin aging lie in the OS induced by the accumulation of ROS, which can lead to lipid, protein, nucleic acid damage, thus leading to the occurrence of cellular senescence (Gu et al., 2020). Photoaging is mainly caused by repeated exposure to UVA radiation. To be more specific, the increased ROS levels will result in DNA damage, collagen degradation and release of inflammatory corpuscles. Besides, ROS can cause destructive OS, activating the arachidonic acid pathway and mediating inflammatory responses (Gu et al., 2020).

Radiation induced DNA damage response (DDR) leads to stimulating p38/MAPK/PKC/NF-κB, contributing to increased intracellular ROS, thus activating the Cyclin-dependent kinase inhibitor 2 A (CDKN2 A) locus, producing p16 INK4A (p16) and p19 INK4D (ARF). p16 INK4A can activate the retinoblastoma protein (pRb) tumor suppressor, then blocks certain proliferative genes by heterochromatinization. Ultimately durable cell-cycle arrest was induced (Nguyen et al., 2018). Besides, UV radiation induced ROS can lead to the phosphorylation and subsequent activation of c-Jun N-terminal kinases. These activated kinases then activate the c-Jun and c-Fos components of the transcription factor activator protein-1 (AP-1), increasing the expression of elastolytic matrixmetallo proteinase (MMPs) (Fitsiou et al., 2021). Saguie et al. found that after irradiation, expression of inflammatory cells, collagenolytic and MMPs increases while elastin expression decreases, thus leading to photoaging (Saguie et al., 2021). MMPs are highly expressed in UV-induced senescent KCs in culture (e.g., MMP-1) and in the epidermis of irradiated human skin samples (e.g., MMP-1, MMP-3, and MMP-9) (Dong et al., 2008; Quan et al., 2009). Proinflammatory cytokines such as TNF-α, IL-1α, IL-1β, and IL-6 also increase in UV-induced senescent KCs (Bashir et al., 2009).

Skin pigmentation is one of the main symptoms of skin aging, which is mainly caused by intracellular melanin deposition. UV radiation-induced DNA damage in keratinocytes activates p53 which initiates the transcription of proopiomelanocortin and subsequently peptides including α-melanocyte-stimulating hormone (α-MSH) are formed. These peptides then combined with MC1R on melanocytes to induce microphthalmia transcription factor (MITF), activating melanogenesis (Lee et al., 2021) (Figure 5).

Many hormone-like mediators are involved in the process of photoaging. For example, level of prostaglandin E2 (PGE-2)

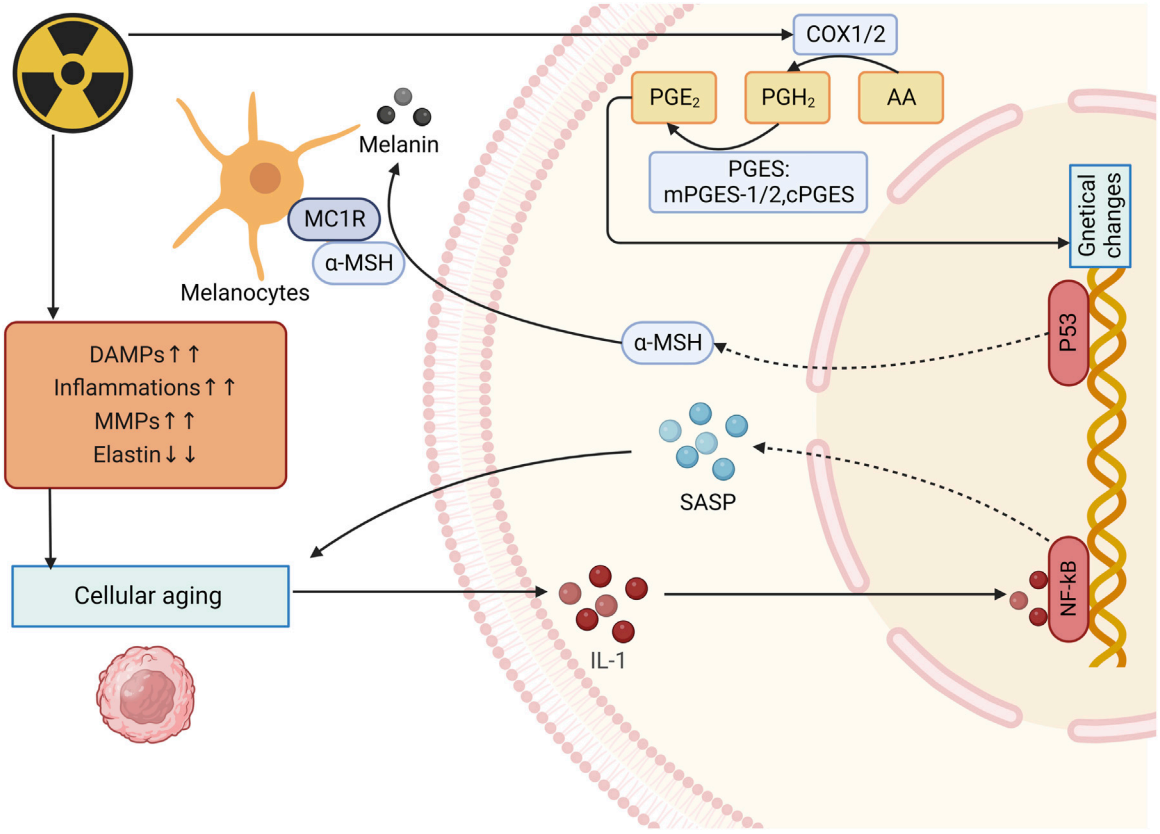

FIGURE 5
Mechanism of radiation-induced skin aging and OS. After irradiation, expression of inflammatory cells, collagenolytic and elastolytic matrixmetallo proteinase (MMPs) increases while elastin expression decreases, thus leading to photoaging and increase of IL-1expression. IL-1 upregulates SASP expression and enhance the photoaging. UV radiation-induced DNA damage activates p53 and eventully activates melanogenesis. (DAMPs: Damage-associated molecular patterns; MMPs: Matrixmetallo proteinases; PGE2: prostaglandin E2; SASP: Senescence-associated secretory phenotype; α-MSH: α-melanocyte-stimulating hormone).

increases quickly when skin is exposed to UVR, causing changes in genetical changes and eventually lead to cell dysfunction (Fuller, 2019) (Figure 5). Biskanaki et al. (2021) found that skin collagen type I (COL I) decreases during aging, even more in photoaging, which indicates that radiation can reduce skin COL I expression and contributes to negative impacts on the skin. Besides, when photoaging occurs, IL-1 expression is upregulated and it can bind to IL-1 receptor/Toll-like receptors to activate NF-κB, thereby increasing the expression of SASP (Gu et al., 2020; Chang et al., 2002). Furthermore, senescence-associated secretory phenotype (SASP) can promote the malignant transformation of adjacent recipient cells, leading to the occur of inflammation, diseases and cells aging (Campisi et al., 2011).

The release of SASP, α-MSH and PGE-2 has a lot to do with the happening of radiation-induced skin aging. The mechanism of radiation-induced skin aging shares many similarities with skin cancer, because skin aging can be seen as a precursor to skin cancer despite the fact that not all skin aging ultimately develops into skin cancer, the relationship between these two is still inseparable. Deeply studying the mechanism of radiation induced skin aging can help identify treatment for managing RISRs and improve patient QoL, besides, provide insights into the pathogenesis of skin cancer.

3 Antioxidant protection

3.1 Antioxidant drugs

Early in 1963, people have realized the effectiveness of corticosteroids in healing RISRs (Jackson, 1963). Corticosteroids have the abilities of anti-inflammatory, reversing the skin related decline in QoL and prohibiting radiation-induced cytokine proliferation (Schmuth et al., 2002a; HARUNA et al., 2017; Hymes et al., 2006), making it exhibit protective effect on skin. Topical usage of corticosteroids has proven be effective in reducing eczema peeling, frequency of serious skin toxicity and delaying the occurrence of grade 1 to 3 dermatitis (HARUNA et al., 2017). However, there is still controversy over whether routine steroid local therapy should be given to patients receiving radiation therapy and its optimal timing of application. The results of three related trials did not show that steroid local therapy can prevent the occurrence of RISR (Glees et al., 1979; Miller et al., 2011; Løkkevik et al., 1996; Yokota et al., 2021; Zenda et al., 2018). Only a small trial of 20 people observed effective differences, indicating that corticosteroids may not be an effective means of preventing RISR (Halnan, 1962). A large clinical trial showed that topical application of 0.1% mometasone furoate cream was not superior to placebo in reducing the maximum

TABLE 1 Antioxidant protections of RISRs.

Methods	Mechanism	Reference
Antioxidant Drugs		
Corticosteroids	Prohibit radiation-induced cytokine proliferation	Haruna et al. (2017)
Trolamine emulsionis	Act as macrophage cell stimulators	Abbas and Bensadoun (2012)
Sucralfate	Act as a mechanical barrier with antibacterial, anti-inflammatory function	Le et al. (2024)
Heme oxygenase-1(HO-1)	Share antioxidant and antiapoptotic properties	Zhang et al. (2012)
Injections of MnSOD	Inhibit of Ferroptosis	Wang et al. (2024)
Antioxidant Materials		
3M barrier film	Reduce friction and irritation	Shaw et al. (2015)
HBOT	Inhibit the TGF-β pathway	Spiegelberg et al. (2014); Pandey et al. (2022)
Triethanolamine cream	Facilitate microcirculation	Yang et al. (2020)
Antioxidant Cytokines and Vesicles		
Sulforaphane (SFN)	Upregulate the expression and function of Nrf2	Wei et al. (2021)
Interleukins (ILs)	Reduce the retention of cutaneous dendritic cells	Gerber et al. (2015)
T-cell protein tyrosine phosphatase	Inhibit Smad2 nuclear translocation	Morales et al. (2019)
Superoxide dismutase (SOD)	Antioxidants that clear ROS	Choung et al. (2004); Pudlarz et al. (2020); Yu et al. (2019)
Aryl hydrocarbon receptor (AHR)	Reduce the UVB-induced expression of fibrosis gene	Tigges et al. (2014)

RISR level or RISR level at 2 weeks after treatment, while two small trials showed that steroid topical treatment was effective in reducing RISR levels (Schmuth et al., 2002b). Nonsteroidal drugs such as hyaluronic acid (HA) and zanzanamine lotion also have some therapeutic effects. HA is a type of carbohydrate polymer. Topical applied HA creams has been suggested to be protective against ROS damage caused by radiation in animal researches. Whether it can help with alleviating human skin injuries remain unclear, for one study found that it reduced the incidence of high-grade RD while the other witnessed more severe dermatitis. Whether it can be used in patients who received RT still need further researches. Trolamine emulsion have similar effect. Serving as macrophage cell stimulators, they are able to remove necrotic tissue, promote fibroblast proliferation, reduce vascular alterations, restore CD34 expression, promote epithelial cell proliferation, and decrease IL-1 expression and collagen secretion (Hymes et al., 2006). Abbas et al. demonstrated that when used in patients who accepted radiation therapy, Trolamine emulsion indeed significantly reduced the intensity of acute dermatitis by its non-steroidal anti-inflammatory properties and ability to recruit macrophages to the wound bed and promote the production of granulation tissue (Abbas and Bensadoun, 2012). 2-Methoxyestradio may also be a potential therapeutic agent for RISRs as it can repair the damaged vessels on the irradiated dermal skin, inhibit endothelial HIF-1 alpha expression and fibrotic changes and accumulate DNA damage in irradiated human dermal microvascular endothelial cells (Kim et al., 2022) (Tables 1, 2).

Ascorbic acid, also known as vitamin C, possesses powerful antioxidant and free radical scavenging qualities. Unfortunately, the benefit of topical ascorbic acid in human being has not been demonstrated yet (Rosenthal et al., 2019), but it seems to have a promising future. Vitamin E also has similar antioxidant properties. Delinasios et al. (2018) found that the use of vitamin E before or after RT can reduce the formation of oxidative purine and cyclobutane pyrimidine dimers (CPD), which supports the use of vitamin E to reduce side effects in patients receiving RT. The effects of antioxidants such as vitamin C and vitamin E are very extensive and powerful. In the past, they often acted through oral administration. They have the characteristic of reducing the formation of CPD, which may still enable them to have effective preventive and therapeutic effects. When added as additives to topical medications such as sun protection.

In recent news, ferroptosis, a form of cell death caused by ROS overload, has been found to be involved in the occurrence of RISRs. Radiation exposure could induce the accumulation of lipid peroxides in human skin keratinocytes, resulting in intracellular Fe2+ overload by regulating the levels of iron exporter ferroportin (FPN) (Su et al., 2022). According to this discovery, local Multiple-site injections of a plasmid harboring human MnSOD may exert protective in patients following RT by inhibiting ferroptosis (Wang et al., 2024). Transdermal delivery of the iron chelator deferoxamine (DFO) can improve tissue perfusion and mitigates chronic RIF (Shen et al., 2020; Lavin et al., 2021). Heme oxygenase-1 (HO-1), the rate-limiting enzyme in heme catabolism, has been reported to have potential antioxidant and antiapoptotic properties, making them potential to be used in alleviating RISRs (Zhang et al., 2012). Similarly, topically applied fibronectin has been found to significantly improve wound healing in irradiated skin due to its effect of decreasing inflammatory infiltrate and increasing angiogenesis (Johnson et al., 2017).

These drugs mentioned above all have antioxidant effects or anti-inflammatory to varying degrees, but currently, most of the

TABLE 2 Clinical trials of antioxidant protection.

Clinical trials	Registration number	Person in charge	Cases	Protocol (study vs. control)	Results
CSMed wound dressing for radiation dermatitis	NCT06001463	Lee et al. (Lee et al., 2024)	30	Half of the irradiated area was covered with CSMed® and the other half was under routine treatment.	CSMed® dressed area had significant lower RTOG score during and after RT than undressed area.
KeraStat(R) cream for radiation dermatitis	NCT03559218	Karen et al. (Winkfield et al., 2024)	25	Study: KeraStat cream for twice daily application; control: standard of care.	The rate of RTOG Grade 2 RD was lower in the study group (30.8%) compared to the control group (54.5%, $P = 0.408$).
Silver-nylon dressing (Silverlon®) to reduce radiation dermatitis	NCT04238728	Julie et al.	31	Silver nylon dressing will be applied daily	3.6% (1/28) patients reported severe adverse skin event and mean healthcare professional assessment scale (HPAS) was 6.31 (95% CL = 5.47–6.94).
Photobiomodulation and photodynamic therapy for the treatment of oral mucositis	—	Erika et al. (Pires Marques et al., 2020)	56	Control: low-level laser applied in the oral cavity; study: additionally gave photosensitizing mouthwash and blue LED.	Both groups observed significant reductions in OM grade ($p < 0.0001$), while study group resulted in a shorter time to resolution of lesions ($p = 0.0005$).
Dakin's solution in preventing radiation dermatitis	NCT02203565	Kathleen et al. (Hejazi et al., 2016)	20	Tropically applied Dakin's solution daily during RT for up to 6 weeks.	15% (3/20) patients experienced grade 3/4 radiation dermatitis.
Oral curcumin for radiation dermatitis	NCT01246973	Julie et al. (Ryan Wolf et al., 2018)	68	Study: curcumin C3 complex (2.0 g) taken orally 3 times/day control: Placebo.	Curcumin did not reduce radiation dermatitis severity (B (95% CI) = 0.044 (- 0.101, 0.188), $p = 0.552$).
Effect of curcumin supplementation during radiotherapy on oxidative status	NCT01917890	Jalal et al. (Ertekin et al., 2004)	40	Study: curcumin capsules (BCM95, Biocurcumin); control: placebos (roasted rice flour of 500 mg).	No significant differences were observed between the 2 groups regarding treatment outcomes.
Oral glutamine on radiation dermatitis	NCT03015077	Huang et al. (Huang et al., 2019)	71	Study: oral glutamine (5 g glutamine and 10 g maltodextrin); control: placebo (15 g maltodextrin).	No difference was found in the incidence and severity of neck dermatitis between the two arms.
Bacterial decolonization for prevention of radiation dermatitis	NCT03883828	Yana et al. (Kost et al., 2023)	80	Study: intranasal mupirocin ointment twice daily and chlorhexidine body cleanser; control: standard of care.	The mean ARD grade was significantly lower for BD group compared with standard of care (1.2 vs. 1.6) ($P = 0.02$).
Topical superoxide dismutase in posttreatment fibrosis	—	Kelly et al. (Landeen et al., 2018)	68	Study: 280 IU/g SOD to the area of fibrosis twice daily control: placebo lotion.	46.4% of study group improved by 1 or more ranks on the CTCAE v4.0 scale, compared to 43.3% of control group.
Oral zinc sulphate on anti-oxidant enzyme activities	—	Ertekin et al. (Ertekin et al., 2004)	30	Study: zinc sulphate capsules (including 50 mg zinc) three times a day; control: placebo.	No difference was detected in any final measurement activities of erythrocyte anti-oxidant enzymes in the direct comparison between two groups.
Phase 3 randomized trial of topical steroid versus placebo for prevention of radiation dermatitis		Tomoya et al. (Yokota et al., 2021)	211	Study: topical steroid when grade 1radiation dermatitis was observed or the total radiation dose reached 30 Gy control: placebo	

more widely used traditional drugs can only alleviate symptoms. New drugs that can truly cause inhibit RISRs from the beginning are either not widely available or are still in the experimental stage. As we gradually establish a deeper understanding of the mechanism of radiation damage, we have found that more and more cytokines, signaling pathways, and other factors are involved. It is possible to achieve the goal of inhibiting RISRs by developing drugs targeting these factors in the future.

3.2 Antioxidant materials

3M barrier can reduce friction and irritation, especially in skin folds and thin areas. A completed observational clinical study from the United States (NCT03546803) showed that the 3M Avilon advanced skin protector can to some extent prevent radiation dermatitis in cancer patients, indicating that using the 3M barrier at the beginning of radiotherapy is a possible method for preventing RISRs (Table 1).

A non-randomized study has confirmed that the RISR was significantly lower in the group receiving the sucralfate gel, highlighting the benefit of sucralfate humid gel in alleviating RISRs. Sucralfate humid gel is the colloidal physical form of the anti-ulcer drug sucralfate, which can form a protective layer, increase bicarbonate production, exhibit anti-peptic effects, and promote tissue growth, regeneration and repair (Le et al., 2024). Similarly, triethanolamine cream, a compound preparation with good hydration, has the ability to drain and cleans the skin, reduce patients' skin dryness, decrease body inflammation and edema response, facilitate patients' body microcirculation and enhance skin tolerance, making it a useful protection in management of RISRs (Yang et al., 2020).

Evoskin and Trixiera are two topical moisturizing and repairing creams, and their effectiveness was compared in a completed clinical trial by a French research team (NCT02334345). The research team included women with cancer who received 50 Gy breast radiation therapy in a prospective randomized trial. Patients used Evoskin in half of the irradiated breasts and Triesiera in the other half, and the results showed that Evoskin was more effective than Trixiera. This indicates that the use of Evoskin is highly recommended for patients undergoing radiation therapy. Similarly, a randomized phase III study (NCT00876642) evaluated the efficacy of aloe vera cream in preventing grade 2 or higher acute radiation dermatitis during postoperative radiotherapy for cancer. However, although many pilot studies have shown that aloe gel has antioxidant and anti-inflammatory properties, it may not be effective for the prevention or treatment of radiation adverse reactions in breast cancer patients, and may only be effective for some patients with cumulative radiation doses greater than 27 Gy and acute radiation proctitis (Farrugia et al., 2019).

Other potential ways of improving RISRs resulted from RT include hyperbaric oxygen therapy (HBOT), surgery, transplantation of endothelial cells and so on. HBOT function mainly through suppressing the TGF-β expression (Spiegelberg et al., 2014). Safra et al. suggested that HBOT be a safe and effective countermeasure to radiation-induced late side-effects (Safra et al., 2008) and particularly can also improve skin elasticity in patients with RIF (Pandey et al., 2022). The future of transplantation of stromal vascular fraction (SVF) in addressing RISRs is promising (Yu et al., 2021). A recruited clinical study conducted by a team from Boston, United States is investigating how to use epidermal skin grafts to improve radiation wound healing (NCT04560803). They mainly use CelluTome, an epidermal transplant system, to form epidermal vesicles to cover the wound, and evaluate the efficacy of epidermal grafts collected using the CelluTome device.

Local application of materials that can achieve antioxidant effects can also help alleviate RISR, such as using 3M barriers, HBOT, and various cell transplants. These materials mainly exert therapeutic effects by establishing barriers, clearing ROS, and inhibiting inflammatory factors. With the continuous development of radiation therapy technology, serious skin reactions have become very rare. Therefore, although studies have shown that cell transplantation can alleviate severe RISR and its clinical application is limited, this does not mean that this research direction is unnecessary. Because RISR shares common mechanisms with other skin diseases, which means that the up-to-date treatment of RISR may also provide ideas for the treatment of other skin diseases, making it a very promising research direction.

3.3 Antioxidant cytokines and vesicles

Interleukins (ILs) are closely involved in multiple steps in the occurrence and development of RISRs. Among which IL-12 has been recognized as a potential mitigator of RISRs by an American team since it can reduce the retention of cutaneous dendritic cells, slow down transepidermal water loss and minimize burn size (Gerber et al., 2015). As stated above, NLRP1 and NLRP3 activation plays a significant role in the happening of RISRs by upregulating the expression and function of Nrf2 and causing OS. Sulforaphane (SFN) may be able to prevent and alleviate RISRs by inhibiting these actions (Wei et al., 2021) (Table 1).

Tetrahydrobiopterin (BH4), also known as Sapropterin, is an important cofactor of nitric oxide synthase (NOS), and guanosine triphosphate hydrolase 1 (GCH1) is a key enzyme in the synthesis of BH4. Overexpression of GCH1 can restore BH4 levels and NO products in irradiated skin cells, reverse and inhibit NOS uncoupling caused by ionizing radiation, thereby eliminating ROS induced by ionizing radiation and reducing DNA damage (Spencer et al., 2005; Schallreuter et al., 1994a; Schallreuter et al., 1994b; Feng et al., 2021; Kraft et al., 2020). In animal experiments, direct subcutaneous injection of BH4 can not only reduce the severity of acute radiation skin injury, but also promote skin repair, reduce the occurrence of radiation skin fibrosis, and maintain normal physiological functions of the skin. In order to explore the efficacy and safety of tetrahydrobiopterin in the treatment of human radiation dermatitis, a related clinical study is being recruited (NCT05114226). The main observation endpoint is the incidence rate of acute radiation dermatitis.

Superoxide dismutase (SOD) is an antioxidant enzyme with multiple metal cofactors that can specifically clear ROS, which plays an important role in a variety of ultraviolet-induced lesions. Therefore, SOD has the anti-ultraviolet radiation effect (Chen et al., 2023; Choung et al., 2004; Pudlarz et al., 2020). The total flavonoids of boxthorn leaves improve resistance to RISRs by regulating SOD level in the skin of mice (Yu et al., 2019). A clinical trial has seen witnessed regression of fibrosis through 2-month follow-up in 34 patients treated with sixintramuscular injections of SOD over a 3-week period (Delanian et al., 1994), directly confirmed the protective role in anti-RISRs. SOD can been regarded as the most representing example of antioxidants functioning in skin protection from radiation, and presents us with faith in exploring more antioxidants to address the side effect of RT.

Antioxidant cytokines and vesicles, whether artificial or natural, can help alleviate RISRs by clearing ROS and inhibiting inflammatory cells. At the same time, mitochondrial dysfunction is one of the important reasons for ROS aggregation, making many mitochondrial targeted antioxidant cytokines a prospective countermeasure to RISRs. Many of these factors are extracted from herbs, indicating that herbs have great potential for RISRs management. However, we still need to explore the specific components in herbs that actually exert therapeutic effects for it

can not only help us understand the mechanism of RISRs, but also avoid unnecessary loads caused by other impurities in herbs as much as possible.

4 Conclusion

In this review we summarize the mechanism of each type of RISRs and briefly conclude some countermeasures. Although traditional treatments like topical steroids, creams, and ointments have been widely used in clinics to alleviate RISRs, they are only symptomatic treatment with unsatisfactory effect. We still need more clinical trials and studies to validate the effectiveness and safety of innovative treatments like antioxidants to prevent the happening of RISRs from the root cause, and to achieve that, further studies focused on the mechanisms of RISRs and corresponding targeting drugs are urgently demanding.

Author contributions

CL: Data curation, Writing–review and editing. JW: Methodology, Writing–review and editing. XW: Visualization, Writing–review and editing. QZ: Investigation, Writing–review and editing. JL: Software, Writing–review and editing. ZT: Formal Analysis, Writing–review and editing. YX: Resources, Validation, Writing–review and editing. XJ: Funding acquisition, Project administration, Supervision, Writing–review and editing.

Funding

The author(s) declare that financial support was received for the research, authorship, and/or publication of this article. This research was funded by Jilin Province Medical and Health Talents Special Foundation (grant numbers: JLSWSRCZX2023-68), The First Hospital of Jilin University Talent Reserve Program (grant numbers: JDYY-TRP-2024012), Jilin Provincial Science and Technology Foundation (grant numbers: 20230508064RC), Jilin Province Medical and Health Talents Special Foundation (grant numbers: JLSWSRCZX2020-064) and Jilin Provincial Department of Education Key Foundation (grant numbers: JJKH20241337KJ).

Conflict of interest

The authors declare that the research was conducted in the absence of any commercial or financial relationships that could be construed as a potential conflict of interest.

Publisher's note

All claims expressed in this article are solely those of the authors and do not necessarily represent those of their affiliated organizations, or those of the publisher, the editors and the reviewers. Any product that may be evaluated in this article, or claim that may be made by its manufacturer, is not guaranteed or endorsed by the publisher.

References

Abbas, H., and Bensadoun, R. J. (2012). Trolamine emulsion for the prevention of radiation dermatitis in patients with squamous cell carcinoma of the head and neck. *Support. Care Cancer* 20 (1), 185–190. doi:10.1007/s00520-011-1110-3

Allegra, A., Pioggia, G., Tonacci, A., Musolino, C., and Gangemi, S. (2020). Oxidative stress and photodynamic therapy of skin cancers: mechanisms, challenges and promising developments. *Antioxidants (Basel)* 9 (5), 448. doi:10.3390/antiox9050448

Bashir, M. M., Sharma, M. R., and Werth, V. P. (2009). UVB and proinflammatory cytokines synergistically activate TNF-alpha production in keratinocytes through enhanced gene transcription. *J. Investigative Dermatology* 129 (4), 994–1001. doi:10.1038/jid.2008.332

Bentzen, S. M. (2006). Preventing or reducing late side effects of radiation therapy: radiobiology meets molecular pathology. *Nat. Rev. Cancer* 6 (9), 702–713. doi:10.1038/nrc1950

Biskanaki, F., Rallis, E., Skouras, G., Stofas, A., Thymara, E., Kavantzas, N., et al. (2021). Impact of solar ultraviolet radiation in the expression of type I collagen in the dermis. *Cosmetics* 8 (2), 46. doi:10.3390/cosmetics8020046

Bray, F. N., Simmons, B. J., Wolfson, A. H., and Nouri, K. (2016). Acute and chronic cutaneous reactions to ionizing radiation therapy. *Dermatol Ther. (Heidelb).* 6 (2), 185–206. doi:10.1007/s13555-016-0120-y

Brown, K. R., and Rzucidlo, E. (2011). Acute and chronic radiation injury. *J. Vasc. Surg.* 53 (1 Suppl. l), 15S-21S–21s. doi:10.1016/j.jvs.2010.06.175

Campisi, J., Andersen, J. K., Kapahi, P., and Melov, S. (2011). Cellular senescence: a link between cancer and age-related degenerative disease? *Seminars Cancer Biol.* 21 (6), 354–359. doi:10.1016/j.semcancer.2011.09.001

Cao, J., Zhu, W., Yu, D., Pan, L., Zhong, L., Xiao, Y., et al. (2019). The involvement of SDF-1α/CXCR4 Axis in radiation-induced acute injury and fibrosis of skin. *Radiat. Res.* 192 (4), 410–421. doi:10.1667/RR15384.1

Chandra, R. A., Keane, F. K., Voncken, F. E. M., and Thomas, C. R., Jr (2021). Contemporary radiotherapy: present and future. *Lancet* 398 (10295), 171–184. doi:10.1016/S0140-6736(21)00233-6

Chang, B. D., Swift, M. E., Shen, M., Fang, J., Broude, E. V., and Roninson, I. B. (2002). Molecular determinants of terminal growth arrest induced in tumor cells by a chemotherapeutic agent. *Proc. Natl. Acad. Sci. U. S. A.* 99 (1), 389–394. doi:10.1073/pnas.012602599

Cheki, M., Yahyapour, R., Farhood, B., Rezaeyan, A., Shabeeb, D., Amini, P., et al. (2018). COX-2 in radiotherapy: a potential target for radioprotection and radiosensitization. *Curr. Mol. Pharmacol.* 11 (3), 173–183. doi:10.2174/1874467211666180219102520

Chen, D., Ai, X., Li, Y., Li, Y., Ao, Y., Rong, J., et al. (2023). Protective effects of Cu/Zn-SOD and Mn-SOD on UVC radiation-induced damage in NIH/3T3 cells and murine skin. *Acta histochem.* 125 (4), 152030. doi:10.1016/j.acthis.2023.152030

Choung, B. Y., Byun, S. J., Suh, J. G., and Kim, T. Y. (2004). Extracellular superoxide dismutase tissue distribution and the patterns of superoxide dismutase mRNA expression following ultraviolet irradiation on mouse skin. *Exp. Dermatol* 13 (11), 691–699. doi:10.1111/j.0906-6705.2004.00209.x

Ciazynska, M., Bednarski, I. A., Wodz, K., Narbutt, J., and Lesiak, A. (2020). NLRP1 and NLRP3 inflammasomes as a new approach to skin carcinogenesis. *Oncol. Lett.* 19 (3), 1649–1656. doi:10.3892/ol.2020.11284

Ciążyńska, M., Olejniczak-Staruch, I., Sobolewska-Sztychny, D., Narbutt, J., Skibińska, M., and Lesiak, A. (2021). Ultraviolet radiation and chronic inflammation-molecules and mechanisms involved in skin carcinogenesis: a narrative review. *Life (Basel)* 11 (4), 326. doi:10.3390/life11040326

D'Arino, A., Caputo, S., Eibenschutz, L., Piemonte, P., Buccini, P., Frascione, P., et al. (2023). Skin cancer microenvironment: what we can learn from skin aging? *Int. J. Mol. Sci.* 24 (18), 14043. doi:10.3390/ijms241814043

Dela Cruz, C. S., and Kang, M.-J. (2018). Mitochondrial dysfunction and damage associated molecular patterns (DAMPs) in chronic inflammatory diseases. *Mitochondrion* 41, 37–44. doi:10.1016/j.mito.2017.12.001

Delanian, S., Baillet, F., Huart, J., Lefaix, J. L., Maulard, C., and Housset, M. (1994). Successful treatment of radiation-induced fibrosis using liposomal Cu/Zn superoxide dismutase: clinical trial. *Radiother. Oncol.* 32 (1), 12–20. doi:10.1016/0167-8140(94)90444-8

Delinasios, G. J., Karbaschi, M., Cooke, M. S., and Young, A. R. (2018). Vitamin E inhibits the UVAI induction of "light" and "dark" cyclobutane pyrimidine dimers, and oxidatively generated DNA damage, in keratinocytes. *Sci. Rep.* 8 (1), 423. doi:10.1038/s41598-017-18924-4

Derynck, R., and Zhang, Y. E. (2003). Smad-dependent and Smad-independent pathways in TGF-beta family signalling. *Nature* 425 (6958), 577–584. doi:10.1038/nature02006

Dong, K. K., Damaghi, N., Picart, S. D., Markova, N. G., Obayashi, K., Okano, Y., et al. (2008). UV-induced DNA damage initiates release of MMP-1 in human skin. *Exp. Dermatol.* 17 (12), 1037–1044. doi:10.1111/j.1600-0625.2008.00747.x

Dong, Z., Wu, L., and Hong, H. (2023). Mitochondrial dysfunction in the pathogenesis and treatment of oral inflammatory diseases. *Int. J. Mol. Sci.* 24 (20), 15483. doi:10.3390/ijms242015483

Ertekin, M. V., Koç, M., Karslioğlu, I., Sezen, O., Taysi, S., and Bakan, N. (2004). The effects of oral zinc sulphate during radiotherapy on anti-oxidant enzyme activities in patients with head and neck cancer: a prospective, randomised, placebo-controlled study. *Int. J. Clin. Pract.* 58 (7), 662–668. doi:10.1111/j.1368-5031.2004.00006.x

Farhood, B., Goradel, N. H., Mortezaee, K., Khanlarkhani, N., Salehi, E., Nashtaei, M. S., et al. (2019). Intercellular communications-redox interactions in radiation toxicity; potential targets for radiation mitigation. *J. Cell Commun. Signal* 13 (1), 3–16. doi:10.1007/s12079-018-0473-3

Farrugia, C. E., Burke, E. S., Haley, M. E., Bedi, K. T., and Gandhi, M. A. (2019). The use of aloe vera in cancer radiation: an updated comprehensive review. *Complement. Ther. Clin. Pract.* 35, 126–130. doi:10.1016/j.ctcp.2019.01.013

Feng, Y., Feng, Y., Gu, L., Liu, P., Cao, J., and Zhang, S. (2021). The critical role of tetrahydrobiopterin (BH4) metabolism in modulating radiosensitivity: BH4/NOS Axis as an angel or a devil. *Front. Oncol.* 11, 720632. doi:10.3389/fonc.2021.720632

Fitsiou, E., Pulido, T., Campisi, J., Alimirah, F., and Demaria, M. (2021). Cellular senescence and the senescence-associated secretory phenotype as drivers of skin photoaging. *J. Invest Dermatol* 141 (4s), 1119–1126. doi:10.1016/j.jid.2020.09.031

Fuller, B. (2019). Role of PGE-2 and other inflammatory mediators in skin aging and their inhibition by topical natural anti-inflammatories. *Cosmetics* 6 (1), 6. doi:10.3390/cosmetics6010006

Gerber, S. A., Cummings, R. J., Judge, J. L., Barlow, M. L., Nanduri, J., Johnson, D. E., et al. (2015). Interleukin-12 preserves the cutaneous physical and immunological barrier after radiation exposure. *Radiat. Res.* 183 (1), 72–81. doi:10.1667/RR13802.1

Glees, J. P., Mameghan-Zadeh, H., and Sparkes, C. G. (1979). Effectiveness of topical steroids in the control of radiation dermatitis: a randomised trial using 1% hydrocortisone cream and 0.05% clobetasone butyrate (Eumovate). *Clin. Radiol.* 30 (4), 397–403. doi:10.1016/s0009-9260(79)80217-2

Gu, Y., Han, J., Jiang, C., and Zhang, Y. (2020). Biomarkers, oxidative stress and autophagy in skin aging. *Ageing Res. Rev.* 59, 101036. doi:10.1016/j.arr.2020.101036

Halnan, K. E. (1962). The effect of corticosteroids on the radiation skin reaction. A random trial to assess the value of local application of prednisolone and neomycin ointment after x-ray treatment of basal cell carcinoma. *Br. J. Radiol.* 35, 403–408. doi:10.1259/0007-1285-35-414-403

Hammouda, M. B., Ford, A. E., Liu, Y., and Zhang, J. Y. (2020). The JNK signaling pathway in inflammatory skin disorders and cancer. *Cells* 9 (4), 857. doi:10.3390/cells9040857

Haruna, F., Lipsett, A., and Marignol, L. (2017). Topical management of acute radiation dermatitis in breast cancer patients: a systematic review and meta-analysis. *Anticancer Res.* 37 (10), 5343–5353. doi:10.21873/anticanres.11960

Hegedus, F., Mathew, L. M., and Schwartz, R. A. (2017). Radiation dermatitis: an overview. *Int. J. Dermatol* 56 (9), 909–914. doi:10.1111/ijd.13371

Hejazi, J., Rastmanesh, R., Taleban, F. A., Molana, S. H., Hejazi, E., Ehtejab, G., et al. (2016). Effect of curcumin supplementation during radiotherapy on oxidative status of patients with prostate cancer: a double blinded, randomized, placebo-controlled study. *Nutr. Cancer* 68 (1), 77–85. doi:10.1080/01635581.2016.1115527

Huang, C. J., Huang, M. Y., Fang, P. T., Chen, F., Wang, Y. T., Chen, C. H., et al. (2019). Randomized double-blind, placebo-controlled trial evaluating oral glutamine on radiation-induced oral mucositis and dermatitis in head and neck cancer patients. *Am. J. Clin. Nutr.* 109 (3), 606–614. doi:10.1093/ajcn/nqy329

Hymes, S. R., Strom, E. A., and Fife, C. (2006). Radiation dermatitis: clinical presentation, pathophysiology, and treatment 2006. *J. Am. Acad. Dermatol* 54 (1), 28–46. doi:10.1016/j.jaad.2005.08.054

Ichihashi, M., Ueda, M., Budiyanto, A., Bito, T., Oka, M., Fukunaga, M., et al. (2003). UV-induced skin damage. *Toxicology* 189 (1), 21–39. doi:10.1016/s0300-483x(03)00150-1

Jackson, R. (1963). CURRENT CONCEPTS IN DERMATOLOGY. III. THE USE OF RADIOTHERAPY AND CORTICOSTEROIDS. *Can. Med. Assoc. J.* 89, 888–892.

Johnson, M. B., Pang, B., Gardner, D. J., Niknam-Benia, S., Soundarajan, V., Bramos, A., et al. (2017). Topical fibronectin improves wound healing of irradiated skin. *Sci. Rep.* 7 (1), 3876. doi:10.1038/s41598-017-03614-y

Kammeyer, A., and Luiten, R. M. (2015). Oxidation events and skin aging. *Ageing Res. Rev.* 21, 16–29. doi:10.1016/j.arr.2015.01.001

Katiyar, S. K., Matsui, M. S., and Mukhtar, H. (2000). Ultraviolet-B exposure of human skin induces cytochromes P450 1A1 and 1B1. *J. Invest Dermatol.* 114 (2), 328–333. doi:10.1046/j.1523-1747.2000.00876.x

Kim, J. H., Nam, J. K., Kim, A. R., Park, M. S., Lee, H. J., Park, J., et al. (2022). 2-Methoxyestradiol inhibits radiation-induced skin injuries. *Int. J. Mol. Sci.* 23 (8), 4171. doi:10.3390/ijms23084171

King, K. E., George, A. L., Sakakibara, N., Mahmood, K., Moses, M. A., and Weinberg, W. C. (2019). Intersection of the p63 and NF-κB pathways in epithelial homeostasis and disease. *Mol. Carcinog.* 58 (9), 1571–1580. doi:10.1002/mc.23081

Kost, Y., Deutsch, A., Mieczkowska, K., Nazarian, R., Muskat, A., Hosgood, H. D., et al. (2023). Bacterial decolonization for prevention of radiation dermatitis: a randomized clinical trial. *JAMA Oncol.* 9 (7), 940–945. doi:10.1001/jamaoncol.2023.0444

Kraft, V. A. N., Bezjian, C. T., Pfeiffer, S., Ringelstetter, L., Müller, C., Zandkarimi, F., et al. (2020). GTP cyclohydrolase 1/tetrahydrobiopterin counteract ferroptosis through lipid remodeling. *ACS Cent. Sci.* 6 (1), 41–53. doi:10.1021/acscentsci.9b01063

Landeen, K. C., Spanos, W. C., and Gromer, L. (2018). Topical superoxide dismutase in posttreatment fibrosis in patients with head and neck cancer. *Head. Neck* 40 (7), 1400–1405. doi:10.1002/hed.25119

Laube, M., Kniess, T., and Pietzsch, J. (2013). Radiolabeled COX-2 inhibitors for non-invasive visualization of COX-2 expression and activity--a critical update. *Molecules* 18 (6), 6311–6355. doi:10.3390/molecules18066311

Laube, M., Kniess, T., and Pietzsch, J. (2016). Development of antioxidant COX-2 inhibitors as radioprotective agents for radiation therapy-A hypothesis-driven review. *Antioxidants (Basel)* 5 (2), 14. doi:10.3390/antiox5020014

Lavin, C. V., Abbas, D. B., Fahy, E. J., Lee, D. K., Griffin, M., Diaz Deleon, N. M., et al. (2021). A comparative analysis of deferoxamine treatment modalities for dermal radiation-induced fibrosis. *J. Cell. Mol. Med.* 25 (21), 10028–10038. doi:10.1111/jcmm.16913

Le, Z., Ramos, M. C., Shou, Y., Li, R. R., Cheng, H. S., Jang, C. J., et al. (2024). Bioactive sucralfate-based microneedles promote wound healing through reprogramming macrophages and protecting endogenous growth factors. *Biomaterials* 311, 122700. doi:10.1016/j.biomaterials.2024.122700

Lee, D. W., Lee, W. J., Cho, J., Yun, C. O., Roh, H., Chang, H. P., et al. (2020). Inhibition of Wnt signaling pathway suppresses radiation-induced dermal fibrosis. *Sci. Rep.* 10 (1), 13594. doi:10.1038/s41598-020-70243-3

Lee, Y. C., Tseng, H. C., Yang, H. F., Lee, Y. H., Ko, Y. F., Chang, S. T., et al. (2024). CSMed(®) wound dressing for prophylaxis and management of radiation dermatitis in breast and head-neck cancer patients: a single hospital prospective clinical trial. *J. Cancer Res. Clin. Oncol.* 150 (2), 101. doi:10.1007/s00432-024-05624-6

Lee, Y. I., Choi, S., Roh, W. S., Lee, J. H., and Kim, T. G. (2021). Cellular senescence and inflammaging in the skin microenvironment. *Int. J. Mol. Sci.* 22 (8), 3849. doi:10.3390/ijms22083849

Loercher, A., Lee, T. L., Ricker, J. L., Howard, A., Geoghegen, J., Chen, Z., et al. (2004). Nuclear factor-kappaB is an important modulator of the altered gene expression profile and malignant phenotype in squamous cell carcinoma. *Cancer Res.* 64 (18), 6511–6523. doi:10.1158/0008-5472.CAN-04-0852

Løkkevik, E., Skovlund, E., Reitan, J. B., Hannisdal, E., and Tanum, G. (1996). Skin treatment with bepanthen cream versus no cream during radiotherapy--a randomized controlled trial. *Acta Oncol.* 35 (8), 1021–1026. doi:10.3109/02841869609100721

Lushchak, V. I. (2011). Environmentally induced oxidative stress in aquatic animals. *Aquat. Toxicol.* 101 (1), 13–30. doi:10.1016/j.aquatox.2010.10.006

Marchi, S., Guilbaud, E., Tait, S. W. G., Yamazaki, T., and Galluzzi, L. (2023). Mitochondrial control of inflammation. *Nat. Rev. Immunol.* 23 (3), 159–173. doi:10.1038/s41577-022-00760-x

Martin, M. T., Vulin, A., and Hendry, J. H. (2016). Human epidermal stem cells: role in adverse skin reactions and carcinogenesis from radiation. *Mutat. Res.* 770 (Pt B), 349–368. doi:10.1016/j.mrrev.2016.08.004

Melia, E., and Parsons, J. L. (2023). DNA damage and repair dependencies of ionising radiation modalities. *Biosci. Rep.* 43 (10), BSR20222586. doi:10.1042/BSR20222586

Miller, R. C., Schwartz, D. J., Sloan, J. A., Griffin, P. C., Deming, R. L., Anders, J. C., et al. (2011). Mometasone furoate effect on acute skin toxicity in breast cancer patients receiving radiotherapy: a phase III double-blind, randomized trial from the North Central Cancer Treatment Group N06C4. *Int. J. Radiat. Oncol. Biol. Phys.* 79 (5), 1460–1466. doi:10.1016/j.ijrobp.2010.01.031

Mittal, M., Siddiqui, M. R., Tran, K., Reddy, S. P., and Malik, A. B. (2014). Reactive oxygen species in inflammation and tissue injury. *Antioxidants and Redox Signal.* 20 (7), 1126–1167. doi:10.1089/ars.2012.5149

Morales, L. D., Archbold, A. K., Olivarez, S., Slaga, T. J., DiGiovanni, J., and Kim, D. J. (2019). The role of T-cell protein tyrosine phosphatase in epithelial carcinogenesis. *Mol. Carcinog.* 58 (9), 1640–1647. doi:10.1002/mc.23078

Nair, S., Kekatpure, V. D., Judson, B. L., Rifkind, A. B., Granstein, R. D., Boyle, J. O., et al. (2009). UVR exposure sensitizes keratinocytes to DNA adduct formation. *Cancer Prev. Res. (Phila)* 2 (10), 895–902. doi:10.1158/1940-6207.CAPR-09-0125

Nguyen, H. Q., To, N. H., Zadigue, P., Kerbrat, S., De La Taille, A., Le Gouvello, S., et al. (2018). Ionizing radiation-induced cellular senescence promotes tissue fibrosis after radiotherapy. A review. *Crit. Rev. Oncol. Hematol.* 129, 13–26. doi:10.1016/j.critrevonc.2018.06.012

Pandey, K., Teguh, D. N., and van Hulst, R. A. (2022). Effect of hyperbaric oxygen treatment on skin elasticity in irradiated patients. *Diving Hyperbaric Med.* 52 (3), 208–212. doi:10.28920/dhm52.3.208-212

Pires Marques, E. C., Piccolo, L. F., Nascimento, I. C., Morelli, J., Pereira, M. V., Machado Meiken, V. M., et al. (2020). Photobiomodulation and photodynamic therapy for the treatment of oral mucositis in patients with cancer. *Photodiagnosis Photodyn. Ther.* 29, 101621. doi:10.1016/j.pdpdt.2019.101621

Pohlers, D., Brenmoehl, J., Löffler, I., Müller, C. K., Leipner, C., Schultze-Mosgau, S., et al. (2009). TGF-beta and fibrosis in different organs - molecular pathway imprints. *Biochim. Biophys. Acta* 1792 (8), 746–756. doi:10.1016/j.bbadis.2009.06.004

Pollet, M., Shaik, S., Mescher, M., Frauenstein, K., Tigges, J., Braun, S. A., et al. (2018). The AHR represses nucleotide excision repair and apoptosis and contributes to UV-induced skin carcinogenesis. *Cell Death Differ.* 25 (10), 1823–1836. doi:10.1038/s41418-018-0160-1

Pudlarz, A. M., Czechowska, E., M, S. K., Ranoszek-Soliwoda, K., Tomaszewska, E., Celichowski, G., et al. (2020). The effect of immobilized antioxidant enzymes on the oxidative stress in UV-irradiated rat skin. *Nanomedicine (Lond).* 15 (1), 23–39. doi:10.2217/nnm-2019-0166

Qiu, Y., Gao, Y., Yu, D., Zhong, L., Cai, W., Ji, J., et al. (2020). Genome-wide analysis reveals zinc transporter ZIP9 regulated by DNA methylation promotes radiation-induced skin fibrosis via the TGF-β signaling pathway. *J. Invest Dermatol.* 140 (1), 94–102. doi:10.1016/j.jid.2019.04.027

Quan, T., Qin, Z., Xia, W., Shao, Y., Voorhees, J. J., and Fisher, G. J. (2009). Matrix-degrading metalloproteinases in photoaging. *J. Investigative Dermatology Symposium Proc.* 14 (1), 20–24. doi:10.1038/jidsymp.2009.8

Richter, K., Konzack, A., Pihlajaniemi, T., Heljasvaara, R., and Kietzmann, T. (2015). Redox-fibrosis: impact of TGFβ1 on ROS generators, mediators and functional consequences. *Redox Biol.* 6, 344–352. doi:10.1016/j.redox.2015.08.015

Rodemann, H. P., and Bamberg, M. (1995). Cellular basis of radiation-induced fibrosis. *Radiother. Oncol.* 35 (2), 83–90. doi:10.1016/0167-8140(95)01540-w

Rosenthal, A., Israilevich, R., and Moy, R. (2019). Management of acute radiation dermatitis: a review of the literature and proposal for treatment algorithm. *J. Am. Acad. Dermatol* 81 (2), 558–567. doi:10.1016/j.jaad.2019.02.047

Ryan Wolf, J., Heckler, C. E., Guido, J. J., Peoples, A. R., Gewandter, J. S., Ling, M., et al. (2018). Oral curcumin for radiation dermatitis: a URCC NCORP study of 686 breast cancer patients. *Support Care Cancer* 26 (5), 1543–1552. doi:10.1007/s00520-017-3957-4

Safra, T., Gutman, G., Fishlev, G., Soyfer, V., Gall, N., Lessing, J. B., et al. (2008). Improved quality of life with hyperbaric oxygen therapy in patients with persistent pelvic radiation-induced toxicity. *Clin. Oncol.* 20 (4), 284–287. doi:10.1016/j.clon.2007.12.005

Saguie, B. O., Martins, R. L., Fonseca, A. S. D., Romana-Souza, B., and Monte-Alto-Costa, A. (2021). An *ex vivo* model of human skin photoaging induced by UVA radiation compatible with summer exposure in Brazil. *J. Photochem Photobiol. B* 221, 112255. doi:10.1016/j.jphotobiol.2021.112255

Sanche, L. (2009). BIOLOGICAL CHEMISTRY beyond radical thinking. *Nature* 461 (7262), 358–359. doi:10.1038/461358a

Schallreuter, K. U., Büttner, G., Pittelkow, M. R., Wood, J. M., Swanson, N. N., and Körner, C. (1994b). Cytotoxicity of 6-biopterin to human melanocytes. *Biochem. Biophys. Res. Commun.* 204 (1), 43–48. doi:10.1006/bbrc.1994.2423

Schallreuter, K. U., Wood, J. M., Pittelkow, M. R., Gütlich, M., Lemke, K. R., Rödl, W., et al. (1994a). Regulation of melanin biosynthesis in the human epidermis by tetrahydrobiopterin. *Science* 263 (5152), 1444–1446. doi:10.1126/science.8128228

Schmuth, M., Wimmer, M. A., Hofer, S., Sztankay, A., Weinlich, G., Linder, D. M., et al. (2002a). Topical corticosteroid therapy for acute radiation dermatitis: a prospective, randomized, double-blind study. *Br. J. Dermatology* 146 (6), 983–991. doi:10.1046/j.1365-2133.2002.04751.x

Schmuth, M., Wimmer, M. A., Hofer, S., Sztankay, A., Weinlich, G., Linder, D. M., et al. (2002b). Topical corticosteroid therapy for acute radiation dermatitis: a prospective, randomized, double-blind study. *Br. J. Dermatol* 146 (6), 983–991. doi:10.1046/j.1365-2133.2002.04751.x

Shaw, S.-Z., Nien, H.-H., Wu, C.-J., Lui, L. T., Su, J.-F., and Lang, C.-H. (2015). 3M Cavilon No-Sting Barrier Film or topical corticosteroid (mometasone furoate) for protection against radiation dermatitis: a clinical trial. *J. Formos. Med. Assoc.* 114 (5), 407–414. doi:10.1016/j.jfma.2013.04.003

Shen, A. H., Borrelli, M. R., Adem, S., Deleon, N. M. D., Patel, R. A., Mascharak, S., et al. (2020). Prophylactic treatment with transdermal deferoxamine mitigates radiation-induced skin fibrosis. *Sci. Rep.* 10 (1), 12346. doi:10.1038/s41598-020-69293-4

Silva Acosta, J. L., Mendoza Santoyo, F., Flores Moreno, J. M., Hernandez Montes, M. S., De la Torre Ibarra, M. H., Frausto, G. R., et al. (2021). Study of skin aging effects induced by near UV radiation using time average digital holographic interferometry. *Opt. Lasers Eng.* 137, 106345. doi:10.1016/j.optlaseng.2020.106345

Soloviev, A. I., Tishkin, S. M., Parshikov, A. V., Ivanova, I. V., Goncharov, E. V., and Gurney, A. M. (2003). Mechanisms of endothelial dysfunction after ionized radiation: selective impairment of the nitric oxide component of endothelium-dependent vasodilation. *Br. J. Pharmacol.* 138 (5), 837–844. doi:10.1038/sj.bjp.0705079

Spencer, J. D., Chavan, B., Marles, L. K., Kauser, S., Rokos, H., and Schallreuter, K. U. (2005). A novel mechanism in control of human pigmentation by {beta}-melanocyte-stimulating hormone and 7-tetrahydrobiopterin. *J. Endocrinol.* 187 (2), 293–302. doi:10.1677/joe.1.06275

Spiegelberg, L., Swagemakers, S. M. A., van Ijcken, W. F. J., Oole, E., Wolvius, E. B., Essers, J., et al. (2014). Gene expression analysis reveals inhibition of radiation-induced tgfβ-signaling by hyperbaric oxygen therapy in mouse salivary glands. *Mol. Med.* 20, 257–269. doi:10.2119/molmed.2014.00003

Straub, J. M., New, J., Hamilton, C. D., Lominska, C., Shnayder, Y., and Thomas, S. M. (2015). Radiation-induced fibrosis: mechanisms and implications for therapy. *J. Cancer Res. Clin. Oncol.* 141 (11), 1985–1994. doi:10.1007/s00432-015-1974-6

Su, J., Bian, C., Zheng, Z., Wang, H., Meng, L., Xin, Y., et al. (2022). Cooperation effects of radiation and ferroptosis on tumor suppression and radiation injury. *Front. Cell Dev. Biol.* 10, 951116. doi:10.3389/fcell.2022.951116

Thompson, K. G., and Kim, N. (2020). Distinguishing myth from fact: photocarcinogenesis and phototherapy. *Dermatol Clin.* 38 (1), 25–35. doi:10.1016/j.det.2019.08.003

Tigges, J., Haarmann-Stemmann, T., Vogel, C. F. A., Grindel, A., Hübenthal, U., Brenden, H., et al. (2014). The new aryl hydrocarbon receptor antagonist E/Z-2-benzylindene-5,6-dimethoxy-3,3-dimethylindan-1-one protects against UVB-induced signal transduction. *J. Invest Dermatol* 134 (2), 556–559. doi:10.1038/jid.2013.362

Tommasino, M. (2019). HPV and skin carcinogenesis. *Papillomavirus Res.* 7, 129–131. doi:10.1016/j.pvr.2019.04.003

van Hogerlinden, M., Rozell, B. L., Ahrlund-Richter, L., and Toftgård, R. (1999). Squamous cell carcinomas and increased apoptosis in skin with inhibited Rel/nuclear factor-kappaB signaling. *Cancer Res.* 59 (14), 3299–3303.

Wang, B., Wei, J., Meng, L., Wang, H., Qu, C., Chen, X., et al. (2020). Advances in pathogenic mechanisms and management of radiation-induced fibrosis. *Biomed. Pharmacother.* 121, 109560. doi:10.1016/j.biopha.2019.109560

Wang, X., Lu, Y., Cheng, X., Zhu, X., Li, D., Duan, H., et al. (2024). Local multiple-site injections of a plasmid encoding human MnSOD mitigate radiation-induced skin injury by inhibiting ferroptosis. *Curr. Drug Deliv.* 21 (5), 763–774. doi:10.2174/1567201820666230508120720

Wei, J., Meng, L., Hou, X., Qu, C., Wang, B., Xin, Y., et al. (2018). Radiation-induced skin reactions: mechanism and treatment. *Cancer Manag. Res.* 11, 167–177. doi:10.2147/CMAR.S188655

Wei, J., Meng, L., Hou, X., Qu, C., Wang, B., Xin, Y., et al. (2019a). Radiation-induced skin reactions: mechanism and treatment. *Cancer Manag. Res.* 11, 167–177. doi:10.2147/CMAR.S188655

Wei, J., Wang, H., Wang, H., Wang, B., Meng, L., Xin, Y., et al. (2019b). The role of NLRP3 inflammasome activation in radiation damage. *Biomed. Pharmacother.* 118, 109217. doi:10.1016/j.biopha.2019.109217

Wei, J., Zhao, Q., Zhang, Y., Shi, W., Wang, H., Zheng, Z., et al. (2021). Sulforaphane-mediated Nrf2 activation prevents radiation-induced skin injury through inhibiting the oxidative-stress-activated DNA damage and NLRP3 inflammasome. *Antioxidants (Basel)* 10 (11), 1850. doi:10.3390/antiox10111850

Wilkinson, B., Hill, M. A., and Parsons, J. L. (2023). The cellular response to complex DNA damage induced by ionising radiation. *Int. J. Mol. Sci.* 24 (5), 4920. doi:10.3390/ijms24054920

Winkfield, K. M., Hughes, R. T., Brown, D. R., Clohessy, R. M., Holder, R. C., Russell, G. B., et al. (2024). Randomized pilot study of a keratin-based topical cream for radiation dermatitis in breast cancer patients. *Technol. Cancer Res. Treat.* 23: 15330338231222137.

Xue, J., Yu, C., Tang, Y., Mo, W., Tang, Z., Sheng, W., et al. (2021). NF-E2-Related factor 2 (Nrf2) ameliorates radiation-induced skin injury. *Front. Oncol.* 11, 680058. doi:10.3389/fonc.2021.680058

Yahyapour, R., Motevaseli, E., Rezaeyan, A., Abdollahi, H., Farhood, B., Cheki, M., et al. (2018). Reduction-oxidation (redox) system in radiation-induced normal tissue injury: molecular mechanisms and implications in radiation therapeutics. *Clin. Transl. Oncol.* 20 (8), 975–988. doi:10.1007/s12094-017-1828-6

Yamamori, T., Sasagawa, T., Ichii, O., Hiyoshi, M., Bo, T., Yasui, H., et al. (2017). Analysis of the mechanism of radiation-induced upregulation of mitochondrial abundance in mouse fibroblasts. *J. Radiat. Res.* 58 (3), 292–301. doi:10.1093/jrr/rrw113

Yang, X., Ren, H., Guo, X., Hu, C., and Fu, J. (2020). Radiation-induced skin injury: pathogenesis, treatment, and management. *Aging (Albany NY)* 12 (22), 23379–23393. doi:10.18632/aging.103932

Yokota, T., Zenda, S., Ota, I., Yamazaki, T., Yamaguchi, T., Ogawa, T., et al. (2021). Phase 3 randomized trial of topical steroid versus placebo for prevention of

radiation dermatitis in patients with head and neck cancer receiving chemoradiation. *Int. J. Radiat. Oncol. Biol. Phys.* 111 (3), 794–803. doi:10.1016/j.ijrobp.2021.05.133

Yu, D., Zhang, S., Mo, W., Jiang, Z., Wang, M., An, L., et al. (2021). Transplantation of the stromal vascular fraction (SVF) mitigates severe radiation-induced skin injury. *Radiat. Res.* 196 (3), 250–260. doi:10.1667/RADE-20-00156.1

Yu, Q., Shen, Y., Gan, Y. D., and Zheng, L. (2019). Protective effect of total flavonoids from boxthorn leaf against UVB irradiation-induced skin injury. *Trop. J. Pharm. Res.* 18 (9), 1943–1947. doi:10.4314/tjpr.v18i9.23

Zenda, S., Yamaguchi, T., Yokota, T., Miyaji, T., Mashiko, T., Tanaka, M., et al. (2018). Topical steroid versus placebo for the prevention of radiation dermatitis in head and neck cancer patients receiving chemoradiotherapy: the study protocol of J-SUPPORT 1602 (TOPICS study), a randomized double-blinded phase 3 trial. *BMC Cancer* 18 (1), 873. doi:10.1186/s12885-018-4763-1

Zhai, Z., Liu, W., Kaur, M., Luo, Y., Domenico, J., Samson, J. M., et al. (2017). NLRP1 promotes tumor growth by enhancing inflammasome activation and suppressing apoptosis in metastatic melanoma. *Oncogene* 36 (27), 3820–3830. doi:10.1038/onc.2017.26

Zhang, D., Shao, S., Shuai, H., Ding, Y., Shi, W., Wang, D., et al. (2013). SDF-1α reduces fibronectin expression in rat mesangial cells induced by TGF-β1 and high glucose through PI3K/Akt pathway. *Exp. Cell Res.* 319 (12), 1796–1803. doi:10.1016/j.yexcr.2013.03.030

Zhang, S., Song, C., Zhou, J., Xie, L., Meng, X., Liu, P., et al. (2012). Amelioration of radiation-induced skin injury by adenovirus-mediated heme oxygenase-1 (HO-1) overexpression in rats. *Radiat. Oncol.* 7, 4. doi:10.1186/1748-717X-7-4

Glossary

AHR	Radiation aryl hydrocarbon receptor
ARF	p19 INK4D
BDDI	E/Z-2-benzylidene-5,6-dimethoxy-3,3-dimethylindan-1-one
CCE	C. costata extract
CDKN2 A	Cyclin-dependent kinase inhibitor 2 A
COL I	Collagen type I
CTS	Cryptotanshinone
DAMPs	Damage-associated molecular patterns
ECM	Extracellular matrix
ERK	Extracellular regulated protein kinases
FPN	Ferroportin
GGR	Global genome repair
HA	Hyaluronic acid
HBOT	Hyperbaric oxygen therapy
HO-1	Heme oxygenase-1
IL	Interleukin
JNK	c-Jun N-terminal kinase
KC	Keratinocytes
MITF	Microphthalmia transcription factor
MMP	Matrixmetallo proteinase
MSCs	Mesenchymal stem cells
mtROS	mitochondria-derived ROS
NADP	Nicotinamide-adenine dinucleotide phosphate
NF-kB	nuclear factor kB
NLRP3	Nucleotide-binding domain and leucine-rich-repeatcontaining family pyrin 3
NOX4	NADPH oxidase 4
OS	Oxidative stress
PAF	Platelet activation factor
PDGF	Platelet-derived growth factor
PGE-2	Prostaglandin E2
PKB	Protein Kinase B
PKC	Protein kinase C
pRb	retinoblastoma protein
QoL	Quality of life
RA	Rosmarinic acid
RIF	Radiation-induced skin fibrosis
RISRs	Radiation-induced skin reactions
RNS	Reactive nitrogen species
ROS	Reactive oxygen species
SASP	Senescence-associated secretory phenotype
SDF-1α	Human stromal cell-derived factor-1 α
SFN	Sulforaphane
SOD	Superoxide dismutase
SOD2	superoxide dismutase 2
SVP	Stromal vascular fraction
TC-PTP	T-cell protein tyrosine phosphatase
TGF-β	Transforming growth factor beta
TM	Thrombomodulin
UV	Ultraviolet
vWF	von Willebrand factor
ZIP9	Zrt-and Irt-like protein 9
8-OHdG	8-hydroxydeoxyguanosine
α-MSH	α-melanocyte-stimulating hormone.

frontiers | Frontiers in Cell and Developmental Biology

TYPE Review
PUBLISHED 09 January 2025
DOI 10.3389/fcell.2024.1500880

Check for updates

OPEN ACCESS

EDITED BY
Jing Pu,
University of New Mexico, United States

REVIEWED BY
Tejeshwar Rao,
University of Houston, United States
Chunyan Wang,
Shenzhen Maternity and Child Healthcare Hospital, China

*CORRESPONDENCE
Kuo-Hui Su,
kuo-hui.su@utoledo.edu

RECEIVED 24 September 2024
ACCEPTED 18 December 2024
PUBLISHED 09 January 2025

CITATION
Ghai S, Shrestha R and Su K-H (2025) HSF1 at the crossroads of chemoresistance: from current insights to future horizons in cell death mechanisms.
Front. Cell Dev. Biol. 12:1500880.
doi: 10.3389/fcell.2024.1500880

COPYRIGHT
© 2025 Ghai, Shrestha and Su. This is an open-access article distributed under the terms of the Creative Commons Attribution License (CC BY). The use, distribution or reproduction in other forums is permitted, provided the original author(s) and the copyright owner(s) are credited and that the original publication in this journal is cited, in accordance with accepted academic practice. No use, distribution or reproduction is permitted which does not comply with these terms.

HSF1 at the crossroads of chemoresistance: from current insights to future horizons in cell death mechanisms

Shruti Ghai, Rejina Shrestha and Kuo-Hui Su*

Department of Cell and Cancer Biology, College of Medicine and Life Sciences, The University of Toledo, Toledo, OH, United States

Heat Shock Factor 1 (HSF1) is a major transcriptional factor regulating the heat shock response and has become a potential target for overcoming cancer chemoresistance. This review comprehensively examines HSF1's role in chemoresistance and its potential as a therapeutic target in cancer. We explore the complex, intricate mechanism that regulates the activation of HSF1, HSF1's function in promoting resistance to chemotherapy, and the strategies used to manipulate HSF1 for therapeutic benefit. In addition, we discuss emerging research implicating HSF1's roles in autophagy, apoptosis, DNA damage repair, drug efflux, and thus chemoresistance. This article highlights the significance of HSF1 in cancer chemoresistance and its potential as a target for enhancing cancer treatment efficacy.

KEYWORDS

heat shock factor 1, chemoresistance, proteotoxic stress response, autophagy, apoptosis, drug efflux

1 Introduction

In 2024, roughly two million people are estimated to be diagnosed with cancer, with 611,720 cancer-related deaths in the United States (Siegel et al., 2024). Approximately 80%–90% of cancer-related deaths are attributed to the development of chemoresistance in responders (Ramos et al., 2021). Chemoresistance is responsible for most relapses, contributing to metastasis and poor rate of survival in patients (Ramos et al., 2021). Chemoresistance often leads to the need for more intensive chemotherapy regimens in second and later lines of cancer treatment as the initial therapies become less effective. The action of chemotherapies typically involves cellular uptake, intracellular activation, acting on the target site, and ultimately inducing cell death (Florea and Busselberg, 2011; Tilsed et al., 2022). Chemoresistance can occur at any of these stages, leading to failure of drug response. Cancers have been shown to develop resistance to various chemotherapies rapidly (Vasan et al., 2019; Ramos et al., 2021; Khan et al., 2024). For example, the resistance to the paclitaxel and 5-fluorouracil combination treatment was observed within 2 years since it being introduced to clinical use (Harris et al., 2006; Szakacs et al., 2006; Murray et al., 2012; Vulsteke et al., 2014). With the advancement in new targeted therapies and drug development, novel drugs show efficacy in many cancer types; however, these treated tumors often develop resistance to these drugs over time, making resistance a significant barrier to successful cancer treatment (Vasan et al., 2019; Khan et al., 2024). Hence, it is no surprise that chemoresistance contributes to about 80%–90% of cancer-related mortality.

Cancer cells utilize complex interplays between innate, intrinsic, and acquired factors to develop resistance to an administered drug during tumor development (Dzobo et al., 2018). In general, intrinsic chemoresistance is due to cell heterogeneity, whereas acquired resistance develops from chemotherapy-induced changes. The intrinsic chemoresistance of a tumor is evident when there is a lack of an initial response to the administered drug. The existence of intrinsic chemoresistance is largely due to the heterogeneity of the cancer cell population, especially the presence of cancer stem cells and mutations in key genes involved in cellular homeostasis and metabolism. These mutations can confer resistance by altering metabolic pathways, enhancing survival signaling, and impairing apoptotic response, thereby allowing cancer cells to survive and proliferate despite chemotherapy (Cancer Genome Atlas Research, 2014; Giordano, 2014; Hasan et al., 2018). Intrinsic chemoresistance is influenced by various factors, including the activation of signaling pathways like phosphoinositide 3-kinase (PI3K)/Akt, hedgehog, nuclear factor-κB (NFkB), and mitogen-activated protein kinase (MAPK), which have been shown to confer resistance to chemotherapeutic agents such as gemcitabine in pancreatic cancer (Rajabpour et al., 2017; He et al., 2021; Guo et al., 2024). The acquired chemoresistance only develops as a response to chemotherapy treatment and involves drug target mutations, tumor microenvironment modifications, and epigenetic changes such as methylation, acetylation, and microRNA (miRNA) expression survival (Mansoori et al., 2017; Emran et al., 2022). These alterations modulate upstream/downstream intracellular cell growth signaling such as MAPK and mammalian target of rapamycin (mTOR), modify the cell cycle checkpoints, inhibit apoptosis, and alter DNA replication, thereby enhancing cancer cell growth.

In addition to the mechanisms mentioned above that contribute to chemoresistance, accumulating evidence shows that stress response pathways are exploited by cancer cells to further support the chemoresistance processes (Vasan et al., 2019; Ramos et al., 2021; Khan et al., 2024). Stress responses, such as those triggered by oxidative stress, hypoxia, and DNA damage, initiate the survival and adaptive responses of cancer cells (Fulda et al., 2010; Dai et al., 2012; Chen and Xie, 2018). Stress responses also play crucial roles in the development and enhancement of resistance to chemotherapy. By inducting cytoprotective responses such as autophagy (Suh et al., 2012), the expression of heat shock proteins (HSPs) (Chatterjee and Burns, 2017), and the unfolded protein response, cancer cells can mitigate the effects of therapeutic stress, thereby promoting their continued growth and survival despite the treatment.

A better understanding of these chemoresistance mechanisms is essential for developing strategies to overcome drug resistance and improve the efficacy of cancer treatments. Recently, heat shock factor 1 (HSF1) has emerged as an intriguing player in tumorigenesis and chemoresistance (Alasady and Mendillo, 2020; Prince et al., 2020; Zhang et al., 2021). HSF1 is originally characterized as a transcription factor for the expression of HSPs responsible for the initiation of the proteotoxic stress response (Alasady and Mendillo, 2020; Zhang et al., 2021). This cellular mechanism safeguards cells from protein misfolding and aggregation under stress conditions (Alasady and Mendillo, 2020; Zhang et al., 2021; Ghai et al., 2024). HSF1 has since also been recognized for its pro-oncogenic properties, contributing to cancer initiation, progression, and chemoresistance (Kijima et al., 2019; Lee et al., 2021; Cyran and Zhitkovich, 2022; Gumilar et al., 2023).

The role of HSF1 in cancer has been extensively studied. HSF1 is downstream of the Kirsten rat sarcoma viral oncogene homolog (KRAS) signaling (Tang et al., 2015; Dai and Sampson, 2016). The *KRAS* gene is one of the most frequently mutated oncogenes in human cancers, with mutations commonly identified in approximately 90%–95% of pancreatic ductal adenocarcinoma (PDAC), 40% of colorectal cancers (CRC), and 25%–30% of non-small cell lung cancers (NSCLC) (Bailey et al., 2016; Zhu et al., 2021; Reita et al., 2022; Nusrat et al., 2024). Cancers with KRAS mutations are particularly lethal due to their role in promoting rapid cell proliferation and resulting in highly aggressive tumor phenotype (Huang et al., 2021). Recent research suggests that by regulating autophagy, apoptosis, DNA damage repair, or drug efflux mechanism, cancer cells can develop resistance to chemotherapy, thereby promoting tumor survival and progression (Dai and Sampson, 2016; Cyran and Zhitkovich, 2022; Gumilar et al., 2023). In this review, we will discuss the role of HSF1 in chemoresistance and its potential as a therapeutic target in tumorigenesis.

2 HSF1 in tumorigenesis

2.1 HSF1 is a key transcription factor in cancer development

When cells undergo proteotoxic stress from exposure to environmental factors such as heat shock, an adaptive cytoprotective mechanism, known as the heat shock response (HSR) or proteotoxic stress response (PSR), is activated. The HSR maintains the protein quality and prevents protein aggregation in the cells, ensuring the proteome homeostasis (proteostasis) in the cells (Lindquist, 1986). Immediately after the accumulation of unfolded proteins, HSF1, a master regulator of proteotoxic stress, is activated and, in turn, activates the transcription of genes encoding HSPs (Ghai et al., 2023). HSPs are molecular chaperones of the cells that enable the proper folding of the unfolded proteins and the degrading of the unrequired proteins through ubiquitination (Bukau et al., 2006; Gidalevitz et al., 2011; Dai and Sampson, 2016) (Figure 1).

HSF1 is a transcription factor and is an evolutionarily conserved member of the HSF family proteins (Wu, 1995; Anckar and Sistonen, 2011). HSF1 comprises the N-terminal helix-turn-helix DNA-binding domain, the oligomerization domain, and the C-terminal transactivation domain. The N-terminal DNA-binding domain of HSF1 binds to the inverted repeats of the heat shock elements (HSE) (Buchwalter et al., 2004). The oligomerization domain of HSF1 comprises four leucine zipper repeats, allowing HSF1 to trimerize and become an active transcription factor (Neudegger et al., 2016; Gomez-Pastor et al., 2018). The C-terminal transactivation domain of HSF1 is essential for the elongation process of transcription (Vihervaara et al., 2017). In cells under normal physiological conditions, HSF1 is present as a monomer and is sequestered by the HSP70, T-complex protein ring complex (TRiC), and histone deacetylase 6 (HDAC6) complex in the

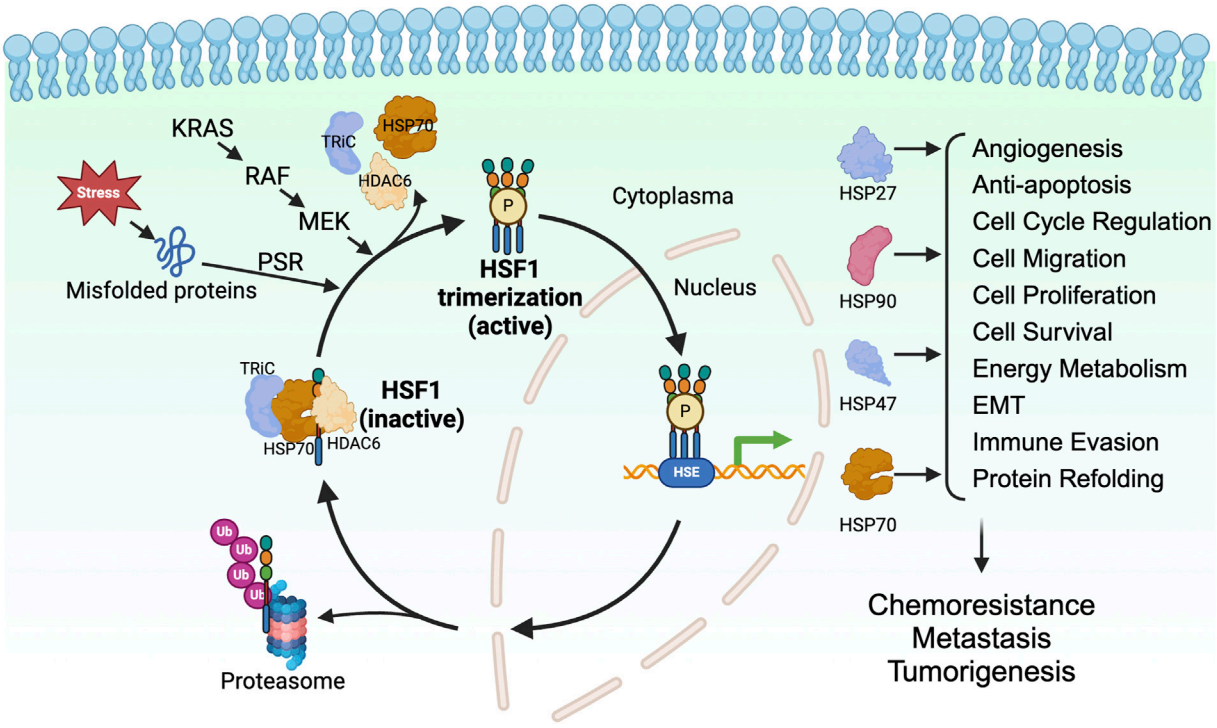

FIGURE 1
HSF1 is a transcriptional factor for HSPs in tumorigenesis. HSF1 is a downstream effector of KRAS-RAF-MEK signaling. HSF1 is activated upon proteotoxic stress in the cells, which allows its trimerization, phosphorylation, and translocation to the nucleus. In the nucleus, HSF1 binds to heat shock elements and allows expression of HSP27, HSP47, HSP70, and HSP90, which directly and indirectly affects tumor progression. EMT, epithelial-mesenchymal transition; HDAC6, histone deacetylase 6; HSE, heat shock element; HSF1, heat shock factor 1; HSP, heat shock protein; KRAS, Kirsten rat sarcoma viral oncogene homolog; MEK, mitogen-activated protein kinase kinase; P, phosphorylation; PSR, proteotoxic stress response; RAF, rapidly accelerated fibrosarcoma; TRiC, T-complex protein ring complex; Ub, ubiquitin.

cytoplasm (Neef et al., 2014). Misfolded proteins resulting from proteotoxic stresses induced by various stimuli compete with HSF1 for binding to the chaperones, allowing the release of HSF1 from the HSP70/HDAC6 complex (Shi et al., 1998; Gomez-Pastor et al., 2018; Kijima et al., 2018). Along with the proteotoxic stress, post-translational modifications such as phosphorylation, SUMOylation, and acetylation are known to regulate the activation of HSF1. Phosphorylation of HSF1 at Ser326 is a commonly used marker for the activation of HSF1. In addition, phosphorylation of HSF1 on Ser230 and Ser320 positively regulates the HSF1 activity (Holmberg et al., 2001; Guettouche et al., 2005; Zhang et al., 2011; Chou et al., 2012a) whereas phosphorylation on Ser121 negatively regulates the activity of HSF1 (Dai et al., 2015; Swan and Sistonen, 2015). The acetylation of HSF1 on K298 prevents the proteosome-dependent degradation of the HSF1, thus increases the stability of HSF1 (Wu, 1995; Anckar and Sistonen, 2011). In contrast, the SUMOylation of HSF1 at K298 inhibits the activity of HSF1 (Wu, 1995; Hietakangas et al., 2003; Anckar and Sistonen, 2011). The activated HSF1 can trans-localize to the nucleus and regulate the transcription of genes encoding chaperone proteins. After the restoration of proteostasis, the HSP90 binds to the HSF1, leading to the inactivation of HSF1 (Gomez-Pastor et al., 2018; Kijima et al., 2018) (Figure 1).

Several studies using different murine models have shown HSF1 as a pro-oncogenic factor. A pioneering work performed in skin carcinogenesis mouse models shows reduced oncogenic Ras-induced tumor formation upon the loss of *Hsf1* (Dai et al., 2007). *Hsf1* deletion also leads to reduced tumor burden in other mouse models, including chemical carcinogenesis-driven hepatocellular carcinoma, mammary tumorigenesis resulting from p53 and neurofibromatosis type 1 (*Nf1*) loss, and lymphomas caused by p53-deficiency (Min et al., 2007; Jin et al., 2011; Xi et al., 2012). Along with that, increased HSF1 expression has been found in a wide range of human cancers, including cervix, colon, breast, lung, liver, pancreatic, and prostate carcinomas (Dudeja et al., 2011; Santagata et al., 2011; Fang et al., 2012; Mendillo et al., 2012). These reports indicate that HSF1 plays a crucial role in mediating tumorigenesis.

The increased rate of protein synthesis in cells allows for a high number of unfolded or misfolded proteins. Similarly, inflammation and stresses, such as hypoxia, activate HSF1 in the cells (Luo et al., 2009; Oromendia et al., 2012; Santagata et al., 2013). Besides this general activation of HSF1, cancer cells can constitutively activate HSF1, thus allowing its cytoprotective effect through various mechanisms. The mammalian target of rapamycin complex 1 (mTORC1) activated by PI3K/AKT phosphorylates HSF1 at Ser326 and accentuates the HSF1 transcriptional activity (Chou et al., 2012b). The HSF1 activation promotes cell proliferation while circumventing the cells' apoptosis and senescence (Meng et al., 2010; Carpenter et al., 2015). Besides, the Ras-MEK signaling phosphorylates HSF1 at Ser326 to activate HSF1's transcriptional activity (Tang et al., 2015). In addition, the metabolic sensor AMP-

activated protein kinase (AMPK) is reported to suppress the activity of HSF1 through phosphorylating the HSF1 Ser121 (Dai et al., 2015; Swan and Sistonen, 2015). In PDAC, the loss of AMPK allows the activation of HSF1, promoting the invasion and migration of PDAC (Chen et al., 2017). In summary, the activity of HSF1 is regulated by multiple upstream kinases and regulatory factors.

HSF1 activation in cancers thus is not only in response to different stresses but also through a wide array of other mechanisms, including those driven by oncogenic signaling and those that elevate HSF1 expression levels. This diverse range of HSF1 activation pathways collectively accounts for the extensive activation and functional roles of HSF1 in tumorigenesis.

2.2 HSF1-mediated upregulation of HSPs

Because HSF1 is a major transcriptional factor for HSPs, we will discuss the role of HSF1 in the chemoresistance mechanism. HSPs, including HSP70, HSP27, HSP90, HSP40, and HSP60, are crucial players in cancer chemoresistance (Zhang et al., 2021). These molecular chaperones facilitate protein folding, maintain protein stability, and, in some conditions, promote the degradation of misfolded or aggregated proteins, contributing to the maintenance of proteostasis within cancer cells. For example, HSP27 regulates the Salvador–Warts–Hippo pathway (Hippo pathway) known to control tumor progression and cancer stem cell reprogramming (Vahid et al., 2016). HSP27 forms multimeric complexes to stabilize denatured and aggregated proteins, making them functional (Vahid et al., 2016). HSP40 aids proper protein folding, translation, translocation, and degradation (Takashima et al., 2018). Several HSP40 family members are highly expressed in various types of human cancer, including colorectal, gastric, and KRAS-mutated lung cancers. Concerning colorectal cancer, HSP40 has demonstrated metastatic promoting behavior (Sterrenberg et al., 2011; He et al., 2015; Yamashita et al., 2016; Yang et al., 2020). Elevated levels of HSPs can promote chemoresistance by aiding the proper folding of oncoproteins, thereby sustaining malignant processes. HSP90 is overexpressed in multiple cancer types and regulates the stability, activity, maturation, and proteolytic degradation of various oncogenic kinases. HSP90 interacts with its substrates through its N-terminal ATPase domain, which is enhanced by the binding of co-chaperones such as HSP70 (Chiosis et al., 2004; Workman et al., 2007; Chatterjee et al., 2016).

HSPs also directly regulate kinases. For example, overexpressed HSP90AA1 upon chemotherapy dissociates phosphorylated AKT and c-Jun N-terminal kinase (JNK), inducing protective autophagy while inhibiting apoptosis and hence contributing to chemoresistance (Xiao et al., 2018). This highlights the important role of HSPs in chemoresistance and underscores how highly regulated cellular pathways are hijacked by cancer cells to survive stress and chemotherapy. Furthermore, cancer cells exploit external signaling by binding extracellular HSP90α to lipoprotein receptor-related protein 1 (LRP1), which has been shown to promote PDAC metastasis via AKT activation. LRP1 is associated with poor PDAC patient survival and LRP1 silencing increases the susceptibility of PDAC cells to doxorubicin and gemcitabine (Xue et al., 2022). Disruption of HSP47 in PDAC cells increases intracellular reactive oxygen species (ROS) and subsequent Ca^{2+} levels, resulting in the activation of the caspase-12/caspase-9/caspase-3 axis, which may sensitize cells to chemotherapy (Yoneda et al., 2021). Inhibition of HSP27 in human colon cancer cells reduces their acquired resistance to 5-fluorouracil (Asada et al., 2021). This suggests that HSPs play a role in protecting cells from ROS-induced damage and cellular stress. There is still a significant gap in our understanding of how HSPs modulate oxidative stress and provide protection against ROS, further investigation into these mechanisms could shed light on their contributions to chemoresistance.

In summary, HSF1-mediated regulation of HSPs provides diverse mechanisms of chemoresistance by preserving proteomic integrity and modulating cell death pathways. The upregulation of HSPs through HSF1 thus promotes tumor growth and contributes to chemoresistance (Figure 1). Given this understanding, targeting HSF1 in various cancers appears to be a promising therapeutic strategy. We will further discuss the role of HSF1 in chemotherapy and its effect on chemoresistance. The combination of HSF1 inhibition with existing chemotherapeutic agents may represent a potential avenue for enhancing treatment efficacy and warrants further investigation. We have summarized recent studies and the current mechanisms on the role of HSF1 in driving chemoresistance, which may provide new avenues for targeting HSF1 in various cancers.

3 HSF1 as a regulator of chemoresistance

3.1 HSF1 and autophagy

PSR regulates both the ubiquitin-proteasome system (UPS) and autophagy for the degradation of dysfunctional and toxic proteins to maintain proteostasis in response to stress. HSF1 induces autophagy by acting as a transcription factor of multiple autophagy-related genes (ATG), such as ATG5, ATG7, and ATG12. HSF1 also induces the autophagy marker sequestosome 1 (SQSTM1)/p62 activity through the regulation of its upstream kinases (Watanabe et al., 2017). However, the autophagy flux and the p62 level are increased in HSF1-deficient mice (Dayalan Naidu et al., 2017). This suggests that the relationship between HSF1 and autophagy may be context dependent.

In the past decade, various studies have demonstrated that autophagy plays an important role in conferring chemoresistance. ATGs, such as ATG3, ATG5, ATG6 (Beclin-1), ATG7, and ATG12, and autophagy markers, such as microtubule-associated protein 1A/1B-light chain 3 (LC3) and p62, are the major regulators of autophagy and chemoresistance (Li et al., 2019). ATG3 facilitates the conversion of LC3-I to LC3-II and promotes endoplasmic reticulum (ER) stress. However, the downregulation of ATG3 increases the sensitivity to erlotinib in the erlotinib-resistant lung cancer cell lines (Lee and Wu, 2012). ATG5 normally participates in the elongation of the autophagosome membrane. However, the interaction of the long non-coding RNA (lncRNA) gallbladder cancer drug resistance-associated lncRNA1 with phosphoglycerate kinase 1 in gallbladder cancer cells prevents ATG5 degradation and induces the ATG5-ATG12 complex formation, promoting autophagy and

doxorubicin resistance (Cai et al., 2019). Additionally, suppression of ATG6, a crucial protein in the ATG6 and Vps-34 complex that promotes autophagosome formation, downregulates HER2 expression and enhances tamoxifen sensitivity in estrogen receptor-positive breast cancer cells *in vitro* (Gu et al., 2017). ATG7, an activator of ATG8 involved in the expansion of phagophore, confers chemoresistance in the acute myeloid leukemia cell lines against cytarabine and idarubicin treatment, knockdown of ATG7 increased apoptosis and DNA damage (Piya et al., 2016). Hence, autophagy is critical in chemoresistance, involving multiple autophagy-related genes and proteins (Debnath et al., 2023; Mohammed et al., 2024). This observation supports the well-established phenomenon of autophagy functioning in an oncogenic manner, contingent upon the stage of tumorigenesis. Autophagy is cytoprotective under stress conditions, such as chemotherapy, and helps maintaining the cellular homeostasis in the surviving cancer cells, such as colorectal and hepatocellular carcinoma cells (Xu et al., 2013; Lan et al., 2024). Therefore, monitoring the stages of tumorigenesis and autophagy and employing autophagy inhibitors may open new therapeutic avenues to combat chemoresistance.

HSF1 is correlated with various ATGs and their activity. Higher levels of nuclear HSF1 result in a higher H3 acetylation level and enhanced activity of the ATG7 promoter. The absence of HSF1 prevents the ATG7 promoter activity and increases the chemosensitivity to carboplatin in the MDA-MB-231 breast cancer cell line (Desai et al., 2013). Thus, inhibiting cytoprotective autophagy induced by HSF1 knockdown could provide a better therapeutic efficacy against drug resistance. In a study showing that BAG3 contributes to chemoresistance, 5-Fluorouracil and Doxorubicin-resistant triple negative breast cancer cell lines show higher expression of ATG5, LC3-II, and Beclin-1, suggesting a correlation between drug resistance and autophagy (Das et al., 2018). Importantly, inhibiting the transcriptional activity of HSF1 significantly increases the sensitivity of these resistant cell lines to the treatment. Bcl2-associated athanogene 3 (BAG3) also works together with the molecular chaperones HSP70 and HSPB8 along with the ubiquitin receptor SQSTM1/p62 to selectively direct aggregation-prone proteins for degradation via autophagy (Minoia et al., 2014; Sturner and Behl, 2017). Moreover, transmission electron microscopy revealed a distinct accumulation of small vacuoles in the cytoplasm of cells expressing BAG3, indicating enhanced autophagic flux, in HepG2 and MCF7 cells. The enhanced autophagic flux is further supported by a significant increase in LC3-II and p62 levels (Zhao et al., 2019). These studies highlight the novel HSF1-BAG3 axis, targeting which may pave the way to increase chemosensitivity to current therapies in cancer (Figure 2).

HSF1 has been shown to induce miR-135b-5p overexpression, which induces protective autophagy, in colorectal cancer following oxaliplatin treatment. MiR135b-5p stabilizes Unc-51 like autophagy activating kinase 1 (ULK1) by inhibiting mitochondrial E3 ubiquitin protein ligase 1 and its E3 ubiquitin ligase activity on ULK1, thereby inducing protective autophagy and resistance against oxaliplatin (Wang et al., 2021). MiR-217 is known to regulate the HSF1-ATG7 axis by inhibiting the NF1 activity and enhancing chemoresistance (Li et al., 2023a). Other microRNAs, such as miR-107, have been shown to inhibit autophagy and decrease breast cancer progression by targeting HMGB1. Therefore, overexpressing miR-107 can serve as a strategy to hinder cancer progression whereas inhibiting miR-217 or miR-135b-5p may aid in regulating autophagy to combat drug resistance (Ai et al., 2019). Given the diverse roles of microRNAs across various cancers and stress factors, it is crucial to adopt a more mechanistic perspective to comprehend the clinical significance of microRNAs in chemoresistance (Figure 2).

The role of HSF1 and HSPs in tumor autophagy remains a topic of ongoing debate. HSF1 promotes autophagy by upregulating ATG10 through binding to the *Atg10* promoter, thereby enhancing the lipidation of LC3-II. In contrast, HSF1 depletion reduces ATG10 expression and increases the production of inflammatory cytokines in lipopolysaccharide-treated peritoneal macrophages (Tan et al., 2023). Manganese exposure induces hepatic mitochondrial oxidative stress, leading to HSF1 phosphorylation at Ser326 and activation of autophagy. Knockdown of HSF1 prevents manganese-induced autophagosome formation in hepatocytes of yellow catfish (Zhao et al., 2024). Conversely, HSF1 regulates JNK1-mediated mTORC1 activation, suggesting an inhibitory role in autophagy (Su et al., 2016; Su and Dai, 2016; Su and Dai, 2017). Furthermore, HSF1 knockdown activates AMPK and promotes mitophagy, leading to reduced mitochondrial mass (Su et al., 2019). Moreover, recent studies show that HSP70 negatively regulates autophagy and that HSP70 inhibition, along with autophagy blockade, promotes cell death in NSCLC cells (Alhasan et al., 2024). These findings demonstrate the complexity of HSF1 in autophagy, highlighting the need for further investigation to clarify its functions in autophagy regulation and its contribution to chemotherapy resistance (Figure 2).

Future research should focus on clarifying the dual role of HSF1 in autophagy regulation, investigating the specific conditions and signaling pathways that determine whether HSF1 acts as a promoter or inhibitor of autophagy. Additionally, exploring the impact of HSF1-mediated autophagy on chemoresistance in cancer could reveal new strategies to enhance the therapeutic sensitivity in autophagy-dependent tumors. Finally, studying the interactions between HSF1, HSP70, and key pathways, such as kinase activities and ATG protein expression, may provide insights into combination therapies targeting autophagy and chemoresistance in cancer treatment.

3.2 HSF1 and apoptosis

Both intrinsic and extrinsic pathways of apoptosis contribute to chemoresistance. The involvement of the intrinsic pathway is indicated by the upregulation of anti-apoptotic proteins, such as BCL-2 family proteins, and the downregulation of proapoptotic proteins, such as BAX and BAK (Singh et al., 2019). Decreased expression and increased endocytosis of molecules involved in the extrinsic pathway, such as tumor necrosis factor superfamily proteins, FAS ligands, and death receptor (DR) 4 and DR5, potentially confer drug resistance (Ashkenazi, 2015).

HSF1 primarily functions as a transcription factor of HSP70 and HSP90, which are well-known for their roles in inhibiting apoptosis. For instance, HSP70 plays a protective role in heat-induced apoptosis by stabilizing the anti-apoptotic protein MCL-1, which

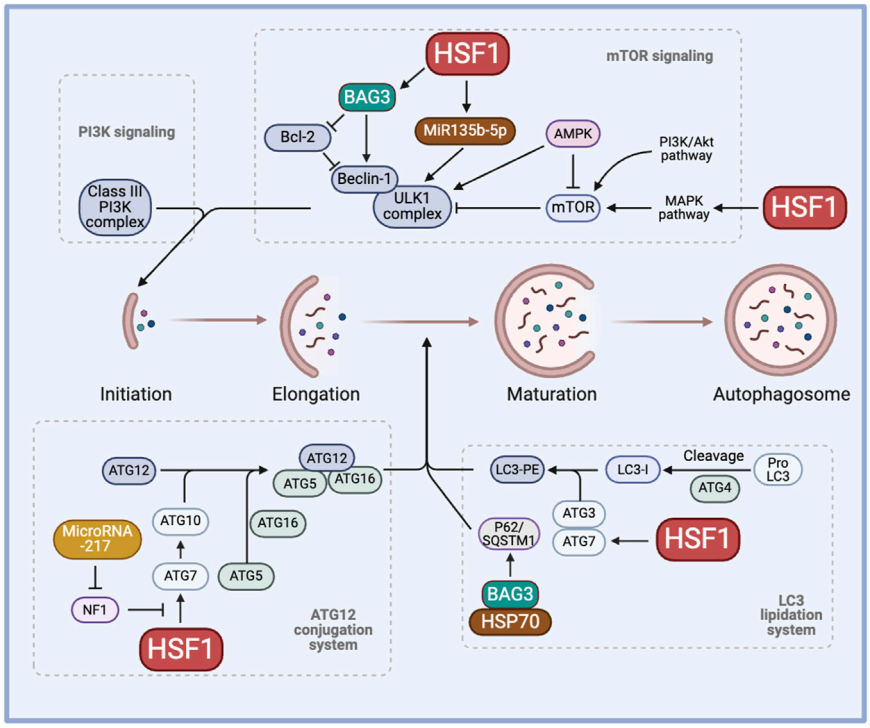

FIGURE 2
The role of HSF1 in cancer autophagy. HSF1 is involved in cancer autophagy by regulating the initiation process through the PI3K-mTOR signaling, the elongation process through the ATG12 conjunction system, and the maturation of autophagosome formation through the LC3 lipidation system. This regulation induces cytoprotective autophagy, hence regulating chemoresistance. AMPK, AMP-activated protein kinase; ATG, autophagy-related genes/proteins; BAG3, Bcl2-associated athanogene 3; HSP, heat shock proteins; HSF1, heat shock factor 1; LC3, microtubule-associated protein 1 light chain 3; LC3-PE, LC3-phosphatidylethanolamine conjugate; MAPK, mitogen-activated protein kinase; miR, micro RNA, mTOR, mammalian target of rapamycin; NF1, neurofibromin 1; PI3K, phosphoinositide 3-kinase; SQSTM1, sequestosome 1/p62; ULK1, Unc-51 like autophagy activating kinase 1.

prevents BAX activation and cytochrome-c release (Stankiewicz et al., 2009). Similarly, HSP90 prevents the release of cytochrome c by inhibiting the activity of the proapoptotic protein FKBP38. Increased HSP90 expression is correlated with elevated levels of antiapoptotic proteins BCL-2 and BCL-xL (Edlich et al., 2007). On the other hand, inhibiting HSP27 triggers the release of SMAC protein, a key regulator of the mitochondrial apoptotic pathway, in dexamethasone-resistant myeloma cell lines and promotes the activation of caspase-9 and caspase-3, suggesting that HSP27 contributes to resistance against dexamethasone (Chauhan et al., 2003).

Moreover, genetic knockdown of HSF1 has been shown to directly link to enhancing apoptosis through the regulation of the mitochondrial apoptosis pathway. In breast cancer, HSF1 knockdown enhances BAX expression and cisplatin-induced apoptosis, whereas restoring HSF1 expression significantly reduces cisplatin-induced apoptosis (Liu and Ma, 2021). In a study on pancreatic tumorigenesis, HSF1 silencing led to the upregulation of pro-apoptotic proteins, including SMAC, cytochrome c, Apaf1, and cleaved caspase-3 and -9, suggesting that HSF1 inhibits the mitochondrial apoptosis pathway to promote tumor growth (Liang et al., 2017). Inhibiting HSP70 prevents HSP70 from stabilizing anti-apoptotic proteins and blocking apoptosis, thus reducing chemoresistance, in bladder cancer (Wei et al., 2024). Inhibiting HSF1 by small molecules enhances the effectiveness of the aurora kinase inhibitor efficacy in NSCLC by promoting apoptosis, potentially overcoming chemoresistance through PI3K/AKT pathway downregulation and ROS activation (Zhang et al., 2024). This suggests that inhibiting HSF1 enhances the effectiveness of chemotherapy by overcoming HSF1- or HSP70-mediated anti-apoptosis mechanisms.

BAG3, a member of the co-chaperone family, is a well-known non-HSP substrate of HSF1 and contributes to chemoresistance in cancer (Jacobs and Marnett, 2009; Antonietti et al., 2017; Guo et al., 2022). Generally, HSP70's function depends on its interactions with other chaperones like HSP90 and the co-chaperone BAG3. In an interesting study, the HSF1/HSP70/BAG3 pathway is investigated and confirmed to contribute to chemoresistance, particularly through its role in the overexpression of pro-survival BCL-2 family proteins and the subsequent resistance to cell death in gliomas (Das et al., 2018). In another study, the overexpression of Bag-1, another protein from the BAG family, modulates HSP levels by phosphorylating HSF1 at Ser326 via the PI3K/AKT/mTOR pathway in HER2-positive and HER2-negative breast cancer cells. BAG1 explicitly enhances the expression of HSP70 and HSP27, contributing to breast cancer cell survival and, potentially, drug resistance (Kizilboga et al., 2024). HSF1 influences apoptosis and chemoresistance through its interactions with co-chaperones like BAG3 and BAG1 and it promotes cell survival by upregulating pro-survival BCL-2 family proteins and HSPs across various cancer types (Figure 3).

Other stress response mechanisms also contribute to the HSF1-mediated chemoresistance. For example, ER stress-induced

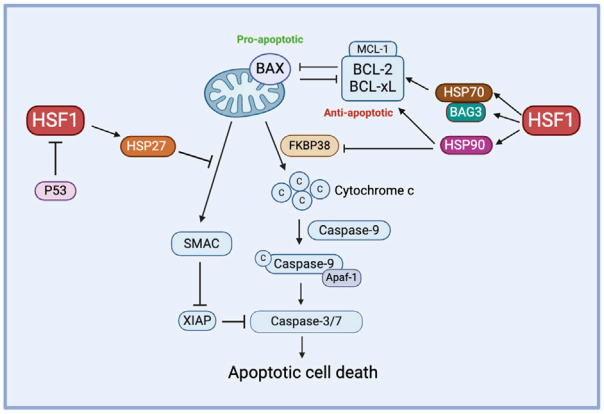

FIGURE 3
The role of HSF1 in cancer apoptosis. HSF1 mediates pro-apoptotic and anti-apoptotic pathways in the chemoresistance by regulating the expression of downstream HSPs. HSP70 controls the function of anti-apoptotic proteins via the HSP70-BAG3 axis, HSP90 regulates anti-apoptotic proteins and inhibits FKBP38, and HSP27 prevents the release of SMAC. Additionally, P53 inhibits HSF1 to avert this process of apoptosis. Apaf-1, apoptotic protease activating factor 1; BAG3, Bcl2-associated athanogene 3; BAX, Bcl-2-associated X protein; BCL-xL, B-cell lymphoma-extra large; c, Cytochrome c; FKBP38, FK506-binding protein 38; HSF1, heat shock factor 1; HSP, heat shock protein; MCL-1, myeloid cell leukemia-1; P53, tumor protein p53; SMAC, second mitochondria-derived activator of caspases; XIAP, X-linked inhibitor of apoptosis protein.

HSF1 promotes chemoresistance to ubiquitin-specific protease 7 (USP7) inhibitors via the protein kinase R-like ER kinase (PERK) pathway, suggesting that targeting HSF1 or PERK could improve USP7 inhibitor-based chemotherapy (Lim et al., 2024). Besides, The Munc18-1 interacting protein 3- (Mint3)-activated hypoxia-indued factor 1α (HIF-1α) signaling promotes chemoresistance in triple-negative breast cancer (TNBC) by increasing the HSP70 expression. Mint3 depletion induces energy stress, which inactivates HSF1 via the AMPK/mTOR pathway, reducing HSP70 levels and enhancing the effectiveness of doxorubicin in TNBC (Tanaka et al., 2023). These findings suggest crosstalk among stress response signaling pathways, with HSF1 driving chemoresistance through mechanisms like ER stress via PERK and HIF-1α signaling, ultimately enhancing cancer cell survival during chemotherapy.

In addition, the interaction of HSF1 with multiple oncogenic transcription factors is crucial for tumorigenesis and apoptosis. The wildtype p53 is a tumor suppressor, inducing cell cycle arrest and apoptosis when DNA damage cannot be repaired. Surprisingly, mutant p53 directly interacts with HSF1, aiding the proper binding of HSF1 to the target HSPs and regulating the activity of HSPs, thereby contributing to cell survival. Moreover, mutant p53 is also known to activate mTOR, MAPK, and PI3K pathways via erythroblastic oncogene B (ErbB) family, including epidermal growth factor receptor (EGFR) and HER2, inducing HSF1 activation and contributing to apoptosis and chemoresistance (Toma-Jonik et al., 2019; Zhang et al., 2021). Furthermore, SUMOylation of HSF1 at the K298 enhances its stability, nuclear localization, and mitochondrial unfolded protein response, which promotes glioblastoma cell proliferation, migration, and resistance to apoptosis (Li et al., 2024). This SUMOylation-modified HSF1 activity contributes to chemoresistance by supporting mitochondrial function and increasing the expression of mitochondrial chaperones, which may help cancer cells to evade chemotherapy-induced stress. Future research should explore how targeting HSF1 and its downstream pathways can be used to overcome chemoresistance, focusing on both intrinsic and extrinsic apoptotic mechanisms and the HSF1's effect on other programmed cell death signaling.

3.3 HSF1 and DNA damage repair

The DNA damage response (DDR) is a complex network of pathways that maintain the genome integrity. A key mechanism of DDR is base excision repair, which is mediated by Poly (ADP-ribose) polymerase (PARP) and AP endonuclease1 (APE1) as the responsible proteins. Other pathways contributing to DDR include non-homologous end joining (NHEJ) and homologous recombination (HR). DNA–dependent protein kinase (DNA-PK) plays an important role in NHEJ for double-strand breaks (DSBs) and contributes to chemo-radiotherapy resistance. DSBs are critical DNA lesions repair mainly by HR or NHEJ. Ataxia-telangiectasia mutated and ataxia telangiectasia and Rad3-related (ATR) kinases detect DSBs, activating p53 for cell cycle arrest or apoptosis and Breast cancer genes (BRCA) 1/2 for accurate repair through HR (Jackson and Bartek, 2009). This coordinated response maintains genomic stability, preventing mutations that can lead to cancer. Cell cycle checkpoint kinases are activated during DDR, of which checkpoint kinase 1 (CHK1) and CHK2 are downstream substrates of ataxia-telangiectasia mutated (ATM)/ATR. ATR and ATM are activated during single-strand and double-strand breaks, respectively. The enhanced DNA damage repair capacity (DRC) in tumor cells contributes significantly to their drug resistance, including targeted and immune therapy For example, cisplatin-resistant tumor cells often demonstrate higher expression of DNA damage repair-related genes and higher DRC (Fujimoto et al., 2017). Furthermore, inhibiting the nucleotide excision repair (NER) pathway further increased the sensitivity of tumor cells to another chemotherapy drug, cisplatin, complementing the cytotoxic effects (Oliver et al., 2010; Wang et al., 2011). HSF1 plays a crucial role in DNA damage repair-mediated chemoresistance, particularly through its involvement in the NHEJ pathway. HSF1 inhibits NHEJ by interacting with Lupus Ku autoantigen protein p70 (Ku70) and Ku86 to disrupt their heterodimeric interaction, leading to defective DNA repair and genomic instability. This is a potential mechanism for HSF1-mediated carcinogenesis (Kang et al., 2015). This inhibition of NHEJ by HSF1 contributes to chemoresistance by promoting genomic instability, which can drive cancer progression and resistance to therapy. Notably, HSF1's function in NHEJ appears to be independent of its traditional role as a transcription factor, it instead operates through direct protein-protein interactions within the DNA damage repair machinery.

Single-strand DNA breaks are repaired through the base excision repair pathway, where PARP detects the damage sites and recruits repair factors to them while proliferating cell nuclear antigen (PCNA) acts as a sliding clamp to facilitate the recruitment of DNA polymerases, ensuring efficient repair and genome stability.

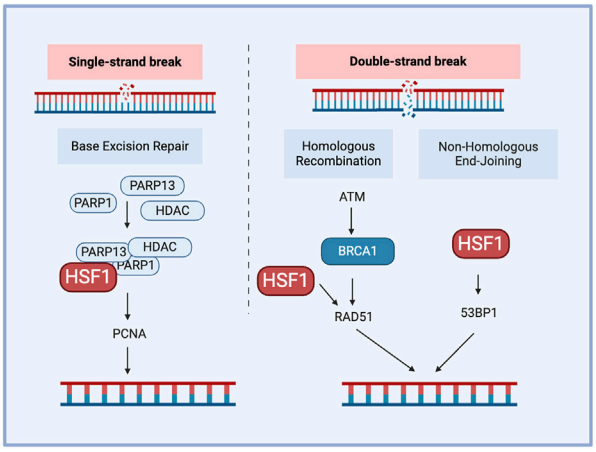

FIGURE 4
The role of HSF1 in cancer DNA damage repair. HSF1 participates in DNA damage repair by forming interactions with PARP1 and PARP13, facilitating the localization of PARP1 to DNA single-strain break sites and regulating RAD51 or 53BP1 during double-strain break repair. 53BP1. tumor protein p53 binding protein 1; ATM, ataxia-telangiectasia mutated; BRCA1, breast cancer type 1 susceptibility protein; HDAC, histone deacetylase; HSF1, heat shock factor 1; PARP, poly (ADP-ribose) polymerase; PCNA, proliferating cell nuclear antigen; RAD51, RAD51 recombinase.

HSF1 also contributes to DNA damage response by forming a complex with PARP1 and PARP13 and redistributing PARP1 to DNA lesions (Fujimoto et al., 2017). PARP1 contains a C-terminal catalytic domain that helps the synthesis of PAR, and autoPARylation of PARP1 regulates chromatin remodeling and DNA damage repair. Deficiency of HSF1 also reduces the expression of DNA damage repair factors such as RAD51 and 53BP1 and reduces DNA damage repair efficiency. BRCA1 and BRCA2 are DNA damage repair genes; many mutations in these genes result in a dysfunctional DNA damage response. HSF1 deficiency has been shown to reduce the proliferation of mammary tumors having dysfunctional HR due to BRCA1 mutations (Fujimoto et al., 2017). This correlated with HSF1's crucial role in maintaining the genome integrity as a part of the PSR, contributing to BRCA-mutated tumor cells' addiction to HSF1 (Figure 4). This addiction can be leveraged as a targeted therapy approach, increasing the susceptibility of BRCA-mutated cells to chemotherapy.

Besides, HSF1 can form a complex with DNA damage kinases ATR and CHK1, facilitating p53 phosphorylation in response to DNA damage (Logan et al., 2009). HSF1 activation increases DNA damage repair, contributing to radiation resistance and promoting cancer cell survival under treatment stress in colorectal cancer (Li et al., 2023b). MDM2-mediated ubiquitination of HSF1 under stress conditions affects HSF1 stability, facilitating DNA damage repair processes and potentially contributing to resistance against DNA-damaging treatments (Xiang et al., 2023). Besides, inhibiting HSF1 with KRIBB11 disrupts these pathways, reduces MDM2 and other survival proteins, induces apoptosis, and enhances sensitivity to HSP90 inhibitors, making HSF1 a promising target to overcome DNA damage repair-mediated chemoresistance in adult T-cell leukemia (Ishikawa and Mori, 2023). These findings highlight the potential for targeting HSF1 as a therapeutic approach to overcome DNA damage repair-mediated chemoresistance.

Although it is promising to target HSF1 in DNA damage repair chemoresistance, currently there are gaps in our understanding of HSF1's role in DNA damage repair involving its dual function in promoting or inhibiting repair pathways, its specific interactions with DNA repair proteins, and its context-specific effects across different cancer types. Addressing these questions could improve our understanding of HSF1 as a potential therapeutic target for developing targeted therapies to overcome chemoresistance.

3.4 HSF1 and drug efflux transporters

ATP-binding cassette (ABC) transporters contribute to drug resistance. At the basal level, these transporters export hydrophobic molecules to the outside of cells. However, in cancer cells, the upregulated efflux of drugs through ABC transporters contributes to another potential drug resistance mechanism (Gumilar et al., 2023). ATP-binding cassette sub-family G member 2 (ABCG2), commonly known as breast cancer resistance protein (BCRP), is an important factor in the development of chemoresistance in many malignancies. ABCG2 actively remove a variety of chemotherapeutic drugs out of cancer cells, lowering intracellular drug accumulation and effectiveness (Doyle and Ross, 2003; Noguchi et al., 2014; Mao and Unadkat, 2015). ABCG2 is extensively expressed in some cancer stem cells and its expression is often increased in response to chemotherapy, which helps these cells surviving treatments. Overexpression of ABCG2 has been associated with resistance to many chemotherapeutic treatments, including mitoxantrone, topotecan, and doxorubicin. Targeting ABCG2-mediated drug efflux therefore has emerged as a promising strategy for combating chemoresistance and improving treatment results in cancer patients (Zhang, 2007; Peng et al., 2010; Mo and Zhang, 2012). ABCG1, another member of the ABCG subfamily of ABC transporter, regulates and maintains cellular cholesterol homeostasis and is critical for the survival and function of normal cells. HSF1 overexpression has been seen in melanoma cell lines, contributing to greater drug efflux (Vydra et al., 2013). HSF1 regulates drug resistance through multiple mechanisms. As the mere binding of HSF1 to the HSE element on the ABCG1 gene is insufficient to activate the ABCG1 expression, the detailed mechanism of HSF1 in regulating ABGC1 protein is not understood. However, there are reasonable hypotheses that the ABCG1 activity is post-transcriptionally regulated by the overexpression of HSF1 (Vydra et al., 2013). Interestingly, ABCG1 and ABCG2 are co-expressed in metastatic colon cancer cells, with ABCG1 influencing ABCG2 expression through the modulation of HIF-1α (Namba et al., 2018). This interaction suggests a crosstalk between ABCG1 and ABCG2, implicating HSF1 in regulating drug resistance and tumorigenesis by affecting ABCG2 through ABCG1.

Another key mechanism is that HSF1 acts as the major transcriptional regulator of the multidrug-resistant 1 gene (*MDR1*), which encodes the ABC transporter P-glycoprotein responsible for driving chemoresistance (Krishnamurthy et al.,

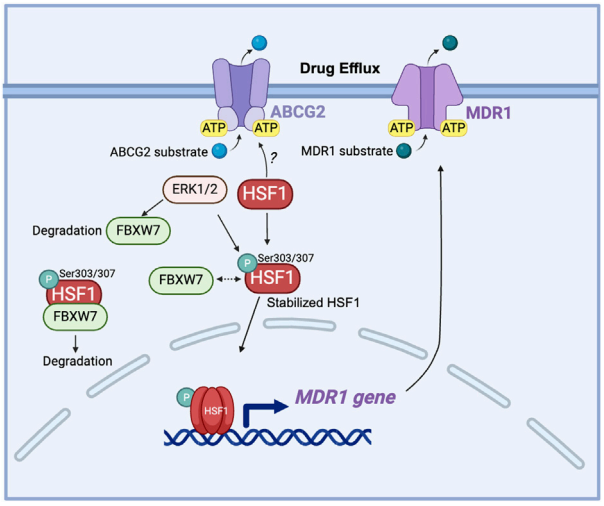

FIGURE 5
The role of HSF1 in cancer drug efflux. HSF1 upregulates the MDR1 gene expression in drug-resistant cells and is associated with the expression of ABCG2. ERK1/2 phosphorylates FBXW7 at the Thr205 residue, leading to the degradation of FBXW7. This degradation of FBXW7 reduces its ability to ubiquitinate and target HSF1 for proteasomal degradation, resulting in the stabilization of HSF1. The stabilized HSF1 then enhances the transcription of the *MDR1* gene, increasing MDR1 protein expression. Elevated levels of MDR1 contribute to drug resistance by actively pumping chemotherapeutic drugs out of cancer cells, thereby reducing their efficacy. Dashed arrow: dissociation. ABCG2, ATP-binding cassette sub-family G member 2; ATP, adenosine triphosphate; ERK: extracellular signal-regulated kinase; FBXW7, F-box and WD repeat domain-containing 7; HSF1, heat shock factor 1; MDR1, multidrug resistance protein 1 (also known as P-glycoprotein); P, phosphorylation; Ser, serine.

2012; Gumilar et al., 2023). Overexpression of activated HSF1 increases the MDR1 mRNA level along with enhanced P-glycoprotein cell surface expression (Vilaboa et al., 2000). Interestingly, this function of HSF1 persists even in HSF1 mutants that are unable to increase the transcription of HSP genes, implying that HSF1 may also activate *MDR1* through a non-transcriptional, stress-independent pathway (Tchenio et al., 2006). This finding expands the understanding of HSF1's role in chemoresistance, which may involve additional, pathways that do not rely solely on stress-induced HSP gene activation. HSF1, through its regulation of HSPs and interaction with SIRT1, contributes to 17-allylamino-17-demethoxygeldanamycin (17-AAG)-mediated chemoresistance in cancer stem-like cells by stabilizing key proteins and enhancing MDR1 drug efflux mechanisms (Kim et al., 2015). F-Box And WD Repeat Domain Containing 7 (FBXW7) has been reported to regulate the stability of nuclear HSF1 by binding to phosphorylated HSF1 at Ser303/307 and leading to HSF1 degradation (Kourtis et al., 2015; Yu et al., 2024). In drug-resistant cells, decreased FBXW7 expression driven by ERK1/2 activation stabilizes phosphorylated HSF1, which in turn enhances the *MDR1* transcription by directly binding to the *MDR1* promoter (Mun et al., 2020). This reveals the post-translational regulation of HSF1 in MDR1-mediated drug resistance (Figure 5).

Targeting HSF1 in conjunction with ABC transporters, particularly ABCG2 and ABCG1, represents a promising strategy for overcoming chemoresistance in various cancers. Inhibiting HSP90 with geldanamycin (GDN) or 17-AAG induces significant apoptotic cell death in glioma cell lines, where ABCG2 shows minimal and ineffective efflux of GDN and 17-AAG (Pastvova et al., 2021). HSP90 inhibitors have been known to induce HSF1 activation (Kijima et al., 2018); however, whether HSF1 regulates ABCG2 stability and expression is still unknown. Furthermore, HSF1 has both transcriptional and non-transcriptional roles in regulating drug efflux pathways, adding complexity to resistance mechanisms but reinforcing its potential as a valuable target for overcoming transporters-mediated resistance, including through MDR1. Further research is needed to elucidate the mechanisms of interaction between HSF1 and ABC transporters to optimize therapeutic strategies in cancer chemoresistance.

3.5 HSF1 inhibition in KRAS-mutated cancer

Cancers driven by KRAS mutants often show significant resistance to conventional and targeted chemotherapies, making them particularly challenging to treat (Negri et al., 2022; Singhal et al., 2024). For example, KRAS mutations are known to confer primary and secondary resistance to EGFR-targeted therapies in CRC and NSCLC. This is mainly because that KRAS functions downstream of receptor tyrosine kinases (RTKs), thus, constitutive KRAS activation will activate downstream signalings independently of the upstream RTK activity (Siddiqui and Piperdi, 2010; Zhao et al., 2017; Zhu et al., 2021). To effectively treat KRAS-driven tumors and to overcome chemoresistance conferred by KRAS mutants, effective inhibition of KRAS mutants would be ideal. Despite four decades of intensive research, targeting KRAS mutations directly remains challenging due to the protein's structural characteristics, which lack deep binding pockets, limiting the efficacy of traditional small-molecule inhibitors (Huang et al., 2021; Wadood et al., 2022; Zhu et al., 2022). Additionally, the mechanisms by which KRAS mutations confer chemoresistance, including interactions with downstream signaling pathways such as HSF1-mediated stress responses, are not fully understood.

An exciting recent advance in inhibiting KRAS mutants is the approval of KRAS(G12C)-mutant inhibitors for the clinical use. Both adagrasib and sotorasib are developed to target the KRAS(G12C)-mutant by covalently binding to the mutant cysteine residue in KRAS(G12C), leading to irreversible inhibition of the KRAS activity and blocking KRAS downstream signaling pathways essential for cancer cell proliferation. Both adagrasib and sotorasib have been approved explicitly for treating KRAS(G12C)-mutant NSCLC (Huang et al., 2021; Janne et al., 2022). However, G12C is only one of many mutations that having been found in KRAS in tumors and acquired resistance to KRAS(G12C) inhibitors has been observed. KRAS mutant tumors treated with KRAS inhibitors often develop resistance to these inhibitors through acquired *KRAS* alternations, *MET* amplification or oncogenic *BRAF* gene fusions and mutations. These tumors may also undergo phenotypic changes, such as epithelial-mesenchymal transition (EMT), or adopt survival mechanisms like metabolic rewiring and autophagy (Awad et al.,

2021; Yaeger et al., 2023). For example, although adagrasib can reverse multidrug resistance mediated by the MDR1 transporter (Zhang et al., 2022), the resistance to adagrasib has emerged through heterogeneous subclonal mutations in RAS-MAPK pathway components (e.g., NRAS, BRAF, and MAP2K1) that enable NSCLC tumor cells to reactivate MAPK signaling and bypass KRAS(G12C) inhibition (Tanaka et al., 2021). In order to obtain more durable responses to KRAS inhibitors, researchers are exploring combination therapies, such as pairing KRAS inhibitors with MEK or SHP2 inhibitors or with immune checkpoint inhibitors (Khan and O'Bryan, 2021; Hegazi et al., 2024). Thus, targeting KRAS for cancer treatment remains challenging, particularly in overcoming chemoresistance.

HSF1 is a downstream effector of the RAS-MEK pathway (Tang et al., 2015; Dai and Sampson, 2016) and KRAS-mutant cancers, due to their elevated levels of cellular stress resulting from rapid proliferation and metabolic demands, have a higher dependence on HSF1. Therefore, HSF1 represents a promising target for KRAS-mutant cancers, potentially addressing some resistance mechanisms by disrupting cancer cell stress responses. By targeting HSF1, it may be possible to exploit this stress vulnerability, making KRAS-mutant cancer cells more susceptible to therapeutic intervention. Targeting HSF1 in KRAS-mutant cancers, such as PDAC and NSCLC, where chemoresistance is common and therapeutic options are limited could open new avenues for treatment. By specifically disrupting the HSF1-mediated stress response in these tumors, HSF1 inhibitors may provide a novel approach to sensitize these cancers to existing therapies and improve clinical outcomes.

3.6 Challenges and opportunities in targeting HSF1 for cancer therapy

Several small molecules targeting HSF1 have been synthesized and their effects have been tested, primarily in *in vitro* and *in vivo* preclinical models. However, because HSF1 is a transcription factor and lacks clearly targetable sites, developing drugs that specifically target HSF1 remains highly challenging (Gumilar et al., 2023). Several HSF1 inhibitors have been discussed broadly (Dong et al., 2019; Cyran and Zhitkovich, 2022). Most current inhibitors target HSF1 indirectly and suffer from limited specificity and potency. Additionally, HSF1's role in tumorigenesis is complex, involving multiple signaling pathways that vary across different cancer types. Although several potential HSF1 inhibitors have been identified, we will mainly discuss current small molecules that directly interact with HSF1 in this review.

KRIBB11 is a small molecule known to directly associate with HSF1, disrupting its functional activity by preventing the recruitment of pTEFB on the promoter region of HSP70, as seen in a colorectal carcinoma cell line (Yoon et al., 2011). This blocks the transcription of *HSP70* and *HSP27* and the downstream stress response while inducing growth arrest and triggering caspase-dependent apoptosis. For example, in lung cancer, KRIBB11 induces apoptosis by reducing the level of Mcl-1, an anti-apoptotic protein (Kang et al., 2017). KRIBB11 induces apoptosis and cell cycle arrest in NSCLC, especially in combination therapies, by inhibiting the PI3K/AKT pathway, increasing ROS, and activating DNA damage responses (Zhang et al., 2024). In another study of NSCLC, KRIBB11 is shown to reduce drug resistance potentially associated with EMT by downregulating EMT-associated proteins, such as N-cadherin and vimentin, and EGFR, along with other key signaling molecules (Shibue and Weinberg, 2017; Lee et al., 2021). Although KRIBB11 directly associates with HSF1, it may also interact with other proteins or pathways, leading to off-target effects that lead to toxicities and narrowing the therapeutic window, thus complicating its clinical application.

DTHIB binds HSF1 directly and degrades HSF1 in the nucleus, thereby decreasing its nuclear activity and ultimately lowering its transcriptional activity in prostate cancer (Dong et al., 2020). DTHIB induces the degradation of HSF1 through the proteasome and the E3 ligase component FBXW7. Additionally, DTHIB effectively attenuated tumor growth in four therapy-resistant prostate cancer animal models, including a neuroendocrine prostate cancer model, where it caused profound tumor regression (Dong et al., 2019; Dong et al., 2020). However, further development and optimization are necessary to assess its efficacy in KRAS mutant cancers before advancing to clinical trials.

NXP800 (CCT361814) is currently the only inhibitor targeting the HSF1 pathway that has advanced to clinical trials, it is now in phase Ib clinical trial in platinum-resistant, ARID1a-mutated ovarian cancer (NCT05226507) (Cheeseman et al., 2017; clinicaltrials.gov 2021; Pasqua et al., 2023). This marks a significant milestone in HSF1-targeted cancer therapy. NXP800 has been shown to inhibit HSF1 transcriptional activity (Menezes et al., 2017; Workman et al., 2022). NXP800 inhibits HSF1 indirectly by activating the integrated stress response (ISR) through the general control nonderepressible 2 (GCN2), Activation of GCN2 leads to phosphorylation of eukaryotic translation initiation factor 2 α (eIF2α), which reduces global protein synthesis and selectively increases the translation of stress-responsive genes like activating transcription factor 4 (ATF4). Elevated ATF4 levels subsequently inhibit HSF1 activation, thereby diminishing the expression of HSF1-regulated genes This mechanism has been observed in human carcinoma cell lines and tumor xenograft models, where NXP800-induced ISR activation resulted in decreased HSF1 activity and reduced tumor cell proliferation (Cheeseman et al., 2017; Pasqua et al., 2023). NXP800-mediated inhibition of HSF1 induces sustained cellular stress, ultimately triggering programmed cell death. This therapeutic mechanism is particularly effective in cancers that heavily rely on HSF1 for protection against stress-induced damage, as it weakens the cells' defenses against therapeutic intervention. However, further extensive research is necessary to optimize this therapeutic approach, including investigations into optimal dosing strategies, potential synergistic effects with various chemotherapy agents, and a deeper understanding of the molecular pathways by which HSF1 inhibition impacts cancer cell survival and treatment resistance.

Technological advancements are revolutionizing the creation of HSF1 inhibitors to address chemoresistance. Proteolysis-targeting chimeras, or PROTACs, offer a strong alternative by completely degrading HSF1 rather than just inhibiting it, which has the potential to reduce the possibility of resistance. A proof-of-concept study has demonstrated the feasibility of HSF1 degradation using a bifunctional PROTAC molecular that

leverages KRIBB11-mediated binding and E3 ligase-mediated proteolysis (Sharma et al., 2022). Although this study has demonstrated the utility of the PROTAC approach for HSF1 inhibition, the effect of this approach on chemoresistance remains to be evaluated. Besides, an RNA aptamer that binds specifically and tightly to the DNA-binding domain of HSF1 has been developed and demonstrated to be able to block HSF1 from binding to DNA when delivered using a synthetic gene and strong promoter (Salamanca et al., 2011). Overall, the study highlights aptamers' potential for precise inhibition of HSF1 in cancer while minimizing off-target effects, providing a novel strategy to suppress cancer cell growth and survival by blocking HSF1's DNA-binding activity (Salamanca et al., 2014). Recently, nanoparticle drug delivery systems have demonstrated effective in enhancing the potency of HSF1 inhibitors by targeting them directly to tumor tissues. This approach reduces off-target side effects and maintains reliable treatment drug concentration. For example, one study shows that functionalized nanomaterials can efficiently transport small-molecule HSP inhibitors to tumor locations, boosting the effectiveness of both photothermal and photodynamic therapies (Premji et al., 2024). In addition, studies on hybrid nanoparticles enhanced with hyaluronic acid for delivering an HSP90 inhibitor emphasize their potential in targeted cancer therapy by enhancing drug delivery efficiency and specificity (Pan et al., 2021). Another study has developed aqueous bovine serum albumin nanoparticles for controlled delivery of the Hsp90 inhibitor luminespib. Through *in vitro* characterization and evaluations, this approach has demonstrated its potential as a nanoformulation for pancreatic and breast cancer therapy (K Rochani et al., 2020). Using advanced patient-derived models like organoids and xenografts allows for the assessment of HSF1 inhibitors in settings that closely resemble human tumors. This method results in more reliable predictions about their effectiveness and possible resistance (Yang et al., 2018). In summary, these advancements are driving the development of more effective HSF1-targeted therapies to tackle the issue of chemoresistance in cancer treatment specifically.

4 Conclusion and perspective

This review explores mechanisms of the HSF1's role in the proteotoxic stress response and its function during chemotherapy exposure. HSF1 regulates multiple pathways that contribute to chemoresistance throughout tumorigenesis. Because HSF1 is active in normal and cancerous cells, complete inhibition of HSF1 as a cancer treatment approach remains challenging. Among autophagy, apoptosis resistance, DNA damage repair, and drug efflux mechanisms, autophagy is often considered the key downstream pathway regulated by HSF1 in the context of chemotherapy resistance. HSF1-mediated autophagy enables cancer cells to manage cellular stress by degrading and recycling damaged proteins and organelles, supporting cell survival under chemotherapy-induced stress. This autophagy-driven survival mechanism is crucial, allowing cancer cells to resist apoptosis and maintain functionality despite therapeutic interventions. Therefore, while drug efflux, apoptosis resistance, and DNA damage repair are important, autophagy is likely the primary downstream pathway through which HSF1 exerts its protective effects against chemotherapy. Given the high expression of HSF1 in various cancer types and its role in chemoresistance, inhibiting HSF1 may offer a promising therapeutic strategy to counteract chemoresistance. This strategy could potentially disrupt the mechanisms that enable cancer cells to resist chemotherapy, enhancing the efficacy of treatment.

Author contributions

SG: Writing–original draft, Writing–review and editing. RS: Writing–original draft, Writing–review and editing. K-HS: Conceptualization, Funding acquisition, Investigation, Project administration, Resources, Supervision, Validation, Visualization, Writing–original draft, Writing–review and editing.

Funding

The author(s) declare that financial support was received for the research, authorship, and/or publication of this article. This work was supported by the University of Toledo Fund Number #110917 and the National Cancer Institute of the National Institutes of Health under Award Number K22CA248616. The content is solely the responsibility of the authors and does not necessarily represent the official views of the National Institutes of Health.

Acknowledgments

The images were created with BioRender.com.

Conflict of interest

The authors declare that the research was conducted in the absence of any commercial or financial relationships that could be construed as a potential conflict of interest.

The author(s) declared that they were an editorial board member of Frontiers, at the time of submission. This had no impact on the peer review process and the final decision.

Publisher's note

All claims expressed in this article are solely those of the authors and do not necessarily represent those of their affiliated organizations, or those of the publisher, the editors and the reviewers. Any product that may be evaluated in this article, or claim that may be made by its manufacturer, is not guaranteed or endorsed by the publisher.

References

Ai, H., Zhou, W., Wang, Z., Qiong, G., Chen, Z., and Deng, S. (2019). microRNAs-107 inhibited autophagy, proliferation, and migration of breast cancer cells by targeting HMGB1. *J. Cell Biochem.* 120 (5), 8696–8705. doi:10.1002/jcb.28157

Alasady, M. J., and Mendillo, M. L. (2020). The multifaceted role of HSF1 in tumorigenesis. *Adv. Exp. Med. Biol.* 1243, 69–85. doi:10.1007/978-3-030-40204-4_5

Alhasan, B., Gladova, Y. A., Sverchinsky, D. V., Aksenov, N. D., Margulis, B. A., and Guzhova, I. V. (2024). Hsp70 negatively regulates autophagy via governing AMPK activation, and dual hsp70-autophagy inhibition induces synergetic cell death in NSCLC cells. *Int. J. Mol. Sci.* 25 (16), 9090. doi:10.3390/ijms25169090

Anckar, J., and Sistonen, L. (2011). Regulation of HSF1 function in the heat stress response: implications in aging and disease. *Annu. Rev. Biochem.* 80, 1089–1115. doi:10.1146/annurev-biochem-060809-095203

Antonietti, P., Linder, B., Hehlgans, S., Mildenberger, I. C., Burger, M. C., Fulda, S., et al. (2017). Interference with the HSF1/HSP70/BAG3 pathway primes glioma cells to matrix detachment and BH3 mimetic-induced apoptosis. *Mol. Cancer Ther.* 16 (1), 156–168. doi:10.1158/1535-7163.MCT-16-0262

Asada, Y., Tsuruta, M., Okabayashi, K., Shigeta, K., Ishida, T., Shimada, T., et al. (2021). Inhibition of heat-shock protein 27 reduces 5-Fluorouracil-acquired resistance in human colon cancer cells. *Anticancer Res.* 41 (3), 1283–1290. doi:10.21873/anticanres.14885

Ashkenazi, A. (2015). Targeting the extrinsic apoptotic pathway in cancer: lessons learned and future directions. *J. Clin. Invest* 125 (2), 487–489. doi:10.1172/JCI80420

Awad, M. M., Liu, S., Rybkin, I. I., Arbour, K. C., Dilly, J., Zhu, V. W., et al. (2021). Acquired resistance to KRAS(G12C) inhibition in cancer. *N. Engl. J. Med.* 384 (25), 2382–2393. doi:10.1056/NEJMoa2105281

Bailey, P., Chang, D. K., Nones, K., Johns, A. L., Patch, A. M., Gingras, M. C., et al. (2016). Genomic analyses identify molecular subtypes of pancreatic cancer. *Nature* 531 (7592), 47–52. doi:10.1038/nature16965

Buchwalter, G., Gross, C., and Wasylyk, B. (2004). Ets ternary complex transcription factors. *Gene* 324, 1–14. doi:10.1016/j.gene.2003.09.028

Bukau, B., Weissman, J., and Horwich, A. (2006). Molecular chaperones and protein quality control. *Cell* 125 (3), 443–451. doi:10.1016/j.cell.2006.04.014

Cai, Q., Wang, S., Jin, L., Weng, M., Zhou, D., Wang, J., et al. (2019). Long non-coding RNA GBCDRlnc1 induces chemoresistance of gallbladder cancer cells by activating autophagy. *Mol. Cancer* 18 (1), 82. doi:10.1186/s12943-019-1016-0

Cancer Genome Atlas Research, N. (2014). Comprehensive molecular profiling of lung adenocarcinoma. *Nature* 511 (7511), 543–550. doi:10.1038/nature13385

Carpenter, R. L., Paw, I., Dewhirst, M. W., and Lo, H. W. (2015). Akt phosphorylates and activates HSF-1 independent of heat shock, leading to Slug overexpression and epithelial-mesenchymal transition (EMT) of HER2-overexpressing breast cancer cells. *Oncogene* 34 (5), 546–557. doi:10.1038/onc.2013.582

Chatterjee, S., Bhattacharya, S., Socinski, M. A., and Burns, T. F. (2016). HSP90 inhibitors in lung cancer: promise still unfulfilled. *Clin. Adv. Hematol. Oncol.* 14 (5), 346–356.

Chatterjee, S., and Burns, T. F. (2017). Targeting heat shock proteins in cancer: a promising therapeutic approach. *Int. J. Mol. Sci.* 18 (9), 1978. doi:10.3390/ijms18091978

Chauhan, D., Li, G., Hideshima, T., Podar, K., Mitsiades, C., Mitsiades, N., et al. (2003). Hsp27 inhibits release of mitochondrial protein Smac in multiple myeloma cells and confers dexamethasone resistance. *Blood* 102 (9), 3379–3386. doi:10.1182/blood-2003-05-1417

Cheeseman, M. D., Chessum, N. E., Rye, C. S., Pasqua, A. E., Tucker, M. J., Wilding, B., et al. (2017). Discovery of a chemical probe bisamide (CCT251236): an orally bioavailable efficacious pirin ligand from a heat shock transcription factor 1 (HSF1) phenotypic screen. *J. Med. Chem.* 60 (1), 180–201. doi:10.1021/acs.jmedchem.6b01055

Chen, K., Qian, W., Li, J., Jiang, Z., Cheng, L., Yan, B., et al. (2017). Loss of AMPK activation promotes the invasion and metastasis of pancreatic cancer through an HSF1-dependent pathway. *Mol. Oncol.* 11 (10), 1475–1492. doi:10.1002/1878-0261.12116

Chen, M., and Xie, S. (2018). Therapeutic targeting of cellular stress responses in cancer. *Thorac. Cancer* 9 (12), 1575–1582. doi:10.1111/1759-7714.12890

Chiosis, G., Vilenchik, M., Kim, J., and Solit, D. (2004). Hsp90: the vulnerable chaperone. *Drug Discov. Today* 9 (20), 881–888. doi:10.1016/S1359-6446(04)03245-3

Chou, C. H., Hwang, C. L., and Wu, Y. T. (2012a). Effect of exercise on physical function, daily living activities, and quality of life in the frail older adults: a meta-analysis. *Arch. Phys. Med. Rehabil.* 93 (2), 237–244. doi:10.1016/j.apmr.2011.08.042

Chou, S. D., Prince, T., Gong, J., and Calderwood, S. K. (2012b). mTOR is essential for the proteotoxic stress response, HSF1 activation and heat shock protein synthesis. *PLoS One* 7 (6), e39679. doi:10.1371/journal.pone.0039679

clinicaltrials.gov (2021). *A phase 1 clinical study of NXP800 in subjects with advanced cancers and expansion in subjects with ovarian cancer.*

Cyran, A. M., and Zhitkovich, A. (2022). Heat shock proteins and HSF1 in cancer. *Front. Oncol.* 12, 860320. doi:10.3389/fonc.2022.860320

Dai, C., Dai, S., and Cao, J. (2012). Proteotoxic stress of cancer: implication of the heat-shock response in oncogenesis. *J. Cell Physiol.* 227 (8), 2982–2987. doi:10.1002/jcp.24017

Dai, C., and Sampson, S. B. (2016). HSF1: guardian of proteostasis in cancer. *Trends Cell Biol.* 26 (1), 17–28. doi:10.1016/j.tcb.2015.10.011

Dai, C., Whitesell, L., Rogers, A. B., and Lindquist, S. (2007). Heat shock factor 1 is a powerful multifaceted modifier of carcinogenesis. *Cell* 130 (6), 1005–1018. doi:10.1016/j.cell.2007.07.020

Dai, S., Tang, Z., Cao, J., Zhou, W., Li, H., Sampson, S., et al. (2015). Suppression of the HSF1-mediated proteotoxic stress response by the metabolic stress sensor AMPK. *EMBO J.* 34 (3), 275–293. doi:10.15252/embj.201489062

Das, C. K., Linder, B., Bonn, F., Rothweiler, F., Dikic, I., Michaelis, M., et al. (2018). BAG3 overexpression and cytoprotective autophagy mediate apoptosis resistance in chemoresistant breast cancer cells. *Neoplasia* 20 (3), 263–279. doi:10.1016/j.neo.2018.01.001

Dayalan Naidu, S., Dikovskaya, D., Gaurilcikaite, E., Knatko, E. V., Healy, Z. R., Mohan, H., et al. (2017). Transcription factors NRF2 and HSF1 have opposing functions in autophagy. *Sci. Rep.* 7 (1), 11023. doi:10.1038/s41598-017-11262-5

Debnath, J., Gammoh, N., and Ryan, K. M. (2023). Autophagy and autophagy-related pathways in cancer. *Nat. Rev. Mol. Cell Biol.* 24 (8), 560–575. doi:10.1038/s41580-023-00585-z

Desai, S., Liu, Z., Yao, J., Patel, N., Chen, J., Wu, Y., et al. (2013). Heat shock factor 1 (HSF1) controls chemoresistance and autophagy through transcriptional regulation of autophagy-related protein 7 (ATG7). *J. Biol. Chem.* 288 (13), 9165–9176. doi:10.1074/jbc.M112.422071

Dong, B., Jaeger, A. M., Hughes, P. F., Loiselle, D. R., Hauck, J. S., Fu, Y., et al. (2020). Targeting therapy-resistant prostate cancer via a direct inhibitor of the human heat shock transcription factor 1. *Sci. Transl. Med.* 12 (574), eabb5647. doi:10.1126/scitranslmed.abb5647

Dong, B., Jaeger, A. M., and Thiele, D. J. (2019). Inhibiting heat shock factor 1 in cancer: a unique therapeutic opportunity. *Trends Pharmacol. Sci.* 40 (12), 986–1005. doi:10.1016/j.tips.2019.10.008

Doyle, L., and Ross, D. D. (2003). Multidrug resistance mediated by the breast cancer resistance protein BCRP (ABCG2). *Oncogene* 22 (47), 7340–7358. doi:10.1038/sj.onc.1206938

Dudeja, V., Chugh, R. K., Sangwan, V., Skube, S. J., Mujumdar, N. R., Antonoff, M. B., et al. (2011). Prosurvival role of heat shock factor 1 in the pathogenesis of pancreatobiliary tumors. *Am. J. Physiol. Gastrointest. Liver Physiol.* 300 (6), G948–G955. doi:10.1152/ajpgi.00346.2010

Dzobo, K., Senthebane, D. A., Thomford, N. E., Rowe, A., Dandara, C., and Parker, M. I. (2018). Not everyone fits the mold: intratumor and intertumor heterogeneity and innovative cancer drug design and development. *OMICS* 22 (1), 17–34. doi:10.1089/omi.2017.0174

Edlich, F., Erdmann, F., Jarczowski, F., Moutty, M. C., Weiwad, M., and Fischer, G. (2007). The Bcl-2 regulator FKBP38-calmodulin-Ca2+ is inhibited by Hsp90. *J. Biol. Chem.* 282 (21), 15341–15348. doi:10.1074/jbc.M611594200

Emran, T. B., Shahriar, A., Mahmud, A. R., Rahman, T., Abir, M. H., Siddiquee, M. F., et al. (2022). Multidrug resistance in cancer: understanding molecular mechanisms, immunoprevention and therapeutic approaches. *Front. Oncol.* 12, 891652. doi:10.3389/fonc.2022.891652

Fang, F., Chang, R., and Yang, L. (2012). Heat shock factor 1 promotes invasion and metastasis of hepatocellular carcinoma *in vitro* and *in vivo*. *Cancer* 118 (7), 1782–1794. doi:10.1002/cncr.26482

Florea, A. M., and Busselberg, D. (2011). Cisplatin as an anti-tumor drug: cellular mechanisms of activity, drug resistance and induced side effects. *Cancers (Basel)* 3 (1), 1351–1371. doi:10.3390/cancers3011351

Fujimoto, M., Takii, R., Takaki, E., Katiyar, A., Nakato, R., Shirahige, K., et al. (2017). The HSF1-PARP13-PARP1 complex facilitates DNA repair and promotes mammary tumorigenesis. *Nat. Commun.* 8 (1), 1638. doi:10.1038/s41467-017-01807-7

Fulda, S., Gorman, A. M., Hori, O., and Samali, A. (2010). Cellular stress responses: cell survival and cell death. *Int. J. Cell Biol.* 2010, 214074. doi:10.1155/2010/214074

Ghai, S., Young, A., and Su, K. H. (2023). Proteotoxic stress response in atherosclerotic cardiovascular disease: emerging role of heat shock factor 1. *Front. Cardiovasc Med.* 10, 1155444. doi:10.3389/fcvm.2023.1155444

Ghai, S., Shrestha, R., Hegazi, A., Boualoy, V., Liu, S. H., and Su, K. H. (2024). The role of heat shock factor 1 in preserving proteomic integrity during copper-induced cellular toxicity. *Int. J. Mol. Sci.* 25 (21), 11657. doi:10.3390/ijms252111657

Gidalevitz, T., Prahlad, V., and Morimoto, R. I. (2011). The stress of protein misfolding: from single cells to multicellular organisms. *Cold Spring Harb. Perspect. Biol.* 3 (6), a009704. doi:10.1101/cshperspect.a009704

Giordano, T. J. (2014). The cancer genome atlas research network: a sight to behold. *Endocr. Pathol.* 25 (4), 362–365. doi:10.1007/s12022-014-9345-4

Gomez-Pastor, R., Burchfiel, E. T., and Thiele, D. J. (2018). Regulation of heat shock transcription factors and their roles in physiology and disease. *Nat. Rev. Mol. Cell Biol.* 19 (1), 4–19. doi:10.1038/nrm.2017.73

Gu, Y., Chen, T., Li, G., Xu, C., Xu, Z., Zhang, J., et al. (2017). Lower Beclin 1 downregulates HER2 expression to enhance tamoxifen sensitivity and predicts a favorable outcome for ER positive breast cancer. *Oncotarget* 8 (32), 52156–52177. doi:10.18632/oncotarget.11044

Guettouche, T., Boellmann, F., Lane, W. S., and Voellmy, R. (2005). Analysis of phosphorylation of human heat shock factor 1 in cells experiencing a stress. *BMC Biochem.* 6, 4. doi:10.1186/1471-2091-6-4

Gumilar, K. E., Chin, Y., Ibrahim, I. H., Tjokroprawiro, B. A., Yang, J. Y., Zhou, M., et al. (2023). Heat shock factor 1 inhibition: a novel anti-cancer strategy with promise for precision oncology. *Cancers (Basel)* 15 (21), 5167. doi:10.3390/cancers15215167

Guo, J., Du, X., and Li, C. (2022). BAG family proteins contributes to autophagy-mediated multidrug resistance of tumor. *Clin. Transl. Oncol.* 24 (8), 1492–1500. doi:10.1007/s12094-022-02819-6

Guo, Q., Jin, Y., Chen, X., Ye, X., Shen, X., Lin, M., et al. (2024). NF-κB in biology and targeted therapy: new insights and translational implications. *Signal Transduct. Target Ther.* 9 (1), 53. doi:10.1038/s41392-024-01757-9

Harris, L. N., Broadwater, G., Lin, N. U., Miron, A., Schnitt, S. J., Cowan, D., et al. (2006). Molecular subtypes of breast cancer in relation to paclitaxel response and outcomes in women with metastatic disease: results from CALGB 9342. *Breast Cancer Res.* 8 (6), R66. doi:10.1186/bcr1622

Hasan, S., Taha, R., and Omri, H. E. (2018). Current opinions on chemoresistance: an overview. *Bioinformation* 14 (2), 80–85. doi:10.6026/97320630014080

He, H. L., Lee, Y. E., Chen, H. P., Hsing, C. H., Chang, I. W., Shiue, Y. L., et al. (2015). Overexpression of DNAJC12 predicts poor response to neoadjuvant concurrent chemoradiotherapy in patients with rectal cancer. *Exp. Mol. Pathol.* 98 (3), 338–345. doi:10.1016/j.yexmp.2015.03.029

He, Y., Sun, M. M., Zhang, G. G., Yang, J., Chen, K. S., Xu, W. W., et al. (2021). Targeting PI3K/Akt signal transduction for cancer therapy. *Signal Transduct. Target Ther.* 6 (1), 425. doi:10.1038/s41392-021-00828-5

Hegazi, A., Rager, L. E., Watkins, D. E., and Su, K. H. (2024). Advancing immunotherapy in pancreatic cancer. *Int. J. Mol. Sci.* 25 (21), 11560. doi:10.3390/ijms252111560

Hietakangas, V., Ahlskog, J. K., Jakobsson, A. M., Hellesuo, M., Sahlberg, N. M., Holmberg, C. I., et al. (2003). Phosphorylation of serine 303 is a prerequisite for the stress-inducible SUMO modification of heat shock factor 1. *Mol. Cell Biol.* 23 (8), 2953–2968. doi:10.1128/MCB.23.8.2953-2968.2003

Holmberg, E. B., Hillman, R. E., Hammarberg, B., Sodersten, M., and Doyle, P. (2001). Efficacy of a behaviorally based voice therapy protocol for vocal nodules. *J. Voice* 15 (3), 395–412. doi:10.1016/S0892-1997(01)00041-8

Huang, L., Guo, Z., Wang, F., and Fu, L. (2021). KRAS mutation: from undruggable to druggable in cancer. *Signal Transduct. Target Ther.* 6 (1), 386. doi:10.1038/s41392-021-00780-4

Ishikawa, C., and Mori, N. (2023). Heat shock factor 1 is a promising therapeutic target against adult T-cell leukemia. *Med. Oncol.* 40 (6), 172. doi:10.1007/s12032-023-02042-5

Jackson, S. P., and Bartek, J. (2009). The DNA-damage response in human biology and disease. *Nature* 461 (7267), 1071–1078. doi:10.1038/nature08467

Jacobs, A. T., and Marnett, L. J. (2009). HSF1-mediated BAG3 expression attenuates apoptosis in 4-hydroxynonenal-treated colon cancer cells via stabilization of anti-apoptotic Bcl-2 proteins. *J. Biol. Chem.* 284 (14), 9176–9183. doi:10.1074/jbc.M808656200

Janne, P. A., Riely, G. J., Gadgeel, S. M., Heist, R. S., Ou, S. I., Pacheco, J. M., et al. (2022). Adagrasib in non-small-cell lung cancer harboring a ^{G12C} mutation. *N. Engl. J. Med.* 387 (2), 120–131. doi:10.1056/NEJMoa2204619

Jin, X., Moskophidis, D., and Mivechi, N. F. (2011). Heat shock transcription factor 1 is a key determinant of HCC development by regulating hepatic steatosis and metabolic syndrome. *Cell Metab.* 14 (1), 91–103. doi:10.1016/j.cmet.2011.03.025

Kang, G. Y., Kim, E. H., Lee, H. J., Gil, N. Y., Cha, H. J., and Lee, Y. S. (2015). Heat shock factor 1, an inhibitor of non-homologous end joining repair. *Oncotarget* 6 (30), 29712–29724. doi:10.18632/oncotarget.5073

Kang, M. J., Yun, H. H., and Lee, J. H. (2017). KRIBB11 accelerates Mcl-1 degradation through an HSF1-independent, Mule-dependent pathway in A549 non-small cell lung cancer cells. *Biochem. Biophys. Res. Commun.* 492 (3), 304–309. doi:10.1016/j.bbrc.2017.08.118

Khan, I., and O'Bryan, J. P. (2021). Probing RAS function with monobodies. *Methods Mol. Biol.* 2262, 281–302. doi:10.1007/978-1-0716-1190-6_17

Khan, S. U., Fatima, K., Aisha, S., and Malik, F. (2024). Unveiling the mechanisms and challenges of cancer drug resistance. *Cell Commun. Signal* 22 (1), 109. doi:10.1186/s12964-023-01302-1

Kijima, T., Prince, T., Neckers, L., Koga, F., and Fujii, Y. (2019). Heat shock factor 1 (HSF1)-targeted anticancer therapeutics: overview of current preclinical progress. *Expert Opin. Ther. Targets* 23 (5), 369–377. doi:10.1080/14728222.2019.1602119

Kijima, T., Prince, T. L., Tigue, M. L., Yim, K. H., Schwartz, H., Beebe, K., et al. (2018). HSP90 inhibitors disrupt a transient HSP90-HSF1 interaction and identify a noncanonical model of HSP90-mediated HSF1 regulation. *Sci. Rep.* 8 (1), 6976. doi:10.1038/s41598-018-25404-w

Kim, H. B., Lee, S. H., Um, J. H., Kim, M. J., Hyun, S. K., Gong, E. J., et al. (2015). Sensitization of chemo-resistant human chronic myeloid leukemia stem-like cells to Hsp90 inhibitor by SIRT1 inhibition. *Int. J. Biol. Sci.* 11 (8), 923–934. doi:10.7150/ijbs.10896

Kizilboga, T., Ozden, C., Can, N. D., Onay Ucar, E., and Dinler Doganay, G. (2024). Bag-1-mediated HSF1 phosphorylation regulates expression of heat shock proteins in breast cancer cells. *FEBS Open Bio* 14 (9), 1559–1569. doi:10.1002/2211-5463.13843

Kourtis, N., Moubarak, R. S., Aranda-Orgilles, B., Lui, K., Aydin, I. T., Trimarchi, T., et al. (2015). FBXW7 modulates cellular stress response and metastatic potential through HSF1 post-translational modification. *Nat. Cell Biol.* 17 (3), 322–332. doi:10.1038/ncb3121

Krishnamurthy, K., Vedam, K., Kanagasabai, R., Druhan, L. J., and Ilangovan, G. (2012). Heat shock factor-1 knockout induces multidrug resistance gene, MDR1b, and enhances P-glycoprotein (ABCB1)-based drug extrusion in the heart. *Proc. Natl. Acad. Sci. U. S. A.* 109 (23), 9023–9028. doi:10.1073/pnas.1200731109

K Rochani, A., Balasubramanian, S., Ravindran Girija, A., Maekawa, T., Kaushal, G., and Kumar, D. S. (2020). Heat shock protein 90 (Hsp90)-Inhibitor-Luminespib-Loaded-Protein-Based nanoformulation for cancer therapy. *Polym. (Basel)* 12 (8), 1798. doi:10.3390/polym12081798

Lan, N., Su, Y., Zeng, Q., Zhou, P., Hu, Y., Zhang, Z., et al. (2024). JD-02, a novel Hsp90 inhibitor, induces ROS/SRC axis-dependent cytoprotective autophagy in colorectal cancer cells. *Mol. Carcinog.* 63 (6), 1038–1050. doi:10.1002/mc.23706

Lee, J. G., and Wu, R. (2012). Combination erlotinib-cisplatin and Atg3-mediated autophagy in erlotinib resistant lung cancer. *PLoS One* 7 (10), e48532. doi:10.1371/journal.pone.0048532

Lee, S., Jung, J., Lee, Y. J., Kim, S. K., Kim, J. A., Kim, B. K., et al. (2021). Targeting HSF1 as a therapeutic strategy for multiple mechanisms of EGFR inhibitor resistance in EGFR mutant non-small-cell lung cancer. *Cancers (Basel)* 13 (12), 2987. doi:10.3390/cancers13122987

Li, W., Yang, C., Li, J., Li, X., and Zhou, P. (2023a). MicroRNA-217 aggravates breast cancer through activation of NF1-mediated HSF1/ATG7 axis and c-Jun/ATF3/MMP13 axis. *Hum. Cell* 36 (1), 377–392. doi:10.1007/s13577-022-00817-y

Li, X., Wang, Z., Gao, B., Dai, K., Wu, J., Shen, K., et al. (2024). Unveiling the impact of SUMOylation at K298 site of heat shock factor 1 on glioblastoma malignant progression. *Neoplasia* 57, 101055. doi:10.1016/j.neo.2024.101055

Li, X., Zhou, Y., Li, Y., Yang, L., Ma, Y., Peng, X., et al. (2019). Autophagy: a novel mechanism of chemoresistance in cancers. *Biomed. Pharmacother.* 119, 109415. doi:10.1016/j.biopha.2019.109415

Li, Y., Wang, B., Ma, F., Jiang, D., Wang, Y., Li, K., et al. (2023b). Proteomic characterization of the colorectal cancer response to chemoradiation and targeted therapies reveals potential therapeutic strategies. *Cell Rep. Med.* 4 (12), 101311. doi:10.1016/j.xcrm.2023.101311

Liang, W., Liao, Y., Zhang, J., Huang, Q., Luo, W., Yu, J., et al. (2017). Heat shock factor 1 inhibits the mitochondrial apoptosis pathway by regulating second mitochondria-derived activator of caspase to promote pancreatic tumorigenesis. *J. Exp. Clin. Cancer Res.* 36 (1), 64. doi:10.1186/s13046-017-0537-x

Lim, C. H., Fang, X. Q., Kang, H., Oh, T., Lee, S., Kim, Y. S., et al. (2024). ER stress-activated HSF1 governs cancer cell resistance to USP7 inhibitor-based chemotherapy through the PERK pathway. *Int. J. Mol. Sci.* 25 (5), 2768. doi:10.3390/ijms25052768

Lindquist, S. (1986). The heat-shock response. *Annu. Rev. Biochem.* 55, 1151–1191. doi:10.1146/annurev.bi.55.070186.005443

Liu, K., and Ma, R. (2021). MicroRNA-615-5p regulates the proliferation and apoptosis of breast cancer cells by targeting HSF1. *Exp. Ther. Med.* 21 (3), 192. doi:10.3892/etm.2021.9624

Logan, I. R., McNeill, H. V., Cook, S., Lu, X., Meek, D. W., Fuller-Pace, F. V., et al. (2009). Heat shock factor-1 modulates p53 activity in the transcriptional response to DNA damage. *Nucleic Acids Res.* 37 (9), 2962–2973. doi:10.1093/nar/gkp180

Luo, J., Solimini, N. L., and Elledge, S. J. (2009). Principles of cancer therapy: oncogene and non-oncogene addiction. *Cell* 136 (5), 823–837. doi:10.1016/j.cell.2009.02.024

Mansoori, B., Mohammadi, A., Davudian, S., Shirjang, S., and Baradaran, B. (2017). The different mechanisms of cancer drug resistance: a brief review. *Adv. Pharm. Bull.* 7 (3), 339–348. doi:10.15171/apb.2017.041

Mao, Q., and Unadkat, J. D. (2015). Role of the breast cancer resistance protein (BCRP/ABCG2) in drug transport--an update. *AAPS J.* 17 (1), 65–82. doi:10.1208/s12248-014-9668-6

Mendillo, M. L., Santagata, S., Koeva, M., Bell, G. W., Hu, R., Tamimi, R. M., et al. (2012). HSF1 drives a transcriptional program distinct from heat shock to support highly malignant human cancers. *Cell* 150 (3), 549–562. doi:10.1016/j.cell.2012.06.031

Menezes, K., Aram, G., Mirabella, F., Johnson, D. C., Sherborne, A. L., Houlston, R. S., et al. (2017). The novel protein HSF1 stress pathway inhibitor bisamide

CCT361814 demonstrates pre-clinical anti-tumor activity in myeloma. *Blood* 130, 3072. doi:10.1182/blood.V130.Suppl_1.3072.3072

Meng, L., Gabai, V. L., and Sherman, M. Y. (2010). Heat-shock transcription factor HSF1 has a critical role in human epidermal growth factor receptor-2-induced cellular transformation and tumorigenesis. *Oncogene* 29 (37), 5204–5213. doi:10.1038/onc.2010.277

Min, J. N., Huang, L., Zimonjic, D. B., Moskophidis, D., and Mivechi, N. F. (2007). Selective suppression of lymphomas by functional loss of Hsf1 in a p53-deficient mouse model for spontaneous tumors. *Oncogene* 26 (35), 5086–5097. doi:10.1038/sj.onc.1210317

Minoia, M., Boncoraglio, A., Vinet, J., Morelli, F. F., Brunsting, J. F., Poletti, A., et al. (2014). BAG3 induces the sequestration of proteasomal clients into cytoplasmic puncta: implications for a proteasome-to-autophagy switch. *Autophagy* 10 (9), 1603–1621. doi:10.4161/auto.29409

Mo, W., and Zhang, J. T. (2012). Human ABCG2: structure, function, and its role in multidrug resistance. *Int. J. Biochem. Mol. Biol.* 3 (1), 1–27.

Mohammed, W. H., Sulaiman, G. M., Abomughaid, M. M., Klionsky, D. J., and Abu-Alghayth, M. H. (2024). The dual role of autophagy in suppressing and promoting hepatocellular carcinoma. *Front. Cell Dev. Biol.* 12, 1472574. doi:10.3389/fcell.2024.1472574

Mun, G. I., Choi, E., Lee, Y., and Lee, Y. S. (2020). Decreased expression of FBXW7 by ERK1/2 activation in drug-resistant cancer cells confers transcriptional activation of MDR1 by suppression of ubiquitin degradation of HSF1. *Cell Death Dis.* 11 (5), 395. doi:10.1038/s41419-020-2600-3

Murray, S., Briasoulis, E., Linardou, H., Bafaloukos, D., and Papadimitriou, C. (2012). Taxane resistance in breast cancer: mechanisms, predictive biomarkers and circumvention strategies. *Cancer Treat. Rev.* 38 (7), 890–903. doi:10.1016/j.ctrv.2012.02.011

Namba, Y., Sogawa, C., Okusha, Y., Kawai, H., Itagaki, M., Ono, K., et al. (2018). Depletion of lipid efflux pump ABCG1 triggers the intracellular accumulation of extracellular vesicles and reduces aggregation and tumorigenesis of metastatic cancer cells. *Front. Oncol.* 8, 376. doi:10.3389/fonc.2018.00376

Neef, D. W., Jaeger, A. M., Gomez-Pastor, R., Willmund, F., Frydman, J., and Thiele, D. J. (2014). A direct regulatory interaction between chaperonin TRiC and stress-responsive transcription factor HSF1. *Cell Rep.* 9 (3), 955–966. doi:10.1016/j.celrep.2014.09.056

Negri, F., Bottarelli, L., de'Angelis, G. L., and Gnetti, L. (2022). KRAS: a druggable target in colon cancer patients. *Int. J. Mol. Sci.* 23 (8), 4120. doi:10.3390/ijms23084120

Neudegger, T., Verghese, J., Hayer-Hartl, M., Hartl, F. U., and Bracher, A. (2016). Structure of human heat-shock transcription factor 1 in complex with DNA. *Nat. Struct. Mol. Biol.* 23 (2), 140–146. doi:10.1038/nsmb.3149

Noguchi, K., Katayama, K., and Sugimoto, Y. (2014). Human ABC transporter ABCG2/BCRP expression in chemoresistance: basic and clinical perspectives for molecular cancer therapeutics. *Pharmgenomics Pers. Med.* 7, 53–64. doi:10.2147/PGPM.S38295

Nusrat, F., Khanna, A., Jain, A., Jiang, W., Lavu, H., Yeo, C. J., et al. (2024). The clinical implications of KRAS mutations and variant allele frequencies in pancreatic ductal adenocarcinoma. *J. Clin. Med.* 13 (7), 2103. doi:10.3390/jcm13072103

Oliver, T. G., Mercer, K. L., Sayles, L. C., Burke, J. R., Mendus, D., Lovejoy, K. S., et al. (2010). Chronic cisplatin treatment promotes enhanced damage repair and tumor progression in a mouse model of lung cancer. *Genes Dev.* 24 (8), 837–852. doi:10.1101/gad.1897010

Oromendia, A. B., Dodgson, S. E., and Amon, A. (2012). Aneuploidy causes proteotoxic stress in yeast. *Genes Dev.* 26 (24), 2696–2708. doi:10.1101/gad.207407.112

Pan, C., Zhang, T., Li, S., Xu, Z., Pan, B., Xu, S., et al. (2021). Hybrid nanoparticles modified by hyaluronic acid loading an HSP90 inhibitor as a novel delivery system for subcutaneous and orthotopic colon cancer therapy. *Int. J. Nanomedicine* 16, 1743–1755. doi:10.2147/IJN.S275805

Pasqua, A. E., Sharp, S. Y., Chessum, N. E. A., Hayes, A., Pellegrino, L., Tucker, M. J., et al. (2023). HSF1 pathway inhibitor clinical candidate (CCT361814/NXP800) developed from a phenotypic screen as a potential treatment for refractory ovarian cancer and other malignancies. *J. Med. Chem.* 66 (8), 5907–5936. doi:10.1021/acs.jmedchem.3c00156

Pastvova, N., Dolezel, P., and Mlejnek, P. (2021). Heat shock protein inhibitor 17-allyamino-17-demethoxygeldanamycin, a potent inductor of apoptosis in human glioma tumor cell lines, is a weak substrate for ABCB1 and ABCG2 transporters. *Pharm. (Basel)* 14 (2), 107. doi:10.3390/ph14020107

Peng, H., Qi, J., Dong, Z., and Zhang, J. T. (2010). Dynamic vs static ABCG2 inhibitors to sensitize drug resistant cancer cells. *PLoS One* 5 (12), e15276. doi:10.1371/journal.pone.0015276

Piya, S., Kornblau, S. M., Ruvolo, V. R., Mu, H., Ruvolo, P. P., McQueen, T., et al. (2016). Atg7 suppression enhances chemotherapeutic agent sensitivity and overcomes stroma-mediated chemoresistance in acute myeloid leukemia. *Blood* 128 (9), 1260–1269. doi:10.1182/blood-2016-01-692244

Premji, T. P., Dash, B. S., Das, S., and Chen, J. P. (2024). Functionalized nanomaterials for inhibiting ATP-dependent heat shock proteins in cancer photothermal/photodynamic therapy and combination therapy. *Nanomater. (Basel).* 14 (1), 112. doi:10.3390/nano14010112

Prince, T. L., Lang, B. J., Guerrero-Gimenez, M. E., Fernandez-Munoz, J. M., Ackerman, A., and Calderwood, S. K. (2020). HSF1: primary factor in molecular chaperone expression and a major contributor to cancer morbidity. *Cells* 9 (4), 1046. doi:10.3390/cells9041046

Rajabpour, A., Rajaei, F., and Teimoori-Toolabi, L. (2017). Molecular alterations contributing to pancreatic cancer chemoresistance. *Pancreatology* 17 (2), 310–320. doi:10.1016/j.pan.2016.12.013

Ramos, A., Sadeghi, S., and Tabatabaeian, H. (2021). Battling chemoresistance in cancer: root causes and strategies to uproot them. *Int. J. Mol. Sci.* 22 (17), 9451. doi:10.3390/ijms22179451

Reita, D., Pabst, L., Pencreach, E., Guerin, E., Dano, L., Rimelen, V., et al. (2022). Direct targeting KRAS mutation in non-small cell lung cancer: focus on resistance. *Cancers (Basel)* 14 (5), 1321. doi:10.3390/cancers14051321

Salamanca, H. H., Antonyak, M. A., Cerione, R. A., Shi, H., and Lis, J. T. (2014). Inhibiting heat shock factor 1 in human cancer cells with a potent RNA aptamer. *PLoS One* 9 (5), e96330. doi:10.1371/journal.pone.0096330

Salamanca, H. H., Fuda, N., Shi, H., and Lis, J. T. (2011). An RNA aptamer perturbs heat shock transcription factor activity in *Drosophila melanogaster*. *Nucleic Acids Res.* 39 (15), 6729–6740. doi:10.1093/nar/gkr206

Santagata, S., Hu, R., Lin, N. U., Mendillo, M. L., Collins, L. C., Hankinson, S. E., et al. (2011). High levels of nuclear heat-shock factor 1 (HSF1) are associated with poor prognosis in breast cancer. *Proc. Natl. Acad. Sci. U. S. A.* 108 (45), 18378–18383. doi:10.1073/pnas.1115031108

Santagata, S., Mendillo, M. L., Tang, Y. C., Subramanian, A., Perley, C. C., Roche, S. P., et al. (2013). Tight coordination of protein translation and HSF1 activation supports the anabolic malignant state. *Science* 341 (6143), 1238303. doi:10.1126/science.1238303

Sharma, C., Choi, M. A., Song, Y., and Seo, Y. H. (2022). Rational design and synthesis of HSF1-PROTACs for anticancer drug development. *Molecules* 27 (5), 1655. doi:10.3390/molecules27051655

Shi, Y., Mosser, D. D., and Morimoto, R. I. (1998). Molecular chaperones as HSF1-specific transcriptional repressors. *Genes Dev.* 12 (5), 654–666. doi:10.1101/gad.12.5.654

Shibue, T., and Weinberg, R. A. (2017). EMT, CSCs, and drug resistance: the mechanistic link and clinical implications. *Nat. Rev. Clin. Oncol.* 14 (10), 611–629. doi:10.1038/nrclinonc.2017.44

Siddiqui, A. D., and Piperdi, B. (2010). KRAS mutation in colon cancer: a marker of resistance to EGFR-I therapy. *Ann. Surg. Oncol.* 17 (4), 1168–1176. doi:10.1245/s10434-009-0811-z

Siegel, R. L., Giaquinto, A. N., and Jemal, A. (2024). Cancer statistics, 2024. *CA Cancer J. Clin.* 74 (1), 12–49. doi:10.3322/caac.21820

Singh, R., Letai, A., and Sarosiek, K. (2019). Regulation of apoptosis in health and disease: the balancing act of BCL-2 family proteins. *Nat. Rev. Mol. Cell Biol.* 20 (3), 175–193. doi:10.1038/s41580-018-0089-8

Singhal, A., Li, B. T., and O'Reilly, E. M. (2024). Targeting KRAS in cancer. *Nat. Med.* 30 (4), 969–983. doi:10.1038/s41591-024-02903-0

Stankiewicz, A. R., Livingstone, A. M., Mohseni, N., and Mosser, D. D. (2009). Regulation of heat-induced apoptosis by Mcl-1 degradation and its inhibition by Hsp70. *Cell Death Differ.* 16 (4), 638–647. doi:10.1038/cdd.2008.189

Sterrenberg, J. N., Blatch, G. L., and Edkins, A. L. (2011). Human DNAJ in cancer and stem cells. *Cancer Lett.* 312 (2), 129–142. doi:10.1016/j.canlet.2011.08.019

Sturner, E., and Behl, C. (2017). The role of the multifunctional BAG3 protein in cellular protein quality control and in disease. *Front. Mol. Neurosci.* 10, 177. doi:10.3389/fnmol.2017.00177

Su, K. H., Cao, J., Tang, Z., Dai, S., He, Y., Sampson, S. B., et al. (2016). HSF1 critically attunes proteotoxic stress sensing by mTORC1 to combat stress and promote growth. *Nat. Cell Biol.* 18 (5), 527–539. doi:10.1038/ncb3335

Su, K. H., and Dai, C. (2016). Protein quantity-quality balance licenses growth. *Cell Cycle* 15 (23), 3155–3156. doi:10.1080/15384101.2016.1220714

Su, K. H., and Dai, C. (2017). mTORC1 senses stresses: coupling stress to proteostasis. *Bioessays* 39 (5). doi:10.1002/bies.201600268

Su, K. H., Dai, S., Tang, Z., Xu, M., and Dai, C. (2019). Heat shock factor 1 is a direct antagonist of AMP-activated protein kinase. *Mol. Cell* 76 (4), 546–561. doi:10.1016/j.molcel.2019.08.021

Suh, D. H., Kim, M. K., Kim, H. S., Chung, H. H., and Song, Y. S. (2012). Unfolded protein response to autophagy as a promising druggable target for anticancer therapy. *Ann. N. Y. Acad. Sci.* 1271 (1), 20–32. doi:10.1111/j.1749-6632.2012.06739.x

Swan, C. L., and Sistonen, L. (2015). Cellular stress response cross talk maintains protein and energy homeostasis. *EMBO J.* 34 (3), 267–269. doi:10.15252/embj.201490757

Szakacs, G., Paterson, J. K., Ludwig, J. A., Booth-Genthe, C., and Gottesman, M. M. (2006). Targeting multidrug resistance in cancer. *Nat. Rev. Drug Discov.* 5 (3), 219–234. doi:10.1038/nrd1984

Takashima, K., Oshiumi, H., Matsumoto, M., and Seya, T. (2018). DNAJB1/HSP40 suppresses melanoma differentiation-associated gene 5-mitochondrial antiviral signaling protein function in conjunction with HSP70. *J. Innate Immun.* 10 (1), 44–55. doi:10.1159/000480740

Tan, H., Huang, F., Huang, M., Wu, X., and Tong, Z. (2023). HSF1 attenuates the release of inflammatory cytokines induced by lipopolysaccharide through transcriptional regulation of Atg10. *Microbiol. Spectr.* 11 (1), e0305922. doi:10.1128/spectrum.03059-22

Tanaka, N., Lin, J. J., Li, C., Ryan, M. B., Zhang, J., Kiedrowski, L. A., et al. (2021). Clinical acquired resistance to KRAS(G12C) inhibition through a novel KRAS switch-II pocket mutation and polyclonal alterations converging on RAS-MAPK reactivation. *Cancer Discov.* 11 (8), 1913–1922. doi:10.1158/2159-8290.CD-21-0365

Tanaka, N., Okada, H., Yamaguchi, K., Seki, M., Matsubara, D., Gotoh, N., et al. (2023). Mint3-depletion-induced energy stress sensitizes triple-negative breast cancer to chemotherapy via HSF1 inactivation. *Cell Death Dis.* 14 (12), 815. doi:10.1038/s41419-023-06352-4

Tang, Z., Dai, S., He, Y., Doty, R. A., Shultz, L. D., Sampson, S. B., et al. (2015). MEK guards proteome stability and inhibits tumor-suppressive amyloidogenesis via HSF1. *Cell* 160 (4), 729–744. doi:10.1016/j.cell.2015.01.028

Tchenio, T., Havard, M., Martinez, L. A., and Dautry, F. (2006). Heat shock-independent induction of multidrug resistance by heat shock factor 1. *Mol. Cell Biol.* 26 (2), 580–591. doi:10.1128/MCB.26.2.580-591.2006

Tilsed, C. M., Fisher, S. A., Nowak, A. K., Lake, R. A., and Lesterhuis, W. J. (2022). Cancer chemotherapy: insights into cellular and tumor microenvironmental mechanisms of action. *Front. Oncol.* 12, 960317. doi:10.3389/fonc.2022.960317

Toma-Jonik, A., Vydra, N., Janus, P., and Widlak, W. (2019). Interplay between HSF1 and p53 signaling pathways in cancer initiation and progression: non-oncogene and oncogene addiction. *Cell Oncol. (Dordr)* 42 (5), 579–589. doi:10.1007/s13402-019-00452-0

Vahid, S., Thaper, D., Gibson, K. F., Bishop, J. L., and Zoubeidi, A. (2016). Molecular chaperone Hsp27 regulates the Hippo tumor suppressor pathway in cancer. *Sci. Rep.* 6, 31842. doi:10.1038/srep31842

Vasan, N., Baselga, J., and Hyman, D. M. (2019). A view on drug resistance in cancer. *Nature* 575 (7782), 299–309. doi:10.1038/s41586-019-1730-1

Vihervaara, A., Mahat, D. B., Guertin, M. J., Chu, T., Danko, C. G., Lis, J. T., et al. (2017). Transcriptional response to stress is pre-wired by promoter and enhancer architecture. *Nat. Commun.* 8 (1), 255. doi:10.1038/s41467-017-00151-0

Vilaboa, N. E., Galan, A., Troyano, A., de Blas, E., and Aller, P. (2000). Regulation of multidrug resistance 1 (MDR1)/P-glycoprotein gene expression and activity by heat-shock transcription factor 1 (HSF1). *J. Biol. Chem.* 275 (32), 24970–24976. doi:10.1074/jbc.M909136199

Vulsteke, C., Pfeil, A. M., Schwenkglenks, M., Pettengell, R., Szucs, T. D., Lambrechts, D., et al. (2014). Impact of genetic variability and treatment-related factors on outcome in early breast cancer patients receiving (neo-) adjuvant chemotherapy with 5-fluorouracil, epirubicin and cyclophosphamide, and docetaxel. *Breast Cancer Res. Treat.* 147 (3), 557–570. doi:10.1007/s10549-014-3105-5

Vydra, N., Toma, A., Glowala-Kosinska, M., Gogler-Piglowska, A., and Widlak, W. (2013). Overexpression of Heat Shock Transcription Factor 1 enhances the resistance of melanoma cells to doxorubicin and paclitaxel. *BMC Cancer* 13, 504. doi:10.1186/1471-2407-13-504

Wadood, A., Ajmal, A., and Rehman, A. U. (2022). Strategies for targeting KRAS: a challenging drug target. *Curr. Pharm. Des.* 28 (23), 1897–1901. doi:10.2174/1381612828666220506144046

Wang, H., Wang, X., Zhang, H., Deng, T., Liu, R., Liu, Y., et al. (2021). The HSF1/miR-135b-5p axis induces protective autophagy to promote oxaliplatin resistance through the MUL1/ULK1 pathway in colorectal cancer. *Oncogene* 40 (28), 4695–4708. doi:10.1038/s41388-021-01898-z

Wang, L. E., Yin, M., Dong, Q., Stewart, D. J., Merriman, K. W., Amos, C. I., et al. (2011). DNA repair capacity in peripheral lymphocytes predicts survival of patients with non-small-cell lung cancer treated with first-line platinum-based chemotherapy. *J. Clin. Oncol.* 29 (31), 4121–4128. doi:10.1200/JCO.2010.34.3616

Watanabe, Y., Tsujimura, A., Taguchi, K., and Tanaka, M. (2017). HSF1 stress response pathway regulates autophagy receptor SQSTM1/p62-associated proteostasis. *Autophagy* 13 (1), 133–148. doi:10.1080/15548627.2016.1248018

Wei, Y., Zhuang, Y., Zhang, Y., Luo, L., Yu, B., and Zeng, J. (2024). Role of heat shock protein 70 in silibinin-induced apoptosis in bladder cancer. *J. Cancer* 15 (1), 79–89. doi:10.7150/jca.88668

Workman, P., Burrows, F., Neckers, L., and Rosen, N. (2007). Drugging the cancer chaperone HSP90: combinatorial therapeutic exploitation of oncogene addiction and tumor stress. *Ann. N. Y. Acad. Sci.* 1113, 202–216. doi:10.1196/annals.1391.012

Workman, P., Clarke, P. A., Te Poele, R., Powers, M., Box, G., De Billy, E., et al. (2022). Discovery and validation of biomarkers to support clinical development of NXP800: a first-in-class orally active, small-molecule HSF1 pathway inhibitor. *Eur. J. Cancer* 174, S35. doi:10.1016/s0959-8049(22)00893-0

Wu, C. (1995). Heat shock transcription factors: structure and regulation. *Annu. Rev. Cell Dev. Biol.* 11, 441–469. doi:10.1146/annurev.cb.11.110195.002301

Xi, J., Liu, Y., Liu, H., Chen, H., Emborg, M. E., and Zhang, S. C. (2012). Specification of midbrain dopamine neurons from primate pluripotent stem cells. *Stem Cells* 30 (8), 1655–1663. doi:10.1002/stem.1152

Xiang, W., Yang, Y., Weng, L., Ye, Z., Ding, P., Li, H., et al. (2023). Hyperhomocysteinemia activates NLRP3 inflammasome to cause hepatic steatosis and insulin resistance via MDM2-mediated ubiquitination of HSF1. *Int. Immunopharmacol.* 118, 110085. doi:10.1016/j.intimp.2023.110085

Xiao, X., Wang, W., Li, Y., Yang, D., Li, X., Shen, C., et al. (2018). HSP90AA1-mediated autophagy promotes drug resistance in osteosarcoma. *J. Exp. Clin. Cancer Res.* 37 (1), 201. doi:10.1186/s13046-018-0880-6

Xu, Y., An, Y., Wang, Y., Zhang, C., Zhang, H., Huang, C., et al. (2013). miR-101 inhibits autophagy and enhances cisplatin-induced apoptosis in hepatocellular carcinoma cells. *Oncol. Rep.* 29 (5), 2019–2024. doi:10.3892/or.2013.2338

Xue, N., Du, T., Lai, F., Jin, J., Ji, M., and Chen, X. (2022). Secreted HSP90α-LRP1 signaling promotes tumor metastasis and chemoresistance in pancreatic cancer. *Int. J. Mol. Sci.* 23 (10), 5532. doi:10.3390/ijms23105532

Yaeger, R., Mezzadra, R., Sinopoli, J., Bian, Y., Marasco, M., Kaplun, E., et al. (2023). Molecular characterization of acquired resistance to KRASG12C-EGFR inhibition in colorectal cancer. *Cancer Discov.* 13 (1), 41–55. doi:10.1158/2159-8290.CD-22-0405

Yamashita, M., Hirohashi, Y., Torigoe, T., Kusumoto, H., Murai, A., Imagawa, T., et al. (2016). Dnajb8, a member of the heat shock protein 40 family has a role in the tumor initiation and resistance to docetaxel but is dispensable for stress response. *PLoS One* 11 (1), e0146501. doi:10.1371/journal.pone.0146501

Yang, H., Sun, L., Liu, M., and Mao, Y. (2018). Patient-derived organoids: a promising model for personalized cancer treatment. *Gastroenterol. Rep. (Oxf).* 6 (4), 243–245. doi:10.1093/gastro/goy040

Yang, S., Ren, X., Liang, Y., Yan, Y., Zhou, Y., Hu, J., et al. (2020). KNK437 restricts the growth and metastasis of colorectal cancer via targeting DNAJA1/CDC45 axis. *Oncogene* 39 (2), 249–261. doi:10.1038/s41388-019-0978-0

Yoneda, A., Minomi, K., and Tamura, Y. (2021). Heat shock protein 47 confers chemoresistance on pancreatic cancer cells by interacting with calreticulin and IRE1α. *Cancer Sci.* 112 (7), 2803–2820. doi:10.1111/cas.14976

Yoon, Y. J., Kim, J. A., Shin, K. D., Shin, D. S., Han, Y. M., Lee, Y. J., et al. (2011). KRIBB11 inhibits HSP70 synthesis through inhibition of heat shock factor 1 function by impairing the recruitment of positive transcription elongation factor b to the hsp70 promoter. *J. Biol. Chem.* 286 (3), 1737–1747. doi:10.1074/jbc.M110.179440

Yu, J., Zhao, Y., and Xie, Y. (2024). Advances of E3 ligases in lung cancer. *Biochem. Biophys. Rep.* 38, 101740. doi:10.1016/j.bbrep.2024.101740

Zhang, B., Fan, Y., Cao, P., and Tan, K. (2021). Multifaceted roles of HSF1 in cell death: a state-of-the-art review. *Biochim. Biophys. Acta Rev. Cancer* 1876 (2), 188591. doi:10.1016/j.bbcan.2021.188591

Zhang, J. T. (2007). Biochemistry and pharmacology of the human multidrug resistance gene product, ABCG2. *Zhong Nan Da Xue Xue Bao Yi Xue Ban.* 32 (4), 531–541.

Zhang, X., Lei, Y., Chen, X., He, J., Liu, Z., Zhu, W., et al. (2024). Suppression of NSCLC progression via the co-administration of Danusertib, an AURK inhibitor, and KRIBB11, an HSF1 inhibitor. *Biochem. Pharmacol.* 223, 116155. doi:10.1016/j.bcp.2024.116155

Zhang, Y., Li, C., Xia, C., Wah To, K. K., Guo, Z., Ren, C., et al. (2022). Adagrasib, a KRAS G12C inhibitor, reverses the multidrug resistance mediated by ABCB1 *in vitro* and *in vivo*. *Cell Commun. Signal* 20 (1), 142. doi:10.1186/s12964-022-00955-8

Zhang, Y., Murshid, A., Prince, T., and Calderwood, S. K. (2011). Protein kinase A regulates molecular chaperone transcription and protein aggregation. *PLoS One* 6 (12), e28950. doi:10.1371/journal.pone.0028950

Zhao, B., Wang, L., Qiu, H., Zhang, M., Sun, L., Peng, P., et al. (2017). Mechanisms of resistance to anti-EGFR therapy in colorectal cancer. *Oncotarget* 8 (3), 3980–4000. doi:10.18632/oncotarget.14012

Zhao, S., Wang, J. M., Yan, J., Zhang, D. L., Liu, B. Q., Jiang, J. Y., et al. (2019). BAG3 promotes autophagy and glutaminolysis via stabilizing glutaminase. *Cell Death Dis.* 10 (4), 284. doi:10.1038/s41419-019-1504-6

Zhao, T., Zheng, H., Xu, J. J., Pantopoulos, K., Xu, Y. C., Liu, L. L., et al. (2024). MnO(2) nanoparticles trigger hepatic lipotoxicity and mitophagy via mtROS-dependent Hsf1(Ser326) phosphorylation. *Free Radic. Biol. Med.* 210, 390–405. doi:10.1016/j.freeradbiomed.2023.11.037

Zhu, C., Guan, X., Zhang, X., Luan, X., Song, Z., Cheng, X., et al. (2022). Targeting KRAS mutant cancers: from druggable therapy to drug resistance. *Mol. Cancer* 21 (1), 159. doi:10.1186/s12943-022-01629-2

Zhu, G., Pei, L., Xia, H., Tang, Q., and Bi, F. (2021). Role of oncogenic KRAS in the prognosis, diagnosis and treatment of colorectal cancer. *Mol. Cancer* 20 (1), 143. doi:10.1186/s12943-021-01441-4

frontiers | Frontiers in Cell and Developmental Biology

TYPE Review
PUBLISHED 05 March 2025
DOI 10.3389/fcell.2025.1545359

Check for updates

OPEN ACCESS

EDITED BY
Aurore Claude-Taupin,
INSERM U1151 Institut Necker Enfants Malades, France

REVIEWED BY
Amadou K. S. Camara,
Medical College of Wisconsin, United States
Chunyan Wang,
Shenzhen Maternity and Child Healthcare Hospital, China

*CORRESPONDENCE
Petr Sergiev,
petya@genebee.msu.ru

RECEIVED 14 December 2024
ACCEPTED 12 February 2025
PUBLISHED 05 March 2025

CITATION
Sergiev P, Averina O, Golubeva J, Vyssokikh M and Dontsova O (2025) Mitoregulin, a tiny protein at the crossroads of mitochondrial functioning, stress, and disease.
Front. Cell Dev. Biol. 13:1545359.
doi: 10.3389/fcell.2025.1545359

COPYRIGHT
© 2025 Sergiev, Averina, Golubeva, Vyssokikh and Dontsova. This is an open-access article distributed under the terms of the Creative Commons Attribution License (CC BY). The use, distribution or reproduction in other forums is permitted, provided the original author(s) and the copyright owner(s) are credited and that the original publication in this journal is cited, in accordance with accepted academic practice. No use, distribution or reproduction is permitted which does not comply with these terms.

Mitoregulin, a tiny protein at the crossroads of mitochondrial functioning, stress, and disease

Petr Sergiev[1,2,3]*, Olga Averina[1], Julia Golubeva[1,2], Mikhail Vyssokikh[1,4] and Olga Dontsova[1,2,3,5]

[1]Belozersky Institute of Physico-Chemical Biology, Lomonosov Moscow State University, Moscow, Russia, [2]Center for Life Sciences, Skolkovo Institute of Science and Technology, Skolkovo, Moscow Region, Russia, [3]Department of Chemistry, Lomonosov Moscow State University, Moscow, Russia, [4]Research Center for Obstetrics, Gynecology and Perinatology, Moscow, Russia, [5]Shemyakin-Ovchinnikov Institute of Bioorganic Chemistry, Russian Academy of Sciences, Moscow, Russia

Mitoregulin (Mtln) is a small mitochondrial protein that was only recently identified. Despite this, a substantial number of studies on its function have already been published. Although sometimes contradictory, these studies have revealed the localization of Mtln, its protein and lipid partners, and its role in lipid homeostasis, energy metabolism, oxidative stress, and other aspects of mitochondrial functioning. Moreover, research using knockout and transgenic mouse models has revealed the important role of Mtln in mammalian physiology. Metabolic changes, along with muscle, kidney, and fat-related phenotypes, have been linked to Mtln dysfunction. In this review, we summarize a comprehensive set of published data on Mtln. While controversies remain, we seek to offer a unified view of its functions, spanning molecular mechanisms to organism-level effects.

KEYWORDS

Mtln, mitochondria, small peptide, respiration, membrane, cardiolipin

1 Introduction

Mitochondria, the powerhouses of the cell, play a central role in responses to several types of stress, including oxidative stress, ischemia–reperfusion, apoptosis, and senescence. Mitochondrial dysfunction may also be a cause of cellular stress. Mitochondrial function is precisely controlled by a set of approximately 1,100 proteins (Palmfeldt and Bross, 2017), among which a surprisingly high proportion are short peptides (sPEPs) (Calvo et al., 2016; Rath et al., 2021) encoded by short open reading frames. These sPEPs were almost overlooked by the standard genome annotation pipeline (Sergiev and Rubtsova, 2021). Over recent years, the development of ribosome profiling and improvements in mass spectrometry and the computational analysis of genome sequences has resulted in a burst of sPEP discoveries (Chugunova et al., 2018).

One recently identified sPEP is a product of a gene originally annotated as *LINC00116* in humans and *1500011k16Rik* in mice (Makarewich et al., 2018; Stein et al., 2018; Chugunova et al., 2019). When our group first investigated this gene, it had largely escaped the attention of the scientific community. However, by 2018–2019, several laboratories almost simultaneously published findings on the functional role of this small protein, now named "mitoregulin" (Mtln—also known as MOXI or MPM), which appeared to be an important part of the mitochondrial proteome (Makarewich et al., 2018; Stein et al., 2018; Chugunova et al., 2019; Lin et al., 2019; Lai et al., 2020). While many conclusions from

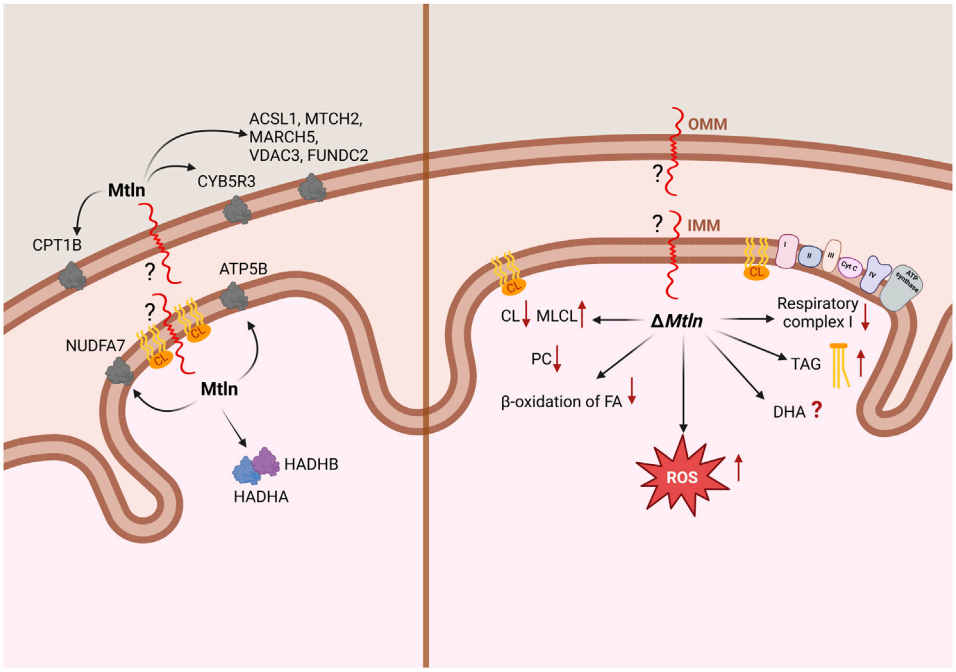

FIGURE 1
Summary of the data relating to Mtln localization and interaction **(A)** and the *Mtln*-knockout (KO) phenotype **(B)** at the level of mitochondria. IMM: inner mitochondrial membrane; OMM: outer mitochondrial membrane. Arrows in the left panel point to Mtln interaction partners; arrows in the right panel correspond to the phenotypes observed following *Mtln* inactivation. CL: cardiolipin; MLCL: monolysocardiolipin; PC: phosphatidylcholine; TAG: triacylglycerol; DHA: docosahexaenoic acid.

studies of this protein agree, controversies remain, obscuring a precise understanding of the molecular mechanism that underlies Mtln function. In this review, we seek to summarize what is known about this small mitochondrial protein.

2 Mtln localization

The initial understanding that the *LINC00116* gene codes for a protein, at least by our group (Chugunova et al., 2019), arose from conservation analysis. The most conserved region of the gene encodes an open reading frame of 56 amino acids. Further analysis by ours and other groups revealed that this sPEP is conserved among vertebrates, whereas invertebrates are generally believed to lack this gene (Makarewich et al., 2018; Stein et al., 2018; Chugunova et al., 2019). An assessment of nucleotide substitutions in the Mtln coding region revealed that most of them lead to the same or similar amino acids. A conserved hydrophobic region in the N-terminus of Mtln is likely to be a transmembrane segment, while the positively charged C-terminus is exposed for functional interactions outside the membrane. There is consensus among studies that Mtln is bound to the mitochondrial membrane, but discrepancies exist regarding whether it localizes to the inner or outer membrane (Figure 1A). Initial work by Makarewich et al. (2018) and Stein et al. (2018) and later by Lin et al. (2019) concluded that Mtln resides in the inner mitochondrial membrane (IMM) based on its resistance to proteinase K digestion. Recently, however, this conclusion has been challenged by the elegant study of Zhang et al. (2023). Their approach involved using a range of digitonin concentrations to selectively solubilize the outer mitochondrial membrane (OMM) and, more conclusively, a split-GFP system, in which a small fragment of GFP (GFP11) was tethered to the N- or C-terminus of Mtln, while the rest of the GFP molecule (GFP1-10) was artificially placed at several mitochondrial locations. Thus, the fluorescent GFP molecule could be formed only if both fragments, GFP11 and GFP1-10, appear in the same compartment. As a result, the authors demonstrated that Mtln resides in the OMM while its N-terminus faces the intermembrane space.

3 Partners of Mtln

The most valuable insight into the localization and function of Mtln is likely to be obtained from the identification of its binding partners. However, experiments employing affinity-tagged Mtln co-precipitation resulted in a list of protein interactors that only partially overlap across studies. For instance, Makarewich et al. (2018) found that Mtln interacts with the inner membrane proteins HADHA and HADHB, which are responsible for the β-oxidation of long-chain fatty acids, while Stein et al. (2018) reported that Mtln interacts with cardiolipin (CL), a highly specific lipid of the IMM. Our group (Chugunova et al., 2019) identified the outer membrane protein NADH-cytochrome b5 reductase 3 (CYB5R3) as a key Mtln-interacting partner. The list was later expanded to include ATP5B (Friesen et al., 2020), NUDFA7 (Xiao et al., 2022), *N*-acetyltransferase 14 (Nat14), and c-Jun (Li et al., 2023). More recently, Zhang et al. (2023) identified more partners of Mtln, including a set of OMM-localized proteins, such as CPT1B,

ACSL1, MTCH2, MARCH5, VDAX3, FUNDC2, and CYB5B (Figure 1A). Additionally, Mtln has been reported to self-oligomerize (Linzer et al., 2024). There is little consensus among the results of different studies, with some exceptions. For example, two laboratories (Makarewich et al., 2018; Friesen et al., 2020) observed that Mtln interacts with HADHB, while both our group (Chugunova et al., 2019) and Zhang et al. (2023) noted that it interacts with CYB5R3. Mtln interacting partners are localized in the mitochondrial matrix, inner (IMM) and outer (OMM) mitochondrial membranes. Meanwhile, Mtln was initially reported to interact with respiratory chain supercomplexes (Stein et al., 2018) within the IMM and influence their activity. However, this assumption was subsequently disputed (Zhang et al., 2023). Mtln knockout appeared to increase the susceptibility of mitochondrial membranes to freezing (Stein et al., 2024), and thus freezing of mitochondria devoid of Mtln resulted in apparent dissociation of respiratory chain supercomplexes.

4 Respiratory phenotypes associated with Mtln deficiency

The main function of mitochondria is respiration. Four respiratory chain complexes transfer electrons from organic substrates to oxygen. Pyruvate generated via glycolysis is transported to mitochondria and converted to acetyl-CoA (AcCoA), concomitant with the production of NADH. AcCoA is oxidized during the tricarboxylic acid cycle, also yielding NADH molecules. The oxidation of fatty and amino acids also fuels the tricarboxylic acid cycle by providing AcCoA and other metabolites. Additionally, the NADH produced in the cytoplasm, such as through glycolysis, is transferred to mitochondria via malate and glutamate shuttle transporters. Ultimately, all mitochondrial NADH molecules are oxidized by respiratory complex I (CI), generating reduced ubiquinone QH_2. Simultaneously, during the tricarboxylic acid cycle, succinate is oxidized to fumarate via respiratory complex II (CII). Apart from the production of AcCoA, fatty acid oxidation also results in the reduction of the ETF protein, which is later oxidized by ETF dehydrogenase. This process also generates reduced ubiquinone QH_2. QH_2 from all sources oxidized by respiratory chain complex III (CIII). Thus, several substrates can be used in model systems aimed at assessing the efficiency of respiratory complexes. For instance, the activity of NADH dehydrogenase in purified respiratory CI can be measured using NADH; pyruvate/malate or glutamate/malate are model substrates for the activity of respiratory chain CI in permeabilized cells or purified mitochondria; palmitoyl carnitine can be used to address the efficiency of both CI and fatty acid β-oxidation; finally, succinate is an exclusive substrate of respiratory chain CII.

The influence of Mtln on respiration has been studied by most groups which have investigated Mtln function using both cell lines and animal models. However, the results have varied to some extent. Our group revealed that Mtln inactivation in both cell (Chugunova et al., 2019) and mouse (Averina et al., 2023c) models affects respiratory CI activity irrespective of the substrate used (e.g., palmitoyl carnitine, pyruvate/malate, or glutamate/malate in permeabilized cells or purified mitochondria—Figure 1B). The activity of CI outside the context of the membrane (purified by immunoprecipitation) was found to be independent of Mtln (Chugunova et al., 2019). This suggested that Mtln is neither a *bona fide* component of CI nor is it involved in its assembly. It also does not favor the idea that Mtln is necessary for a particular type of CI fueling. Furthermore, respiration mediated by CII via succinate oxidation was found to be unaffected by Mtln inactivation, indicating that only CI, and not the rest of the respiratory chain, is dependent on it (Chugunova et al., 2019; Averina et al., 2023b, 2023c).

Two groups have reported that Mtln is involved in the β-oxidation of fatty acids. Makarewich et al. (2018) demonstrated that respiration efficiency is decreased in muscle and heart mitochondria from Mtln-KO mice when palmitoyl carnitine is used as the metabolic substrate, but not when pyruvate is used. They also showed that etomoxir, a specific inhibitor of carnitine palmitoyltransferase I (CPT-1), attenuates the difference in mitochondrial respiration between wild-type and Mtln-KO mice. Perfusion of the respiration substrates labeled with a stable ^{13}C isotope followed by NMR analysis demonstrated that Mtln-KO mice preferentially oxidize carbohydrates at the expense of fatty acids (Makarewich et al., 2018). Friesen et al. (2020) also demonstrated that respiration efficiency was decreased in Mtln-KO adipocytes when palmitoyl carnitine served as the respiration substrate but was increased when glucose was utilized instead.

Lin et al. (2019) reported that respiration was dependent on Mtln when pyruvate is used as the respiratory substrate, as demonstrated by the XF Cell Mito Stress Test (Seahorse Bioscience). This implies that Mtln promotes CI-dependent respiration supported by substrates other than palmitoyl carnitine. However, in a later study, the same group found that respiration efficiency was increased with Mtln knockdown. The negative influence of Mtln on CI activity was attributed to its inhibitory interaction with the CI subunit NDUFA7 (Xiao et al., 2022). The discrepancy between the stimulatory (Lin et al., 2019) and the inhibitory (Xiao et al., 2022) effects of Mtln on mitochondrial respiration might be explained by differences in the cell lines used in these studies. The former experiments were conducted with murine myoblasts, while the latter were performed with human hepatocellular carcinoma cells. Further adding to the debate, Zhang et al. (2023) found no evidence of a dependence of respiration on Mtln.

Respiration in mitochondria occurs within the unique spatial architecture of cristae. Proper structural context is crucial for the activities of the respiratory complexes. Initially, Mtln was found to stimulate CI association into respiratory chain supercomplexes (Stein et al., 2018), although this finding was later challenged (Zhang et al., 2023). Mtln influence on supercomplex assembly appeared to be indirect and observed only if samples of mitochondria were frozen before the analysis by blue-native gel electrophoresis (Stein et al., 2024). Still, this finding is valuable since it indicates that a lack of Mtln makes inner mitochondrial membrane sensitive to freezing. Our group observed that the loss of Mtln decreased the amount of mitochondrial creatine kinase octamers ($mtCK_8$) with the increase of the corresponding dimer ($mtCK_2$) concentration (Averina et al., 2023b). This effect could also be explained by an impairment in the structural organization of the IMM upon Mtln depletion since cardiolipin located in the IMM is known to interact with mtCK and stabilize its octameric form.

5 The effect of Mtln on lipid composition

While debate regarding Mtln function persists, there is broad consensus that Mtln affects cellular and, presumably, mitochondrial lipid composition, thereby potentially influencing other mitochondrial functions. We undertook an analysis of lipid composition in Mtln-KO and corresponding control cell lines NIH 3T3 and NS0 (Chugunova et al., 2019). The major findings were a decrease in the concentrations of phosphatidylcholine lipids and an increase in triacylglycerol (TAG) levels in Mtln-KO cells (Figure 1B), with the biggest increase being detected in the concentrations of TAGs containing docosahexaenoic acid (DHA). Similarly, a subsequent study using C2C12 myoblasts deficient for Mtln reported an increase in total polyunsaturated fatty acids, with DHA concentrations exhibiting the most pronounced rise (Zhang et al., 2023). These findings contrast with Stein et al. (2024), who reported that the concentrations of DHA-containing triglycerides were decreased in the hearts of Mtln-KO mice whereas those of long-chain triglycerides were increased. These findings are puzzling, and the effect of Mtln deficiency on DHA-containing lipids remains contradictory.

The IMM contains a specific lipid, CL, which is needed to facilitate the bending of the IMM for cristae formation. CL is also known to interact directly with the respiratory chain complexes, especially CI, whose activity is critically dependent on this interaction (Jussupow et al., 2019). A direct interaction between CL and CI was demonstrated using an *in vitro* model system (Figure 1; Stein et al., 2018). Subsequent studies reported the CL levels being substantially reduced in muscles (Averina et al., 2023b) and kidneys (Averina et al., 2023c) of Mtln-KO mice, accompanied by a significant rise in the levels of monolysocardiolipin (MLCL), an intermediate product of CL damage and remodeling (Figure 1B). This finding was confirmed in a later study (Stein et al., 2024). CL is known to be damaged primarily by reactive oxygen species (ROS) (Dudek, 2017), and Mtln inactivation has been associated with an increase in ROS production in some (Stein et al., 2018; Choi and Kang, 2023), although not all (Chugunova et al., 2019), studies. Additionally, Mtln overexpression was observed to decrease ROS production (Choi and Kang, 2023; Figure 1B). The repair of oxidized CL proceeds via iPLA2γ-dependent fatty acid (FA) removal, yielding Mtln , whose concentrations are elevated in Mtln-KO mice. Cyb5r3, a partner of Mtln (Chugunova et al., 2019), plays a role in reducing ROS generation (Martin-Montalvo et al., 2016), and its levels were also found to be reduced in mice lacking Mtln (Averina et al., 2023c). Two major models for Mtln-mediated CL protection can be postulated, one involving direct interaction and the other involving indirect effects via Mtln protein partners, such as Cyb5r3.

6 The effect of Mtln on metabolite concentrations

To investigate the role of Mtln in mouse health and wellbeing, many Mtln-KO mouse models have been generated (Makarewich et al., 2018; Stein et al., 2018; Lin et al., 2019; Friesen et al., 2020; Wang et al., 2020; Averina et al., 2023a; Li et al., 2023; Zhang et al., 2023). Major characteristics, such as weight dynamics, have been addressed in several studies, resulting in somewhat controversial outcomes. Both neutral (Makarewich et al., 2018; Lin et al., 2019; Friesen et al., 2020; Averina et al., 2023a; Zhang et al., 2023) and inhibitory (Wang et al., 2020) effects on weight dynamics have been reported for Mtln-KO mice when fed a standard chow. Similarly, contradictory results regarding weight were obtained for Mtln-KO mice fed a high-fat diet, including an increase (Averina et al., 2023a), no change (Friesen et al., 2020), and a decrease (Zhang et al., 2023) in weight gain and fat accumulation. Serum triglyceride levels in Mtln-KO mice are also controversial, with both increases (Averina et al., 2023a) and decreases (Friesen et al., 2020) being reported. Nevertheless, increases in triglyceride accumulation have been observed in the hearts (Stein et al., 2024) and adipocytes (Friesen et al., 2020) of Mtln-KO mice, NS0 myeloma cells, and NIH 3T3 fibroblasts (Chugunova et al., 2019; Figures 1, 2). Curiously, an SNP associated with intramuscular fat accumulation was detected near the pig Mtln gene (Shen et al., 2024). Thus, despite controversies, it is likely that Mtln inactivation leads to fat accumulation, at least in some tissues or under some conditions.

The concentrations of a large set of serum metabolites were compared between Mtln-KO mice and wild-type controls (Averina et al., 2023a). An increase in lactate concentrations was observed following Mtln inactivation, which was expected given that lactate serves as a common marker for many human mitochondrial diseases as well as for mouse models of mitochondrial dysfunction (Averina et al., 2024). However, no other studies have observed an increase in serum lactate levels with Mtln deficiency (Makarewich et al., 2018; Zhang et al., 2023). Serum concentrations of several other metabolites were compared between the wild type and Mtln-KO mice. While we observed a decrease in the serum concentrations of citrate, malate, succinate, betaine, and glycine, concomitant with an increase in the contents of lysine and valine (Averina et al., 2023a), these results were not corroborated by Zhang et al. (2023).

In one study (Averina et al., 2023a), we also measured the serum concentrations of free fatty acids and acylcarnitines in Mtln-KO mice and found very moderate differences relative to wild-type controls. This was unexpected given that the major impact of Mtln inactivation is a deficiency in fatty acid β-oxidation (Makarewich et al., 2018; Stein et al., 2018; Friesen et al., 2020). Defects in fatty acid β-oxidation caused by HADHA dysfunction are expected to result in manyfold or even an order of magnitude difference in the levels of the acylcarnitines C14OH, C16OH, and C18:1OH (Sander et al., 2005)—not observed in Mtln-KO mice. Concurrently, we noted a decrease in the concentrations of the saturated free fatty acids C16:0, C18:0, and C20:0 and an increase in that of DHA. The latter was in agreement with our earlier observation in cell models, where we detected an increase in docosahexaenoic acid-containing triglyceride concentrations (Chugunova et al., 2019), and with that Zhang et al. (2023) relating to C2C12 myoblasts. However, this was not in line with an earlier study (Stein et al., 2024) which reported that the concentrations of DHA-containing triglycerides were decreased in the hearts of Mtln-KO mice.

It seems likely that Mtln inactivation influences the metabolic profile of mice to varying degrees, both positively and negatively. This influence also depends on subtle differences in genetic

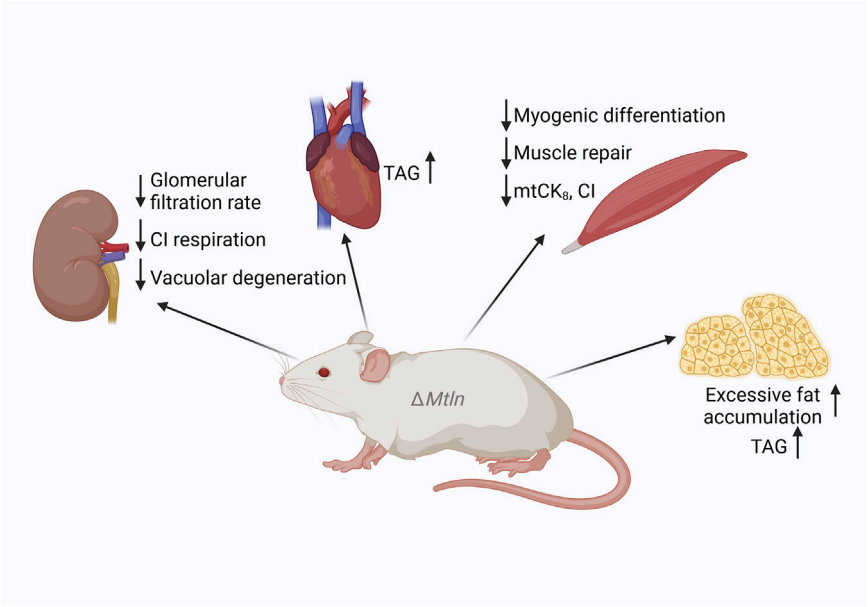

FIGURE 2
Summary of the phenotypes of *Mtln*-knockout (KO) mice. Downward arrows correspond to a decrease and upward arrows to an increase in function or activity following *Mtln* inactivation. CI: respiratory complex I; TAG: triacylglycerol.

background as well as diet, age, sex, or other factors that are difficult to standardize across laboratories. At worst, the observed differences may simply result from random fluctuations.

7 The effect of Mtln on muscle physiology

The Mtln gene is highly expressed in muscles (Makarewich et al., 2018; Stein et al., 2018; Lin et al., 2019; Averina et al., 2023b)—expected, given that muscles, especially oxidative ones, contain a substantial number of mitochondria. Both forelimb grip strength (Lin et al., 2019; Averina et al., 2023b) and performance in the exhaustion running test were found to be decreased in mice devoid of Mtln (Wang et al., 2020). Mtln supports myogenic differentiation in C2C12 myoblasts (Lin et al., 2019; Wang et al., 2020) and muscle repair in several models (Lin et al., 2019; Wang et al., 2020; Averina et al., 2023b). A general decrease in muscle fiber diameter and a specific decrease in the diameter of muscle fibers with centralized nuclei at the regeneration stage following cardiotoxin-induced damage was observed (Lin et al., 2019). A reduction in the steady-state muscle fiber diameter in Mtln-KO mice was also noted (Wang et al., 2020). The same group reported that the weight of the tibialis anterior muscle was decreased in Mtln-KO mice, accompanied by a reduction in tetanic force. Muscle regeneration was found to be delayed following cardiotoxin-induced damage in mice lacking Mtln (Wang et al., 2020), in line with earlier findings (Lin et al., 2019). In our studies, we did not detect any differences in myofiber diameter due to Mtln inactivation. However, we did observe a tendency toward an increase in the number of myofibers with centrally located nuclear chains, indicative of augmented muscle remodeling (Averina et al., 2023b).

Muscle degeneration has also been reported in transgenic mice overexpressing Mtln (Makarewich et al., 2018; Figure 2). Acute Mtln inactivation in mouse hearts was achieved using AAV9 encoding Mtln-targeted guide RNAs in combination with cardiomyocyte-specific *Cas9* expression (Stein et al., 2024). This tissue-specific Mtln inactivation was found to increase the susceptibility of mice to myocardial infarction following heart ischemia reperfusion.

Although Gomori trichrome staining, which provides relatively low resolution, did not show evidence of mitochondrial damage in the muscles of Mtln-KO mice (Averina et al., 2023b), Makarewich et al. (2018) observed severe mitochondrial disorganization, including disrupted and enlarged cristae, using confocal microscopy.

Muscles use the creatine shuttle mechanism to transfer energy from the mitochondrial reticulum to myosin motors. As the diffusion of ATP is slower than that of creatine phosphate (CrP), a set of creatine kinases convert ATP to CrP and back, enabling CrP to act as a diffusible energy shuttle between the sites of ATP generation in mitochondria and ATP consumption by myosin. MtCK is a protein localized in the mitochondrial intermembrane space where it can persist in either a highly active octameric form $mtCK_8$ or less active dimer $mtCK_2$. The octameric form of the mitochondrial creatine kinase is bound to ATP/ADP antiporter and voltage-dependent anion channel (VDAC) (Vial, 2006; Puurand et al., 2018). Octamer formation is facilitated by an interaction with CL-containing IMM (Schlattner and Wallimann, 2000). We noted that the efficiency of muscle mitochondria respiration coupled with Cr phosphorylation was decreased in Mtln-KO mice (Averina et al., 2023b), which was paralleled by a decrease in mtCK octamerization and excessive CL damage (Figure 2). Thus, the creatine shuttle, an important mechanism in muscle physiology, was also found to be affected by Mtln inactivation. Combined, these observations indicate that suboptimal respiration and attenuated creatine shuttling may

underlie the reduction in muscle performance detected following Mtln inactivation.

8 The effect of Mtln on kidney physiology

The kidney is the organ responsible for blood filtering and urine excretion. It is needed for the maintenance of water, ion, and solute balance, as well as for the excretion of metabolic waste and toxins. Kidney-related illnesses, such as chronic kidney disease, lead to kidney fibrosis and life-threatening conditions that require transplantation or constant dialysis. The kidney is enriched in mitochondria (Li et al., 2020), which are required to produce energy for its solute pumps. Many mitochondrial diseases, such as mitochondrial encephalomyopathy, lactic acidosis, and stroke-like symptoms (MELAS), myoclonic epilepsy with ragged-red fibers (MERRF), Pearson, Kearns–Sayre, and Leigh syndromes, result in kidney damage (O'Toole, 2014).

Several studies have focused on the role of Mtln in kidney physiology (Averina et al., 2023c; Li et al., 2023). In our studies (Averina et al., 2023a, 2023b), we found that the kidney exhibits relatively high Mtln expression, as determined by immunoblotting. However, this result was not replicated (Makarewich et al., 2018).

Mtln was observed to be highly expressed in patients with kidney fibrosis as well as in mouse models of kidney fibrosis, such as folic acid nephropathy and unilateral ureteral obstruction (Li et al., 2023). However, the upregulation of Mtln expression might not be a cause but rather a consequence of kidney damage, possibly a sort of a compensatory mechanism. Li et al. (2023) utilized artificial Mtln downregulation to investigate whether Mtln contributes to kidney fibrosis. The grade of kidney fibrosis induced by both folic acid nephropathy and unilateral ureteral obstruction was assessed by α-smooth muscle actin staining. The severity of kidney fibrosis was found to be attenuated in Mtln-KO mice and mice treated with locked nucleic acid antisense oligonucleotides that target Mtln-encoding mRNA (Li et al., 2023). The authors proposed that Mtln promotes a fibrotic response by acting as a bridge for the transcription factor c-Jun and the putative acetyltransferase Nat14. It would be surprising if a gene such as Mtln would be preserved in evolution if it was responsible for a pathology. More likely, Mtln is beneficial in conditions other than folic acid nephropathy and unilateral ureteral obstruction.

Our group investigated the age-dependent kidney-related physiological function of Mtln after unexpectedly detecting a severe kidney pathology in an 18-month-old Mtln-KO male mouse (Averina et al., 2023c). Follow-up studies on 12-month-old male mice revealed vacuolar degeneration in kidney proximal tubules in seven out of nine (78%) Mtln-KO mice compared with the four out of 14 (29%) recorded for wild-type mice. Simultaneously, we noted that glomerular filtration rates were reduced in 24-month-old female mice lacking Mtln (Averina et al., 2023c). Importantly, these pathologies were not detected in young, 6-month-old Mtln-KO mice, both male and female mice.

We also found that CI-dependent respiration was reduced while CL damage was enhanced in both the kidney (Averina et al., 2023c; Figure 2) and muscle mitochondria (Averina et al., 2023b) of Mtln-KO mice.

9 The effect of Mtln on human health

Despite being a very short gene with limited potential for genetic variability, Mtln was identified as being linked with serum triglyceridemia in genome-wide association studies (Surendran et al., 2012; Weissglas-Volkov et al., 2013). This finding aligns well with the increase in serum triglyceride levels and obesity observed in Mtln-KO model mice (Averina et al., 2023a).

Although sparse, several clinical studies have reported Mtln-related findings. Mtln was shown to be highly expressed in M2 (activated) macrophages at the sites of echinococcosis lesions (Ma et al., 2024). Mtln expression levels were also associated with later stages of echinococcosis infection in a mouse model, which ultimately resulted in liver fibrosis. Elevated Mtln expression has also been linked to kidney fibrosis, as mentioned above (Li et al., 2023). Another study described an increase in Mtln expression in osteoarthritis (Choi et al., 2024). Mtln upregulation was also observed in a synovial cell model following the activation of the inflammatory response by TNF-α and lipopolysaccharide. Similarly, Mtln KO in a synovial cell line resulted in the upregulation of inflammatory cytokine production (Choi et al., 2024).

Some studies have linked Mtln with cancer. For instance, Mtln expression is increased in lung cancer (Tomida et al., 2009). The inactivation of the Mtln gene in breast cancer cell lines was found to reduce the frequency of mitochondrial contacts with the ER under conditions of ER stress. In addition, the lack of Mtln resulted in the decreased viability of a breast cancer cell line following treatment with ER-stress inducers, such as tunicamycin (Choi and Kang, 2023). The loss of Mtln in lung cancer cell lines resulted in p53 activation and increased susceptibility to apoptosis, although these effects were attributed to the activity of Mtln-encoding RNA (Iwai et al., 2023). Proliferation and mobility in cervical cancer cell lines were also found to be dependent on Mtln expression (Lai et al., 2020). In contrast, hepatocellular carcinoma cell lines exhibited lower average Mtln expression, with elevated expression levels being indicative of a better prognosis (Xiao et al., 2022). In line with this, Mtln was shown to reduce metastatic potential, whereas its knockdown promoted migration and metastasis.

10 The extramitochondrial functions of Mtln

While the consensus view is that Mtln functions within mitochondria, alternative roles for Mtln have also been proposed. Most unusual, perhaps, is the finding that Mtln-encoding RNA functions as a *bona fide* lincRNA independently of its coding potential. As an RNA entity, LINC00116 binds to the PCBP2 protein, thereby enhancing its ability to repress p53 translation (Iwai et al., 2023). Alternatively, LINC00116 mRNA has been reported to enhance tumorigenesis by acting as a sponge for miR-106a, which, in turn, represses *c-Jun* expression (Lai et al., 2020). Notably, Mtln was observed to bind to and form a complex with both c-Jun and Nat14 in the nucleus (Li et al., 2023), which was assumed to activate fibrotic gene promoters.

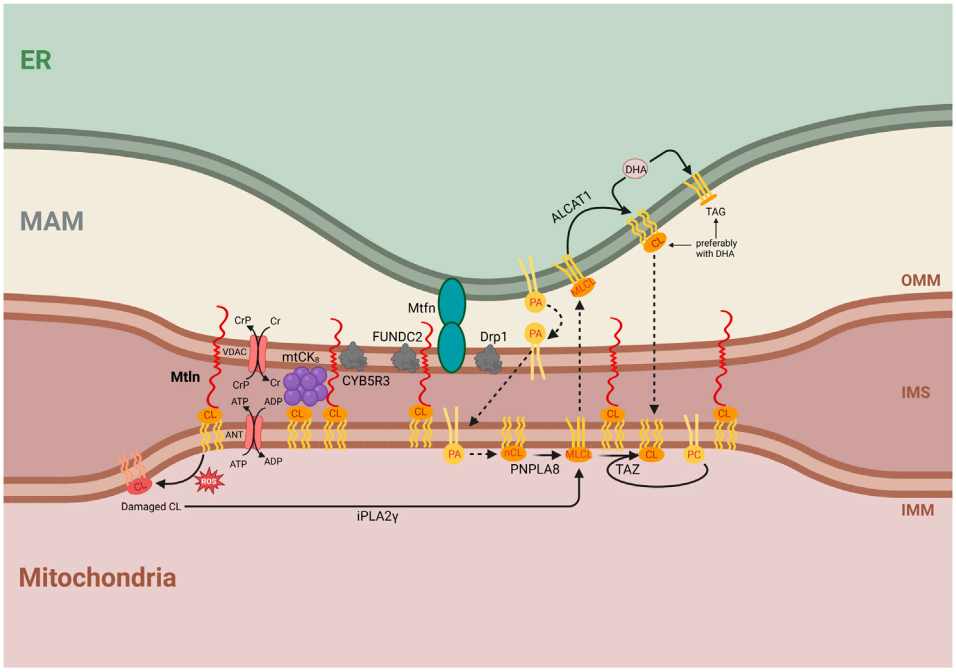

FIGURE 3
Integrative model for the molecular function of Mtln. Central is a proposed function of Mtln as a molecular tether between the inner mitochondrial membrane (IMM), outer mitochondrial membrane (OMM), and mitochondria-associated membrane (MAM). The labeled compartments are mitochondria, the intermembrane space (IMS), and the endoplasmic reticulum (ER). Shown are the interactions of Mtln with CL that arrange the contacts between the OMM and IMM. Shown are protein partners of Mtln, such as the CYB5R3, FUNDC2, mitofusin (Mtfn), and Drp1 localized in the membrane contact sites. The interaction of Mtln with CL could also protect CL from oxidation damage (shown on the left), which initiates CL repair via fatty acid removal by iPLA2γ forming monolysocardiolipin (shown below). CL synthesis is initiated by phosphatidic acid transport at the site of contacts between MAM, OMM, and IMM membranes (shown in the center). Initially formed newly synthesized cardiolipin (nCL) is processed by PNPLA8 to monolysocardiolipin (MLCL). MLCL might be transported to the ER membrane, where it is repaired by ALCAT1 with the addition of DHA. Alternatively, taffazin (TAZ) transfers a fatty acid, preferentially C18:2, from phosphatidylcholine (PC) to MLCL inside the mitochondria. CL synthesis, damage, and repair pathways are shown with an emphasis on the essential influence of the intermembrane exchange processes, which require membrane tethering. The Cr shuttle system is shown as dependent on the interaction with CL and facilitated by the contacts between the membranes. Mitochondrial creatine kinase (mtCK) is shown as an octamer, stabilized by an interaction with both IMM and OMM. ATP/ADP antiporter and VDAC used to arrange Cr shuttling are shown next to $mtCK_8$. Mtln interaction with CL is shown to stabilize intermembrane contacts made by the $mtCK_8$.

11 Toward an integrative model of Mtln function

Initially, the Mtln-encoding gene was misannotated as a long non-coding RNA with no known protein product. Since its identification, there has been a surge in studies related to the localization, partners, molecular function, and physiological role of this protein. While every reported finding about Mtln has been met with some degree of controversy, several of its features have obtained support from at least two independent research groups. Accordingly, a clearer picture of the function of Mtln is beginning to emerge, as summarized below in Figure 3.

Despite conflicting reports (Makarewich et al., 2018; Stein et al., 2018), a recent robust study demonstrated that Mtln is a mitochondrial peptide, the transmembrane segment of which is inserted into the OMM, while its N-terminus faces the intermembrane space (Zhang et al., 2023). This arrangement is consistent with its reported ability to interact with CL (Stein et al., 2018) within the IMM. Moreover, taken together, these results suggest that Mtln functions as a link between the IMM and the OMM (Figure 3).

The pleiotropic and sometimes contradictory phenotypes observed with Mtln inactivation in both cell culture and mice support Mtln KO manifestations being highly influenced by subtle differences in the genotypes of mice or the nature of cell cultures, the amounts of specific nutrients, such as fatty acids, and the age of mice. These findings make it unlikely that Mtln is a *bona fide* component of a specific enzymatic protein complex, or a much stronger and robust phenotype would be anticipated. The location of Mtln in the OMM while its N-terminus is facing the IMM and interacts with the IMM lipid CL supports it playing a structural role by acting as a membrane tether (Figure 3). The possibility that Mtln acts in the tethering of the IMM and OMM may explain its effect on mitochondrial creatine kinase octamerization (Averina et al., 2023b). The octameric form of mtCK is known to interact with the cardiolipin located in the IMM and tether both IMM and OMM (Rojo et al., 1991). Additional IMM to OMM bridging by Mtln should stabilize $mtCK_8$ binding to both mitochondrial membranes (Schlattner and Wallimann, 2000; Schlattner et al., 2006), thus stabilizing $mtCK_8$ formation.

The transport of lipids between the IMM and the OMM is linked to the transport between the OMM and endoplasmic reticulum (ER) membranes (mitochondria-associated membranes [MAMs]) as

many lipid components are exchanged between ER and IMM via OMM (see below). Mtln was reported to be present in the OMM–MAM contact proteome, as revealed by Contact-ID, a method for specifically labelling and purifying proteins localized at the contact sites between particular cellular compartments (Kwak et al., 2020). The contact proteome was similarly enriched in Mtln-interacting partners, such as Cyb5r3 (Chugunova et al., 2019; Zhang et al., 2023) and FUNDC2 (Zhang et al., 2023). The proteins Drp1 and Mfn2, which are responsible for mitochondrial fission (Smirnova et al., 2001; Tábara et al., 2024) and fusion (Santel and Fuller, 2001; Tábara et al., 2024), respectively, are localized to OMM–MAM contact sites (de Brito and Scorrano, 2008; Friedman et al., 2011). Mtln inactivation decreases the abundance of Drp1 (Choi and Kang, 2023) while increasing that of Mfn2 (Averina et al., 2023c). In addition, Mtln inactivation was shown to reduce the number of OMM–MAM contacts, especially under ER stress (Choi and Kang, 2023). This suggests that Mtln may not only contribute to the tethering between OMM and IMM but also to the stabilization of OMM–MAM contacts via its C-terminal domain and protein partners (Figure 3). Hypothetically, Mtln might facilitate the formation of the triple IMM–OMM–MAM contacts.

Contact sites between the IMM and OMM, as well as between the OMM and MAM, are important for lipid exchange, which is necessary for CL synthesis. The CL precursor, phosphatidic acid (PA), is imported into the IMM from the MAM through membrane contact sites (Jiang et al., 2022). This suggests that a reduction in the number and stability of contact sites between the MAM and OMM and the OMM and IMM would affect PA import into the mitochondria and consequently impede CL synthesis. Newly synthesized CL must be converted to its mature form by fatty acid exchange, initiated by iPLA2γ-dependent fatty acid removal, which is also used for the repair of CL following ROS-induced damage. CL remodeling may proceed via mitochondrial TAZ protein, which transfers a fatty acid, preferentially linoleic acid (C18:2), from phosphatidylcholine to MLCL (Schlame et al., 2017). Alternatively, MLCL could be exported to the ER. In the latter case, ALCAT1 converts MLCL into CL, with a preference for DHA incorporation (Figure 3). Several studies have reported differences in DHA contents with Mtln depletion. We observed that DHA-containing triglycerides accumulate in *MTLN*-KO cell lines whereas the phosphatidylcholine content is depleted (Chugunova et al., 2019). This might be explained by a deficiency in MLCL traffic between the mitochondria and ER, such that an excess of DHA would be used for triglyceride synthesis, while phosphatidylcholine would be depleted due to excessive TAZ-mediated MLCL remodeling. Another consequence of Mtln inactivation—the accumulation of MLCL and the reduction of CL contents (Averina et al., 2023b; Stein et al., 2024)—might also be explained by reduced CL remodeling associated with transmembrane transport (Figure 3). Other explanations are possible, such as the protection of CL from oxidative damage through direct interaction with Mtln or the prevention of an increase in ROS production mediated by Mtln. The loss of Mtln was found to be associated with enhanced ROS generation (Stein et al., 2018), while a partner of Mtln, Cyb5r3 (Chugunova et al., 2019; Zhang et al., 2023), which is known to protect cells against oxidative damage (Hall et al., 2022), seems to decay under conditions of Mtln deficiency (Averina et al., 2023c).

12 Future perspectives

Despite a surge in studies on Mtln, there is still no unequivocal mechanistic understanding of Mtln function. To address this knowledge gap, membrane tethering by Mtln can be assessed in *in vitro* experiments, while the effects of Mtln on lipid transportation across mitochondrial membranes require a careful examination of lipidome composition in the IMM, OMM, and MAM after Mtln inactivation. Given recent outstanding progress in mitochondrial structural biology, it may soon be possible to directly observe Mtln.

Author contributions

PS: writing–original draft and writing–review and editing. OA: writing–review and editing. JG: visualization and writing–review and editing. MV: writing–review and editing. OD: writing–review and editing.

Funding

The authors declare that financial support was received for the research, authorship, and/or publication of this article. This work was supported by the Russian Science Foundation [24-14-00048] (PS, JG) and the state assignment of Lomonosov Moscow State University (OA, MV, OD).

Acknowledgments

The authors are grateful to all members of the laboratory for fruitful discussion and constant inspiration.

Conflict of interest

The authors declare that the research was conducted in the absence of any commercial or financial relationships that could be construed as a potential conflict of interest.

Generative AI statement

The authors declare that no generative AI was used in the creation of this manuscript.

Publisher's note

All claims expressed in this article are solely those of the authors and do not necessarily represent those of their affiliated organizations, or those of the publisher, the editors and the reviewers. Any product that may be evaluated in this article, or claim that may be made by its manufacturer, is not guaranteed or endorsed by the publisher.

References

Averina, O. A., Kuznetsova, S. A., Permyakov, O. A., and Sergiev, P. V. (2024). Animal models of mitochondrial diseases associated with nuclear gene mutations. *Acta Naturae* 15, 4–22. doi:10.32607/actanaturae.25442

Averina, O. A., Permyakov, O. A., Emelianova, M. A., Grigoryeva, O. O., Gulyaev, M. V., Pavlova, O. S., et al. (2023a). Mitochondrial peptide Mtln contributes to oxidative metabolism in mice. *Biochimie* 204, 136–139. doi:10.1016/j.biochi.2022.09.009

Averina, O. A., Permyakov, O. A., Emelianova, M. A., Grigoryeva, O. O., Lovat, M. L., Egorova, A. E., et al. (2023b). Mitoregulin contributes to creatine shuttling and cardiolipin protection in mice muscle. *IJMS* 24, 7589. doi:10.3390/ijms24087589

Averina, O. A., Permyakov, O. A., Emelianova, M. A., Guseva, E. A., Grigoryeva, O. O., Lovat, M. L., et al. (2023c). Kidney-related function of mitochondrial protein mitoregulin. *Int. J. Mol. Sci.* 24, 9106. doi:10.3390/ijms24109106

Calvo, S. E., Clauser, K. R., and Mootha, V. K. (2016). MitoCarta2.0: an updated inventory of mammalian mitochondrial proteins. *Nucleic Acids Res.* 44, D1251–D1257. doi:10.1093/nar/gkv1003

Choi, M., and Kang, K. W. (2023). Mitoregulin controls mitochondrial function and stress-adaptation response during early phase of endoplasmic reticulum stress in breast cancer cells. *Biochimica Biophysica Acta (BBA) - Mol. Basis Dis.* 1869, 166570. doi:10.1016/j.bbadis.2022.166570

Choi, M., Min, J.-S., Moon, S. W., Jeon, J., Do, H.-K., and Kim, W. (2024). Mitoregulin modulates inflammation in osteoarthritis: insights from synovial transcriptomics and cellular studies. *Biochem. Biophysical Res. Commun.* 734, 150652. doi:10.1016/j.bbrc.2024.150652

Chugunova, A., Loseva, E., Mazin, P., Mitina, A., Navalayeu, T., Bilan, D., et al. (2019). *LINC00116* codes for a mitochondrial peptide linking respiration and lipid metabolism. *Proc. Natl. Acad. Sci. U.S.A.* 116, 4940–4945. doi:10.1073/pnas.1809105116

Chugunova, A., Navalayeu, T., Dontsova, O., and Sergiev, P. (2018). Mining for small translated ORFs. *J. Proteome Res.* 17, 1–11.

de Brito, O. M., and Scorrano, L. (2008). Mitofusin 2 tethers endoplasmic reticulum to mitochondria. *Nature* 456, 605–610. doi:10.1038/nature07534

Dudek, J. (2017). Role of cardiolipin in mitochondrial signaling pathways. *Front. Cell Dev. Biol.* 5, 90. doi:10.3389/fcell.2017.00090

Friedman, J. R., Lackner, L. L., West, M., DiBenedetto, J. R., Nunnari, J., and Voeltz, G. K. (2011). ER tubules mark sites of mitochondrial division. *Science* 334, 358–362. doi:10.1126/science.1207385

Friesen, M., Warren, C. R., Yu, H., Toyohara, T., Ding, Q., Florido, M. H. C., et al. (2020). Mitoregulin controls β-oxidation in human and mouse adipocytes. *Stem Cell Rep.* 14, 590–602. doi:10.1016/j.stemcr.2020.03.002

Hall, R., Yuan, S., Wood, K., Katona, M., and Straub, A. C. (2022). Cytochrome b5 reductases: redox regulators of cell homeostasis. *J. Biol. Chem.* 298, 102654. doi:10.1016/j.jbc.2022.102654

Iwai, M., Kajino, T., Nakatochi, M., Yanagisawa, K., Hosono, Y., Isomura, H., et al. (2023). Long non-coding RNA TILR constitutively represses TP53 and apoptosis in lung cancer. *Oncogene* 42, 364–373. doi:10.1038/s41388-022-02546-w

Jiang, Z., Shen, T., Huynh, H., Fang, X., Han, Z., and Ouyang, K. (2022). Cardiolipin regulates mitochondrial ultrastructure and function in mammalian cells. *Genes* 13, 1889. doi:10.3390/genes13101889

Jussupow, A., Di Luca, A., and Kaila, V. R. I. (2019). How cardiolipin modulates the dynamics of respiratory complex I. *Sci. Adv.* 5, eaav1850. doi:10.1126/sciadv.aav1850

Kwak, C., Shin, S., Park, J.-S., Jung, M., Nhung, T. T. M., Kang, M.-G., et al. (2020). Contact-ID, a tool for profiling organelle contact sites, reveals regulatory proteins of mitochondrial-associated membrane formation. *Proc. Natl. Acad. Sci. U.S.A.* 117, 12109–12120. doi:10.1073/pnas.1916584117

Lai, Y., Zhou, B., Tan, Q., Xu, J., Wan, T., and Zhang, L. (2020). LINC00116 enhances cervical cancer tumorigenesis through miR-106a/c-Jun pathway. *J Cell. Biochem.* 121, 2247–2257. doi:10.1002/jcb.29447

Li, J., Qu, X., Guan, C., Luo, N., Chen, H., Li, A., et al. (2023). Mitochondrial micropeptide MOXI promotes fibrotic gene transcription by translocation to the nucleus and bridging N-acetyltransferase 14 with transcription factor c-Jun. *Kidney Int.* 103, 886–902. doi:10.1016/j.kint.2023.01.024

Li, X., Zhang, W., Cao, Q., Wang, Z., Zhao, M., Xu, L., et al. (2020). Mitochondrial dysfunction in fibrotic diseases. *Cell Death Discov.* 6, 80. doi:10.1038/s41420-020-00316-9

Lin, Y.-F., Xiao, M.-H., Chen, H.-X., Meng, Y., Zhao, N., Yang, L., et al. (2019). A novel mitochondrial micropeptide MPM enhances mitochondrial respiratory activity and promotes myogenic differentiation. *Cell Death Dis.* 10, 528. doi:10.1038/s41419-019-1767-y

Linzer, C. R., Stein, C. S., Witmer, N. H., Xu, Z., Schnicker, N. J., and Boudreau, R. L. (2024). Mitoregulin self-associates to form likely homo-oligomeric pore-like structures. *bioRxiv.*, 601956. doi:10.1101/2024.07.10.601956

Ma, Y., Li, J., Liu, Y., Zhao, H., Qi, X., Sun, Y., et al. (2024). Identification and exploration of a new M2 macrophage marker MTLN in alveolar echinococcosis. *Int. Immunopharmacol.* 131, 111808. doi:10.1016/j.intimp.2024.111808

Makarewich, C. A., Baskin, K. K., Munir, A. Z., Bezprozvannaya, S., Sharma, G., Khemtong, C., et al. (2018). MOXI is a mitochondrial micropeptide that enhances fatty acid β-oxidation. *Cell Rep.* 23, 3701–3709. doi:10.1016/j.celrep.2018.05.058

Martin-Montalvo, A., Sun, Y., Diaz-Ruiz, A., Ali, A., Gutierrez, V., Palacios, H. H., et al. (2016). Cytochrome b_5 reductase and the control of lipid metabolism and healthspan. *NPJ Aging Mech. Dis.* 2, 16006. doi:10.1038/npjamd.2016.6

O'Toole, J. (2014). Renal manifestations of genetic mitochondrial disease. *IJNRD* 57, 57–67. doi:10.2147/IJNRD.S37887

Palmfeldt, J., and Bross, P. (2017). Proteomics of human mitochondria. *Mitochondrion* 33, 2–14. doi:10.1016/j.mito.2016.07.006

Puurand, M., Tepp, K., Klepinin, A., Klepinina, L., Shevchuk, I., and Kaambre, T. (2018). Intracellular energy-transfer networks and high-resolution respirometry: a convenient approach for studying their function. *IJMS* 19, 2933. doi:10.3390/ijms19102933

Rath, S., Sharma, R., Gupta, R., Ast, T., Chan, C., Durham, T. J., et al. (2021). MitoCarta3.0: an updated mitochondrial proteome now with sub-organelle localization and pathway annotations. *Nucleic Acids Res.* 49, D1541–D1547. doi:10.1093/nar/gkaa1011

Rojo, M., Hovius, R., Demel, R. A., Nicolay, K., and Wallimann, T. (1991). Mitochondrial creatine kinase mediates contact formation between mitochondrial membranes. *J. Biol. Chem.* 266, 20290–20295. doi:10.1016/S0021-9258(18)54921-8

Sander, J., Sander, S., Steuerwald, U., Janzen, N., Peter, M., Wanders, R. J. A., et al. (2005). Neonatal screening for defects of the mitochondrial trifunctional protein. *Mol. Genet. Metabolism* 85, 108–114. doi:10.1016/j.ymgme.2005.02.002

Santel, A., and Fuller, M. T. (2001). Control of mitochondrial morphology by a human mitofusin. *J. Cell Sci.* 114, 867–874. doi:10.1242/jcs.114.5.867

Schlame, M., Xu, Y., and Ren, M. (2017). The basis for acyl specificity in the tafazzin reaction. *J. Biol. Chem.* 292, 5499–5506. doi:10.1074/jbc.M116.769182

Schlattner, U., Tokarska-Schlattner, M., and Wallimann, T. (2006). Mitochondrial creatine kinase in human health and disease. *Biochimica Biophysica Acta (BBA) - Mol. Basis Dis.* 1762, 164–180. doi:10.1016/j.bbadis.2005.09.004

Schlattner, U., and Wallimann, T. (2000). Octamers of mitochondrial creatine kinase isoenzymes differ in stability and membrane binding. *J. Biol. Chem.* 275, 17314–17320. doi:10.1074/jbc.M001919200

Sergiev, P. V., and Rubtsova, M. P. (2021). Little but loud. The diversity of functions of small proteins and peptides - translational products of short reading frames. *Biochem. (Mosc)* 86, 1139–1150. doi:10.1134/S0006297921090091

Shen, Y., Chen, Y., Zhang, S., Wu, Z., Lu, X., Liu, W., et al. (2024). Smartphone-based digital phenotyping for genome-wide association study of intramuscular fat traits in longissimus dorsi muscle of pigs. *Anim. Genet.* 55, 230–237. doi:10.1111/age.13401

Smirnova, E., Griparic, L., Shurland, D.-L., and Van Der Bliek, A. M. (2001). Dynamin-related protein Drp1 is required for mitochondrial division in mammalian cells. *MBoC* 12, 2245–2256. doi:10.1091/mbc.12.8.2245

Stein, C. S., Jadiya, P., Zhang, X., McLendon, J. M., Abouassaly, G. M., Witmer, N. H., et al. (2018). Mitoregulin: a lncRNA-encoded microprotein that supports mitochondrial supercomplexes and respiratory efficiency. *Cell Rep.* 23, 3710–3720.e8. doi:10.1016/j.celrep.2018.06.002

Stein, C. S., Zhang, X., Witmer, N. H., Pennington, E. R., Shaikh, S. R., and Boudreau, R. L. (2024). Mitoregulin supports mitochondrial membrane integrity and protects against cardiac ischemia-reperfusion injury. *bioRxiv.*, 596875. doi:10.1101/2024.05.31.596875

Surendran, R. P., Visser, M. E., Heemelaar, S., Wang, J., Peter, J., Defesche, J. C., et al. (2012). Mutations in LPL, APOC2, APOA5, GPIHBP1 and LMF1 in patients with severe hypertriglyceridaemia. *J. Intern Med.* 272, 185–196. doi:10.1111/j.1365-2796.2012.02516.x

Tábara, L.-C., Segawa, M., and Prudent, J. (2024). Molecular mechanisms of mitochondrial dynamics. *Nat. Rev. Mol. Cell Biol.* 26, 123–146. doi:10.1038/s41580-024-00785-1

Tomida, S., Takeuchi, T., Shimada, Y., Arima, C., Matsuo, K., Mitsudomi, T., et al. (2009). Relapse-related molecular signature in lung adenocarcinomas identifies patients with dismal prognosis. *JCO* 27, 2793–2799. doi:10.1200/JCO.2008.19.7053

Vial, C. (2006). *Creatine kinase* (New York: Nova Science).

Wang, L., Fan, J., Han, L., Qi, H., Wang, Y., Wang, H., et al. (2020). The micropeptide LEMP plays an evolutionarily conserved role in myogenesis. *Cell Death Dis.* 11, 357. doi:10.1038/s41419-020-2570-5

Weissglas-Volkov, D., Aguilar-Salinas, C. A., Nikkola, E., Deere, K. A., Cruz-Bautista, I., Arellano-Campos, O., et al. (2013). Genomic study in Mexicans identifies a new locus for triglycerides and refines European lipid loci. *J. Med. Genet.* 50, 298–308. doi:10.1136/jmedgenet-2012-101461

Xiao, M.-H., Lin, Y.-F., Xie, P.-P., Chen, H.-X., Deng, J.-W., Zhang, W., et al. (2022). Downregulation of a mitochondrial micropeptide, MPM, promotes hepatoma metastasis by enhancing mitochondrial complex I activity. *Mol. Ther.* 30, 714–725. doi:10.1016/j.ymthe.2021.08.032

Zhang, S., Guo, Y., Fidelito, G., Robinson, D. R. L., Liang, C., Lim, R., et al. (2023). LINC00116-encoded microprotein mitoregulin regulates fatty acid metabolism at the mitochondrial outer membrane. *iScience* 26, 107558. doi:10.1016/j.isci.2023.107558

frontiers | Frontiers in Cell and Developmental Biology

TYPE Mini Review
PUBLISHED 11 March 2025
DOI 10.3389/fcell.2025.1559504

Check for updates

OPEN ACCESS

EDITED BY
Jing Pu,
University of New Mexico, United States

REVIEWED BY
S. Joseph Endicott,
University of New Mexico Health Sciences Center, United States
Rui Jia,
Shandong University, China

*CORRESPONDENCE
Fulong Wang,
fulongwang@seu.edu.cn

†These authors have contributed equally to this work

‡Lead contact

RECEIVED 12 January 2025
ACCEPTED 18 February 2025
PUBLISHED 11 March 2025

CITATION
Wang Q, Wang R, Hu H, Huo X and Wang F (2025) Lysosomes' fallback strategies: more than just survival or death.
Front. Cell Dev. Biol. 13:1559504.
doi: 10.3389/fcell.2025.1559504

COPYRIGHT
© 2025 Wang, Wang, Hu, Huo and Wang. This is an open-access article distributed under the terms of the Creative Commons Attribution License (CC BY). The use, distribution or reproduction in other forums is permitted, provided the original author(s) and the copyright owner(s) are credited and that the original publication in this journal is cited, in accordance with accepted academic practice. No use, distribution or reproduction is permitted which does not comply with these terms.

Lysosomes' fallback strategies: more than just survival or death

Quan Wang[1†], Ruolin Wang[1†], Haihui Hu[1†], Xiaoqing Huo[2†] and Fulong Wang[1*‡]

[1]Key Laboratory of Developmental Genes and Human Disease, School of Life Science and Technology, Southeast University, Nanjing, China, [2]Huaian Maternity and Child Healthcare Hospital of JiangSu Province, Huaian, China

Lysosomes are heterogeneous, acidic organelles whose proper functionality is critically dependent on maintaining the integrity of their membranes and the acidity within their lumen. When subjected to stress, the lysosomal membrane can become permeabilized, posing a significant risk to the organelle's survival and necessitating prompt repair. Although numerous mechanisms for lysosomal repair have been identified in recent years, the progression of lysosome-related diseases is more closely linked to the organelle's alternative strategies when repair mechanisms fail, particularly in the contexts of aging and pathogen infection. This review explores lysosomal responses to damage, including the secretion of lysosomal contents and the interactions with lysosome-associated organelles in the endolysosomal system. Furthermore, it examines the role of organelles outside this system, such as the endoplasmic reticulum (ER) and Golgi apparatus, as auxiliary organelles of the endolysosomal system. These alternative strategies are crucial to understanding disease progression. For instance, the secretion and spread of misfolded proteins play key roles in neurodegenerative disease advancement, while pathogen escape via lysosomal secretion and lysosomotropic drug expulsion underlie cancer treatment resistance. Reexamining these lysosomal fallback strategies could provide new perspectives on lysosomal biology and their contribution to disease progression.

KEYWORDS

lysosomal damage, secretion, exosome, autophagy, golgi apparatus, endoplasmic reticulum

Introduction

Lysosomes are the primary degradation organelles of the cell and serve as the terminal compartments within the endolysosomal system (Ballabio and Bonifacino, 2020). This system comprises a network of dynamic and interconnected organelles, including endosomes, multivesicular bodies (MVBs), lysosomes, lysosome-related organelles (e.g., granules in immune cells), phagosomes, and autophagosomes (Figure 1). From a spatiotemporal perspective, rather than functioning as isolated compartments, the endolysosomal system operates as a highly coordinated and adaptive "digestive tract," facilitating the sequestration, sorting, and degradation of cargo derived from both intracellular and extracellular sources (Hu et al., 2015; Neel et al., 2024). Endosomes, phagosomes, and autophagosomes act as intermediary hubs within this network, directing cargo toward lysosomes, which serve as the terminal degradative compartments where cellular digestion and recycling

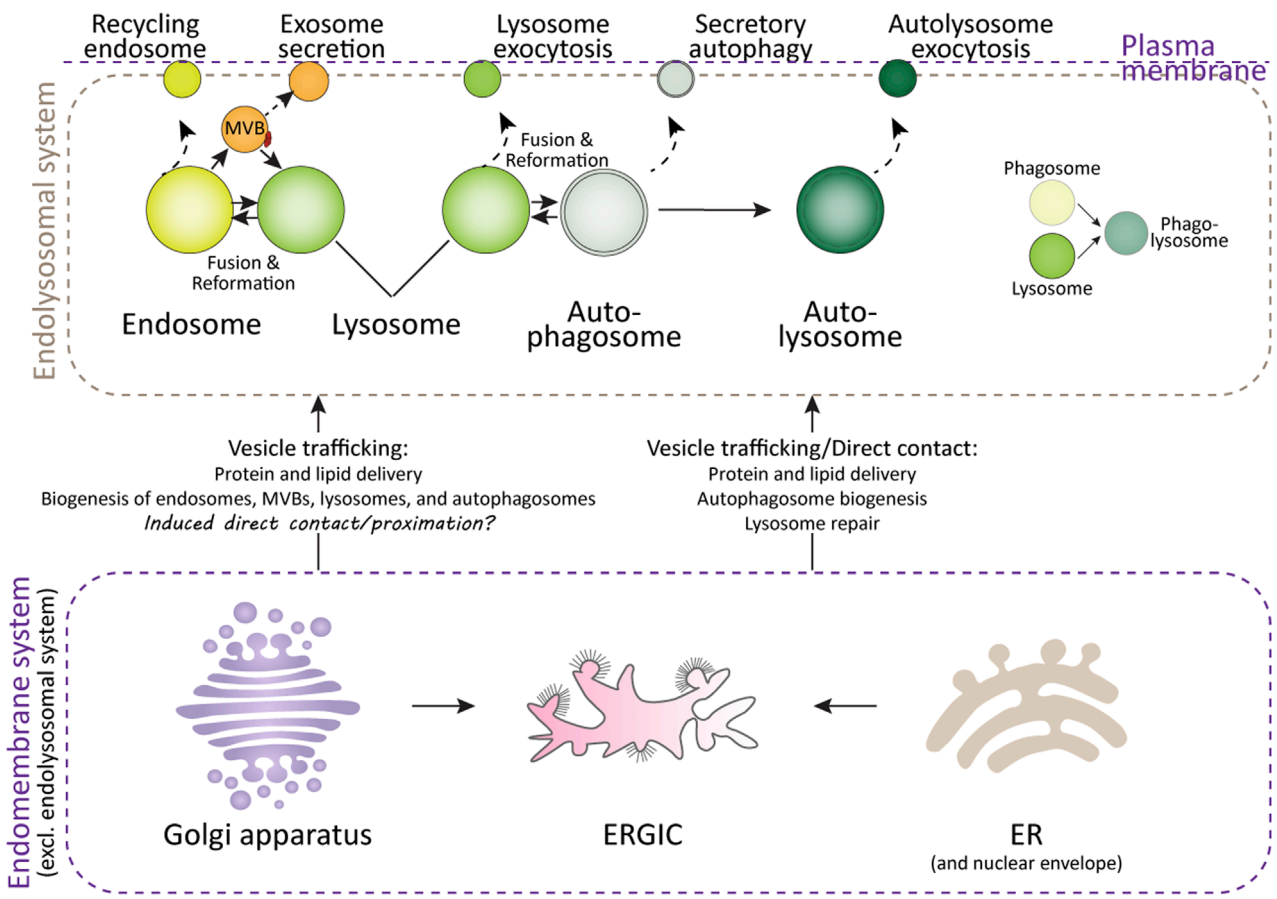

FIGURE 1
Lysosomes and their interacting organelles. Top panel: Overview of lysosomes and their interacting organelles within the endolysosomal system. Lysosomal fusion and fission with endosomes, autophagosomes, and phagosomes are critical for their maturation, functional maintenance, reformation, and repair after damage. However, when lysosomal damage exceeds the capacity for repair, both lysosomes and the organelles within the endolysosomal system may undergo secretion in various forms. Bottom panel: Interaction of lysosomes with organelles in the endomembrane system. The delivery of proteins and lipids from the ER and Golgi apparatus is essential for lysosomal function and repair. Additionally, the ER, ER-Golgi intermediate compartment (ERGIC), and Golgi apparatus contribute to autophagosome formation, a process critical for the clearance of damaged lysosomes.

occur. Beyond their degradative role, components of this system are involved in specialized secretion pathways (Figure 1): autophagosomes facilitate secretory autophagy, MVBs mediate the release of exosomes, and lysosomes participate in lysosome-associated exocytosis, thereby expelling undigested material, especially when the degradation function of the lysosomes is compromised (Buratta et al., 2020; Han et al., 2022; Ponpuak et al., 2015).

From an endolysosome-centric perspective, other organelles within the broader endomembrane system—such as the ER, Golgi apparatus, and plasma membrane—serve as auxiliary organelles or components of the endolysosomal system (Figure 1). These organelles support lysosomal function by synthesizing and delivering lipids, proteins, and membranes via vesicular trafficking, membrane budding, and direct membrane contact sites. These interactions ensure the proper functioning of the endolysosomal system and maintain cellular homeostasis (De Tito et al., 2020; Nascimbeni et al., 2017; Sun et al., 2024; Tan and Finkel, 2023).

Therefore, when lysosomes are exposed to various stresses and their membrane integrity is compromised, organelles within the endolysosomal and endomembrane systems may play critical roles in facilitating lysosomal repair. These stresses can arise from physiological, pathological, and external factors that impair membrane integrity and enzymatic function. Physiologically, aging contributes to lysosomal damage by promoting the accumulation of indigestible materials, such as lipofuscin, which reduces degradation efficiency, while oxidative stress induces lipid peroxidation within lysosomal membranes, weakening their structure and leading to enzyme leakage (Gahlot et al., 2024; Pan et al., 2021; Zhang et al., 2023). Pathological conditions—including neurodegenerative diseases (Root et al., 2021), lysosomal storage disorders (Parenti et al., 2021), metabolic disturbances (Almeida et al., 2020), and infections (Richards et al., 2022)—exacerbate these effects by causing substrate overload, protein aggregation, and inflammation, further destabilizing lysosomes. Additionally, external agents such as lysosomotropic drugs, ionophores, toxins, and environmental pollutants can directly damage lysosomal membranes, triggering

the excessive release of lysosomal enzymes. In research settings, compounds like L-leucyl-L-leucine methyl ester (LLOMe), Glycyl-L-phenylalanine 2-naphthylamide (GPN), methyl-serine dodecylqamide hydrochloride (MSDH), chloroquine, Bafilomycin A1, ammonium chloride, silica crystals, and overexpression of mutant proteins associated with neurodegenerative diseases and lysosomal storage disorders—such as alpha-synuclein, amyloid-beta, Tau, Huntingtin, TDP43, SOD1, PANK2, NPC1, NPC2, CLN3, GBA1, HEXA, GAA, MPS, ASAH1, CTNS, and GALC—are commonly used to mimic these conditions (Parenti et al., 2021; Root et al., 2021; Udayar et al., 2022). Pathogen-derived factors, such as SapM, PtpA, and ESAT-6 from *Mycobacterium tuberculosis* (Ramon-Luing et al., 2023); Listeriolysin O (LLO) from *Listeria monocytogenes* (Shaughnessy et al., 2006); SopB from *Salmonella enterica* (Bakowski et al., 2010); Nef from HIV (Sanfridson et al., 1997); and ORF3a from SARS-CoV-2 (Walia et al., 2024), are also employed to study lysosomal dysfunction.

To date, a wide array of key proteins and complexes have been identified as being recruited to the damaged lysosomal sites to mediate repair processes. These include the Endosomal Sorting Complexes Required for Transport (ESCRT) machinery (Jia et al., 2020b; Radulovic et al., 2018; Skowyra et al., 2018), Annexins (Ebstrup et al., 2023; Yim et al., 2022), mTOR (Jia et al., 2018; Jia et al., 2019), AMPK (Jia et al., 2020a), PI4K2A (Tan and Finkel, 2022), and stress granules (Bussi et al., 2023; Duran et al., 2024; Jia et al., 2022). However, the successful execution of lysosomal repair or resolution of lysosomal stress is heavily dependent on the collaboration and interactions with other organelles. This includes fusion and fission events involving lysosomes, endosomes, and autophagosomes (Bhattacharya et al., 2023; Maejima et al., 2013; Rodgers et al., 2022; Saffi and Botelho, 2019), as well as both direct and indirect interactions with the ER (Radulovic et al., 2022; Tan and Finkel, 2022; Wang et al., 2024), Golgi apparatus (Lie et al., 2021; Vitry et al., 2010), and plasma membrane (Domingues et al., 2024; Sho et al., 2024; Wang et al., 2023; Zhong et al., 2023) (Figure 1).

The progression of lysosome-related diseases often correlates more closely with alternative strategies employed by lysosomes when conventional repair mechanisms fail, particularly in the contexts of age-related diseases and pathogen infections. This review aims to critically examine these alternative strategies, including different forms of lysosomal damage-related secretion, and the role ER and Golgi aparatus play in the repair and handling of damged lysosomes—other important aspects related to lysosomal damage repair, such as lysosomal repositioning and reformation, and lysosomal cell death (Figure 2) are reviewed elsewhere (Aits and Jäättelä, 2013; Gómez-Sintes et al., 2016; Pu et al., 2016; Scerra et al., 2022; Wang et al., 2018), therefore would not be covered here. By addressing these relatively neglected areas of lysosomal adaptation and alterations following lysosomal damage, this review seeks to provide a better understanding of the underlying mechanisms and their implications for cellular homeostasis and disease.

Lysosomal damage and secretion

Under pathological conditions where lysosomes are severely damaged—such as during cancer treatment, pathogen infections, and neurodegenerative diseases—their repair capacities are often compromised or overwhelmed. In these scenarios, cells frequently adopt an alternative mechanism of expelling compromised lysosomes along with their enzymatic content and undigested materials (Chen et al., 2021; Domingues et al., 2024; Sho et al., 2024; Wang et al., 2023; Zhitomirsky and Assaraf, 2017; Zhong et al., 2023). These expelled materials may include lysosomotropic agents, engulfed pathogens, and aggregated pathogenic proteins. Furthermore, vesicles and organelles within the endolysosomal system that are primed to fuse with lysosomes—such as autophagosomes, endosomes, and MVBs—as well as damaged organelles engulfed by autophagosomes or endosomes [e.g., mitochondria (Bao et al., 2022; Liang et al., 2023)], may also be secreted concurrently or in parallel with lysosomal expulsion.

These lysosome-associated secretion processes can significantly influence disease susceptibility and progression (Groth-Pedersen and Jaattela, 2013; Scotto Rosato et al., 2022; Xu et al., 2021). For instance, the expulsion of aggregated proteins or pathogens through this mechanism has been linked to the spread of pathogenic agents in neurodegenerative diseases and the survival of invasive pathogens in infections. In cancer, lysosomal exocytosis contributes to drug resistance by releasing lysosomotropic chemotherapeutic agents from cells (Machado et al., 2015; Zhitomirsky and Assaraf, 2017). Conversely, under specific circumstances, lysosomal secretion may serve a protective role, such as by removing cytotoxic material or reducing intracellular stress (Tsunemi et al., 2019; Zhong et al., 2023).

The impact of lysosome-associated secretion on diseases underscores a potentially underappreciated relationship between this process and disease mechanisms. By better understanding the molecular pathways governing lysosomal secretion, therapeutic targeting of lysosome-associated secretion could represent a novel and promising strategy for managing diseases characterized by lysosomal dysfunction, including neurodegenerative disorders, infectious diseases, and cancers.

Lysosomal exocytosis

Lysosomal exocytosis is a calcium-dependent process in which lysosomes fuse directly with the plasma membrane to release their contents into the extracellular space (Zhong et al., 2023). This mechanism is present in all cell types and is activated by a variety of stimuli. It plays a crucial role in numerous physiological processes, including plasma membrane repair (Reddy et al., 2001), bone resorption (Kim et al., 2024; Lee et al., 2024), pigmentation (Stinchcombe et al., 2004; Wünkhaus et al., 2024), immune responses (Brady et al., 2018; Jin et al., 2021; Sáez et al., 2019), mitosis (Hämälistö et al., 2020; Nugues et al., 2022), and ATP release in the nervous system (Jung et al., 2013; Shin et al., 2012; Zhang et al., 2007). Moreover, when lysosomes are damaged or their functions are compromised, the exocytosis process is typically enhanced (Bogacki et al., 2025; Chen et al., 2011; Domingues et al., 2024; Eriksson et al., 2020; Ghosh et al., 2020; Sivaramakrishnan et al., 2012; Wang et al., 2023). This enhancement is triggered by events such as lysosomal membrane permeabilization, alkalinization, and the consequent release of Ca^{2+}, all of which can induce cellular stress and inflammation.

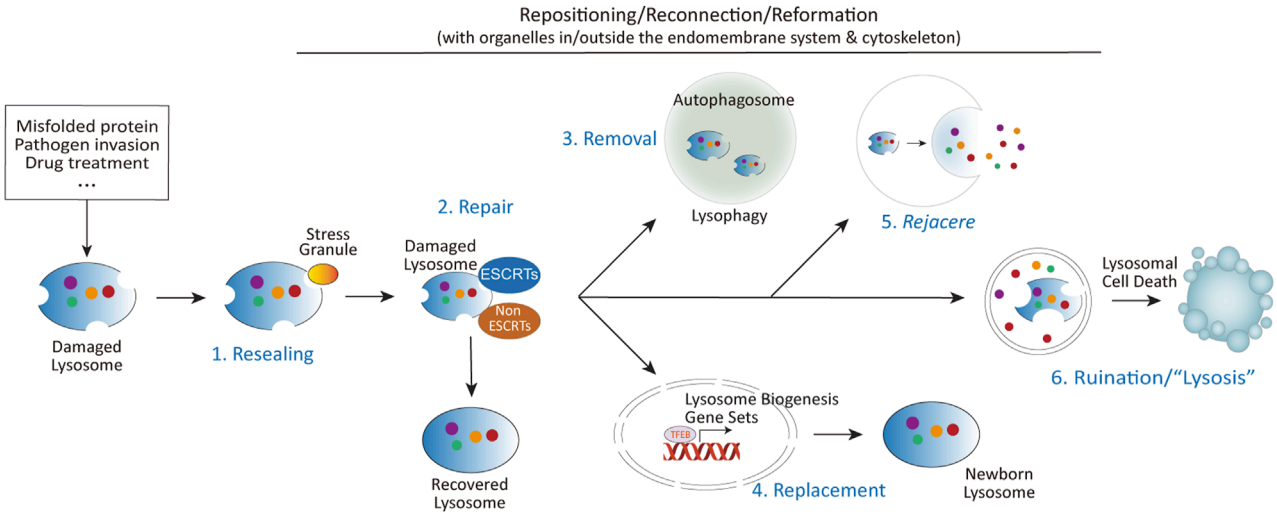

FIGURE 2
The diverse fates of damaged lysosomes. Upon lysosomal damage caused by aggregated proteins, invading pathogens, chemical insults, or other stressors, several outcomes are possible: (1) Immediate resealing of lysosomal membranes through stress granule-mediated repair. (2) Activation of multiple repair mechanisms, including ESCRTs dependent and independent mechanisms. (3) Mildly damaged lysosomes can be repaired, while severely damaged lysosomes are targeted for removal via autophagy (lysophagy). (4) Lysosomal damage also promotes lysosomal biogenesis through the activation of TFEB, regulated by mTORC1, calcium signaling, and other pathways. (5) In cases where repair is insufficient, damaged lysosomes may be expelled through fusion with the plasma membrane. The term *rejacere* (Latin: to expel) is used here to describe the active expulsion of lysosomal contents, emphasizing its mechanistic and evolutionary context. (6) If repair and removal mechanisms fail, the release of lysosomal contents such as cathepsins, coupled with altered signaling pathways at the lysosomal signaling hub, can trigger lysosomal cell death via multiple mechanisms.

Enhanced lysosomal exocytosis can have both beneficial and detrimental effects, depending on the pathological context. For instance, in cancer treatment, the release of lysosomal enzymes through lysosomal exocytosis is often associated with increased metastasis and reduced patient survival (Machado et al., 2015; Ren et al., 2025). Conversely, the expulsion of lysosomotropic agents via lysosomal exocytosis in renal proximal tubular epithelial cells—mediated by the activation of the lysosomal Ca^{2+} channel TRPML1—has been shown to mitigate uranium-induced nephrotoxicity (Zhong et al., 2023). This dichotomy underscores the critical influence of the specific components released during lysosomal exocytosis.

In neurodegenerative diseases, the accumulation of aggregated misfolded proteins is a central factor in disease progression. The role of lysosomes in degrading these proteins—or alternatively, in their activation, accumulation, or release—is paramount. For example, in synucleinopathy models, lysosomal exocytosis-mediated release of degradation-resistant α-synuclein species from neurons has been identified as a key mechanism for the propagation of pathogenic α-synuclein in mouse brains (Xie et al., 2022). However, contrasting findings indicate that activation of TRPML1 can protect human dopaminergic neurons by rescuing defective α-synuclein secretion and preventing its accumulation (Tsunemi et al., 2019). This again suggests that the effects of lysosomal exocytosis in neurodegenerative diseases may vary depending on the specific cellular context involved.

Similarly, during pathogen infections, lysosomal damage-induced exocytosis serves as an effective mechanism to expel overwhelmed pathogens (Chen et al., 2021; Deretic and Wang, 2023; Ghosh et al., 2020; Koo et al., 2008; Shtuhin-Rahav et al., 2023; Wang et al., 2023). However, this process can be hijacked by pathogens to facilitate their own survival and dissemination. For example, both severe acute respiratory syndrome coronavirus 2 (SARS-CoV-2) (Chen et al., 2021) and its β-coronavirus relative MHV (Ghosh et al., 2020) induce lysosomal damage and exocytosis through multiple Ca^{2+}-dependent mechanisms, enabling their egress from infected cells. Additionally, in bacterial infections, lysosomal exocytosis from immune and other cell types is associated with the cytolytic effects of bacteria, allowing bacteria within lysosomes and phagosomes to evade digestion and enhance their survival (Koo et al., 2008; Shtuhin-Rahav et al., 2023; Wang et al., 2023).

These studies illustrate that lysosomal exocytosis plays a complex role in disease dynamics, acting as a double-edged sword. On one hand, it can protect cells by removing toxic substances and pathogens; on the other hand, it can facilitate disease progression by promoting metastasis, protein propagation, and pathogen survival. Understanding the specific context of lysosomal exocytosis is therefore crucial.

Alternative secretion mechanisms

Besides lysosomal exocytosis, at least two additional secretion mechanisms are linked to lysosomal damage and compromised lysosomal function: exosome secretion and secretory autophagy. Exosome secretion is a process in which small extracellular vesicles, known as exosomes, are released following the fusion of MVBs with the plasma membrane (Han et al., 2022). The formation of exosomes is facilitated by the ESCRT complexes, which sort cargo into

intraluminal vesicles and drive membrane inward budding events. These exosomes, which transport proteins, lipids, and nucleic acids, play a crucial role in intercellular communication and modulate various physiological and pathological processes. Secretory autophagy, on the other hand, repurposes the cellular autophagic machinery to facilitate the secretion of cellular components, rather than their degradation (Buratta et al., 2020; Debnath and Leidal, 2022; Solvik et al., 2022). Unlike the classical autophagic pathway, which typically directs cargo to lysosomes for degradation, secretory autophagy allows the release of cellular materials, such as proteins and lipids, into the extracellular space. This process is particularly important for cellular communication, immune responses, and tissue homeostasis, providing an alternative route for the secretion of factors like cytokines and extracellular matrix components. Both exosome secretion and secretory autophagy serve as alternative pathways for managing cargo within the endolysosomal system, contributing to cellular responses and disease progression by facilitating the extracellular release of materials that would otherwise be degraded.

A significant feature of approximately half of the lysosomal storage disorders (LSDs)—a group of over 70 rare inherited metabolic diseases caused by lysosomal dysfunction—is the increased secretion of exosomes, highlighting the correlation between lysosomal impairment and exosome release (Abe et al., 2024; Alvarez-Erviti et al., 2011). The exosome-mediated release of pathogenic α-synuclein from macrophage lineage cells or neuroblastoma cells has been attributed to lysosomal stress-induced dysfunction (Abe et al., 2024; Alvarez-Erviti et al., 2011). In another model of lysosomal dysfunction, the contents released via exosomes include amyloid precursor protein C-terminal fragments (APP-CTFs), specific sphingolipids, and the phospholipid bis(monoacylglycero)phosphate (BMP), which normally reside in the internal vesicles of endolysosomes (Miranda et al., 2018). Notably, disruption of endolysosome fusion also increases exosome secretion (Shelke et al., 2023), indicating that the physical interaction between lysosomes and MVBs inherently predicts exosome release.

However, when lysosomal inhibition is induced by agents such as chloroquine or Bafilomycin A, cells tend to utilize secretory autophagy instead of exosome secretion, as evidenced by increased secretion of autophagy cargo receptors in extracellular vesicles and particles (EVPs) but negligible changes in classical exosome markers such as TSG101, ALIX, and CD9 (Solvik et al., 2022). This observation is consistent with several other studies demonstrating that lysosomal damage or stress can induce secretory autophagy (Chang et al., 2024; Dash et al., 2024; Kimura et al., 2017). Considering the significant roles of secretory autophagy and exosome secretion in the progression of diseases such as neurodegenerative disorders and cancer, as well as the use of exosomes for drug delivery, the interplay between lysosomal damage and secretion warrants further attention.

Lysosomal damage and endomembrane system

While much attention has been given to the endolysosomal system itself, emerging research reveals that lysosomes rely heavily on interactions with other organelles—particularly the endoplasmic reticulum (ER) and Golgi apparatus—to repair damage and restore homeostasis.

ER and lysosomal damage

Emerging evidence underscores the critical role of endoplasmic reticulum (ER)-lysosome membrane contact sites (MCSs) in mediating lysosomal repair. Central to this process is the phosphatidylinositol-4 kinase type 2α (PI4K2A), which generates phosphatidylinositol-4-phosphate (PI4P) at lysosomal membranes. PI4P recruits oxysterol-binding protein (OSBP)-related protein (ORP) family members, including ORP9, ORP10, ORP11, and OSBP, to orchestrate the formation of ER-lysosome MCSs (Tan and Finkel, 2022). These dynamic contact sites facilitate the transfer of phosphatidylserine and cholesterol from the ER to damaged lysosomes, enabling rapid membrane restoration. Complementary studies emphasize the role of cholesterol and ER-resident tethering proteins, such as VAPA/B and ORP1L, in stabilizing these interactions and promoting lysosomal integrity (Radulovic et al., 2022).

A parallel mechanism involves the lipid transfer protein ATG2, which is recruited to damaged lysosomes to mediate direct lipid transfer for membrane repair (Tan and Finkel, 2022). ATG2's interaction with the lipid scramblase ATG9, essential for ER-phagophore contact site formation and autophagosome maturation (Gomez-Sanchez et al., 2018; van Vliet et al., 2022), suggests a coordinated interplay between lysosomal repair and lysophagy. This duality highlights a potential regulatory axis where ER-driven lipid redistribution supports both autophagosome biogenesis and lysosomal membrane restoration.

Pathophysiological insights emerge from studies linking ER-lysosome interactions to Parkinson's disease (PD). VPS13C and LRRK2, two PD-associated proteins, are recruited to damaged lysosomes: VPS13C facilitates ER-lysosome tethering, while LRRK2 promotes lysosomal membrane tubulation and cargo sorting (Bonet-Ponce and Cookson, 2022; Wang et al., 2024). Similarly, PDZD8, a tubular lipid-binding protein (TULIP) superfamily member, tethers ER-lysosome MCSs to regulate lysosome maturation and autophagy (Guillén-Samander et al., 2019; Thakur and O'Connor-Giles, 2023). Behavioral abnormalities observed in PDZD8-deficient mice (Kurihara et al., 2023) raise intriguing questions about whether these phenotypes come partially from disrupted ER-lysosome communication, underscoring the need to explore MCS dysfunction in neurodegenerative contexts.

The endoplasmic reticulum (ER) may contribute to lysosomal damage repair through additional mechanisms. For example, during lysosomal injury, calcium efflux from damaged lysosomes has been shown to trigger compensatory ER-mediated calcium refilling in multiple models of lysosomal dysfunction (Garrity et al., 2016; Kang et al., 2024; Liu and Lieberman, 2019). Given the central role of calcium signaling in lysosomal repair and adaptation, future studies should investigate whether ER-lysosome membrane contact sites (MCSs) directly facilitate this calcium replenishment process. Such work could reveal how spatial and temporal coordination between calcium homeostasis and lipid transfer synergistically

enhances lysosomal membrane repair. Beyond calcium dynamics, the ER and ER-Golgi intermediate compartment (ERGIC) also play critical roles in autophagy, a process tightly linked to lysosomal recovery. The ER and ERGIC are well-known sources of membranes for autophagosome biogenesis, supplying lipids and proteins required for phagophore expansion (Han et al., 2023; Melia et al., 2020). Building on these findings, the interplay between ER/ERGIC-driven autophagosome formation and lysosomal repair mechanisms—such as lysophagy—remains an open question. For instance, it is unclear whether ER-derived autophagosomes are preferentially recruited to engulf damaged lysosomes or if their maturation is synchronized with lysophagy. Elucidating these interactions could clarify how membrane trafficking pathways converge to restore lysosomal function, offering insights into the integration of autophagy and organelle repair. By exploring these mechanisms, researchers could refine models of lysosomal recovery, emphasizing the ER's dual role in calcium regulation and membrane supply, and how these functions are coordinated to resolve lysosomal stress.

Golgi apparatus and lysosomal damage

In contrast to the ER and ERGIC, which directly interact with lysosomes through membrane contact sites to repair damage, the Golgi apparatus engages with lysosomes in a more indirect and unidirectional manner. This interaction primarily occurs via two pathways: 1) Protein Transport: Proteins, including hydrolases processed by the Golgi apparatus, are transported to endosomes through vesicular trafficking. These proteins ultimately reach lysosomes through acidification and fusion within the endolysosomal pathway (Melia et al., 2020; Scheuring et al., 2011). Therefore, deficiencies in posttranslational modifications within the Golgi apparatus are strongly associated with lysosomal dysfunction-related diseases (Akaaboune and Wang, 2024; Sou et al., 2024). 2) Autophagosome Biogenesis: The Golgi apparatus also serves as a source of key proteins and membrane components necessary for autophagosome formation (Gao et al., 2016; Sawa-Makarska et al., 2020). These components are incorporated into autophagosomes, which subsequently fuse with lysosomes to form autolysosomes, thereby delivering their cargo for degradation.

Despite these established pathways, the interactions between the Golgi apparatus and lysosomes might be more complex. In numerous diseases characterized by lysosomal dysfunction—such as lysosomal storage disorders (Lojewski et al., 2014; Shammas et al., 2019), neurodegenerative diseases (Gosavi et al., 2002; Martínez-Menárguez et al., 2019), COVID-19 infection (Cortese et al., 2020; Zhang et al., 2024), nicotine exposure (Govind et al., 2021), and epilepsy or other mental disorders triggered by electrical signal disturbances (Thayer et al., 2013)—morphological alterations in the Golgi apparatus have been consistently observed. These alterations include fragmentation (reduction in Golgi stack organization and increased dispersal), vesiculation (increased formation of Golgi-derived vesicles), and depolarization (randomized Golgi distribution), indicating that lysosomal damage and Golgi apparatus disorganization are concomitant events in these pathologies.

Similar to the ER, several Golgi-resident proteins may be recruited to or localized near damaged lysosomes, further suggesting a more complex interplay between the Golgi apparatus and lysosomal dysfunction. For example, Rab34, a Golgi-localized protein, plays a significant role in lysosome positioning and function. Overexpression or constitutive activation of Rab34 relocates lysosomes to the peri-Golgi area (Kumar et al., 2024; Wang and Hong, 2002) and facilitates the fusion of phagosomes with lysosomes (Seto et al., 2011). Additionally, loss-of-function variants of Rab34 are associated with various ciliopathies (Batkovskyte et al., 2024; Bruel et al., 2023), suggesting the possibility that dysregulation of Rab34-mediated Golgi-lysosome interactions may contribute to the pathogenesis of human diseases. The possibility of Golgi–lysosome interaction is further supported by single-organelle immunoprecipitation–coupled mass spectrometry studies of the Golgi (Fasimoye et al., 2023) and lysosomes (Eapen et al., 2021; Jia et al., 2022; Tan and Finkel, 2022; Wyant et al., 2018), underscoring the need for continued investigation.

Discussion

Lysosomal quality control is vital for cellular homeostasis and disease progression, with lysosomes employing alternative secretion pathways, such as exocytosis, exosome release, and secretory autophagy, when traditional repair mechanisms fail. Interactions with the endomembrane system, particularly the ER and Golgi apparatus, are also essential for lysosomal repair and function. These pathways play key roles in diseases, such as neurodegenerative disorders, where exosome-mediated spread of aggregated proteins accelerates progression, and cancer, where lysosomal exocytosis contributes to drug resistance and metastasis. Pathogens also exploit lysosomal secretion to enhance survival and spread, highlighting its complex role in disease.

Targeting lysosomal secretion and enhancing organelle interactions offer promising treatment strategies for lysosome-related diseases. Modulating exosome release could limit pathogenic protein spread in neurodegeneration, while inhibiting lysosomal exocytosis may help overcome cancer drug resistance. Strengthening ER-lysosome and Golgi-lysosome interactions could enhance lysosomal resilience in various diseases. These approaches aim to mitigate lysosomal dysfunction and improve cellular stress responses, offering new therapeutic perspectives.

Despite progress, key questions remain in lysosomal biology. Future research should focus on how lysosomal positioning impacts quality control, identifying specialized lysosome subpopulations, and understanding coordination with organelles like mitochondria. Additionally, the molecular triggers behind Golgi morphological changes in response to lysosomal damage and their role in repair need further investigation. Addressing these questions is critical to fully understanding lysosomal function and its integration within the cellular network.

In conclusion, lysosomes employ diverse strategies, including alternative secretion pathways and organelle interactions, to maintain cellular homeostasis under stress. These mechanisms are crucial in diseases like neurodegeneration, cancer, and infections. A deeper understanding of lysosomal-endomembrane interactions will uncover new therapeutic targets and

help improve strategies for managing diseases linked to lysosomal dysfunction.

Author contributions

QW: Visualization, Writing–review and editing. RW: Visualization, Writing–review and editing. HH: Visualization, Writing–review and editing. XH: Visualization, Writing–review and editing. FW: Conceptualization, Funding acquisition, Investigation, Project administration, Resources, Supervision, Visualization, Writing–original draft, Writing–review and editing.

Funding

The author(s) declare that financial support was received for the research, authorship, and/or publication of this article. This study was supported by the Start-up Research Fund of Southeast University to FW.

Conflict of interest

The authors declare that the research was conducted in the absence of any commercial or financial relationships that could be construed as a potential conflict of interest.

Generative AI statement

The author(s) declare that no Generative AI was used in the creation of this manuscript.

Publisher's note

All claims expressed in this article are solely those of the authors and do not necessarily represent those of their affiliated organizations, or those of the publisher, the editors and the reviewers. Any product that may be evaluated in this article, or claim that may be made by its manufacturer, is not guaranteed or endorsed by the publisher.

References

Abe, T., Kuwahara, Suenaga, T., Sakurai, S., Takatori, M. S., and Iwatsubo, T. (2024). Lysosomal stress drives the release of pathogenic α-synuclein from macrophage lineage cells via the LRRK2-Rab10 pathway. *iScience* 27, 108893. doi:10.1016/j.isci.2024.108893

Aits, S., and Jäättelä, M. (2013). Lysosomal cell death at a glance. *J. Cell Sci.* 126, 1905–1912. doi:10.1242/jcs.091181

Akaaboune, S. R., and Wang, Y. (2024). Golgi defect as a major contributor to lysosomal dysfunction. *Front. Cell Dev. Biol.* 12, 1386149. doi:10.3389/fcell.2024.1386149

Almeida, M. F., Bahr, B. A., and Kinsey, S. T. (2020). Endosomal-lysosomal dysfunction in metabolic diseases and Alzheimer's disease. *Int. Rev. Neurobiol.* 154, 303–324. doi:10.1016/bs.irn.2020.02.012

Alvarez-Erviti, L., Seow, Y., Schapira, A. H., Gardiner, C., Sargent, I. L., Wood, M. J., et al. (2011). Lysosomal dysfunction increases exosome-mediated alpha-synuclein release and transmission. *Neurobiol. Dis.* 42, 360–367. doi:10.1016/j.nbd.2011.01.029

Bakowski, M. A., Braun, V., Lam, G. Y., Yeung, T., Heo, W. D., Meyer, T., et al. (2010). The phosphoinositide phosphatase SopB manipulates membrane surface charge and trafficking of the Salmonella-containing vacuole. *Cell Host Microbe* 7, 453–462. doi:10.1016/j.chom.2010.05.011

Ballabio, A., and Bonifacino, J. S. (2020). Lysosomes as dynamic regulators of cell and organismal homeostasis. *Nat. Rev. Mol. Cell Biol.* 21, 101–118. doi:10.1038/s41580-019-0185-4

Bao, F., Zhou, L., Zhou, R., Huang, Q., Chen, J., Zeng, S., et al. (2022). Mitolysosome exocytosis, a mitophagy-independent mitochondrial quality control in flunarizine-induced parkinsonism-like symptoms. *Sci. Adv.* 8, eabk2376. doi:10.1126/sciadv.abk2376

Batkovskyte, D., Komatsu, M., Hammarsjö, A., Pooh, R., Shimokawa, O., Ikegawa, S., et al. (2024). Compound heterozygous variants in RAB34 in a rare skeletal ciliopathy syndrome. *Clin. Genet.* 105, 87–91. doi:10.1111/cge.14419

Bhattacharya, A., Mukherjee, R., Kuncha, S. K., Brunstein, M. E., Rathore, R., Junek, S., et al. (2023). A lysosome membrane regeneration pathway depends on TBC1D15 and autophagic lysosomal reformation proteins. *Nat. Cell Biol.* 25, 685–698. doi:10.1038/s41556-023-01125-9

Bogacki, E. C., Longmore, G., Lewis, P. A., and Herbst, S. (2025). GPNMB is a biomarker for lysosomal dysfunction and is secreted via LRRK2-modulated lysosomal exocytosis. bioRxiv, 2001–630988. doi:10.1101/2025.01.01.630988

Bonet-Ponce, L., and Cookson, M. R. (2022). The endoplasmic reticulum contributes to lysosomal tubulation/sorting driven by LRRK2. *Mol. Biol. Cell* 33, ar124. doi:10.1091/mbc.E22-04-0139

Brady, O. A., Martina, J. A., and Puertollano, R. (2018). Emerging roles for TFEB in the immune response and inflammation. *Autophagy* 14, 181–189. doi:10.1080/15548627.2017.1313943

Bruel, A. L., Ganga, A. K., Nosková, L., Valenzuela, I., Martinovic, J., Duffourd, Y., et al. (2023). Pathogenic RAB34 variants impair primary cilium assembly and cause a novel oral-facial-digital syndrome. *Hum. Mol. Genet.* 32, 2822–2831. doi:10.1093/hmg/ddad109

Buratta, S., Tancini, B., Sagini, K., Delo, F., Chiaradia, E., Urbanelli, L., et al. (2020). Lysosomal exocytosis, exosome release and secretory autophagy: the autophagic- and endo-lysosomal systems go extracellular. *Int. J. Mol. Sci.* 21, 2576. doi:10.3390/ijms21072576

Bussi, C., Mangiarotti, A., Vanhille-Campos, C., Aylan, B., Pellegrino, E., Athanasiadi, N., et al. (2023). Stress granules plug and stabilize damaged endolysosomal membranes. *Nature* 623, 1062–1069. doi:10.1038/s41586-023-06726-w

Chang, Y.-C., Gao, Y., Lee, J. Y., Peng, Y.-J., Langen, J., and Chang, K. T. (2024). Identification of secretory autophagy as a mechanism modulating activity-induced synaptic remodeling, *Proc. Natl. Acad. Sci. U. S. A.*, 121, e2315958121, doi:10.1073/pnas.2315958121

Chen, D., Zheng, Q., Sun, L., Ji, M., Li, Y., Deng, H., et al. (2021). ORF3a of SARS-CoV-2 promotes lysosomal exocytosis-mediated viral egress. *Dev. Cell* 56, 3250–3263.e5. doi:10.1016/j.devcel.2021.10.006

Chen, P. M., Gombart, Z. J., and Chen, J. W. (2011). Chloroquine treatment of ARPE-19 cells leads to lysosome dilation and intracellular lipid accumulation: possible implications of lysosomal dysfunction in macular degeneration. *Cell and Biosci.* 1, 10. doi:10.1186/2045-3701-1-10

Cortese, M., Lee, J. Y., Cerikan, B., Neufeldt, C. J., Oorschot, V. M. J., Kohrer, S., et al. (2020). Integrative imaging reveals SARS-CoV-2-induced reshaping of subcellular morphologies. *Cell Host Microbe* 28, 853–866. doi:10.1016/j.chom.2020.11.003

Dash, B. K., Urano, Y., and Noguchi, N. (2024). Lysosomal damage promotes autophagy-based unconventional secretion of the Parkinson's disease protein PARK7. *Redox Exp. Med. 2024* 2024. doi:10.1530/rem-24-0014

Debnath, J., and Leidal, A. M. (2022). Secretory autophagy during lysosome inhibition (SALI). *Autophagy* 18, 2498–2499. doi:10.1080/15548627.2022.2095788

Deretic, V., and Wang, F. (2023). Autophagy is part of the answer to tuberculosis. *Nat. Microbiol.* 8, 762–763. doi:10.1038/s41564-023-01373-3

De Tito, S., Hervás, J. H., van Vliet, A. R., and Tooze, S. A. (2020). The Golgi as an assembly line to the autophagosome. *Trends Biochem. Sci.* 45, 484–496. doi:10.1016/j.tibs.2020.03.010

Domingues, N., Catarino, S., Cristóvão, B., Rodrigues, L., Carvalho, F. A., Sarmento, M. J., et al. (2024). Connexin43 promotes exocytosis of damaged lysosomes through actin remodelling. *Embo J.* 43, 3627–3649. doi:10.1038/s44318-024-00177-3

Duran, J., Salinas, J. E., Wheaton, R. P., Poolsup, S., Allers, L., Rosas-Lemus, M., et al. (2024). Calcium signaling from damaged lysosomes induces cytoprotective stress granules. *EMBO J.* 43, 6410–6443. doi:10.1038/s44318-024-00292-1

Eapen, V. V., Swarup, S., Hoyer, M. J., Paulo, J. A., and Harper, J. W. (2021). Quantitative proteomics reveals the selectivity of ubiquitin-binding autophagy receptors in the turnover of damaged lysosomes by lysophagy. *Elife* 10, e72328. doi:10.7554/eLife.72328

Ebstrup, M. L., Sonder, S. L., Fogde, D. L., Heitmann, A. S. B., Dietrich, T. N., Dias, C., et al. (2023). Annexin A7 mediates lysosome repair independently of ESCRT-III. *Front. Cell Dev. Biol.* 11, 1211498. doi:10.3389/fcell.2023.1211498

Eriksson, I., Waster, P., and Ollinger, K. (2020). Restoration of lysosomal function after damage is accompanied by recycling of lysosomal membrane proteins. *Cell Death Dis.* 11, 370. doi:10.1038/s41419-020-2527-8

Fasimoye, R., Dong, W., Nirujogi, R. S., Rawat, E. S., Iguchi, M., Nyame, K., et al. (2023). Golgi-IP, a tool for multimodal analysis of Golgi molecular content, *Proc. Natl. Acad. Sci. U. S. A.*, 120, e2219953120, doi:10.1073/pnas.2219953120

Gahlot, P., Kravic, B., Rota, G., van den Boom, J., Levantovsky, S., Schulze, N., et al. (2024). Lysosomal damage sensing and lysophagy initiation by SPG20-ITCH. *Mol. Cell* 84, 1556–1569.e10. doi:10.1016/j.molcel.2024.02.029

Gao, Y., Liu, Y., Hong, L., Yang, Z., Cai, X., Chen, X., et al. (2016). Golgi-associated LC3 lipidation requires V-ATPase in noncanonical autophagy. *Cell Death and Dis.* 7, e2330. doi:10.1038/cddis.2016.236

Garrity, A. G., Wang, W., Collier, C. M., Levey, S. A., Gao, Q., and Xu, H. (2016). The endoplasmic reticulum, not the pH gradient, drives calcium refilling of lysosomes. *Elife* 5, e15887. doi:10.7554/eLife.15887

Ghosh, S., Dellibovi-Ragheb, T. A., Kerviel, A., Pak, E., Qiu, Q., Fisher, M., et al. (2020). β-Coronaviruses use lysosomes for egress instead of the biosynthetic secretory pathway. *Cell* 183, 1520–1535. doi:10.1016/j.cell.2020.10.039

Gomez-Sanchez, R., Rose, J., Guimaraes, R., Mari, M., Papinski, D., Rieter, E., et al. (2018). Atg9 establishes Atg2-dependent contact sites between the endoplasmic reticulum and phagophores. *J. Cell Biol.* 217, 2743–2763. doi:10.1083/jcb.201710116

Gómez-Sintes, R., Ledesma, M. D., and Boya, P. (2016). Lysosomal cell death mechanisms in aging. *Ageing Res. Rev.* 32, 150–168. doi:10.1016/j.arr.2016.02.009

Gosavi, N., Lee, H. J., Lee, J. S., Patel, S., and Lee, S. J. (2002). Golgi fragmentation occurs in the cells with prefibrillar alpha-synuclein aggregates and precedes the formation of fibrillar inclusion. *J. Biol. Chem.* 277, 48984–48992. doi:10.1074/jbc.M208194200

Govind, A. P., Jeyifous, O., Russell, T. A., Yi, Z., Weigel, A. V., Ramaprasad, A., et al. (2021). Activity-dependent Golgi satellite formation in dendrites reshapes the neuronal surface glycoproteome. *Elife* 10, e68910. doi:10.7554/eLife.68910

Groth-Pedersen, L., and Jaattela, M. (2013). Combating apoptosis and multidrug resistant cancers by targeting lysosomes. *Cancer Lett.* 332, 265–274. doi:10.1016/j.canlet.2010.05.021

Guillén-Samander, A., Bian, X., and De Camilli, P. (2019). PDZD8 mediates a Rab7-dependent interaction of the ER with late endosomes and lysosomes. *Proc. Natl. Acad. Sci.* 116, 22619–22623. doi:10.1073/pnas.1913509116

Hämälistö, S., Stahl, J. L., Favaro, E., Yang, Q., Liu, B., Christoffersen, L., et al. (2020). Spatially and temporally defined lysosomal leakage facilitates mitotic chromosome segregation. *Nat. Commun.* 11, 229. doi:10.1038/s41467-019-14009-0

Han, Q. F., Li, W. J., Hu, K. S., Gao, J., Zhai, W. L., Yang, J. H., et al. (2022). Exosome biogenesis: machinery, regulation, and therapeutic implications in cancer. *Mol. Cancer* 21, 207. doi:10.1186/s12943-022-01671-0

Han, Y., Li, S., and Ge, L. (2023). Biogenesis of autophagosomes from the ERGIC membrane system. *J. Genet. Genomics* 50, 3–6. doi:10.1016/j.jgg.2022.07.001

Hu, Y.-B., Dammer, E. B., Ren, R.-J., and Wang, G. (2015). The endosomal-lysosomal system: from acidification and cargo sorting to neurodegeneration. *Transl. Neurodegener.* 4, 18. doi:10.1186/s40035-015-0041-1

Jia, J., Abudu, Y. P., Claude-Taupin, A., Gu, Y., Kumar, S., Choi, S. W., et al. (2018). Galectins control mTOR in response to endomembrane damage. *Mol. Cell* 70, 120–135. doi:10.1016/j.molcel.2018.03.009

Jia, J., Abudu, Y. P., Claude-Taupin, A., Gu, Y., Kumar, S., Choi, S. W., et al. (2019). Galectins control MTOR and AMPK in response to lysosomal damage to induce autophagy. *Autophagy* 15, 169–171. doi:10.1080/15548627.2018.1505155

Jia, J., Bissa, B., Brecht, L., Allers, L., Choi, S. W., Gu, Y., et al. (2020a). AMPK, a regulator of metabolism and autophagy, is activated by lysosomal damage via a novel galectin-directed ubiquitin signal transduction system. *Mol. Cell* 77, 951–969. doi:10.1016/j.molcel.2019.12.028

Jia, J., Claude-Taupin, A., Gu, Y., Choi, S. W., Peters, R., Bissa, B., et al. (2020b). Galectin-3 coordinates a cellular system for lysosomal repair and removal. *Dev. Cell* 52, 69–87. doi:10.1016/j.devcel.2019.10.025

Jia, J., Wang, F., Bhujabal, Z., Peters, R., Mudd, M., Duque, T., et al. (2022). Stress granules and mTOR are regulated by membrane atg8ylation during lysosomal damage. *J. Cell Biol.* 221, e202207091. doi:10.1083/jcb.202207091

Jin, J., Zhang, H., Weyand, C. M., and Goronzy, J. J. (2021). Lysosomes in T Cell immunity and aging. *Front. Aging* 2, 809539. doi:10.3389/fragi.2021.809539

Jung, J., Shin, Y. H., Konishi, H., Lee, S. J., and Kiyama, H. (2013). Possible ATP release through lysosomal exocytosis from primary sensory neurons. *Biochem. Biophysical Res. Commun.* 430, 488–493. doi:10.1016/j.bbrc.2012.12.009

Kang, H., Choi, S. W., Kim, J. Y., Oh, S.-J., Kim, S. J., and Lee, M.-S. (2024). ER-to-lysosome Ca2+ refilling followed by K+ efflux-coupled store-operated Ca2+ entry in inflammasome activation and metabolic inflammation. *eLife Sci. Publ. Ltd.* 12. doi:10.7554/elife.87561.3

Kim, M., Park, J. H., Go, M., Lee, N., Seo, J., Lee, H., et al. (2024). RUFY4 deletion prevents pathological bone loss by blocking endo-lysosomal trafficking of osteoclasts. *Bone Res.* 12, 29. doi:10.1038/s41413-024-00326-8

Kimura, T., Jia, J., Kumar, S., Choi, S. W., Gu, Y., Mudd, M., et al. (2017). Dedicated SNAREs and specialized TRIM cargo receptors mediate secretory autophagy. *EMBO J.* 36, 42–60. doi:10.15252/embj.201695081

Koo, I. C., Wang, C., Raghavan, S., Morisaki, J. H., Cox, J. S., and Brown, E. J. (2008). ESX-1-dependent cytolysis in lysosome secretion and inflammasome activation during mycobacterial infection. *Cell Microbiol.* 10, 1866–1878. doi:10.1111/j.1462-5822.2008.01177.x

Kumar, R., Khan, M., Francis, V., Aguila, A., Kulasekaran, G., Banks, E., et al. (2024). DENND6A links Arl8b to a Rab34/RILP/dynein complex, regulating lysosomal positioning and autophagy. *Nat. Commun.* 15, 919. doi:10.1038/s41467-024-44957-1

Kurihara, Y., Mitsunari, K., Mukae, N., Shoji, H., Miyakawa, T., and Shirane, M. (2023). PDZD8-deficient mice manifest behavioral abnormalities related to emotion, cognition, and adaptation due to dyslipidemia in the brain. *Mol. Brain* 16, 11. doi:10.1186/s13041-023-01002-4

Lee, J. J., Wang, T., Wiggins, K., Lu, P. N., Underwood, C., Ochenkowska, K., et al. (2024). Dysregulated lysosomal exocytosis drives protease-mediated cartilage pathogenesis in multiple lysosomal disorders. *iScience* 27, 109293. doi:10.1016/j.isci.2024.109293

Liang, W., Sagar, S., Ravindran, R., Najor, R. H., Quiles, J. M., Chi, L., et al. (2023). Mitochondria are secreted in extracellular vesicles when lysosomal function is impaired. *Nat. Commun.* 14, 5031. doi:10.1038/s41467-023-40680-5

Lie, P. P. Y., Yang, D. S., Stavrides, P., Goulbourne, C. N., Zheng, P., Mohan, P. S., et al. (2021). Post-Golgi carriers, not lysosomes, confer lysosomal properties to pre-degradative organelles in normal and dystrophic axons. *Cell Rep.* 35, 109034. doi:10.1016/j.celrep.2021.109034

Liu, E. A., and Lieberman, A. P. (2019). The intersection of lysosomal and endoplasmic reticulum calcium with autophagy defects in lysosomal diseases. *Neurosci. Lett.* 697, 10–16. doi:10.1016/j.neulet.2018.04.049

Lojewski, X., Staropoli, J. F., Biswas-Legrand, S., Simas, A. M., Haliw, L., Selig, M. K., et al. (2014). Human iPSC models of neuronal ceroid lipofuscinosis capture distinct effects of TPP1 and CLN3 mutations on the endocytic pathway. *Hum. Mol. Genet.* 23, 2005–2022. doi:10.1093/hmg/ddt596

Machado, E., White-Gilbertson, S., van de Vlekkert, D., Janke, L., Moshiach, S., Campos, Y., et al. (2015). Regulated lysosomal exocytosis mediates cancer progression. *Sci. Adv.* 1, e1500603. doi:10.1126/sciadv.1500603

Maejima, I., Takahashi, A., Omori, H., Kimura, T., Takabatake, Y., Saitoh, T., et al. (2013). Autophagy sequesters damaged lysosomes to control lysosomal biogenesis and kidney injury. *EMBO J.* 32, 2336–2347. doi:10.1038/emboj.2013.171

Martínez-Menárguez, J., Tomás, M., Martínez-Martínez, N., and Martínez-Alonso, E. (2019). Golgi fragmentation in neurodegenerative diseases: is there a common cause? *Cells* 8, 748. doi:10.3390/cells8070748

Melia, T. J., Lystad, A. H., and Simonsen, A. (2020). Autophagosome biogenesis: from membrane growth to closure. *J. Cell Biol.* 219, e202002085. doi:10.1083/jcb.202002085

Miranda, A. M., Lasiecka, Z. M., Xu, Y., Neufeld, J., Shahriar, S., Simoes, S., et al. (2018). Neuronal lysosomal dysfunction releases exosomes harboring APP C-terminal fragments and unique lipid signatures. *Nat. Commun.* 9, 291. doi:10.1038/s41467-017-02533-w

Nascimbeni, A. C., Giordano, F., Dupont, N., Grasso, D., Vaccaro, M. I., Codogno, P., et al. (2017). ER-plasma membrane contact sites contribute to autophagosome biogenesis by regulation of local PI3P synthesis. *EMBO J.* 36, 2018–2033. doi:10.15252/embj.201797006

Neel, E., Chiritoiu-Butnaru, M., Fargues, W., Denus, M., Colladant, M., Filaquier, A., et al. (2024). The endolysosomal system in conventional and unconventional protein secretion. *J. Cell Biol.* 223, e202404152. doi:10.1083/jcb.202404152

Nugues, C., Rajamanoharan, D., Burgoyne, R. D., Haynes, L. P., and Helassa, N. (2022). Lysosome exocytosis is required for mitosis in mammalian cells. *Biochem. Biophys. Res. Commun.* 626, 211–219. doi:10.1016/j.bbrc.2022.08.024

Pan, C., Banerjee, K., Lehmann, G. L., Almeida, D., Hajjar, K. A., Benedicto, I., et al. (2021). Lipofuscin causes atypical necroptosis through lysosomal membrane permeabilization, *Proc. Natl. Acad. Sci. U. S. A.*, 118, e2100122118, doi:10.1073/pnas.2100122118

Parenti, G., Medina, D. L., and Ballabio, A. (2021). The rapidly evolving view of lysosomal storage diseases. *EMBO Mol. Med.* 13, e12836. doi:10.15252/emmm.202012836

Ponpuak, M., Mandell, M. A., Kimura, T., Chauhan, S., Cleyrat, C., and Deretic, V. (2015). Secretory autophagy. *Curr. Opin. Cell Biol.* 35, 106–116. doi:10.1016/j.ceb.2015.04.016

Pu, J., Guardia, C. M., Keren-Kaplan, T., and Bonifacino, J. S. (2016). Mechanisms and functions of lysosome positioning. *J. Cell Sci.* 129, 4329–4339. doi:10.1242/jcs.196287

Radulovic, M., Schink, K. O., Wenzel, E. M., Nahse, V., Bongiovanni, A., Lafont, F., et al. (2018). ESCRT-mediated lysosome repair precedes lysophagy and promotes cell survival. *EMBO J.* 37, e99753. doi:10.15252/embj.201899753

Radulovic, M., Wenzel, E. M., Gilani, S., Holland, L. K., Lystad, A. H., Phuyal, S., et al. (2022). Cholesterol transfer via endoplasmic reticulum contacts mediates lysosome damage repair. *EMBO J.* 41, e112677. doi:10.15252/embj.2022112677

Ramon-Luing, L. A., Palacios, Y., Ruiz, A., Téllez-Navarrete, N. A., and Chavez-Galan, L. (2023). Virulence factors of *Mycobacterium tuberculosis* as modulators of cell death mechanisms. *Pathogens* 12, 839. doi:10.3390/pathogens12060839

Reddy, A., Caler, E. V., and Andrews, N. W. (2001). Plasma membrane repair is mediated by Ca(2+)-regulated exocytosis of lysosomes. *Cell* 106, 157–169. doi:10.1016/s0092-8674(01)00421-4

Ren, W.-W., Kawahara, R., Suzuki, K. G. N., Dipta, P., Yang, G., Thaysen-Andersen, M., et al. (2025). MYO18B promotes lysosomal exocytosis by facilitating focal adhesion maturation. *J. Cell Biol.* 224, e202407068. doi:10.1083/jcb.202407068

Richards, C. M., Jabs, S., Qiao, W., Varanese, L. D., Schweizer, M., Mosen, P. R., et al. (2022). The human disease gene LYSET is essential for lysosomal enzyme transport and viral infection. *Science* 378, eabn5648. doi:10.1126/science.abn5648

Rodgers, S. J., Jones, E. I., Arumugam, S., Hamila, S. A., Danne, J., Gurung, R., et al. (2022). Endosome maturation links PI3Kα signaling to lysosome repopulation during basal autophagy. *EMBO J.* 41, e110398. doi:10.15252/embj.2021110398

Root, J., Merino, P., Nuckols, A., Johnson, M., and Kukar, T. (2021). Lysosome dysfunction as a cause of neurodegenerative diseases: lessons from frontotemporal dementia and amyotrophic lateral sclerosis. *Neurobiol. Dis.* 154, 105360. doi:10.1016/j.nbd.2021.105360

Sáez, J. J., Diaz, J., Ibañez, J., Bozo, J. P., Cabrera Reyes, F., Alamo, M., et al. (2019). The exocyst controls lysosome secretion and antigen extraction at the immune synapse of B cells. *J. Cell Biol.* 218, 2247–2264. doi:10.1083/jcb.201811131

Saffi, G. T., and Botelho, R. J. (2019). Lysosome fission: planning for an exit. *Trends Cell Biol.* 29, 635–646. doi:10.1016/j.tcb.2019.05.003

Sanfridson, A., Hester, S., and Doyle, C. (1997). Nef proteins encoded by human and simian immunodeficiency viruses induce the accumulation of endosomes and lysosomes in human T cells. *Proc. Natl. Acad. Sci.* 94, 873–878. doi:10.1073/pnas.94.3.873

Sawa-Makarska, J., Baumann, V., Coudevylle, N., von Bülow, S., Nogellova, V., Abert, C., et al. (2020). Reconstitution of autophagosome nucleation defines Atg9 vesicles as seeds for membrane formation. *Science* 369, eaaz7714. doi:10.1126/science.aaz7714

Scerra, G., De Pasquale, V., Scarcella, M., Caporaso, M. G., Pavone, L. M., and D'Agostino, M. (2022). Lysosomal positioning diseases: beyond substrate storage. *Open Biol.* 12, 220155. doi:10.1098/rsob.220155

Scheuring, D., Viotti, C., Krüger, F., Künzl, F., Sturm, S., Bubeck, J., et al. (2011). Multivesicular bodies mature from the trans-Golgi network/early endosome in Arabidopsis. *Plant Cell* 23, 3463–3481. doi:10.1105/tpc.111.086918

Scotto Rosato, A., Krogsaeter, E. K., Jaslan, D., Abrahamian, C., Montefusco, S., Soldati, C., et al. (2022). TPC2 rescues lysosomal storage in mucolipidosis type IV, Niemann-Pick type C1, and Batten disease. *EMBO Mol. Med.* 14, e15377. doi:10.15252/emmm.202115377

Seto, S., Tsujimura, K., and Koide, Y. (2011). Rab GTPases regulating phagosome maturation are differentially recruited to mycobacterial phagosomes. *Traffic* 12, 407–420. doi:10.1111/j.1600-0854.2011.01165.x

Shammas, H., Kuech, E.-M., Rizk, S., Das, A. M., and Naim, H. Y. (2019). Different niemann-pick C1 genotypes generate protein phenotypes that vary in their intracellular processing, trafficking and localization. *Sci. Rep-Uk* 9, 5292. doi:10.1038/s41598-019-41707-y

Shaughnessy, L. M., Hoppe, A. D., Christensen, K. A., and Swanson, J. A. (2006). Membrane perforations inhibit lysosome fusion by altering pH and calcium in Listeria monocytogenes vacuoles. *Cell Microbiol.* 8, 781–792. doi:10.1111/j.1462-5822.2005.00665.x

Shelke, G. V., Williamson, C. D., Jarnik, M., and Bonifacino, J. S. (2023). Inhibition of endolysosome fusion increases exosome secretion. *J. Cell Biol.* 222, e202209084. doi:10.1083/jcb.202209084

Shin, Y. H., Lee, S. J., and Jung, J. (2012). Secretion of ATP from Schwann cells through lysosomal exocytosis during Wallerian degeneration. *Biochem. Biophysical Res. Commun.* 429, 163–167. doi:10.1016/j.bbrc.2012.10.121

Sho, T., Li, Y., Jiao, H., and Yu, L. (2024). Migratory autolysosome disposal mitigates lysosome damage. *J. Cell Biol.* 223, e202403195. doi:10.1083/jcb.202403195

Shtuhin-Rahav, R., Olender, A., Zlotkin-Rivkin, E., Bouman, E. A., Danieli, T., Nir-Keren, Y., et al. (2023). Enteropathogenic *E. coli* infection co-elicits lysosomal exocytosis and lytic host cell death. *mBio* 14, e0197923. doi:10.1128/mbio.01979-23

Sivaramakrishnan, V., Bidula, S., Campwala, H., Katikaneni, D., and Fountain, S. J. (2012). Constitutive lysosome exocytosis releases ATP and engages P2Y receptors in human monocytes. *J. Cell Sci.* 125, 4567–4575. doi:10.1242/jcs.107318

Skowyra, M. L., Schlesinger, P. H., Naismith, T. V., and Hanson, P. I. (2018). Triggered recruitment of ESCRT machinery promotes endolysosomal repair. *Science* 360, eaar5078. doi:10.1126/science.aar5078

Solvik, T. A., Nguyen, T. A., Tony Lin, Y. H., Marsh, T., Huang, E. J., Wiita, A. P., et al. (2022). Secretory autophagy maintains proteostasis upon lysosome inhibition. *J. Cell Biol.* 221, e202110151. doi:10.1083/jcb.202110151

Sou, Y. S., Yamaguchi, J., Masuda, K., Uchiyama, Y., Maeda, Y., and Koike, M. (2024). Golgi pH homeostasis stabilizes the lysosomal membrane through N-glycosylation of membrane proteins. *Life Sci. Alliance* 7, e202402677. doi:10.26508/lsa.202402677

Stinchcombe, J., Bossi, G., and Griffiths, G. M. (2004). Linking albinism and immunity: the secrets of secretory lysosomes. *Science* 305, 55–59. doi:10.1126/science.1095291

Sun, S., Zhao, G., Jia, M., Jiang, Q., Li, S., Wang, H., et al. (2024). Stay in touch with the endoplasmic reticulum. *Sci. China Life Sci.* 67, 230–257. doi:10.1007/s11427-023-2443-9

Tan, J. X., and Finkel, T. (2022). A phosphoinositide signalling pathway mediates rapid lysosomal repair. *Nature* 609, 815–821. doi:10.1038/s41586-022-05164-4

Tan, J. X., and Finkel, T. (2023). Lysosomes in senescence and aging. *EMBO Rep.* 24, e57265. doi:10.15252/embr.202357265

Thakur, R. S., and O'Connor-Giles, K. M. (2023). PDZD8 promotes autophagy at ER-Lysosome contact sites to regulate synaptogenesis. bioRxiv 2023. doi:10.1101/2023.10.30.564828

Thayer, D. A., Jan, Y. N., and Jan, L. Y. (2013). Increased neuronal activity fragments the Golgi complex. *Proc. Natl. Acad. Sci. U. S. A.* 110, 1482–1487. doi:10.1073/pnas.1220978110

Tsunemi, T., Perez-Rosello, T., Ishiguro, Y., Yoroisaka, A., Jeon, S., Hamada, K., et al. (2019). Increased lysosomal exocytosis induced by lysosomal Ca(2+) channel agonists protects human dopaminergic neurons from α-synuclein toxicity. *J. Neurosci.* 39, 5760–5772. doi:10.1523/JNEUROSCI.3085-18.2019

Udayar, V., Chen, Y., Sidransky, E., and Jagasia, R. (2022). Lysosomal dysfunction in neurodegeneration: emerging concepts and methods. *Trends Neurosci.* 45, 184–199. doi:10.1016/j.tins.2021.12.004

van Vliet, A. R., Chiduza, G. N., Maslen, S. L., Pye, V. E., Joshi, D., De Tito, S., et al. (2022). ATG9A and ATG2A form a heteromeric complex essential for autophagosome formation. *Mol. Cell* 82, 4324–4339.e8. doi:10.1016/j.molcel.2022.10.017

Vitry, S., Bruyere, J., Hocquemiller, M., Bigou, S., Ausseil, J., Colle, M. A., et al. (2010). Storage vesicles in neurons are related to Golgi complex alterations in mucopolysaccharidosis IIIB. *Am. J. Pathol.* 177, 2984–2999. doi:10.2353/ajpath.2010.100447

Walia, K., Sharma, A., Paul, S., Chouhan, P., Kumar, G., Ringe, R., et al. (2024). SARS-CoV-2 virulence factor ORF3a blocks lysosome function by modulating TBC1D5-dependent Rab7 GTPase cycle. *Nat. Commun.* 15, 2053. doi:10.1038/s41467-024-46417-2

Wang, F., Gómez-Sintes, R., and Boya, P. (2018). Lysosomal membrane permeabilization and cell death. *Traffic* 19, 918–931. doi:10.1111/tra.12613

Wang, F., Peters, R., Jia, J., Mudd, M., Salemi, M., Allers, L., et al. (2023). ATG5 provides host protection acting as a switch in the atg8ylation cascade between autophagy and secretion. *Dev. Cell* 58, 866–884.e8. doi:10.1016/j.devcel.2023.03.014

Wang, T., and Hong, W. (2002). Interorganellar regulation of lysosome positioning by the Golgi apparatus through Rab34 interaction with Rab-interacting lysosomal protein. *Mol. Biol. Cell* 13, 4317–4332. doi:10.1091/mbc.e02-05-0280

Wang, X., Xu, P., Bentley-DeSousa, A., Hancock-Cerutti, W., Cai, S., Johnson, B. T., et al. (2024). Lysosome damage triggers acute formation of ER to lysosomes membrane tethers mediated by the bridge-like lipid transport protein VPS13C. bioRxiv. doi:10.1101/2024.06.08.598070

Wünkhaus, D., Tang, R., Nyame, K., Laqtom, N. N., Schweizer, M., Scotto Rosato, A., et al. (2024). TRPML1 activation ameliorates lysosomal phenotypes in CLN3 deficient retinal pigment epithelial cells. *Sci. Rep-Uk* 14, 17469. doi:10.1038/s41598-024-67479-8

Wyant, G. A., Abu-Remaileh, M., Frenkel, E. M., Laqtom, N. N., Dharamdasani, V., Lewis, C. A., et al. (2018). NUFIP1 is a ribosome receptor for starvation-induced ribophagy. *Science* 360, 751–758. doi:10.1126/science.aar2663

Xie, Y. X., Naseri, N. N., Fels, J., Kharel, P., Na, Y., Lane, D., et al. (2022). Lysosomal exocytosis releases pathogenic α-synuclein species from neurons in synucleinopathy models. *Nat. Commun.* 13, 4918. doi:10.1038/s41467-022-32625-1

Xu, Y., Du, S., Marsh, J. A., Horie, K., Sato, C., Ballabio, A., et al. (2021). TFEB regulates lysosomal exocytosis of tau and its loss of function exacerbates tau pathology and spreading. *Mol. Psychiatry* 26, 5925–5939. doi:10.1038/s41380-020-0738-0

Yim, W. W., Yamamoto, H., and Mizushima, N. (2022). Annexins A1 and A2 are recruited to larger lysosomal injuries independently of ESCRTs to promote repair. *FEBS Lett.* 596, 991–1003. doi:10.1002/1873-3468.14329

Zhang, J., Kennedy, A., de Melo Jorge, D. M., Xing, L., Reid, W., Bui, S., et al. (2024). SARS-CoV-2 remodels the Golgi apparatus to facilitate viral assembly and secretion. bioRxiv, doi:10.1101/2022.03.04.483074

Zhang, K. R., Jankowski, C. S. R., Marshall, R., Nair, R., Más Gómez, N., Alnemri, A., et al. (2023). Oxidative stress induces lysosomal membrane permeabilization and ceramide accumulation in retinal pigment epithelial cells. *Dis. Models and Mech.* 16, dmm050066. doi:10.1242/dmm.050066

Zhang, Z., Chen, G., Zhou, W., Song, A., Xu, T., Luo, Q., et al. (2007). Regulated ATP release from astrocytes through lysosome exocytosis. *Nat. Cell Biol.* 9, 945–953. doi:10.1038/ncb1620

Zhitomirsky, B., and Assaraf, Y. G. (2017). Lysosomal accumulation of anticancer drugs triggers lysosomal exocytosis. *Oncotarget* 8, 45117–45132. doi:10.18632/oncotarget.15155

Zhong, D., Wang, R., Zhang, H., Wang, M., Zhang, X., and Chen, H. (2023). Induction of lysosomal exocytosis and biogenesis via TRPML1 activation for the treatment of uranium-induced nephrotoxicity. *Nat. Commun.* 14, 3997. doi:10.1038/s41467-023-39716-7

frontiers | Frontiers in Cell and Developmental Biology

TYPE Review
PUBLISHED 27 March 2025
DOI 10.3389/fcell.2025.1559125

Check for updates

OPEN ACCESS

EDITED BY
Bhawana Bissa,
Central University of Rajasthan, India

REVIEWED BY
Ruheena Javed,
University of New Mexico, United States
Fulong Wang,
Southeast University, China

*CORRESPONDENCE
Alf Håkon Lystad,
alfly@medisin.uio.no

RECEIVED 11 January 2025
ACCEPTED 12 March 2025
PUBLISHED 27 March 2025

CITATION
Kaur N, Carlsson SR and Lystad AH (2025) Lysosome-associated CASM: from upstream triggers to downstream effector mechanisms. *Front. Cell Dev. Biol.* 13:1559125. doi: 10.3389/fcell.2025.1559125

COPYRIGHT
© 2025 Kaur, Carlsson and Lystad. This is an open-access article distributed under the terms of the Creative Commons Attribution License (CC BY). The use, distribution or reproduction in other forums is permitted, provided the original author(s) and the copyright owner(s) are credited and that the original publication in this journal is cited, in accordance with accepted academic practice. No use, distribution or reproduction is permitted which does not comply with these terms.

Lysosome-associated CASM: from upstream triggers to downstream effector mechanisms

Namrita Kaur[1,2], Sven R. Carlsson[3] and Alf Håkon Lystad[1,2]*

[1]Centre for Cancer Cell Reprogramming, Faculty of Medicine, University of Oslo, Oslo, Norway, [2]Department of Molecular Cell Biology, Institute for Cancer Research, Oslo University Hospital, Oslo, Norway, [3]Department of Medical Biochemistry and Biophysics, University of Umeå, Umeå, Sweden

Lysosomes are dynamic organelles critical for cellular degradation and signaling, safeguarded by a limiting membrane that prevents leakage of harmful contents into the cytoplasm. Upon lysosomal damage, cells deploy defensive mechanisms, including a key process called CASM (conjugation of ATG8 to single membranes), which lipidates ATG8 proteins onto the limiting membrane to support protective pathways. CASM operates through two pathways: VAIL, induced by lysosomal pH changes via V-ATPase and ATG16L1, and STIL, triggered by sphingomyelin exposure and mediated by TECPR1. This review examines CASM's role in lysosomal damage responses, exploring the mechanisms of damaging agents, distinctions between VAIL and STIL, and the downstream effects of decorating lysosomes with ATG8, including effector recruitment for membrane repair or removal.

KEYWORDS

CASM, VAIL, STIL, autophagy, lysosome damage, atg8ylation, Atg8

1 Introduction

The degradative system that resides inside lysosomes is highly effective, comprising a large array of highly active enzymes in an acidic environment (pH 4-5) that is capable of degrading most of the incoming material (De Duve and Wattiaux, 1966; Ballabio and Bonifacino, 2020; Settembre and Perera, 2024). This destructive capacity underscores the need for a robust and tightly regulated cellular response to lysosomal damage, ensuring that harmful contents do not leak into the cytoplasm and compromise cell viability. Recent studies have uncovered a range of protective mechanisms that either restore or eliminate damaged lysosomes, including membrane repair pathways and targeted degradation processes (Papadopoulos et al., 2020; Zhen et al., 2021; Zoncu and Perera, 2022; Duran et al., 2024). These mechanisms rely on sophisticated protein machinery, including the ATG8 conjugation system, first characterized in autophagy, a conserved pathway for cellular recycling and homeostasis (Mizushima et al., 2011; Yim and Mizushima, 2020; Durgan and Florey, 2022; Figueras-Novoa et al., 2024). In response to lysosomal damage, ATG8 proteins and their conjugation machinery function in two distinct pathways: autophagy and CASM. While we will briefly discuss both processes, this review primarily focuses on CASM and its established roles at compromised lysosomes.

1.1 Autophagy and selective autophagy

The principal mechanisms of canonical autophagy (often referred to as macroautophagy) are now well-established, including an initiation phase near the ER membrane, the growth of a double-membraned phagophore/isolation membrane, followed by capture of cargo to be degraded as bulk, or through specific adaptors/receptors in a process called selective autophagy (Yamamoto et al., 2023). Closed phagophores, called autophagosomes, with its captured cargo (which can be whole organelles tagged for destruction) then fuse with functional lysosomes forming autolysosomes in which the degradation takes place through the action of lysosomal enzymes.

The selective autophagic process responsible for removing non-functional damaged lysosomes is called macrolysophagy (Maejima et al., 2013; Gatica et al., 2018; Vargas et al., 2023). The recognition of such lysosomes is thought to be mediated through the exposure of internal structures (caused by disruption of its limiting membrane), which are recognized by lectin-type proteins present in the cytosol belonging to the galectin family (Johannes et al., 2018; Jacob and Gorek, 2024). The galectin reaction leads to ubiquitination of the lysosome that is recognized by autophagy receptors, which function to cross-link the damaged lysosome with the phagophore membrane, facilitating sequestration and delivery to a healthy lysosome (Lamark and Johansen, 2021).

1.2 Atg8ylation

Generally, the role of receptors in selective autophagy depends on the lipid-conjugation of mammalian Atg8 homologs—here referred to as ATG8 — which decorate the surface of the phagophore. These receptors typically bind to ATG8 through specific sequences known as LIR (LC3-interacting region) motifs (Johansen and Lamark, 2020). ATG8 proteins have been exploited during evolution and come in slightly different versions and in varying numbers in different species (Mizushima, 2020). In humans, six alternative homologs are expressed: LC3A, LC3B, LC3C, GABARAP, GABARAPL1, and GABARAPL2. Additionally, a seventh variant designated LC3B2 is described (Shpilka et al., 2011), distinct from LC3B by just one amino acid. Although they have been extensively studied for many years, their differential functions are still not entirely clear (Rogov et al., 2023). However, phylogenetic analyses have shown that members of the GABARAP subfamily are more ancient in evolution and appear to have more prominent roles in specific reactions such as receptor binding and generation of functional phagophores (Johansen and Lamark, 2020; Mizushima, 2020).

The lipid conjugation reaction of ATG8 proteins is a dynamic multi-factorial process (Mizushima et al., 2011; Ohsumi, 2014; Lystad et al., 2019) (Figure 1). The last reaction step is the transfer of activated ATG8 from ATG3 to aminophospholipids (phosphatidylethanolamine, PE, or phosphatidylserine, PS) in the receiving membrane (Durgan et al., 2021). This reaction is enhanced by the E3-like ligase ATG16L1, which, together with other factors, determines the specific target membrane within the cell (Fujita et al., 2008). Collectively, this process of covalently attaching ATG8 to membrane lipids, specifically PE or PS, is referred to as "membrane atg8ylation" or "ATG8 lipidation" (Deretic and Lazarou, 2022). While atg8ylation is reported to also occur on proteins (Agrotis et al., 2019; Nguyen et al., 2021), this review focuses exclusively on its lipidation. Therefore, we hereafter use "atg8ylation" specifically to denote the lipidation of ATG8 proteins.

1.3 CASM

Classically, the atg8ylation reaction proceeds on the autophagic membrane, forming the foundation for the functional phagophore. In recent years, atg8ylation has been found to also occur on non-autophagic membranes (Durgan and Florey, 2022), where ATG8 proteins have roles separate from those at the phagophores. Such processes were formerly called "non-canonical autophagy" to distinguish them from canonical autophagy but was renamed as CASM (conjugation of ATG8 to single membranes) which better denote the cellular structures where they appear and further discriminate them from autophagy (Durgan et al., 2021). The designation CASM is now used as an umbrella term for atg8ylations that appear on single-membrane structures at various locations in the cell (Durgan and Florey, 2022; Deretic, 2024; Figueras-Novoa et al., 2024; Kaur et al., 2024).

The lysosome appears to be particularly susceptible to CASM, especially in response to damage, but can also occur on other structures such as Golgi (Gao et al., 2016), ER (Sun et al., 2023), endosomes (Heckmann et al., 2019), phagosomes (Sanjuan et al., 2007), and lipid droplets (Omrane et al., 2023) (note: in the latter case atg8ylation occurs on a single-layer of phospholipids, not a bilayer). The reactions leading to the lipidation of ATG8 differ from those in canonical autophagy, such that factors important in the initiation phase of canonical autophagy (ULK kinase complex, class III PI3kinase complex, and WIPI2) are not needed in CASM (Fletcher et al., 2018; Lystad et al., 2019). Furthermore, although several factors are the same in the later steps of the conjugation reaction (ATG3, ATG5, ATG7, ATG10, and ATG12), there are important differences in the E3-like reaction that are related to its site of action. While canonical autophagy can proceed with only the amino-terminal part of ATG16L1 (which in size and function corresponds to the yeast ortholog Atg16), CASM is strictly dependent on a carboxyl-terminal WD40 domain for binding to the endolysosomal surface (Fletcher et al., 2018; Lystad et al., 2019; Rai et al., 2019). Under specific conditions, the WD40 domain of ATG16L1 engages the proton transporter V-ATPase (vacuolar ATPase), initiating a pathway known as VAIL (V-ATPase-ATG16L1-Induced LC3-lipidation) (Fischer et al., 2020) (Figure 1).

Complementing this, we and others have recently identified a second type of E3-like ligase, TECPR1 (tectonin β-propeller repeat-containing protein 1), which activates during endolysosomal damage in response to sphingomyelin (SM) exposure on the lysosomal surface (Boyle et al., 2023; Corkery et al., 2023; Kaur et al., 2023; Wang Y. et al., 2023), forming an alternative axis termed

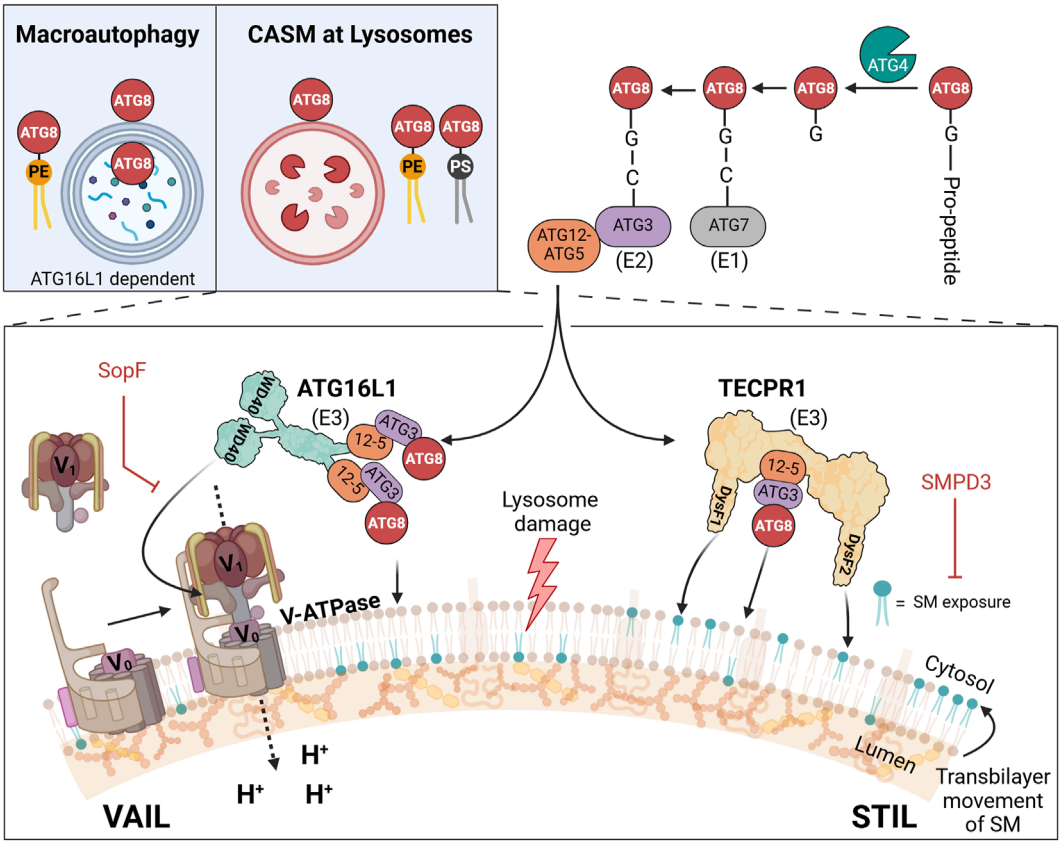

FIGURE 1
CASM at lysosomes: distinct VAIL and STIL axes in ATG8 lipidation upon membrane damage. Upper left inset: comparison of double-membrane atg8ylation in macroautophagy and single-membrane atg8ylation in CASM at lysosomes. In macroautophagy (left), ATG8 proteins are lipidated by phosphatidylethanolamine (PE, yellow) on double-membraned phagophores, which mature into autophagosomes. In CASM at lysosomes (right), ATG8 proteins are lipidated by PE or phosphatidylserine (PS, black) directly on the single membrane of lysosomes in response to damage. Illustration of the two known CASM axes that respond to lysosomal damage: the VAIL axis (left) and the STIL axis (right). In the VAIL axis, dissipation of the proton gradient triggers assembly of the V-ATPase complex, which consists of the cytosolic V_1 subunits and the membrane-integral V_0 subunits. This assembly creates a conformational state recognized by ATG16L1 via its WD40 domain, facilitating ATG8 lipidation on de-acidified lysosomes. In the STIL axis, sphingomyelin (SM) exposure on the cytosolic leaflet of the lysosomal membrane recruits TECPR1 through its DysF domains, also leading to ATG8 lipidation. The ATG12-ATG5 ("**12-5**") conjugate interact with ATG16L1 (VAIL) or TECPR1 (STIL) to form E3-like complexes. ATG8 proteins are processed by ATG4, activated by ATG7 (E1-like enzyme), transferred to ATG3 (E2-like enzyme), and conjugated to PE or PS on the membrane via either E3 complex.

STIL (Sphingomyelin-TECPR1-Induced LC3-lipidation) (Figueras-Novoa et al., 2024). Although the search for additional E3-like ligases in CASM remains an active research area (Deretic, 2024), only the two E3 complexes—those containing ATG16L1 and TECPR1—currently have documented activity in ATG8 lipidation. Accordingly, we limit our discussion here to the well-characterized VAIL and STIL axes of CASM, mediated by ATG16L1 and TECPR1, respectively.

2 The lysosome and its limiting membrane

The lysosome is not a discrete static organelle, but continuously goes through dynamic changes by means of fusion and fission reactions (Bright et al., 2016; Ballabio and Bonifacino, 2020; Settembre and Perera, 2024). The result is that the collection of lysosomes in a cell can vary in size, location, pH, and enzyme content (Bohnert and Johnson, 2022). During the late stages of endocytosis multi-vesicular bodies (MVBs) are formed (also referred to as late endosomes), containing newly synthesized hydrolytic enzymes and material to be degraded (Gruenberg, 2020). MVBs can fuse with old lysosomes with the purpose of reusing enzymes and other material. The fused structure is usually referred to as an "endolysosome," and it is believed that this organelle is the principle degradative compartment having an optimal low pH and the full set of enzymes (Bright et al., 2016; Johnson et al., 2016; Sava et al., 2024). The endolysosome contains in addition to enzymes and cofactors intraluminal vesicles (ILVs) and lamellar membrane sheets, originating from MVB formation, that have important roles in lipid degradation (Breiden and Sandhoff, 2019b) (see below). During degradation and export of products out to the cytosol, the endolysosome change in appearance and matures into a "terminal lysosome," accompanied by content condensation

and an increase in luminal pH to almost neutral at the final stage (Bright et al., 2016). The latter phenomenon was described to be dependent on the assembly regulation of active V-ATPase (Sava et al., 2024). The terminal lysosome can be reused through fusion with a new incoming late endosome. In addition, at certain stages in the maturation process, membrane tubules are formed from the endolysosomal surface that undergo scission, a process that is believed to give rise to nascent lysosomes but can also have other functions and be cell-type specific (Li et al., 2016; Yang and Wang, 2021; Bohnert and Johnson, 2022). Disturbances in this recycling process is thought to be linked to neurological and other degenerative diseases. Due to its complexity, in many experimental setups it is uncertain which stage in lysosome biogenesis that is affected, for example, during drug treatment. Therefore, in this text the use of "lysosome" or "endolysosome" refers to any structure from late endosomes to terminal lysosomes.

2.1 Lysosome limiting membrane components

The lysosomal limiting membrane has a unique, but variable, structure in order to accomplish its special roles (Kolter and Sandhoff, 2005; Saftig and Klumperman, 2009). The inner surface is covered with a thick glycocalyx, a carbohydrate-rich layer mainly composed of two highly glycosylated integral membrane glycoproteins LAMP-1 and LAMP-2 (Fukuda, 1991; Eskelinen et al., 2003). Special glycan structures (polylactosaminoglycans) present on LAMP-1 and LAMP-2 make them vastly resistant to degradation by glycosidases and proteases in the lumen (Carlsson et al., 1988; Kundra and Kornfeld, 1999), and the glycocalyx therefore yields an effective protection for the lipid bilayer and for other proteins on or in the membrane. Most likely, it is β-galactosides within this glycocalyx that is recognized by cytosolic galectins to signal for rupture of the membrane and to trigger removal of the lysosome by macrolysophagy (Maejima et al., 2013). Other membrane glycoproteins constituting the glycocalyx in lower amounts are LIMP-1 and LIMP-2 (lysosomal integral membrane proteins) (Fukuda, 1991; Eskelinen et al., 2003).

2.1.1 Lipids

The limiting membrane of lysosomes is highly asymmetric and is, with some important exceptions, essentially a mirror of the asymmetry of the plasma membrane and endosomes (van Meer, 2011). SM is normally found only on the luminal side while PS, PE, and phosphatidylinositol (PI) are mainly on the cytosolic side. Phosphatidylcholine (PC) is distributed in both leaflets whereas free cholesterol is normally low in the lysosomal membrane but may have important roles in the regulation of lysosomal activities (Maxfield and van Meer, 2010; Meng et al., 2020). Apart from these common membrane lipids, the lysosomal membrane contains in addition an atypical lipid, bis[monoacylglycero]phosphate (BMP), also termed lysobisphosphatidic acid (LBPA) (Kolter and Sandhoff, 2005; Gruenberg, 2020). This lipid, which is not detected elsewhere in the cell, is asymmetrically located on the luminal side of the limiting membrane, and also present on lysosomal internal membranes such as ILVs. BMP is believed to play an important role in protection and activation of the performing lipases and other hydrolytic enzymes in the lysosome (Gallala and Sandhoff, 2011). As described later, the disturbance of asymmetry and/or interference of BMP-dependent binding mediated by foreign substances in the lumen has crucial consequences for the response by proteins in the cytosol.

At certain stages during the lifetime of a lysosome, lipid headgroups on the cytosol-facing monolayer are covalently modified to signal for actions required. As mentioned above, atg8ylation is a model of such an alteration, and phosphorylation of PI are other important examples of modifications of the lysosome that are currently being revealed (Posor et al., 2022). Multiple specific lipid kinases can produce a series of PI variants (called phosphoinositides), of which PI(3)P, PI(4)P, PI(3,4)P_2, PI(3,5)P_2, and PI(4,5)P_2 are found to have differential roles in the complex regulation of lysosome function. For instance, PI(4)P is generated through activation and recruitment of PI4K2A to the lysosomal membrane during damage (Radulovic et al., 2022; Tan and Finkel, 2022). PI(3,5)P_2, synthesized by PIKfyve (Hasegawa et al., 2017), mediates processes such as tubulation during lysosomal reformation and formation of ILVs that degrade lysosomal membrane proteins following damage (Rodgers et al., 2022; Klein et al., 2024).

2.1.2 Proteins

The limiting membrane has in addition to the major glycoproteins described above a large number of membrane proteins in lower amounts, such as transporters of nutrients and ions, signaling complexes, motor protein adaptors, small GTPases, tethering factors, and SNAREs (Ballabio and Bonifacino, 2020). Perhaps the best studied among them is the active membrane-translocator of protons, termed vacuolar ATPase (V-ATPase) (Collins and Forgac, 2020; Freeman et al., 2023). Its action is fundamental for generating the optimal acidic environment for degradation in the lumen, and in addition the protein complex is crucial for signaling to the cytosol that the desired acidity is not reached or lost (Hooper et al., 2022). V-ATPase is a multi-subunit structure that consists of a membrane-integral part (V_0) and a catalytic cytosolic part (V_1). Pump activity is achieved when the full quaternary structure is assembled, and when the desired pH is reached V_1 dissociates from V_0 and pumping is blocked (Sava et al., 2024).

When damage disrupts the proton gradient—such as from proton leakage through the membrane—the V-ATPase subunits reassemble. However, this reassembly occurs in a manner that prevents active proton pumping (Timimi et al., 2024). Instead, a conformational change occurs in the V_1 domain, which is specifically recognized by ATG16L1. This recognition triggers CASM activation as part of the VAIL response (Timimi et al., 2024). This dynamic assembly and disassembly cycle of the V-ATPase is regulated by additional factors, including the RAVE complex (Jaskolka et al., 2021), as well as mTOR and its associated proteins (Liu and Sabatini, 2020). Importantly, CASM appears to rely not merely on the assembly state of the V-ATPase but also on the unique presence of assembled yet inactive complexes. This suggests a dual regulatory mechanism, wherein both the loss of proton gradients and the resulting inactive V-ATPase state serve as critical cues for CASM activation.

Of the so far identified proteins with roles in induction or as effectors of CASM (apart from V-ATPase) only a few are

resident in the lysosomal outer membrane. Mostly based on microscopy analysis, a majority of the participating proteins appear to be recruited to (or detached from) the limiting membrane only during the damage response. The role of several such proteins will be described below under "Downstream effectors of CASM." However, the recruitment of at least some of the cytosolic proteins that participate in damage signaling depend on integral membrane proteins, such as the binding of mTOR to the amino acid transporter SLC38A9 via Ragulator and Rag GTPases (Rebsamen et al., 2015). Another well-studied integral membrane protein is NPC1, which is the principle transporter of cholesterol to the outside of the lysosomal limiting membrane (Meng et al., 2020). Its role in the response to damage remains to be elucidated, but as cholesterol homeostasis is known to be central for lysosomal function, such as in the regulation of mTOR activity (Davis et al., 2021), a contribution of NPC1 is anticipated also in defense reactions when lysosomes are injured (Kendall and Holian, 2023).

Lysosomal resident integral membrane proteins with evident roles in the defense against injury are the various ion channels with different specificities (Riederer et al., 2023), although their involvement in CASM is not fully elucidated. The major Ca^{2+}-channel, TRPML1, responds to damage by translocating Ca^{2+} from the intraluminal store to the cytosol where several factors are activated in a Ca^{2+}-dependent manner. Interestingly, CASM can be induced by agonists to TRPML1, and in this case atg8ylation occurs without an increase in lysosomal pH or severe membrane damage (Goodwin et al., 2021). Drug and bacteria-induced Ca^{2+}-release was also found to trigger a rapid Ca^{2+}-dependent scrambling of the lysosomal membrane lipids and exposure of SM to the cytosol (Niekamp et al., 2022). This effect led to the removal of membrane, which was suggested to occur through invagination based on ceramide production by neutral sphingomyelinase on the cytosolic side of the membrane. It can be anticipated that additional resident lysosomal proteins with functions in the damage response will be discovered in the coming years. For example, the Ca^{2+}-dependent scramblase described above is yet to be defined (Niekamp et al., 2022).

While this text discusses various aspects of CASM in lysosomal damage responses, it is important to note that certain atg8ylation related findings—such as LC3-Dependent Extracellular Vesicle Loading and Secretion (LDELS) (Leidal et al., 2020) and retromer-dependent trafficking (Paddar et al., 2025)—are not covered in detail here. For example, LDELS involves ATG8-family protein–driven cargo secretion via extracellular vesicles (EVs) but does not involve compromised lysosomes, and neither VAIL or STIL has yet been linked to this process. Likewise, the retromer complex reinforces lysosomal integrity through trafficking, relying on ATG5 and atg8ylation, however no role for VAIL or STIL was identified in this study either. Although these processes are important, they do not fall within the scope of CASM as presented here.

Having discussed these essential aspects of lysosomal architecture and composition, we next look at how a variety of agents—both external and endogenous—are known to induce lysosomal damage and thereby provoke a CASM response.

3 Different types of damage that can induce a CASM response

As cells are exposed to many different types of substances, through uptake by endocytosis or by other means, damage to lysosomes can occur in a variety of ways. Lysosomes are designed to take care of natural macromolecules, degrade them into smaller constituents, such as amino acids, monosaccharides, nucleosides, cholesterol, fatty acids, and glycerol, and then transport them over the limiting membrane to be used at other locations in the cell. Although certain substrates in the lumen can possess difficulties for enzymes or in transport, for example, lipid substrates to overcome the phase problem with water (Breiden and Sandhoff, 2019b), intricate systems have evolved that will ensure that no build-up of indigestible material occurs. If that happens it will inevitably lead to disease, as seen in the large group of lysosomal storage diseases (LSDs) (Platt et al., 2018).

3.1 Pore-forming proteins

Much of what has been learnt about responses to lysosomal damage comes from studies with pathogenic infectious microorganisms and viruses (Durgan and Florey, 2022; Wang et al., 2022; Figueras-Novoa et al., 2024). A number of different strategies have been revealed that are used by pathogens to overcome the problems with the harsh conditions in the endolysosomal system. A common theme is the production of proteins that assemble and form ion conducting pores in the membrane, denoted pore-forming toxins (PFTs) (Barisch et al., 2023). The assembly of PFTs in the endolysosomal system leads to neutralization of the lumen and, in the case of larger pores, egress of effector proteins or whole bacteria into the cytosol. The VAIL system immediately responds to proton leakage and act to diminish the damage. In certain cases, such as during *Salmonella* infection (Ellison et al., 2020; Boyle et al., 2023), asymmetry of lysosomal membrane lipids is also disturbed leading to activation of the STIL system, responding to cytosolic exposure of SM through TECPR1, to yield a versatile CASM response. Interestingly, the STIL response appears to be faster than the exposure of luminal glycans, meaning that asymmetry defects precede the breakage of the membrane (Ellison et al., 2020). The cause of asymmetry deterioration during bacterial infection is not yet clear but may be due to effects on endogenous scramblases by bacterial effectors (Ellison et al., 2020; Barisch et al., 2023).

Another well-documented process is that of influenza A virus (IAV) infection, where a viral protein is involved to generate pores in the membranes of the endolysosomal system (Pinto et al., 1992; Chizhmakov et al., 1996; Durgan and Florey, 2022). During infection, proton conducting channels are formed by the M2 viroprotein, which has multiple functions during the viral life cycle. Proton gradient dissipation leads to activation of VAIL and atg8ylation of affected membranes (Fletcher et al., 2018; Ulferts et al., 2021; Hooper et al., 2022).

Recent findings (Fischer et al., 2020; Liu et al., 2023) have revealed an example that also endogenous pore-forming proteins can be activated and engaged as part of a response to infection through VAIL. The protein STING (Stimulator of interferon genes) classically acts at the transcriptional level to induce

expression of interferons and cytokines. In addition, when activated, dimerized STING is transported to endolysosomes and forms proton conducting channels in the membrane which will induce CASM (Liu et al., 2023; Bentley-DeSousa et al., 2025).

3.2 Ionophores and lysosomotropic drugs

Many recent experimental studies on lysosomal damaging phenomena utilize substances that in certain aspects mimick those of pathogens, but they also have a value in its own right as such chemicals often are used as drugs in human and veterinary medicine (Breiden and Sandhoff, 2019a). To distinguish damage caused by chemicals taken up by cells from that triggered by viruses and microorganisms, the former is referred to as "sterile" damage. The term "ionophore" is used to describe a set of amphiphilic molecules that bind different cations and partition into bilayers, enhancing ion movement through membranes (Ekinci et al., 2023). In the endolysosomal system, treatments with ionophores are often accompanied with an increase in luminal pH, resulting from an exchange of cations with protons, leading to activation of VAIL through V-ATPase (Florey et al., 2015). The disturbance of ionic balance results in swelling of the compartments due to osmosis that eventually may lead to rupture of the membrane (Jacquin et al., 2017). Monensin and Nigericin are two commonly used ionophores in CASM research. Interestingly, these drugs do not elicit a STIL response, indicating that the asymmetry of lipids is intact, at least for SM (Kaur et al., 2023), and they can therefore be used in experiments to selectively activate the VAIL axis of CASM.

While ionophore drugs affect ionic balances in multiple cellular compartments, lysosomotropic agents predominantly alter conditions within acidic organelles, such as lysosomes (Durgan and Florey, 2022; Meyer and Kravic, 2024). Many lysosomotropic drugs are weak nitrogen bases that possess amphiphilic properties. Upon diffusing into the lysosome, these molecules become protonated at low pH and are therefore trapped, leading to their enrichment in the lumen. Such agents are often referred to as cationic amphiphilic drugs (CADs), which consume protons and partially buffer the lysosomal environment at a higher-than-normal pH. The increase in pH is recognized by the VAIL-system through V-ATPase (Durgan and Florey, 2022). Certain lysosomotropic agents inhibits the activity of luminal acid sphingomyelinase. This enzyme is normally protected from degradation by charge-dependent binding to internal membranes of lysosomes containing the lipid BMP (which is unique among the membrane phospholipids being negatively charged also at lysosomal acidity) (Gallala and Sandhoff, 2011). Acid sphingomyelinase, together with several other lipases, is thought to be released from internal membranes by lysosomotropic substances through competition, and are quickly degraded by cathepsins in the lumen (Breiden and Sandhoff, 2021). Such drugs are therefore also referred to as FIASMAs (functional inhibitors of acid sphingomyelinase) (Kornhuber et al., 2010). The inhibition leads to build-up of SM and other sphingolipids in the lumen that can affect a variety of processes in lysosomes, such as the maintenance of bilayer asymmetry (Breiden and Sandhoff, 2019a). Several drugs of this class activate the STIL system (Kaur et al., 2023), which may be caused by indirect effects through accumulation of sphingolipid metabolites or by direct surfactant action of the drugs on the lipid bilayer (Meyer and Kravic, 2024).

Lysosomotropic substances can have a variety of structures and their biological effects are therefore different. The most commonly used lysosome damaging lysosomotropic agent in recent reports is LLOMe (L-leucyl-L-leucine methyl ester). LLOMe is quickly taken up by cells and gets enriched in lysosomes where it is cleaved by cathepsin C, and a mixture of polymers ((leucyl-leucin)$_n$-OMe) is generated through dipeptidyl transferase activity of the enzyme (Thiele and Lipsky, 1990; Repnik et al., 2017). The mechanism of action is not entirely clear, but the polyleucine products are thought to act as weak surfactants, affecting the organization of the lysosomal bilayer lipids, leading to transiently increased water and proton permeability (Repnik et al., 2017; Meyer and Kravic, 2024) (Figure 2). A similar drug is the dipeptide GPN (glycyl-L-phenylalanine 2-naphtylamide) (Jadot et al., 1984), but this compound may have effects different from LLOMe in terms of Ca^{2+} permeability and osmosis (Chen et al., 2024). An early effect in cells after administration of LLOMe or GPN is the appearance of SM on the cytosolic side of lysosomes which is detected by SM-reporters, and by TECPR1 inducing STIL (Kaur et al., 2023), indicating that lipid asymmetry is disturbed by these agents (Figure 2).

Weak surfactants are amphiphilic substances that have a propensity to intercalate with membrane lipids and perturb lipid order without solubilizing the membrane (Meyer and Kravic, 2024). Several agents that induce an early STIL response in cells may in fact act as surfactants on the limiting membrane bilayer, as exemplified by LLOMe and certain CADs, which could affect lipid asymmetry (Repnik et al., 2014; Meyer and Kravic, 2024). In line with this, a recent report showed that LLOMe treatment of cultured cells caused rapid lipid-packing defects in the lysosomal limiting membrane that were specifically sensed by an amphipathic helix-containing protein in the cytosol (SPG20) (Gahlot et al., 2024). It may be that the STIL effects that we see with various drugs is due to surfactant action by the drug itself, mediating translocation of SM to the cytosolic side (Meyer and Kravic, 2024). In addition, effects on potential scramblases to disturb asymmetry (several of which are still to be identified) (Niekamp et al., 2022), or the formation of pores in the membrane (Meyer and Kravic, 2024), cannot be ruled out. Indeed, as mentioned above, infection of cells with *Salmonella* induced a similar phenotype of SM exposure on bacteria-containing vacuoles, which may argue for more specific effects on the bilayer (Ellison et al., 2020; Boyle et al., 2023). Ammonium chloride, Chloroquine (CQ), and Hydroxychloroquine (HCQ) are all lysosomotropic compounds that diffuse into lysosomes in their uncharged basic forms and then become protonated, raising the lysosomal pH, thereby inducing VAIL (Jacquin et al., 2017). Because CQ and HCQ can accept two protons, they undergo further protonation and thus accumulate more extensively than the ammonium ion (Chen and Geiger, 2020), which may lead to greater osmotic stress and explain why they—unlike ammonium chloride—can also induce STIL (Wang Y. et al., 2023), possibly through membrane rupture.

Thus, while ionophores selectively trigger VAIL without disrupting SM asymmetry, lysosomotropic agents and FIASMA-type compounds often exhibit broader effects. These include raising lysosomal pH, acting as weak surfactants, or inhibiting key lysosomal enzymes such as acid sphingomyelinase, ultimately

10.3389/fcell.2025.1559125

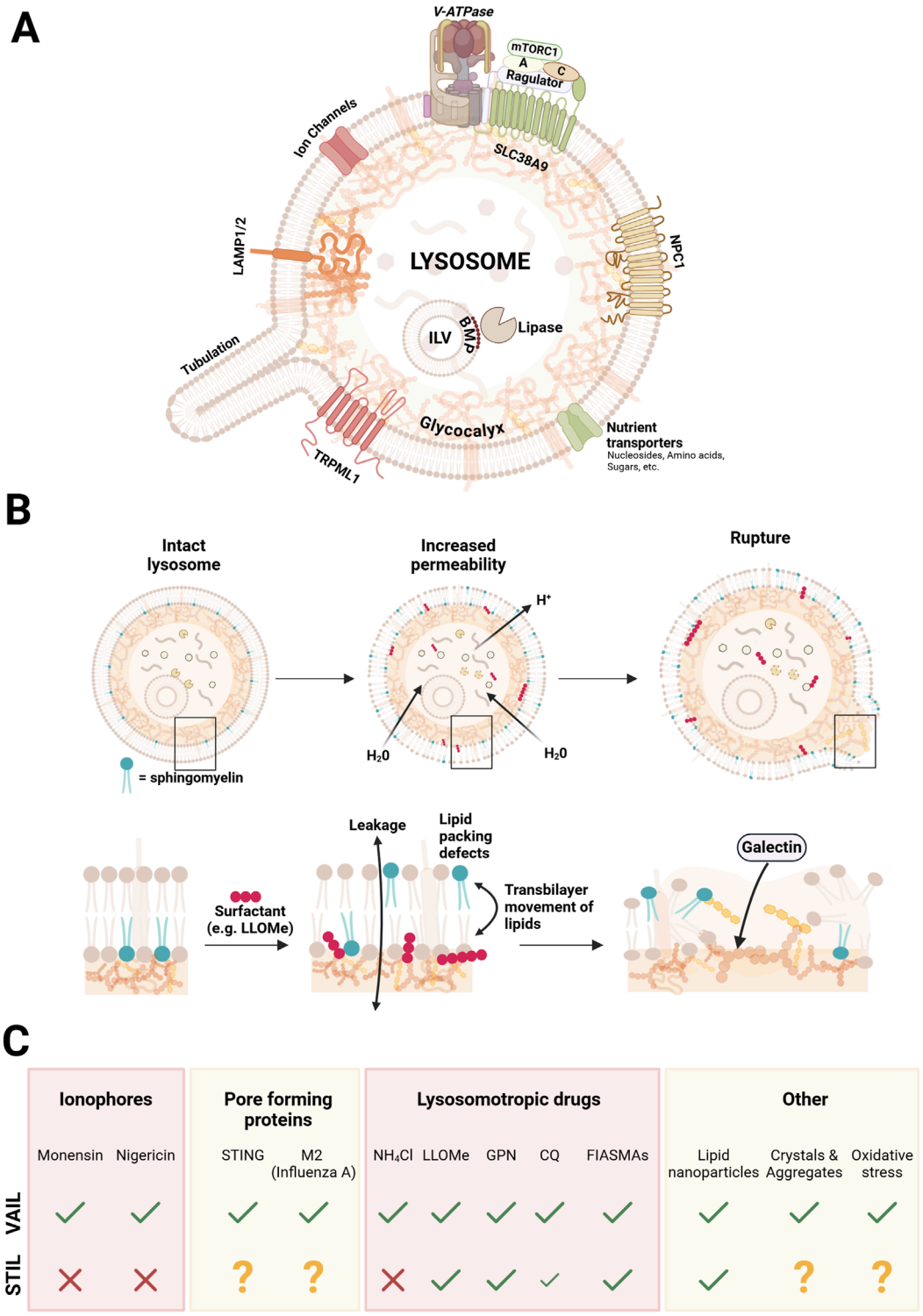

FIGURE 2
Simplified illustration of the lysosomal structure, stages of surfactant-induced damage, and the CASM response to distinct damage-inducing agents. Panel **(A)** depicts an intact lysosome, highlighting key structural and functional components, including the glycocalyx, intraluminal vesicles (ILVs), ion channels, the major Ca^{2+} channel TRPML1, nutrient transporters, amino acid transporter SLC38A9 with its associated proteins, lysosomal-associated membrane proteins (LAMP1/2), the major cholesterol transporter NPC1, and the V-ATPase complex that maintains the acidic lysosomal environment. Panel **(B)** depicts the progressive stages of lysosomal damage caused by surfactants integrating with the lipid bilayer. The process begins with increased permeability, leading to membrane leakiness and lipid scrambling, and culminates in membrane rupture, marked by exposure of the glycocalyx and recognition by galectins. Panel **(C)** summarizes the response by the two CASM axes (VAIL and STIL) induced by various agents and stressors that cause lysosomal damage, including ionophores, pore forming proteins, lysosomotrophic drugs, lipid nanoparticles, crystals and aggregates, and oxidative stress. A question mark denotes that the effect has not been reported.

culminating in STIL activation. Notably, ammonium chloride serves as an exception among lysosomotropic agents; while it neutralizes lysosomal pH and activates VAIL, it does not induce STIL (Kaur et al., 2023). This distinction is likely due to its monoprotic nature and lack of surfactant activity, which prevent significant perturbation of the lysosomal membrane.

3.3 Lipid nanoparticles (LNPs)/vaccines/transfection reagents

One of our early findings, when testing different agents for their effects on TECPR1-dependent CASM, was the surprising result that certain common transfection reagents, such as JetMessenger®, gave a strong STIL response (Kaur et al., 2023). This indicated that the formulation affects the limiting membrane, leading to exposure of SM, which may be one of the reasons for the enhancement of polynucleotide delivery. The same result was obtained with clinically relevant lipid nanoparticles (DLin-MC3-DMA), initially used for delivery of siRNA and lately also for mRNA vaccines (Karp and Peer, 2018; Akinc et al., 2019). To enhance the endosomal escape of polynucleotides, modern formulations of LNPs, such as those used in mRNA vaccines, consist of a mixture of four different lipid constituents: a phospholipid, an ionizable lipid, cholesterol, and a PEG (polyethyleneglycol)-modified lipid (Dowdy, 2017; Mukai et al., 2022; Wu et al., 2024). The effect in lysosomes is mediated by the ionizable lipid, having a role similar to the lysosomotropic drugs described above, affecting the organization of the limiting membrane and permitting escape of its cargo through the membrane. The cellular response is immediate, orchestrating a powerful CASM reaction through recognition of SM exposure in addition to activation of VAIL (Kaur et al., 2023). It can be envisioned that elaboration with the CASM response in future research may have a potential to enhance the efficiency of vaccine delivery.

3.4 Other types of processes that can elicit a CASM response

The generation, or uptake into cells, of substances that have a propensity to form crystals or large aggregates have also been shown to provoke a CASM response. Examples are silica, ureate, and cholesterol crystals, and amyloid proteins such as α-synuclein, amyloid-β, and tau (Papadopoulos and Meyer, 2017; Papadopoulos et al., 2020; Meyer and Kravic, 2024). A current view is that the accumulation of large structures in lysosomes will invoke penetration of the limiting membrane leading to leakage of ions and enzymes into the cytosol. The VAIL system is activated (Durgan and Florey, 2022), but since the damage often is severe the main response appears to rely on macrolysophagy (through exposure of luminal glycans and ubiquitination) to remove the damaged lysosomes (Maejima et al., 2013).

An alternative CASM-dependent mechanism associated with aggregated proteins is LANDO (LC3-associated endocytosis), which was identified in a murine model of Alzheimer's disease (Heckmann et al., 2019). In this pathway, Rab5-positive endosomes become decorated with ATG8 in response to amyloid-β build-up, ultimately triggering innate immune responses and inflammation. However, because LANDO takes place on early endosomal compartments and has been reviewed elsewhere (Magne and Green, 2022; Pena-Martinez et al., 2022), we will not address it further here.

Oxidative stress on cells can alter the lipid metabolism in lysosomes resulting in products, such as peroxidated lipids, that may have harmful consequences on lysosome function due to effects on its limiting membrane, causing, for example, lipid-packing defects (Gahlot et al., 2024; Meyer and Kravic, 2024). Also physiological processes may create reactive oxygen species (ROS) that is recognized by CASM. The best example is that of LAP (LC3-associated phagocytosis), which actually was the first described case of "non-canonical autophagy" (Sanjuan et al., 2007). In LAP, phagocytosis of pathogens or dead cells leads to formation of phagosomes, which matures into degradative compartments through a series of reactions culminating in the production of ROS by the enzyme NOX2 (NADPH oxidase 2). This reaction consumes protons that is sensed by the VAIL system and results in atg8ylation of the phagosome membrane (Hooper et al., 2022).

4 Downstream effectors of CASM

Since the initial characterization of non-canonical autophagy, or CASM, a key question has been to elucidate the role of ATG8 proteins downstream of their membrane attachment. It has become evident that the ATG8 conjugation machinery is adept at detecting membrane damage or insults, and that ATG8 proteins, acting as a scaffold, together with specific cellular factors like phosphoinositides and Rab GTPases, facilitate the recruitment and stabilization of various protein complexes required for lysosomal repair and maintenance. This relies on effector proteins distinct from those involved in canonical autophagy, emphasizing the role of additional factors in determining specificity of ATG8 interactions. Here, we explore key effector proteins recruited by CASM and their roles in addressing lysosomal damage (Figure 3).

4.1 Lysosomal tubulation events

Lysosomal tubules are dynamic membrane structures that form from lysosomes and related organelles under various physiological and pathological conditions—such as shifts in nutrient availability, cellular stress, and organelle damage—thereby helping to maintain lysosomal homeostasis and participating in essential recycling processes like autophagic lysosome reformation (ALR) and phagolysosome resolution (Yu et al., 2010; Krajcovic et al., 2013).

During ALR, which follows autophagy, mTOR reactivation at autolysosomes triggers the formation of tubular extensions. These tubules then undergo scission to produce proto-lysosomes that mature into fully functional lysosomes (Yu et al., 2010). A comparable mechanism operates in antigen-presenting cells, where lysosomal tubules form from phagosomes through phagolysosome resolution, contributing to antigen processing and presentation (Krajcovic et al., 2013; Lancaster et al., 2021). Lysosome reformation can also occur from endosomal compartments, where hybrid endosome-lysosome structures are generated. These structures

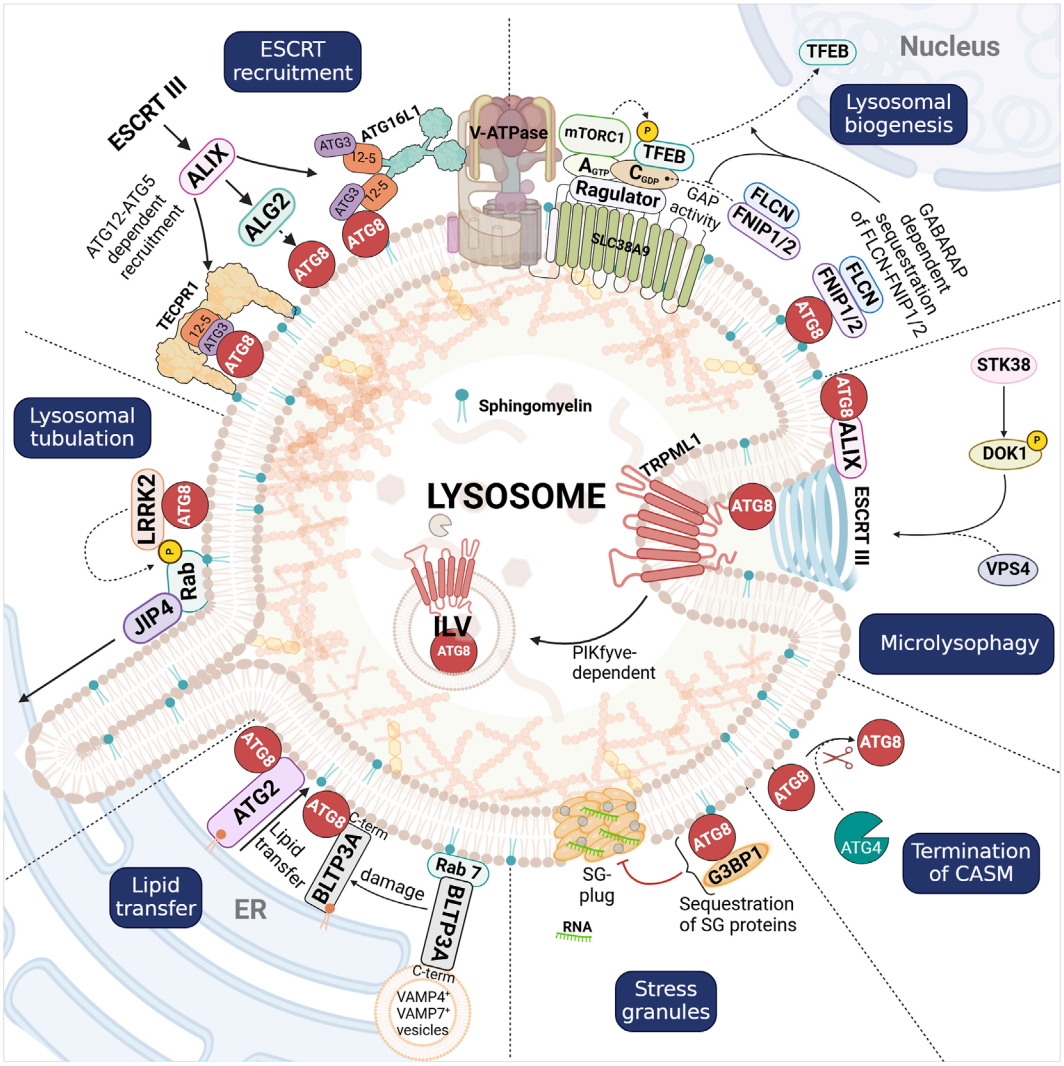

FIGURE 3
Overview of CASM pathways activated in response to lysosomal damage, and the role of membrane-anchored ATG8 proteins (red filled circles), as detailed in the main text. CASM supports Lysosomal biogenesis through TFEB activation, where the inhibition of FLCN-FNIP1/2 via GABARAP enables TFEB nuclear translocation to drive lysosomal gene expression and stress response pathways. ESCRT recruitment is initiated by the recruitment of ALIX and ESCRT-III components to ATG12-ATG5/GABARAP on damaged lysosomal membranes, facilitating membrane scission and resealing. Lysosomal tubulation is driven by the CASM-dependent recruitment of LRRK2, which phosphorylates Rab GTPases to promote tubule formation and membrane sorting. Lipid transfer through BLTPs (BLTP3A and ATG2) at ER-lysosome contact sites, provide essential lipids to restore and stabilize membrane integrity. Stress granule formation regulated by ATG8, which sequesters components like G3BP1 to prevent granule assembly. Termination of CASM occurs through ATG4-dependent cleavage of lipidated ATG8. Microlysophagy involves CASM-induced PIKfyve-dependent intraluminal vesicle (ILV) formation, which contributes to membrane turnover and damage resolution. Although CASM can proceed via two branches (VAIL and STIL), it remains unclear whether either pathway yields distinct downstream effects; for this reason, we have not distinguished between VAIL- and STIL-mediated ATG8 conjugation in the figure.

undergo fission and maturation to regenerate lysosomes, thereby supporting lysosomal homeostasis and recycling under specific physiological conditions (Pryor et al., 2000; Bright et al., 2005).

However, when lysosomes are damaged, a CASM-dependent pathway produces an unconventional class of tubules lacking the lysosomal membrane protein LAMP-1. A principal driver of this CASM-dependent tubulation is Leucine-Rich Repeat Kinase 2 (LRRK2) (Eguchi et al., 2024; Bentley-DeSousa et al., 2025).

LRRK2 is a large, multifunctional kinase that phosphorylates members of the Rab GTPase family, such as Rab8A, Rab10, and Rab35 (Steger et al., 2016; Steger et al., 2017). It is broadly expressed throughout the body, and its dysfunction has been associated with Parkinson's Disease (PD) and Crohn's Disease (CD) (Hui et al., 2018). *In vivo*, loss or inhibition of LRRK2 leads to enlarged lysosomes in organs like the kidney and lung, while familial LRRK2 mutations alter lysosomal morphology (Henry et al., 2015; Hockey et al., 2015).

Under lysosomal stress, LRRK2 is recruited to lysosomes through a CASM-dependent mechanism by directly interacting with GABARAP via two LIR motifs (Bentley-DeSousa et al., 2025), a process triggered by diverse stressors—such as Chloroquine, Monensin, Nigericin, STING agonists, TRPML1 agonists, and

LLOMe—and also occurring during LC3-associated phagocytosis (LAP) (Eguchi et al., 2024; Bentley-DeSousa et al., 2025). Importantly, CASM is essential for LRRK2 recruitment; depletion of CASM disrupts LRRK2 localization, whereas knockdown of autophagy-essential genes like ULK kinase complex subunits FIP200 or ATG13 does not, highlighting a CASM-specific, rather than a general atg8ylation-dependent pathway (Eguchi et al., 2024). Bentley-DeSousa et al. (2025) further proposed that LRRK2's preference for CASM-positive compartments may be explained by a coincidence detection mechanism that relies on the co-recognition of GABARAP and specific Rab GTPases (e.g., Rab10, Rab12, Rab29, Rab32), which collectively facilitate its recruitment (Bentley-DeSousa et al., 2025).

Once at compromised lysosomes, LRRK2 phosphorylates Rab GTPases, inhibiting their interaction with GDP dissociation inhibitors (GDIs) and thus keeping them active on the lysosomal membrane (Bonet-Ponce et al., 2020). Activated Rabs recruit JNK-interacting protein 4 (JIP4) to lysosomal surfaces, with Rab10 playing the primary role. JIP4 then facilitates the formation of LRRK2-driven tubules, known as LYTL (LYsosomal Tubulation/sorting driven by LRRK2) (Bonet-Ponce et al., 2020). These tubules, which lack LAMP-1/LIMP-2 and Dextran-555 labeling, differ from ALR tubules both in composition and in their utilization of distinct motor proteins, underscoring separate mechanistic pathways (Bonet-Ponce et al., 2020).

The pathogenic G2019S mutation in LRRK2, associated with PD, enhances its recruitment to compromised lysosomes, leading to excessive JIP4 recruitment and lysosomal tubulation (Bonet-Ponce et al., 2020). This excessive remodeling of lysosomal membranes underscores the central role of LRRK2 in lysosomal dynamics and its broader implications in disease mechanisms. While the specific roles of the LRRK2-driven tubules are not yet fully understood, they are unlikely to participate in proto-lysosome reformation, as they lack lysosomal membrane markers such as LAMP-1 and LIMP-2.

In contrast, a distinct lysosomal tubulation pathway mediated by TBC1D15—a Rab7 GTPase-activating protein (GAP)—also relies on atg8ylation at lysosomes yet independently of a "classical" CASM mechanism (Bhattacharya et al., 2023). Following acute lysosomal damage, TBC1D15 is recruited to damaged membranes through interactions with ATG8 proteins. Acting as a scaffold, TBC1D15 assembles and stabilizes components of the lysosomal tubulation machinery—including dynamin-2, kinesin-5B, and clathrin—thereby driving tubule formation and scission to promote lysosomal recovery independently of lysosomal biogenesis. Surprisingly, TBC1D15 recruitment and the resulting tubulation is not dependent on VAIL, as normal TBC1D15 recruitment is seen with a CASM-deficient ATG16L1 mutant. Instead, it seems that TBC1D15 relies on canonical macroautophagy factors (e.g., ATG13) for its recruitment and function in lysosomal tubulation and recovery.

4.2 Lysosomal biogenesis

Transcription factor EB (TFEB) serves as a master regulator of the autophagy-lysosomal pathway by driving gene expression through its binding to Coordinated Lysosomal Expression and Regulation (CLEAR) elements in target gene promoters (Sardiello et al., 2009). Its activity is tightly regulated by mTORC1, which phosphorylates TFEB to retain it in the cytosol, preventing its nuclear translocation (Martina et al., 2012; Roczniak-Ferguson et al., 2012; Settembre et al., 2012). However, accumulating evidence now indicates that CASM can override this block on TFEB, even in contexts where mTORC1 remains active toward other targets.

Unlike other mTORC1 targets, such as S6K and 4EBP1, TFEB requires active RagC to be recruited to the lysosome for phosphorylation (Napolitano et al., 2020). RagC's activation, converting it to its GDP-bound state, is mediated by the GAP complex FLCN-FNIP1/2 (Tsun et al., 2013).

CASM supports TFEB's nuclear translocation by utilizing a GABARAP-specific LIR motif within FNIP1 and FNIP2 (Goodwin et al., 2021). Lipidated GABARAP binds this motif, sequestering the FLCN-FNIP1/2 complex and preventing it from activating RagC. As a result, RagC remains inactive, allowing TFEB to dissociate from the lysosome and move into the nucleus (Goodwin et al., 2021).

Several agents can trigger CASM-mediated TFEB translocation, including STING agonists, TRPML1 agonists, and the ionophore Monensin (Nakamura et al., 2020; Goodwin et al., 2021; Lv et al., 2024). The GABARAP-dependent sequestration of FLCN-FNIP1/2 has also been observed in xenophagy and mitophagy, indicating that this mechanism extends beyond CASM (Goodwin et al., 2021; Schmuckli-Maurer et al., 2024). Interestingly, high concentrations of STING agonists can induce TFEB translocation through CASM-independent pathways, suggesting the presence of additional regulatory layers that remain to be explored (Lv et al., 2024).

4.3 Lipid transfer proteins

Maintaining the lysosomal membrane is crucial for protecting the cytoplasm from the harsh lysosomal environment. When lysosomes are damaged or permeabilized, lipids are rapidly introduced to restore and protect membrane integrity. The endoplasmic reticulum (ER) serves as the main source of these lipids, and upon lysosomal injury, specialized ER–lysosome membrane contact sites (EL-MCS) form to facilitate non-vesicular lipid transfer (Radulovic et al., 2022; Tan and Finkel, 2022; Hanna et al., 2023).

A key factor in this process is PI(4)P on lysosomal membranes, generated by PI4K2A (Radulovic et al., 2022; Tan and Finkel, 2022). PI(4)P drives the formation of EL-MCS and helps recruit oxysterol-binding protein (OSBP) and oxysterol-binding protein-related proteins (ORPs). These shuttle-like proteins bind lipids in a hydrophobic cleft, extracting them from the ER and delivering them to lysosomes across an aqueous gap (Radulovic et al., 2022; Tan and Finkel, 2022). For instance, ORP1L transfers cholesterol in exchange for PI(4)P, whereas ORP9, ORP10, and ORP11 transport PS. Notably, PS on lysosomal membranes activates ATG2, a bridge-like lipid transfer protein (BLTP) capable of bulk lipid transport (Tan and Finkel, 2022).

BLTPs, such as ATG2 (BLTP4), adopt a rod-like structure with a hydrophobic groove optimized for lipid transfer (Hanna et al., 2023). They feature a repeating β-groove (RBG) domain, whose

role in lipid selectivity remains unclear, and a chorein motif in the N-terminal region, typically localized to the ER which is the lipid donor (Leonzino et al., 2021; Hanna et al., 2023). Structural studies reveal that BLTPs can accommodate a single lipid at the groove's narrowest point, supporting unidirectional lipid flow. These proteins bridge membrane gaps at contact sites, enabling low-energy bulk lipid transfer essential for membrane repair (Hanna et al., 2023). This mechanism highlights their role in preventing further membrane damage through efficient lipid replenishment.

Recent work shows that BLTPs can interact with ATG8 on lysosomes in a CASM-dependent manner. For example, ATG2 and ATG8 associate on lysosomal membranes after permeabilization and osmotic stress (Cross et al., 2023). While this interaction is not strictly required for ATG2's recruitment, it helps stabilize ATG2 at the damaged lysosome. BLTP3A, in contrast, is recruited to lysosomes directly through CASM (Hanna et al., 2025). Under normal conditions, BLTP3A localizes to VAMP7- and VAMP4-positive vesicles tethered via its N-terminal region to lysosome-bound Rab7. Upon damage, Rab7-dependent tethering is disrupted, but CASM leads to BLTP3A reassociation through a LIR domain in its C-terminal region. This interaction appears to expose the protein's N-terminal chorein motif, enabling ER engagement and lipid transfer to the lysosome.

Because BLTPs only access the cytosolic leaflets at MCS, lipid flow can unbalance the bilayer of donor and acceptor membranes (Hanna et al., 2023). Therefore, BLTPs cooperate with scramblases for balancing this asymmetry during lipid flow at MCS. For example, *in vitro* work has demonstrated that ATG2 can interact with scramblases on both donor membranes (VMP1 and TMEM41B) and acceptor membranes (ATG9) in an artificial system modeling autophagosome biogenesis (Ghanbarpour et al., 2021). However, a model explaining how BLTP-induced leaflet imbalance is managed following lysosomal damage has yet to be proposed.

In addition to ATG2 and BLTP3A, VPS13C (also known as BLTP5C) has been observed on lysosomes following damage, apparently independent of VAIL; whether its recruitment depends on STIL remains to be tested. As a BLTP, VPS13C is expected to promote net lipid flow to compromised membranes (Cai et al., 2022; Wang et al., 2025).

Increasing evidence suggests that CASM is vital for stabilizing BLTPs (e.g., ATG2 and BLTP3A) at lysosomes, though the exact molecular details remain unclear. This mechanism may enable CASM to compensate for membrane thinning and prevent rupture. Although several studies have examined lipid transfer following membrane-perforation damage, the impact on de-acidified and swelling lysosomes—where VAIL is triggered but the limiting membrane remains intact—remains largely unexplored.

4.4 ESCRT recruitment

The Endosomal Sorting Complexes Required for Transport (ESCRT) machinery is essential for a variety of cellular processes, including multivesicular endosome formation, virus budding, cytokinetic abscission, and nuclear envelope reassembly (Christ et al., 2017; Vietri et al., 2020). It also plays a crucial role in membrane repair, including restoring integrity of the plasma membrane and lysosomes following damage. The ESCRT machinery consists of four subcomplexes: ESCRT-0, ESCRT-I, ESCRT-II, and ESCRT-III. ESCRT-I is crucial for recruiting ESCRT-III, with ALG2-interacting protein X (ALIX), a Bro1 domain-containing protein, serving as a bridge between them (Christ et al., 2017).

As demonstrated by Skowyra et al. (2018) and Radulovic et al. (2018), the reparative role of ESCRTs in lysosomal membrane damage precedes macrolysophagy, with TSG101 (an ESCRT-I component) and ALIX (a critical ESCRT-nucleating factor) being recruited to damaged lysosomes before the appearance of galectin-3, which marks severe membrane damage (Radulovic et al., 2018; Skowyra et al., 2018). This early recruitment is considered as the first line of defense against membrane damage, as failure in this repair mechanism can lead to irreversible damage and cell death. In addition, ESCRTs recruitment to damaged lysosomes is dependent on Ca^{2+}, where cytoplasmic Ca^{2+} signals the recruitment of ALG-2, which, upon binding to the membrane, undergoes a conformational change and interacts with ALIX (Skowyra et al., 2018; Shukla et al., 2022; Chen et al., 2024). Besides repairing membrane perforations caused by LLOMe, ESCRTs are activated by elevated peri-lysosomal Ca^{2+} levels, which can result from TRPML1 activation even without membrane perforation, thereby protecting lysosomes from rupture (Chen et al., 2024).

It has also been reported that ALIX recruitment occurs in a GABARAP-dependent manner during microlysophagy (discussed below) triggered by lysosomal damage or osmotic stress (Ogura et al., 2023). In this study, cells lacking the atg8ylation machinery (ATG16L1, ATG7, ATG8 or ATG3) failed to recruit ESCRT components (ALIX, VPS4 and CHMP4B) following lysosome damage. In contrast, autophagy deficient FIP200 knockout (KO) cells showed no defect in ESCRT recruitment. Further analysis revealed that ALIX directly interacts with ATG8 proteins, with specificity for the GABARAP subfamily. This finding highlighted the essential role of CASM in mediating ALIX dependent nucleation of the ESCRT machinery on compromised lysosomes (Ogura et al., 2023).

Later, another study found that ALIX recruitment following membrane damage is primarily dependent on ATG12-ATG5, which is recruited by either ATG16L1 or TECPR1, rather than on GABARAP (Corkery et al., 2024). This study showed that ALIX could still be recruited in the absence of atg8ylation, provided ATG12-ATG5 was present. However, in atg8ylation deficient cells, the ESCRT machinery's distribution on damaged membranes was fragmented and incomplete. This impaired recruitment was attributed to the lack of CASM-dependent stabilization of ALG-2 on damaged lysosomes, facilitated by a direct interaction with LC3B. Importantly, lysosome recovery, following damage, was equally impaired in ATG8 KO cells as it was in cells lacking ATG5, or ATG16L1 and TECPR1 (Corkery et al., 2024), highlighting the necessity of both the ATG8 conjugation machinery and CASM for efficient ESCRT-mediated repair (Corkery et al., 2024).

An interesting phenomenon to note is the formation of an alternative ATG12 complex, where ATG12 is conjugated to ATG3 instead of ATG5, a situation that becomes more pronounced with ATG5 depletion (Murrow et al., 2015; Wang F. et al., 2023). This ATG12-ATG3 complex, which lacks the ability to interact with ATG16L1 or TECPR1, has been shown to impact ALIX-dependent pathways, such as exosome biogenesis and lysosomal exocytosis. In

the absence of ATG5, ALIX exhibits a strong affinity for ATG12-ATG3, impairing its recruitment to lysosomes and compromising the lysosomal repair process.

Together, these studies underline the vital role of ESCRTs as a first line of defense against lysosomal damage and highlight the intricate contributions of CASM in optimizing ESCRT function. While ESCRT components such as TSG101 and ALIX initiate repair in a Ca^{2+}-dependent manner, the atg8ylation machinery ensures the proper stabilization and distribution of ESCRT proteins on compromised membranes. Moreover, the interplay between distinct E3-like ligase complexes (ATG16L1–ATG12–ATG5 vs. TECPR1–ATG12–ATG5) and the alternative formation of ATG12–ATG3 reveal additional layers of complexity. These findings emphasize the critical interplay between CASM and ESCRTs in lysosomal repair, with CASM not only stabilizing key repair components but also dictating the spatial organization of ESCRT machinery required for effective membrane restoration.

4.5 Microlysophagy

Microautophagy is a selective process that removes organelles and cytoplasmic components through invagination of the lysosomal limiting membrane, a mechanism observed in both yeast and mammalian systems (Sahu et al., 2011; Schuck et al., 2014). Various cargoes—including mitochondria, ER, peroxisomes, and nuclear material—have been described to undergo selective microautophagy. A specialized form of this pathway, known as microlysophagy, mediates lysosome membrane turnover in mammalian cells independently of macroautophagy, facilitating lysosome size control through the formation of ILVs. Microlysophagy can be divided into ATG8-dependent and ATG8-independent processes, both relying on the ESCRT machinery, with the ATG8-independent route rather requiring ubiquitin (Wang L. et al., 2023).

ATG8-dependent microlysophagy requires the core conjugation machinery (ATG5, ATG7, and ATG3), but it does not depend on the ULK-complex (ATG13 and ULK1) required for macroautophagy (Lee et al., 2020). Under conditions of extreme cellular stress, lysosomal turnover becomes essential for reducing lysosomal damage. For instance, stressors such as LLOMe or ionophores induce CASM on lysosomes, and trigger the degradation of select lysosomal membrane proteins, including TRPML1 and SNAT7 (Lee et al., 2020). In earlier sections, we discussed how CASM is vital for recruiting the ESCRT machinery that mediates ILV formation in response to agents like Monensin and LLOMe. Recent findings, however, have highlighted additional factors involved in the ATG8-dependent microlysophagy pathway.

Specifically, both the phosphoinositide kinase PIKfyve and the lysosomal Ca^{2+} channel TRPML1 act as critical downstream effectors in CASM-dependent microlysophagy. Monensin-induced ILV formation is disrupted when either PIKfyve or TRPML1 is inhibited (Klein et al., 2024). Notably, blocking either protein does not reduce Monensin-induced LC3 lipidation, rather, it appears to enhance it, indicating that TRPML1 and PIKfyve are required for ILV formation but not for LC3 lipidation in ionophore-treated cells. Collectively, these observations underscore the roles of PIKfyve and TRPML1 in lysosomal homeostasis and highlight their importance in orchestrating ILV formation during microlysophagy.

Another study highlighted the essential role of serine-threonine kinase 38 (STK38) in microlysophagy, more specifically a role in the disassembly of the ESCRT complex (Ogura et al., 2023). STK38 achieves this by phosphorylating the scaffold protein DOK1 at a specific serine residue (S269), which facilitates the recruitment of VPS4 to damaged lysosomes. This recruitment is critical for the final disassembly of the ESCRT complex, ultimately leading to the formation of ILVs within lysosomes.

As mentioned above, ESCRT-mediated microautophagy can occur with or without the involvement of CASM (Li et al., 2015; Ogura et al., 2023). However, the factors determining which pathway is prioritized remain unclear. Under conditions of severe lysosomal stress, it is plausible that membrane atg8ylation accelerates ESCRT-mediated microlysophagy. Additionally, the specific circumstances under which ESCRT- and PIKfyve-dependent microlysophagy are preferentially activated require further investigation, highlighting the intricacy of lysosomal quality control and size regulation.

4.6 Stress granule assembly at lysosomal damage sites

We will also briefly mention stress granules (SGs), as atg8ylation and potentially CASM have been implicated in their formation. SG are cytoplasmic, membrane-less liquid-liquid phase-separated biomolecular condensates that contain translation factors, mRNAs, RNA-binding proteins (RBPs), including G3BP1, and other associated proteins, such as NUFIP2.

The formation of SGs can be induced by lysosomal damage (Jia et al., 2022). Interestingly, *in vitro* experiments using giant unilamellar vesicles (GUVs) have shown that G3BP1-RNA condensates can stabilize damaged membranes and prevent the leakage of luminal content, while their absence results in vesicle collapse (Bussi et al., 2023). Consistently, the inhibition of SG formation (via knockdown of G3BP proteins) affects ESCRT-mediated repair and pushes damaged lysosomes towards macrolysophagy (Bussi et al., 2023).

SG formation increases in situations where the CASM machinery is compromised (Jia et al., 2022). Additionally, it was demonstrated that GABARAP, when conjugated to the lysosome, suppresses SG formation by sequestering essential components G3BP1 and NUFIP2 through direct interaction (Jia et al., 2022).

4.7 Termination of lysosome-associated CASM

A key hallmark of CASM, as mentioned above, is the conjugation of ATG8 proteins not only to PE but also to PS (Durgan et al., 2021). This has been observed across a range of CASM-inducing stimuli, including pharmacological treatments with Monensin or LLOMe, LC3-associated phagocytosis, and influenza A virus infection (Durgan et al., 2021; Cross et al., 2023).

In both autophagy and CASM, the terminal step for ATG8 proteins involves either their degradation or de-lipidation. De-lipidation in humans is carried out by the ATG4 protease family, which consists of four isoforms: ATG4A, ATG4B, ATG4C, and ATG4D (Scherz-Shouval et al., 2003; Tanida et al., 2004; Kauffman et al., 2018). Notably, ATG4D exhibits a unique role in CASM, as it demonstrates little to no activity toward ATG8-PE but shows the highest activity among ATG4 isoforms toward ATG8-PS (Durgan et al., 2021).

This specificity of ATG4D for ATG8-PS, rather than ATG8-PE, elucidates a key mechanism for distinguishing CASM from autophagy. It raises two important considerations: (1) ATG8-PS may recruit different interaction partners, and (2) ATG4 isoforms may selectively target ATG8 attached to different lipids to regulate its removal during autophagy versus CASM. An alternative explanation suggests that conjugating ATG8 to PS could alter the lipid's biophysical properties, thereby influencing charge-dependent processes, for example, during phagocytosis (Yeung et al., 2009; Durgan et al., 2021).

5 Concluding remarks

From the research done on CASM so far, it is clear that ATG8 decoration of damaged lysosomal membranes can occur through different mechanisms, and also that the outcome can vary depending on cell-type, the nature of the damage, and the duration of the insult. As new data emerge, one can start to see certain patterns in how cells respond to lysosomal injury in ways that rely on, or are enhanced by, ATG8. Nevertheless, many outstanding questions remain before we can fully appreciate the integrated system in which CASM operates, and its precise roles in different cellular contexts continue to be an active area of investigation.

In several cases it appears that atg8ylation on single membranes acts to stabilize the membrane and to provide efficient platforms for recruitment of key proteins, perhaps to enhance the kinetics of repair (Radulovic et al., 2018; Skowyra et al., 2018), removal (Lee et al., 2020), or formation of new membrane (Cross et al., 2023; Eguchi et al., 2024; Bentley-DeSousa et al., 2025). Thus far, almost all studies report that ATG8-dependent recruitment of factors occur via interactions between LIR-sequences in the recruited proteins and the LIR-docking site on membrane-anchored ATG8s. Minor variations on this theme has been described (Johansen and Lamark, 2020), but in essence it seems that an early response after damage is to present anchor points for dedicated proteins involved in various specific processes as outlined above. Mechanistically, although it may be possible to implement, for example, a repair process without ATG8s, the kinetics is likely enhanced several-fold if factors are enriched at certain sites. This principle may be especially important when the cell has to deal with potentially life-threatening danger.

Generally, the effects of lysosomal damage can be divided into early and late phases. Early on, events such as Ca^{2+}-leakage through the Ca^{2+}-specific channels (Hu et al., 2024; Meyer and Kravic, 2024), loss of proton gradient (Durgan and Florey, 2022; Figueras-Novoa et al., 2024), disruption in membrane lipid-packing (Gahlot et al., 2024), and collapse of membrane leaflet asymmetry (leading to SM exposure) take place (Ellison et al., 2020; Niekamp et al., 2022). These cues trigger ATG8 lipidation via VAIL or STIL, enabling repair mechanisms like microlysophagy, where CASM facilitates the internalization of small damaged membrane portions to stabilize and restore lysosomal function. If the damaging agent is removed at this stage, the cell can heal the membrane. At a late stage, however, severe breakdown exposes internal glycans in the glycocalyx (Gahlot et al., 2024; Jacob and Gorek, 2024), rendering salvage futile as much of the lysosomal contents escape. The irreversibly damaged lysosome is then cleared through macrolysophagy, dependent on galectins and ubiquitination, with autophagy receptors like TAX1BP1 linking ubiquitin-tagged lysosomes to ATG8-decorated phagophores (Eapen et al., 2021). One intriguing possibility is that the early CASM at the lysosomal membranes might also serve to enhance a subsequent macrolysophagy response, should it be needed, and thereby reduce the risk of excessive leakage of lysosomal contents. Still, CASM's involvement in macrolysophagy is uncertain, and how it might prepare lysosomes for clearance remains to be explored.

Emerging evidence suggests that, while LC3B-lipidation is often used as a convenient readout in CASM studies, members of the GABARAP subfamily may play a more prominent role in recruiting LIR-containing proteins in both canonical autophagy and CASM (Johansen and Lamark, 2020; Mizushima, 2020). Although much research has focused on direct interactions between ATG8 proteins and LIR motifs, other factors, such as membrane lipid composition (e.g., phosphoinositides), membrane curvature, the type of lipid conjugated to ATG8 (PE or PS), and membrane-associated proteins like Rabs, can substantially influence these interactions. Investigating how these factors act in concert could provide deeper insights into the underlying mechanisms of CASM.

We now know of two distinct systems that drive ATG8-lipidation at lysosomal membranes upon damage, named VAIL and STIL, and more pathways may be uncovered in the future (Deretic, 2024; Deretic and Klionsky, 2024; Figueras-Novoa et al., 2024). VAIL and STIL use different E3-like ligase complexes (ATG16L1-ATG12-ATG5 and TECPR1-ATG12-ATG5, respectively), but otherwise share a similar conjugation mechanism. Their activation, however, differs: VAIL responds to signals from the V-ATPase (Xu et al., 2019), whereas STIL is triggered by SM exposure following membrane asymmetry defects (Boyle et al., 2023; Corkery et al., 2023; Kaur et al., 2023; Wang Y. et al., 2023). This division of labor presumably provides spatio-temporal flexibility in atg8ylation during damage responses, allowing scenarios in which one E3 can act more rapidly, or exclusively, compared to the other. Another interesting difference is that STIL remains unaffected by the bacterial effector SopF, which irreversibly blocks V-ATPase-mediated signaling (Kaur et al., 2023). Thus, during *Salmonella* infections, SopF would selectively inhibit VAIL but leave STIL functionality intact, providing an additional layer of importance to their diverging functionality (Xu et al., 2019; Kaur et al., 2023).

Mouse models deficient in VAIL or STIL have been generated separately, and both show normal macroautophagy (Ogawa et al., 2011; Rai et al., 2019). Interestingly, VAIL-deficient mice are extremely vulnerable to infections with low-pathogenicity IAV, exhibiting high viral replication in the lungs, dysregulated cytokine responses, and lethality rates that mirror those seen with highly pathogenic IAV (Wang et al., 2021). Although TECPR1-deficient mice have yet to be investigated specifically in the context

of CASM, TECPR1-deficient MEFs display diminished LC3 responses to infections with *Shigella* ΔicsB, resulting in markedly higher bacterial survival (Ogawa et al., 2011). These observations underscore the importance of disrupting both STIL and VAIL in future research to determine their interplay and to establish how each pathway can compensate for the other in defending against infections.

It also remains to be determined whether STIL alone can be triggered under specific conditions that go beyond SopF-mediated disruptions of VAIL. Pinpointing situations where STIL operates independently would yield insight into its specialized functions in cellular processes and how it contributes to maintaining endolysosomal balance. Moreover, studying mice that lack both STIL and VAIL will be a crucial step toward revealing how these pathways coordinate and back up one another. Observing how double-deficient mice respond to different bacterial and viral infections, as well as to challenges within their endolysosomal networks, could highlight new ways these mechanisms control host defense and cellular stress responses. Such investigations might even uncover new weaknesses that could be targeted for treatments in diseases involving disruptions of these protective pathways.

Author contributions

NK: Writing–original draft, Writing–review and editing. SC: Writing–original draft, Writing–review and editing. AL: Writing–original draft, Writing–review and editing.

Funding

The author(s) declare that financial support was received for the research and/or publication of this article. This work was partly supported by a Young Research Talents Grant from the Research Council of Norway (Project number 325305) and through its Centres of Excellence funding scheme (project number 262652).

Acknowledgments

Figures created in https://BioRender.com.

Conflict of interest

The authors declare that the research was conducted in the absence of any commercial or financial relationships that could be construed as a potential conflict of interest.

Generative AI statement

The authors declare that no Generative AI was used in the creation of this manuscript.

Publisher's note

All claims expressed in this article are solely those of the authors and do not necessarily represent those of their affiliated organizations, or those of the publisher, the editors and the reviewers. Any product that may be evaluated in this article, or claim that may be made by its manufacturer, is not guaranteed or endorsed by the publisher.

References

Agrotis, A., von Chamier, L., Oliver, H., Kiso, K., Singh, T., and Ketteler, R. (2019). Human ATG4 autophagy proteases counteract attachment of ubiquitin-like LC3/GABARAP proteins to other cellular proteins. *J. Biol. Chem.* 294 (34), 12610–12621. doi:10.1074/jbc.AC119.009977

Akinc, A., Maier, M. A., Manoharan, M., Fitzgerald, K., Jayaraman, M., Barros, S., et al. (2019). The Onpattro story and the clinical translation of nanomedicines containing nucleic acid-based drugs. *Nat. Nanotechnol.* 14 (12), 1084–1087. doi:10.1038/s41565-019-0591-y

Ballabio, A., and Bonifacino, J. S. (2020). Lysosomes as dynamic regulators of cell and organismal homeostasis. *Nat. Rev. Mol. Cell. Biol.* 21 (2), 101–118. doi:10.1038/s41580-019-0185-4

Barisch, C., Holthuis, J. C. M., and Cosentino, K. (2023). Membrane damage and repair: a thin line between life and death. *Biol. Chem.* 404 (5), 467–490. doi:10.1515/hsz-2022-0321

Bentley-DeSousa, A., Roczniak-Ferguson, A., and Ferguson, S. M. (2025). A STING-CASM-GABARAP pathway activates LRRK2 at lysosomes. *J. Cell. Biol.* 224 (2), e202310150. doi:10.1083/jcb.202310150

Bhattacharya, A., Mukherjee, R., Kuncha, S. K., Brunstein, M. E., Rathore, R., Junek, S., et al. (2023). A lysosome membrane regeneration pathway depends on TBC1D15 and autophagic lysosomal reformation proteins. *Nat. Cell. Biol.* 25 (5), 685–698. doi:10.1038/s41556-023-01125-9

Bohnert, K. A., and Johnson, A. E. (2022). Branching off: new insight into lysosomes as tubular organelles. *Front. Cell. Dev. Biol.* 10, 863922. doi:10.3389/fcell.2022.863922

Bonet-Ponce, L., Beilina, A., Williamson, C. D., Lindberg, E., Kluss, J. H., Saez-Atienzar, S., et al. (2020). LRRK2 mediates tubulation and vesicle sorting from lysosomes. *Sci. Adv.* 6 (46), eabb2454. doi:10.1126/sciadv.abb2454

Boyle, K. B., Ellison, C. J., Elliott, P. R., Schuschnig, M., Grimes, K., Dionne, M. S., et al. (2023). TECPR1 conjugates LC3 to damaged endomembranes upon detection of sphingomyelin exposure. *EMBO J.* 42 (17), e113012. doi:10.15252/embj.2022113012

Breiden, B., and Sandhoff, K. (2019a). Emerging mechanisms of drug-induced phospholipidosis. *Biol. Chem.* 401 (1), 31–46. doi:10.1515/hsz-2019-0270

Breiden, B., and Sandhoff, K. (2019b). Lysosomal glycosphingolipid storage diseases. *Annu. Rev. Biochem.* 88, 461–485. doi:10.1146/annurev-biochem-013118-111518

Breiden, B., and Sandhoff, K. (2021). Acid sphingomyelinase, a lysosomal and secretory phospholipase C, is key for cellular phospholipid catabolism. *Int. J. Mol. Sci.* 22 (16), 9001. doi:10.3390/ijms22169001

Bright, N. A., Davis, L. J., and Luzio, J. P. (2016). Endolysosomes are the principal intracellular sites of acid hydrolase activity. *Curr. Biol.* 26 (17), 2233–2245. doi:10.1016/j.cub.2016.06.046

Bright, N. A., Gratian, M. J., and Luzio, J. P. (2005). Endocytic delivery to lysosomes mediated by concurrent fusion and kissing events in living cells. *Curr. Biol.* 15 (4), 360–365. doi:10.1016/j.cub.2005.01.049

Bussi, C., Mangiarotti, A., Vanhille-Campos, C., Aylan, B., Pellegrino, E., Athanasiadi, N., et al. (2023). Stress granules plug and stabilize damaged endolysosomal membranes. *Nature* 623 (7989), 1062–1069. doi:10.1038/s41586-023-06726-w

Cai, S., Wu, Y., Guillen-Samander, A., Hancock-Cerutti, W., Liu, J., and De Camilli, P. (2022). *In situ* architecture of the lipid transport protein VPS13C at ER-lysosome membrane contacts. *Proc. Natl. Acad. Sci. U. S. A.* 119 (29), e2203769119. doi:10.1073/pnas.2203769119

Carlsson, S. R., Roth, J., Piller, F., and Fukuda, M. (1988). Isolation and characterization of human lysosomal membrane glycoproteins, h-lamp-1 and h-lamp-2. Major sialoglycoproteins carrying polylactosaminoglycan. *J. Biol. Chem.* 263 (35), 18911–18919. doi:10.1016/s0021-9258(18)37369-1

Chen, W., Motsinger, M. M., Li, J., Bohannon, K. P., and Hanson, P. I. (2024). Ca(2+)-sensor ALG-2 engages ESCRTs to enhance lysosomal membrane resilience to osmotic stress. *Proc. Natl. Acad. Sci. U. S. A.* 121 (22), e2318412121. doi:10.1073/pnas.2318412121

Chen, X., and Geiger, J. D. (2020). Janus sword actions of chloroquine and hydroxychloroquine against COVID-19. *Cell. Signal* 73, 109706. doi:10.1016/j.cellsig.2020.109706

Chizhmakov, I. V., Geraghty, F. M., Ogden, D. C., Hayhurst, A., Antoniou, M., and Hay, A. J. (1996). Selective proton permeability and pH regulation of the influenza virus M2 channel expressed in mouse erythroleukaemia cells. *J. Physiol.* 494 (2), 329–336. doi:10.1113/jphysiol.1996.sp021495

Christ, L., Raiborg, C., Wenzel, E. M., Campsteijn, C., and Stenmark, H. (2017). Cellular functions and molecular mechanisms of the ESCRT membrane-scission machinery. *Trends Biochem. Sci.* 42 (1), 42–56. doi:10.1016/j.tibs.2016.08.016

Collins, M. P., and Forgac, M. (2020). Regulation and function of V-ATPases in physiology and disease. *Biochim. Biophys. Acta Biomembr.* 1862 (12), 183341. doi:10.1016/j.bbamem.2020.183341

Corkery, D. P., Castro-Gonzalez, S., Knyazeva, A., Herzog, L. K., and Wu, Y. W. (2023). An ATG12-ATG5-TECPR1 E3-like complex regulates unconventional LC3 lipidation at damaged lysosomes. *EMBO Rep.* 24 (9), e56841. doi:10.15252/embr.202356841

Corkery, D. P., Li, S., Wijayatunga, D., Herzog, L. K., Knyazeva, A., and Wu, Y.-W. (2024). ESCRT recruitment to damaged lysosomes is dependent on the ATG8 E3-like ligases. *bioRxiv* 2024, 591897. doi:10.1101/2024.04.30.591897

Cross, J., Durgan, J., McEwan, D. G., Tayler, M., Ryan, K. M., and Florey, O. (2023). Lysosome damage triggers direct ATG8 conjugation and ATG2 engagement via non-canonical autophagy. *J. Cell. Biol.* 222 (12), e202303078. doi:10.1083/jcb.202303078

Davis, O. B., Shin, H. R., Lim, C. Y., Wu, E. Y., Kukurugya, M., Maher, C. F., et al. (2021). NPC1-mTORC1 signaling couples cholesterol sensing to organelle homeostasis and is a targetable pathway in niemann-pick type C. *Dev. Cell.* 56 (3), 260–276.e7. doi:10.1016/j.devcel.2020.11.016

De Duve, C., and Wattiaux, R. (1966). Functions of lysosomes. *Annu. Rev. Physiol.* 28, 435–492. doi:10.1146/annurev.ph.28.030166.002251

Deretic, V. (2024). *Atg8ylation and its manifestations*. Newcastle-upon-Tyne: Cambridge Scholars Publishing.

Deretic, V., and Klionsky, D. J. (2024). An expanding repertoire of E3 ligases in membrane Atg8ylation. *Nat. Cell. Biol.* 26 (3), 307–308. doi:10.1038/s41556-023-01329-z

Deretic, V., and Lazarou, M. (2022). A guide to membrane atg8ylation and autophagy with reflections on immunity. *J. Cell. Biol.* 221 (7), e202203083. doi:10.1083/jcb.202203083

Dowdy, S. F. (2017). Overcoming cellular barriers for RNA therapeutics. *Nat. Biotechnol.* 35 (3), 222–229. doi:10.1038/nbt.3802

Duran, J., Salinas, J. E., Wheaton, R. P., Poolsup, S., Allers, L., Rosas-Lemus, M., et al. (2024). Calcium signaling from damaged lysosomes induces cytoprotective stress granules. *EMBO J.* 43 (24), 6410–6443. doi:10.1038/s44318-024-00292-1

Durgan, J., and Florey, O. (2022). Many roads lead to CASM: diverse stimuli of noncanonical autophagy share a unifying molecular mechanism. *Sci. Adv.* 8 (43), eabo1274. doi:10.1126/sciadv.abo1274

Durgan, J., Lystad, A. H., Sloan, K., Carlsson, S. R., Wilson, M. I., Marcassa, E., et al. (2021). Non-canonical autophagy drives alternative ATG8 conjugation to phosphatidylserine. *Mol. Cell.* 81 (9), 2031–2040.e8. doi:10.1016/j.molcel.2021.03.020

Eapen, V. V., Swarup, S., Hoyer, M. J., Paulo, J. A., and Harper, J. W. (2021). Quantitative proteomics reveals the selectivity of ubiquitin-binding autophagy receptors in the turnover of damaged lysosomes by lysophagy. *Elife* 10, e72328. doi:10.7554/eLife.72328

Eguchi, T., Sakurai, M., Wang, Y., Saito, C., Yoshii, G., Wileman, T., et al. (2024). The V-ATPase-ATG16L1 axis recruits LRRK2 to facilitate the lysosomal stress response. *J. Cell. Biol.* 223 (3), e202302067. doi:10.1083/jcb.202302067

Ekinci, I. B., Chlodowska, A., and Olejnik, M. (2023). Ionophore toxicity in animals: a review of clinical and molecular aspects. *Int. J. Mol. Sci.* 24 (2), 1696. doi:10.3390/ijms24021696

Ellison, C. J., Kukulski, W., Boyle, K. B., Munro, S., and Randow, F. (2020). Transbilayer movement of sphingomyelin precedes catastrophic breakage of enterobacteria-containing vacuoles. *Curr. Biol.* 30 (15), 2974–2983. doi:10.1016/j.cub.2020.05.083

Eskelinen, E. L., Tanaka, Y., and Saftig, P. (2003). At the acidic edge: emerging functions for lysosomal membrane proteins. *Trends Cell. Biol.* 13 (3), 137–145. doi:10.1016/s0962-8924(03)00005-9

Figueras-Novoa, C., Timimi, L., Marcassa, E., Ulferts, R., and Beale, R. (2024). Conjugation of ATG8s to single membranes at a glance. *J. Cell. Sci.* 137 (15), jcs261031. doi:10.1242/jcs.261031

Fischer, T. D., Wang, C., Padman, B. S., Lazarou, M., and Youle, R. J. (2020). STING induces LC3B lipidation onto single-membrane vesicles via the V-ATPase and ATG16L1-WD40 domain. *J. Cell. Biol.* 219 (12), e202009128. doi:10.1083/jcb.202009128

Fletcher, K., Ulferts, R., Jacquin, E., Veith, T., Gammoh, N., Arasteh, J. M., et al. (2018). The WD40 domain of ATG16L1 is required for its non-canonical role in lipidation of LC3 at single membranes. *EMBO J.* 37 (4), e97840. doi:10.15252/embj.201797840

Florey, O., Gammoh, N., Kim, S. E., Jiang, X., and Overholtzer, M. (2015). V-ATPase and osmotic imbalances activate endolysosomal LC3 lipidation. *Autophagy* 11 (1), 88–99. doi:10.4161/15548627.2014.984277

Freeman, S. A., Grinstein, S., and Orlowski, J. (2023). Determinants, maintenance, and function of organellar pH. *Physiol. Rev.* 103 (1), 515–606. doi:10.1152/physrev.00009.2022

Fujita, N., Itoh, T., Omori, H., Fukuda, M., Noda, T., and Yoshimori, T. (2008). The Atg16L complex specifies the site of LC3 lipidation for membrane biogenesis in autophagy. *Mol. Biol. Cell.* 19 (5), 2092–2100. doi:10.1091/mbc.e07-12-1257

Fukuda, M. (1991). Lysosomal membrane glycoproteins. Structure, biosynthesis, and intracellular trafficking. *J. Biol. Chem.* 266 (32), 21327–21330. doi:10.1016/s0021-9258(18)54636-6

Gahlot, P., Kravic, B., Rota, G., van den Boom, J., Levantovsky, S., Schulze, N., et al. (2024). Lysosomal damage sensing and lysophagy initiation by SPG20-ITCH. *Mol. Cell.* 84 (8), 1556–1569.e10. doi:10.1016/j.molcel.2024.02.029

Gallala, H. D., and Sandhoff, K. (2011). Biological function of the cellular lipid BMP-BMP as a key activator for cholesterol sorting and membrane digestion. *Neurochem. Res.* 36 (9), 1594–1600. doi:10.1007/s11064-010-0337-6

Gao, Y., Liu, Y., Hong, L., Yang, Z., Cai, X., Chen, X., et al. (2016). Golgi-associated LC3 lipidation requires V-ATPase in noncanonical autophagy. *Cell. Death Dis.* 7 (8), e2330. doi:10.1038/cddis.2016.236

Gatica, D., Lahiri, V., and Klionsky, D. J. (2018). Cargo recognition and degradation by selective autophagy. *Nat. Cell. Biol.* 20 (3), 233–242. doi:10.1038/s41556-018-0037-z

Ghanbarpour, A., Valverde, D. P., Melia, T. J., and Reinisch, K. M. (2021). A model for a partnership of lipid transfer proteins and scramblases in membrane expansion and organelle biogenesis. *Proc. Natl. Acad. Sci. U. S. A.* 118 (16), e2101562118. doi:10.1073/pnas.2101562118

Goodwin, J. M., Walkup, W. G. t., Hooper, K., Li, T., Kishi-Itakura, C., Ng, A., et al. (2021). GABARAP sequesters the FLCN-FNIP tumor suppressor complex to couple autophagy with lysosomal biogenesis. *Sci. Adv.* 7 (40), eabj2485. doi:10.1126/sciadv.abj2485

Gruenberg, J. (2020). Life in the lumen: the multivesicular endosome. *Traffic* 21 (1), 76–93. doi:10.1111/tra.12715

Hanna, M., Guillen-Samander, A., and De Camilli, P. (2023). RBG motif bridge-like lipid transport proteins: structure, functions, and open questions. *Annu. Rev. Cell. Dev. Biol.* 39, 409–434. doi:10.1146/annurev-cellbio-120420-014634

Hanna, M. G., Rodriguez Cruz, H. O., Fujise, K., Wu, Y., Xu, C. S., Pang, S., et al. (2025). BLTP3A is associated with membranes of the late endocytic pathway and is an effector of CASM. *bioRxiv* 2024, 615015. doi:10.1101/2024.09.28.615015

Hasegawa, J., Strunk, B. S., and Weisman, L. S. (2017). PI5P and PI(3,5)P(2): minor, but essential phosphoinositides. *Cell. Struct. Funct.* 42 (1), 49–60. doi:10.1247/csf.17003

Heckmann, B. L., Teubner, B. J. W., Tummers, B., Boada-Romero, E., Harris, L., Yang, M., et al. (2019). LC3-Associated endocytosis facilitates beta-amyloid clearance and mitigates neurodegeneration in murine Alzheimer's disease. *Cell.* 178 (3), 536–551. doi:10.1016/j.cell.2019.05.056

Henry, A. G., Aghamohammadzadeh, S., Samaroo, H., Chen, Y., Mou, K., Needle, E., et al. (2015). Pathogenic LRRK2 mutations, through increased kinase activity, produce enlarged lysosomes with reduced degradative capacity and increase ATP13A2 expression. *Hum. Mol. Genet.* 24 (21), 6013–6028. doi:10.1093/hmg/ddv314

Hockey, L. N., Kilpatrick, B. S., Eden, E. R., Lin-Moshier, Y., Brailoiu, G. C., Brailoiu, E., et al. (2015). Dysregulation of lysosomal morphology by pathogenic LRRK2 is corrected by TPC2 inhibition. *J. Cell. Sci.* 128 (2), 232–238. doi:10.1242/jcs.164152

Hooper, K. M., Jacquin, E., Li, T., Goodwin, J. M., Brumell, J. H., Durgan, J., et al. (2022). V-ATPase is a universal regulator of LC3-associated phagocytosis and non-canonical autophagy. *J. Cell. Biol.* 221 (6), e202105112. doi:10.1083/jcb.202105112

Hu, M., Feng, X., Liu, Q., Liu, S., Huang, F., and Xu, H. (2024). The ion channels of endomembranes. *Physiol. Rev.* 104 (3), 1335–1385. doi:10.1152/physrev.00025.2023

Hui, K. Y., Fernandez-Hernandez, H., Hu, J., Schaffner, A., Pankratz, N., Hsu, N. Y., et al. (2018). Functional variants in the LRRK2 gene confer shared effects on risk for Crohn's disease and Parkinson's disease. *Sci. Transl. Med.* 10 (423), eaai7795. doi:10.1126/scitranslmed.aai7795

Jacob, R., and Gorek, L. S. (2024). Intracellular galectin interactions in health and disease. *Semin. Immunopathol.* 46 (1-2), 4. doi:10.1007/s00281-024-01010-z

Jacquin, E., Leclerc-Mercier, S., Judon, C., Blanchard, E., Fraitag, S., and Florey, O. (2017). Pharmacological modulators of autophagy activate a parallel noncanonical pathway driving unconventional LC3 lipidation. *Autophagy* 13 (5), 854–867. doi:10.1080/15548627.2017.1287653

Jadot, M., Colmant, C., Wattiaux-De Coninck, S., and Wattiaux, R. (1984). Intralysosomal hydrolysis of glycyl-L-phenylalanine 2-naphthylamide. *Biochem. J.* 219 (3), 965–970. doi:10.1042/bj2190965

Jaskolka, M. C., Winkley, S. R., and Kane, P. M. (2021). RAVE and rabconnectin-3 complexes as signal dependent regulators of organelle acidification. *Front. Cell. Dev. Biol.* 9, 698190. doi:10.3389/fcell.2021.698190

Jia, J., Wang, F., Bhujabal, Z., Peters, R., Mudd, M., Duque, T., et al. (2022). Stress granules and mTOR are regulated by membrane atg8ylation during lysosomal damage. *J. Cell. Biol.* 221 (11), e202207091. doi:10.1083/jcb.202207091

Johannes, L., Jacob, R., and Leffler, H. (2018). Galectins at a glance. *J. Cell. Sci.* 131 (9), jcs208884. doi:10.1242/jcs.208884

Johansen, T., and Lamark, T. (2020). Selective autophagy: ATG8 family proteins, LIR motifs and cargo receptors. *J. Mol. Biol.* 432 (1), 80–103. doi:10.1016/j.jmb.2019.07.016

Johnson, D. E., Ostrowski, P., Jaumouille, V., and Grinstein, S. (2016). The position of lysosomes within the cell determines their luminal pH. *J. Cell. Biol.* 212 (6), 677–692. doi:10.1083/jcb.201507112

Karp, J. M., and Peer, D. (2018). Focus on RNA interference: from nanoformulations to *in vivo* delivery. *Nanotechnology* 29 (1), 010201. doi:10.1088/1361-6528/aa98e3

Kauffman, K. J., Yu, S., Jin, J., Mugo, B., Nguyen, N., O'Brien, A., et al. (2018). Delipidation of mammalian Atg8-family proteins by each of the four ATG4 proteases. *Autophagy* 14 (6), 992–1010. doi:10.1080/15548627.2018.1437341

Kaur, N., Carlsson, S. R., and Lystad, A. H. (2024). The separate axes of TECPR1 and ATG16L1 in CASM. *Autophagy* 20 (1), 214–215. doi:10.1080/15548627.2023.2255462

Kaur, N., de la Ballina, L. R., Haukaas, H. S., Torgersen, M. L., Radulovic, M., Munson, M. J., et al. (2023). TECPR1 is activated by damage-induced sphingomyelin exposure to mediate noncanonical autophagy. *EMBO J.* 42 (17), e113105. doi:10.15252/embj.2022113105

Kendall, R. L., and Holian, A. (2023). Cholesterol-dependent molecular mechanisms contribute to cationic amphiphilic drugs' prevention of silica-induced inflammation. *Eur. J. Cell. Biol.* 102 (2), 151310. doi:10.1016/j.ejcb.2023.151310

Klein, A. D., Petruzzi, K. L., Lee, C., and Overholtzer, M. (2024). Stress-induced microautophagy is coordinated with lysosome biogenesis and regulated by PIKfyve. *Mol. Biol. Cell.* 35 (5), ar70. doi:10.1091/mbc.E23-08-0332

Kolter, T., and Sandhoff, K. (2005). Principles of lysosomal membrane digestion: stimulation of sphingolipid degradation by sphingolipid activator proteins and anionic lysosomal lipids. *Annu. Rev. Cell. Dev. Biol.* 21, 81–103. doi:10.1146/annurev.cellbio.21.122303.120013

Kornhuber, J., Tripal, P., Reichel, M., Muhle, C., Rhein, C., Muehlbacher, M., et al. (2010). Functional Inhibitors of Acid Sphingomyelinase (FIASMAs): a novel pharmacological group of drugs with broad clinical applications. *Cell. Physiol. Biochem.* 26 (1), 9–20. doi:10.1159/000315101

Krajcovic, M., Krishna, S., Akkari, L., Joyce, J. A., and Overholtzer, M. (2013). mTOR regulates phagosome and entotic vacuole fission. *Mol. Biol. Cell.* 24 (23), 3736–3745. doi:10.1091/mbc.E13-07-0408

Kundra, R., and Kornfeld, S. (1999). Asparagine-linked oligosaccharides protect Lamp-1 and Lamp-2 from intracellular proteolysis. *J. Biol. Chem.* 274 (43), 31039–31046. doi:10.1074/jbc.274.43.31039

Lamark, T., and Johansen, T. (2021). Mechanisms of selective autophagy. *Annu. Rev. Cell. Dev. Biol.* 37, 143–169. doi:10.1146/annurev-cellbio-120219-035530

Lancaster, C. E., Fountain, A., Dayam, R. M., Somerville, E., Sheth, J., Jacobelli, V., et al. (2021). Phagosome resolution regenerates lysosomes and maintains the degradative capacity in phagocytes. *J. Cell. Biol.* 220 (9), e202005072. doi:10.1083/jcb.202005072

Lee, C., Lamech, L., Johns, E., and Overholtzer, M. (2020). Selective lysosome membrane turnover is induced by nutrient starvation. *Dev. Cell.* 55 (3), 289–297. doi:10.1016/j.devcel.2020.08.008

Leidal, A. M., Huang, H. H., Marsh, T., Solvik, T., Zhang, D., Ye, J., et al. (2020). The LC3-conjugation machinery specifies the loading of RNA-binding proteins into extracellular vesicles. *Nat. Cell. Biol.* 22 (2), 187–199. doi:10.1038/s41556-019-0450-y

Leonzino, M., Reinisch, K. M., and De Camilli, P. (2021). Insights into VPS13 properties and function reveal a new mechanism of eukaryotic lipid transport. *Biochim. Biophys. Acta Mol. Cell. Biol. Lipids* 1866 (10), 159003. doi:10.1016/j.bbalip.2021.159003

Li, M., Rong, Y., Chuang, Y. S., Peng, D., and Emr, S. D. (2015). Ubiquitin-dependent lysosomal membrane protein sorting and degradation. *Mol. Cell.* 57 (3), 467–478. doi:10.1016/j.molcel.2014.12.012

Li, X., Rydzewski, N., Hider, A., Zhang, X., Yang, J., Wang, W., et al. (2016). A molecular mechanism to regulate lysosome motility for lysosome positioning and tubulation. *Nat. Cell. Biol.* 18 (4), 404–417. doi:10.1038/ncb3324

Liu, B., Carlson, R. J., Pires, I. S., Gentili, M., Feng, E., Hellier, Q., et al. (2023). Human STING is a proton channel. *Science* 381 (6657), 508–514. doi:10.1126/science.adf8974

Liu, G. Y., and Sabatini, D. M. (2020). mTOR at the nexus of nutrition, growth, ageing and disease. *Nat. Rev. Mol. Cell. Biol.* 21 (4), 183–203. doi:10.1038/s41580-019-0199-y

Lv, B., Dion, W. A., Yang, H., Xun, J., Kim, D. H., Zhu, B., et al. (2024). A TBK1-independent primordial function of STING in lysosomal biogenesis. *Mol. Cell.* 84 (20), 3979–3996.e9. doi:10.1016/j.molcel.2024.08.026

Lystad, A. H., Carlsson, S. R., de la Ballina, L. R., Kauffman, K. J., Nag, S., Yoshimori, T., et al. (2019). Distinct functions of ATG16L1 isoforms in membrane binding and LC3B lipidation in autophagy-related processes. *Nat. Cell. Biol.* 21 (3), 372–383. doi:10.1038/s41556-019-0274-9

Maejima, I., Takahashi, A., Omori, H., Kimura, T., Takabatake, Y., Saitoh, T., et al. (2013). Autophagy sequesters damaged lysosomes to control lysosomal biogenesis and kidney injury. *EMBO J.* 32 (17), 2336–2347. doi:10.1038/emboj.2013.171

Magne, J., and Green, D. R. (2022). LC3-associated endocytosis and the functions of Rubicon and ATG16L1. *Sci. Adv.* 8 (43), eabo5600. doi:10.1126/sciadv.abo5600

Martina, J. A., Chen, Y., Gucek, M., and Puertollano, R. (2012). MTORC1 functions as a transcriptional regulator of autophagy by preventing nuclear transport of TFEB. *Autophagy* 8 (6), 903–914. doi:10.4161/auto.19653

Maxfield, F. R., and van Meer, G. (2010). Cholesterol, the central lipid of mammalian cells. *Curr. Opin. Cell. Biol.* 22 (4), 422–429. doi:10.1016/j.ceb.2010.05.004

Meng, Y., Heybrock, S., Neculai, D., and Saftig, P. (2020). Cholesterol handling in lysosomes and beyond. *Trends Cell. Biol.* 30 (6), 452–466. doi:10.1016/j.tcb.2020.02.007

Meyer, H., and Kravic, B. (2024). The endo-lysosomal damage response. *Annu. Rev. Biochem.* 93 (1), 367–387. doi:10.1146/annurev-biochem-030222-102505

Mizushima, N. (2020). The ATG conjugation systems in autophagy. *Curr. Opin. Cell. Biol.* 63, 1–10. doi:10.1016/j.ceb.2019.12.001

Mizushima, N., Yoshimori, T., and Ohsumi, Y. (2011). The role of Atg proteins in autophagosome formation. *Annu. Rev. Cell. Dev. Biol.* 27, 107–132. doi:10.1146/annurev-cellbio-092910-154005

Mukai, H., Ogawa, K., Kato, N., and Kawakami, S. (2022). Recent advances in lipid nanoparticles for delivery of nucleic acid, mRNA, and gene editing-based therapeutics. *Drug Metab. Pharmacokinet.* 44, 100450. doi:10.1016/j.dmpk.2022.100450

Murrow, L., Malhotra, R., and Debnath, J. (2015). ATG12-ATG3 interacts with Alix to promote basal autophagic flux and late endosome function. *Nat. Cell. Biol.* 17 (3), 300–310. doi:10.1038/ncb3112

Nakamura, S., Shigeyama, S., Minami, S., Shima, T., Akayama, S., Matsuda, T., et al. (2020). LC3 lipidation is essential for TFEB activation during the lysosomal damage response to kidney injury. *Nat. Cell. Biol.* 22 (10), 1252–1263. doi:10.1038/s41556-020-00583-9

Napolitano, G., Di Malta, C., Esposito, A., de Araujo, M. E. G., Pece, S., Bertalot, G., et al. (2020). A substrate-specific mTORC1 pathway underlies Birt-Hogg-Dube syndrome. *Nature* 585 (7826), 597–602. doi:10.1038/s41586-020-2444-0

Nguyen, T. N., Padman, B. S., Zellner, S., Khuu, G., Uoselis, L., Lam, W. K., et al. (2021). ATG4 family proteins drive phagophore growth independently of the LC3/GABARAP lipidation system. *Mol. Cell.* 81 (9), 2013–2030.e9. doi:10.1016/j.molcel.2021.03.001

Niekamp, P., Scharte, F., Sokoya, T., Vittadello, L., Kim, Y., Deng, Y., et al. (2022). Ca(2+)-activated sphingomyelin scrambling and turnover mediate ESCRT-independent lysosomal repair. *Nat. Commun.* 13 (1), 1875. doi:10.1038/s41467-022-29481-4

Ogawa, M., Yoshikawa, Y., Kobayashi, T., Mimuro, H., Fukumatsu, M., Kiga, K., et al. (2011). A Tecpr1-dependent selective autophagy pathway targets bacterial pathogens. *Cell. Host Microbe* 9 (5), 376–389. doi:10.1016/j.chom.2011.04.010

Ogura, M., Kaminishi, T., Shima, T., Torigata, M., Bekku, N., Tabata, K., et al. (2023). Microautophagy regulated by STK38 and GABARAPs is essential to repair lysosomes and prevent aging. *EMBO Rep.* 24 (12), e57300. doi:10.15252/embr.202357300

Ohsumi, Y. (2014). Historical landmarks of autophagy research. *Cell. Res.* 24 (1), 9–23. doi:10.1038/cr.2013.169

Omrane, M., Ben M'Barek, K., Santinho, A., Nguyen, N., Nag, S., Melia, T. J., et al. (2023). LC3B is lipidated to large lipid droplets during prolonged starvation for noncanonical autophagy. *Dev. Cell.* 58 (14), 1266–1281 e1267. doi:10.1016/j.devcel.2023.05.009

Paddar, M. A., Wang, F., Trosdal, E. S., Hendrix, E., He, Y., Salemi, M. R., et al. (2025). Noncanonical roles of ATG5 and membrane atg8ylation in retromer assembly and function. *Elife* 13. doi:10.7554/eLife.100928

Papadopoulos, C., Kravic, B., and Meyer, H. (2020). Repair or lysophagy: dealing with damaged lysosomes. *J. Mol. Biol.* 432 (1), 231–239. doi:10.1016/j.jmb.2019.08.010

Papadopoulos, C., and Meyer, H. (2017). Detection and clearance of damaged lysosomes by the endo-lysosomal damage response and lysophagy. *Curr. Biol.* 27 (24), R1330–R1341. doi:10.1016/j.cub.2017.11.012

Pena-Martinez, C., Rickman, A. D., and Heckmann, B. L. (2022). Beyond autophagy: LC3-associated phagocytosis and endocytosis. *Sci. Adv.* 8 (43), eabn1702. doi:10.1126/sciadv.abn1702

Pinto, L. H., Holsinger, L. J., and Lamb, R. A. (1992). Influenza virus M2 protein has ion channel activity. *Cell.* 69 (3), 517–528. doi:10.1016/0092-8674(92)90452-i

Platt, F. M., d'Azzo, A., Davidson, B. L., Neufeld, E. F., and Tifft, C. J. (2018). Lysosomal storage diseases. *Nat. Rev. Dis. Prim.* 4 (1), 27. doi:10.1038/s41572-018-0025-4

Posor, Y., Jang, W., and Haucke, V. (2022). Phosphoinositides as membrane organizers. *Nat. Rev. Mol. Cell. Biol.* 23 (12), 797–816. doi:10.1038/s41580-022-00490-x

Pryor, P. R., Mullock, B. M., Bright, N. A., Gray, S. R., and Luzio, J. P. (2000). The role of intraorganellar Ca(2+) in late endosome-lysosome heterotypic fusion and in the reformation of lysosomes from hybrid organelles. *J. Cell. Biol.* 149 (5), 1053–1062. doi:10.1083/jcb.149.5.1053

Radulovic, M., Schink, K. O., Wenzel, E. M., Nahse, V., Bongiovanni, A., Lafont, F., et al. (2018). ESCRT-mediated lysosome repair precedes lysophagy and promotes cell survival. *EMBO J.* 37 (21), e99753. doi:10.15252/embj.201899753

Radulovic, M., Wenzel, E. M., Gilani, S., Holland, L. K., Lystad, A. H., Phuyal, S., et al. (2022). Cholesterol transfer via endoplasmic reticulum contacts mediates lysosome damage repair. *EMBO J.* 41 (24), e112677. doi:10.15252/embj.2022112677

Rai, S., Arasteh, M., Jefferson, M., Pearson, T., Wang, Y., Zhang, W., et al. (2019). The ATG5-binding and coiled coil domains of ATG16L1 maintain autophagy and tissue homeostasis in mice independently of the WD domain required for LC3-associated phagocytosis. *Autophagy* 15 (4), 599–612. doi:10.1080/15548627.2018.1534507

Rebsamen, M., Pochini, L., Stasyk, T., de Araujo, M. E., Galluccio, M., Kandasamy, R. K., et al. (2015). SLC38A9 is a component of the lysosomal amino acid sensing machinery that controls mTORC1. *Nature* 519 (7544), 477–481. doi:10.1038/nature14107

Repnik, U., Borg Distefano, M., Speth, M. T., Ng, M. Y. W., Progida, C., Hoflack, B., et al. (2017). L-leucyl-L-leucine methyl ester does not release cysteine cathepsins to the cytosol but inactivates them in transiently permeabilized lysosomes. *J. Cell. Sci.* 130 (18), 3124–3140. doi:10.1242/jcs.204529

Repnik, U., Hafner Cesen, M., and Turk, B. (2014). Lysosomal membrane permeabilization in cell death: concepts and challenges. *Mitochondrion* A, 49–57. doi:10.1016/j.mito.2014.06.006

Riederer, E., Cang, C., and Ren, D. (2023). Lysosomal ion channels: what are they good for and are they druggable targets? *Annu. Rev. Pharmacol. Toxicol.* 63, 19–41. doi:10.1146/annurev-pharmtox-051921-013755

Roczniak-Ferguson, A., Petit, C. S., Froehlich, F., Qian, S., Ky, J., Angarola, B., et al. (2012). The transcription factor TFEB links mTORC1 signaling to transcriptional control of lysosome homeostasis. *Sci. Signal* 5 (228), ra42. doi:10.1126/scisignal.2002790

Rodgers, S. J., Jones, E. I., Arumugam, S., Hamila, S. A., Danne, J., Gurung, R., et al. (2022). Endosome maturation links PI3Kα signaling to lysosome repopulation during basal autophagy. *EMBO J.* 41 (19), e110398. doi:10.15252/embj.2021110398

Rogov, V. V., Nezis, I. P., Tsapras, P., Zhang, H., Dagdas, Y., Noda, N. N., et al. (2023). Atg8 family proteins, LIR/AIM motifs and other interaction modes. *Autophagy Rep.* 2 (1), 2188523. doi:10.1080/27694127.2023.2188523

Saftig, P., and Klumperman, J. (2009). Lysosome biogenesis and lysosomal membrane proteins: trafficking meets function. *Nat. Rev. Mol. Cell. Biol.* 10 (9), 623–635. doi:10.1038/nrm2745

Sahu, R., Kaushik, S., Clement, C. C., Cannizzo, E. S., Scharf, B., Follenzi, A., et al. (2011). Microautophagy of cytosolic proteins by late endosomes. *Dev. Cell.* 20 (1), 131–139. doi:10.1016/j.devcel.2010.12.003

Sanjuan, M. A., Dillon, C. P., Tait, S. W., Moshiach, S., Dorsey, F., Connell, S., et al. (2007). Toll-like receptor signalling in macrophages links the autophagy pathway to phagocytosis. *Nature* 450 (7173), 1253–1257. doi:10.1038/nature06421

Sardiello, M., Palmieri, M., di Ronza, A., Medina, D. L., Valenza, M., Gennarino, V. A., et al. (2009). A gene network regulating lysosomal biogenesis and function. *Science* 325 (5939), 473–477. doi:10.1126/science.1174447

Sava, I., Davis, L. J., Gray, S. R., Bright, N. A., and Luzio, J. P. (2024). Reversible assembly and disassembly of V-ATPase during the lysosome regeneration cycle. *Mol. Biol. Cell.* 35 (5), ar63. doi:10.1091/mbc.E23-08-0322

Scherz-Shouval, R., Sagiv, Y., Shorer, H., and Elazar, Z. (2003). The COOH terminus of GATE-16, an intra-Golgi transport modulator, is cleaved by the human cysteine protease HsApg4A. *J. Biol. Chem.* 278 (16), 14053–14058. doi:10.1074/jbc.M212108200

Schmuckli-Maurer, J., Bindschedler, A. F., Wacker, R., Wurgler, O. M., Rehmann, R., Lehmberg, T., et al. (2024). Plasmodium berghei liver stage parasites exploit host GABARAP proteins for TFEB activation. *Commun. Biol.* 7 (1), 1554. doi:10.1038/s42003-024-07242-x

Schuck, S., Gallagher, C. M., and Walter, P. (2014). ER-phagy mediates selective degradation of endoplasmic reticulum independently of the core autophagy machinery. *J. Cell. Sci.* 127 (18), 4078–4088. doi:10.1242/jcs.154716

Settembre, C., and Perera, R. M. (2024). Lysosomes as coordinators of cellular catabolism, metabolic signalling and organ physiology. *Nat. Rev. Mol. Cell. Biol.* 25 (3), 223–245. doi:10.1038/s41580-023-00676-x

Settembre, C., Zoncu, R., Medina, D. L., Vetrini, F., Erdin, S., Erdin, S., et al. (2012). A lysosome-to-nucleus signalling mechanism senses and regulates the lysosome via mTOR and TFEB. *EMBO J.* 31 (5), 1095–1108. doi:10.1038/emboj.2012.32

Shpilka, T., Weidberg, H., Pietrokovski, S., and Elazar, Z. (2011). Atg8: an autophagy-related ubiquitin-like protein family. *Genome Biol.* 12 (7), 226. doi:10.1186/gb-2011-12-7-226

Shukla, S., Larsen, K. P., Ou, C., Rose, K., and Hurley, J. H. (2022). *In vitro* reconstitution of calcium-dependent recruitment of the human ESCRT machinery in lysosomal membrane repair. *Proc. Natl. Acad. Sci. U. S. A.* 119 (35), e2205590119. doi:10.1073/pnas.2205590119

Skowyra, M. L., Schlesinger, P. H., Naismith, T. V., and Hanson, P. I. (2018). Triggered recruitment of ESCRT machinery promotes endolysosomal repair. *Science* 360 (6384), eaar5078. doi:10.1126/science.aar5078

Steger, M., Diez, F., Dhekne, H. S., Lis, P., Nirujogi, R. S., Karayel, O., et al. (2017). Systematic proteomic analysis of LRRK2-mediated Rab GTPase phosphorylation establishes a connection to ciliogenesis. *Elife* 6, e31012. doi:10.7554/eLife.31012

Steger, M., Tonelli, F., Ito, G., Davies, P., Trost, M., Vetter, M., et al. (2016). Phosphoproteomics reveals that Parkinson's disease kinase LRRK2 regulates a subset of Rab GTPases. *Elife* 5, e12813. doi:10.7554/eLife.12813

Sun, Y., Wang, X., Yang, X., Wang, L., Ding, J., Wang, C. C., et al. (2023). V-ATPase recruitment to ER exit sites switches COPII-mediated transport to lysosomal degradation. *Dev. Cell.* 58 (23), 2761–2775.e5. doi:10.1016/j.devcel.2023.10.007

Tan, J. X., and Finkel, T. (2022). A phosphoinositide signalling pathway mediates rapid lysosomal repair. *Nature* 609 (7928), 815–821. doi:10.1038/s41586-022-05164-4

Tanida, I., Sou, Y. S., Ezaki, J., Minematsu-Ikeguchi, N., Ueno, T., and Kominami, E. (2004). HsAtg4B/HsApg4B/autophagin-1 cleaves the carboxyl termini of three human Atg8 homologues and delipidates microtubule-associated protein light chain 3- and GABAA receptor-associated protein-phospholipid conjugates. *J. Biol. Chem.* 279 (35), 36268–36276. doi:10.1074/jbc.M401461200

Thiele, D. L., and Lipsky, P. E. (1990). Mechanism of L-leucyl-L-leucine methyl ester-mediated killing of cytotoxic lymphocytes: dependence on a lysosomal thiol protease, dipeptidyl peptidase I, that is enriched in these cells. *Proc. Natl. Acad. Sci. U. S. A.* 87 (1), 83–87. doi:10.1073/pnas.87.1.83

Timimi, L., Wrobel, A. G., Chiduza, G. N., Maslen, S. L., Torres-Mendez, A., Montaner, B., et al. (2024). The V-ATPase/ATG16L1 axis is controlled by the V(1)H subunit. *Mol. Cell.* 84 (15), 2966–2983.e9. doi:10.1016/j.molcel.2024.07.003

Tsun, Z. Y., Bar-Peled, L., Chantranupong, L., Zoncu, R., Wang, T., Kim, C., et al. (2013). The folliculin tumor suppressor is a GAP for the RagC/D GTPases that signal amino acid levels to mTORC1. *Mol. Cell.* 52 (4), 495–505. doi:10.1016/j.molcel.2013.09.016

Ulferts, R., Marcassa, E., Timimi, L., Lee, L. C., Daley, A., Montaner, B., et al. (2021). Subtractive CRISPR screen identifies the ATG16L1/vacuolar ATPase axis as required for non-canonical LC3 lipidation. *Cell. Rep.* 37 (4), 109899. doi:10.1016/j.celrep.2021.109899

van Meer, G. (2011). Dynamic transbilayer lipid asymmetry. *Cold Spring Harb. Perspect. Biol.* 3 (5), a004671. doi:10.1101/cshperspect.a004671

Vargas, J. N. S., Hamasaki, M., Kawabata, T., Youle, R. J., and Yoshimori, T. (2023). The mechanisms and roles of selective autophagy in mammals. *Nat. Rev. Mol. Cell. Biol.* 24 (3), 167–185. doi:10.1038/s41580-022-00542-2

Vietri, M., Radulovic, M., and Stenmark, H. (2020). The many functions of ESCRTs. *Nat. Rev. Mol. Cell. Biol.* 21 (1), 25–42. doi:10.1038/s41580-019-0177-4

Wang, F., Peters, R., Jia, J., Mudd, M., Salemi, M., Allers, L., et al. (2023a). ATG5 provides host protection acting as a switch in the atg8ylation cascade between autophagy and secretion. *Dev. Cell.* 58 (10), 866–884.e8. doi:10.1016/j.devcel.2023.03.014

Wang, L., Klionsky, D. J., and Shen, H. M. (2023b). The emerging mechanisms and functions of microautophagy. *Nat. Rev. Mol. Cell. Biol.* 24 (3), 186–203. doi:10.1038/s41580-022-00529-z

Wang, X., Xu, P., Bentley-DeSousa, A., Hancock-Cerutti, W., Cai, S., Johnson, B. T., et al. (2025). Lysosome damage triggers acute formation of ER to lysosomes membrane tethers mediated by the bridge-like lipid transport protein VPS13C. *bioRxiv* 2024, 598070. doi:10.1101/2024.06.08.598070

Wang, Y., Jefferson, M., Whelband, M., Kreuzer, K., Mccoll, J., Verkade, P., et al. (2023c). TECPR1 provides E3-ligase like activity to the ATG5-ATG12 complex to conjugate LC3/ATG8 to damaged lysosomes. *bioRxiv* 2023. 2006.2024.546289. doi:10.1101/2023.06.24.546289

Wang, Y., Ramos, M., Jefferson, M., Zhang, W., Beraza, N., Carding, S., et al. (2022). Control of infection by LC3-associated phagocytosis, CASM, and detection of raised vacuolar pH by the V-ATPase-ATG16L1 axis. *Sci. Adv.* 8 (43), eabn3298. doi:10.1126/sciadv.abn3298

Wang, Y., Sharma, P., Jefferson, M., Zhang, W., Bone, B., Kipar, A., et al. (2021). Non-canonical autophagy functions of ATG16L1 in epithelial cells limit lethal infection by influenza A virus. *EMBO J.* 40 (6), e105543. doi:10.15252/embj.2020105543

Wu, S., Lin, L., Shi, L., and Liu, S. (2024). An overview of lipid constituents in lipid nanoparticle mRNA delivery systems. *Wiley Interdiscip. Rev. Nanomed Nanobiotechnol* 16 (4), e1978. doi:10.1002/wnan.1978

Xu, Y., Zhou, P., Cheng, S., Lu, Q., Nowak, K., Hopp, A. K., et al. (2019). A bacterial effector reveals the V-ATPase-ATG16L1 axis that initiates xenophagy. *Cell.* 178 (3), 552–566. doi:10.1016/j.cell.2019.06.007

Yamamoto, H., Zhang, S., and Mizushima, N. (2023). Autophagy genes in biology and disease. *Nat. Rev. Genet.* 24 (6), 382–400. doi:10.1038/s41576-022-00562-w

Yang, C., and Wang, X. (2021). Lysosome biogenesis: regulation and functions. *J. Cell. Biol.* 220 (6), e202102001. doi:10.1083/jcb.202102001

Yeung, T., Heit, B., Dubuisson, J. F., Fairn, G. D., Chiu, B., Inman, R., et al. (2009). Contribution of phosphatidylserine to membrane surface charge and protein targeting during phagosome maturation. *J. Cell. Biol.* 185 (5), 917–928. doi:10.1083/jcb.200903020

Yim, W. W., and Mizushima, N. (2020). Lysosome biology in autophagy. *Cell. Discov.* 6, 6. doi:10.1038/s41421-020-0141-7

Yu, L., McPhee, C. K., Zheng, L., Mardones, G. A., Rong, Y., Peng, J., et al. (2010). Termination of autophagy and reformation of lysosomes regulated by mTOR. *Nature* 465 (7300), 942–946. doi:10.1038/nature09076

Zhen, Y., Radulovic, M., Vietri, M., and Stenmark, H. (2021). Sealing holes in cellular membranes. *EMBO J.* 40 (7), e106922. doi:10.15252/embj.2020106922

Zoncu, R., and Perera, R. M. (2022). Built to last: lysosome remodeling and repair in health and disease. *Trends Cell. Biol.* 32 (7), 597–610. doi:10.1016/j.tcb.2021.12.009

frontiers | Frontiers in Cell and Developmental Biology

TYPE Original Research
PUBLISHED 28 April 2025
DOI 10.3389/fcell.2025.1571198

Check for updates

OPEN ACCESS

EDITED BY
Jingyue Jia Cassano,
University of New Mexico, United States

REVIEWED BY
Fulong Wang,
Southeast University, China
Chunqing Wang,
University of New Mexico, United States

*CORRESPONDENCE
Wenyan Bi,
biwenyan@hpu.edu.cn

RECEIVED 05 February 2025
ACCEPTED 03 April 2025
PUBLISHED 28 April 2025

CITATION
Li W, Yang X, Bi W, Song L and Liu B (2025) Effect of low-frequency assisted ultrasonic on cryopreservation of L-02 hepatocyte cells. *Front. Cell Dev. Biol.* 13:1571198. doi: 10.3389/fcell.2025.1571198

COPYRIGHT
© 2025 Li, Yang, Bi, Song and Liu. This is an open-access article distributed under the terms of the Creative Commons Attribution License (CC BY). The use, distribution or reproduction in other forums is permitted, provided the original author(s) and the copyright owner(s) are credited and that the original publication in this journal is cited, in accordance with accepted academic practice. No use, distribution or reproduction is permitted which does not comply with these terms.

Effect of low-frequency assisted ultrasonic on cryopreservation of L-02 hepatocyte cells

Weijie Li[1], Xi Yang[1], Wenyan Bi[2]*, Liyong Song[1,3,4] and Baolin Liu[1,3,4]

[1]Institute of Biothermal Science and Technology, University of Shanghai for Science and Technology, Shanghai, China, [2]College of Chemistry and Chemical Engineering, Henan Polytechnic University, Jiaozuo, Henan, China, [3]Co-Innovation Center for Energy Therapy of Tumors, Shanghai, China, [4]Shanghai Technical Service Platform for Cryopreservation of Biological Resources, Shanghai, China

Developing bioartificial liver and hepatocyte transplantation technology causes increasing hepatocyte cell demand. Effective long-term hepatocyte cell preservation methods are necessary to promote. Progressive cooling is a key preservation technology for cell banks. However, the cell solution needs to be supercooled in a slow freezing process. The high degree of supercooling possibly induces uncontrollable intracellular ice formation. This work designs an ultrasonic ice-seeding system for L-02 hepatocyte cell preservation, reducing supercooling and improving cell survival rate. The effect of ultrasonic intensities on the hepatocyte's survival rate was investigated and optimized. The results prove the calorimetric method can efficiently measure the ultrasonic intensity dissipated in the hepatocyte cell preservation solution. When the ultrasonic intensity is 0.0329 W/cm^2 ~ 0.4316 W/cm^2, the hepatocyte survival rate is over 90%. There is no significant difference between experiment groups ($p < 0.05$) when the ultrasonic intensity is larger than 0.4316 W/cm^2. The hepatocyte cell survival rate reduced significantly with the increase of ultrasonic intensity. The 7-day hepatic function indicator experiment results indicate that the ultrasonic ice seeding has the weakest impact on hepatocyte cells in the four groups. The secretion of urea, albumin and glucose proved that ultrasonic ice seeding technology does not affect cell secretion and has an enormous advantage in cryopreservation. It can be widely applied to cell freezing fields.

KEYWORDS

ultrasonic ice seeding, ultrasonic intensity, hepatocyte, cryopreservation, hepatic function

1 Introduction

Low temperature is beneficial for the cell's long-term preservation. The cooling rate has an enormous impact on the cell's survival. In the long-term hepatocyte preservation process, cells were slowly cooled down to below the freezing point of the cryoprotection solution. Crystal nuclei were then placed in the cryoprotectant to accelerate the nucleation of the cell solution. Finally, continue to cool the cells to below −80°C. Ice nucleates and grows in the extracellular space (Da Costa et al., 2024). However, uncontrolled spontaneous ice nucleation is stochastic. It is detrimental and lethal to cells (Baklanov and Kiselev, 2023; D'Adamo et al., 2023; Qin et al., 2024; Silva et al., 2024). The lower the ice nucleation temperature, the more ice embryo nucleation (Silva et al., 2024). At a low subzero temperature like −10°C or below, the fine ice crystals formed outside cells easily

pierce the cell membrane, causing physical damage and inducing intracellular water to form fine ice crystals. Supercooling conditions will lead to a high intracellular ice formation (IIF) tendency, which is lethal to cells (Baklanov and Kiselev, 2023; D'Adamo et al., 2023; Qin et al., 2024; Silva et al., 2024). In addition, sudden/rapid ice formation will cause the rapid osmosis of the extracellular solution around the growing ice crystals, inducing osmotic shock-type cell damage (OSD) (Silva et al., 2024).

In contrast, controlled ice nucleation at a high subzero temperature enables a reduced nucleation of ice embryos. They gradually grow into large ice crystals outside cells with further cooling, which leaves enough time for intracellular water to diffuse out of cells progressively and minimizes both the IIF and the OSD (Baklanov and Kiselev, 2023; D'Adamo et al., 2023; Qin et al., 2024; Silva et al., 2024). It is crucial for cryopreserving stress-sensitive cells like embryos. The impact degree of cryopreservation is possibly cell-type dependent (Silva et al., 2024; Vorobeva et al., 2023). Several methods control the ice nucleation number of samples during cryopreservation to reduce the damage (Vorobeva et al., 2023; Karasor et al., 2022). Early studies introduced ice crystals into an undercooled sample to manually "seed" ice (O'Kelly Boit, 2023). Later, to reduce the risk of sample contamination, pre-cooled probes, metal rods, or forceps were used to create cold spots from the outside wall of the container (e.g., cryovial), thereby providing localized deep supercooling (usually below −20°C) to induce ice nucleation in a sample that is above −10°C (Silva et al., 2024; Vorobeva et al., 2023; Karasor et al., 2022; O'Kelly Boit, 2023; Parihar et al., 2023). However, manual ice seeding is complex and lengthy to standardize because it often requires multiple trials to induce ice formation. Ice seeding can reduce cell supercooling, produce smaller ice crystals and reduce cell damage. At the same time, it can effectively avoid recrystallization during the rewarming process, improving cell survival (Ahmed et al., 2018; William and Acker, 2020; Mousazadehkasin et al., 2023; Najafi et al., 2023).

The traditional ice seeding method places the cell cryovial in an ice bath at −4°C to pre-cool to sub-zero temperature. Then, the cryovial wall was touched with tweezers or metal needles and pre-cooled in liquid nitrogen (Altmaier et al., 2022; Daily et al., 2020; Jiang et al., 2023; Lindow, 2023; Liu et al., 2021; Mutsenko et al., 2023; Yadegari et al., 2024; Zhang et al., 2024), creating the cryostat local overcooling to induce crystallization. However, these ice seeding methods cause uneven formation of ice crystals. The temperature near the position where tweezers or metal needles touched is lower, and the ice crystals formed are larger. It is easy to cause damage to cells and affect the survival rate and integrity during cell cryopreservation.

In addition, adding ice nucleation bacteria can also induce freezing (Zhang et al., 2024; Abir and Shin, 2024; Daily et al., 2023; Dunn et al., 2023; Tomas et al., 2023), as well as electrodes (Eskandari et al., 2024; Javitt et al., 2023; Mehanna and Abla, 2022; William et al., 2023; Zheng et al., 2018), shaking, vibration, ultrasound (Chen et al., 2024; Maharana et al., 2023; Zilei et al., 2023), etc. Many methods, including changing the cooling rate (Andres et al., 2023), the pressure (Juckers et al., 2024), etc., are also used to induce freezing nucleation. The ultrasound-induced nucleation research focuses on freezing food materials, such as freeze-concentration, freeze-drying of food (Midya and Bandyopadhyay, 2024), medicines, vaccines (Midya and Bandyopadhyay, 2024; Grover and Negi, 2023; Kazarin et al., 2023; Mokhova et al., 2023; Parale et al., 2024; Song et al., 2024), etc.

However, literature on ultrasound-assisted cryopreservation of cells remains limited. Existing research mainly investigates the effects of ultrasound on the permeation of cryoprotectants into cells, tissues, or organs. For instance, ultrasound treatment has been shown to enhance the penetration of cryoprotectants in fish embryos. Yet, it fails to achieve a sufficiently high intracellular cryoprotectant concentration for successful vitrification (Rahman et al., 2017; Bart and Kyaw, 2003). Moreover, the excessive permeation of cryoprotectants at high concentrations poses a risk of cytotoxicity. Thus, further exploration is required to elucidate the role of ultrasound in the cryopreservation of biological tissues and cells. This study focuses on the effect of ultrasound on ice nucleation during cryopreservation, aiming to determine whether appropriate ultrasound treatment can overcome the limitations of conventional cryopreservation methods and improve cell survival rates after freezing.

In studying ultrasonic ice seeding-assisted crystallization, many factors are usually used to describe sonochemical power, including ultrasonic power, meter power, input ultrasonic power, output ultrasonic power, and so on (Nogueira et al., 2023). Thus, comparing the sonochemical results reported by different laboratories isn't easy. It is called the "reproducibility problem in sonochemistry" (Xing et al., 2021). The energy is a kind of mechanical energy that converts electrical energy into ultrasonic waves through the vibrator. The converting efficiency depends not only on the model of the instrument but also on the size of the vibrator, the specifications of the ultrasonic container, etc. Energy loss occurs when the sensor converts electrical energy into ultrasonic energy. The energy dissipated in the ultrasonic container is less than the electrical power energy. Therefore, electrical energy can not describe sound energy accurately. Although it is not necessary to measure the energy as mechanical energy converted from electrical energy in all cases, there are some representative standard methods to determine ultrasonic energy generated by a particular instrument. There are two main methods to measure the ultrasonic power dissipated in the sample solution. One is the chemical dosimeter method, the Weissler reaction (Rajamma et al., 2021). The ultrasonic power dissipated in the chemical reaction system is indirectly determined by measuring the change of certain chemical substances. For example, ultrasonic water treatment containing carbon tetrachloride will produce chlorine molecules, reacting quickly with iodine ions in the solution to release iodine molecules. The amount of iodine released by potassium iodide under ultrasound can determine the ultrasonic power (P_s). Measuring the amount of HNO_3 produced by NO_3 in the water under ultrasonic waves can also determine Ps.

However, not all liquid sound-transmitting media have sonochemical reactions and chemical dosing methods are rarely used. The other is calorimetry (Hamdaoui and Alghyamah, 2023). The heat energy received by the sample is measured to express the ultrasonic power dissipated.

This method assumes that the released ultrasonic energy can be absorbed by the liquid sound-transmitting medium and turned into thermal energy. Many experts recommend calorimetry as an effective method to obtain the power dissipated in the sample (Orozco M. A. et al., 2021). The power level measured by the calorimetry method is proportional to the instruments'

electrical input power, and the ultrasonic ice seeding instrument with different volumes and different shapes of containers can obtain more consistent results. Based on the above discussion of the method of ultrasonic power dissipated in the sample solution, this article adopts calorimetry to measure the ultrasonic power and ultrasonic intensity dissipated in the cell solution of different concentrations.

2 Materials and methods

2.1 Materials

L-02 primary hepatocyte (purchased from FuHeng Biology, Shanghai), fetal bovine serum (Gemini, Shanghai), medium RPMI-1640 (Gibco, Thermo Fisher Scientific), trypsin (TBD, Tianjin), dimethyl sulfoxide Me_2SO (Aladdin, Shanghai), PBS buffer (TBD, Tianjin), ethylene glycol (Macklin, Shanghai), optical microscope (Nikon, Japan), fluorescence microscope (Nikon, Japan), low-speed Benchtop centrifuge (Anke, Shanghai), CO_2 cell incubator (BoXun, Shanghai), program cooling box (Thermo Fisher Scientific, America), ultra-low temperature refrigerator (Haier, Qingdao), low-temperature thermostat (Tianheng, Ningbo), intelligent multi-channel Temperature tester (Anbai, Changzhou), differential scanning calorimeter (Netzsh, Germany).

2.2 Construction of ultrasonic ice seeding system

Figure 1 is the schematic diagram of the ultrasonic ice seeding system. It consists of five parts: (I) The ultrasonic container model is designed according to the model of the program cooling box. The control cryotube and hepatocyte cryotubes can be placed in the sample tank. The bottom of the sample tank is connected with the phase change liquid, and the sample tank is placed in the ultrasonic inner box. The bottom material of the ultrasonic container is selected as an aluminium sheet. (II) Temperature detection system: It comprises the first thermocouple electrode, the second thermocouple electrode and the temperature data acquisition module. The first thermocouple electrode is placed in the control cryotube to detect the temperature of the cell solution in real-time. The thermocouple electrode is placed in the phase change liquid in the ultrasonic inner box for real-time detection of the temperature of the control phase change liquid. (III) Ultrasonic system: It consists of an ultrasonic vibrator and an ultrasonic generator (Shanghai Shengpu Ultrasonic Equipment Factory), in which the ultrasonic vibrator (diameter d = 45 mm) is uniformly bonded to the bottom of the ultrasonic container, and the ultrasonic wave propagates upward from the ultrasonic container to the tube. The ultrasonic frequency is 40 kHz, and the electric power range is 0~150 W adjustable. (IV) Cooling circulation system: A low-temperature thermostat provides a cold source. Its temperature control range is - 25°C ± 0.1°C–25°C ± 0.1°C. Because ethylene glycol has the advantages of high boiling point, not easy to evaporate, not easy to catch fire, and good safety, this article uses 38.5% ethylene glycol as the freezing liquid, which can be cooled to −20°C without freezing. The ultrasonic inner box and the low-temperature thermostat are loaded with refrigerant, causing the closed circulation loop. The low-temperature thermostat has a refrigeration cycle system, and the temperature distribution in the ultrasonic container is uniform. (V) Photographic recording system: The CCD high-speed camera (Sony E3ISPM06300KPB, resolution 3,072 × 2,048 pixels, 59 frames/s) transmitted the video signal to the computer, and the effect of ultrasonic ice seeding is recorded in real-time.

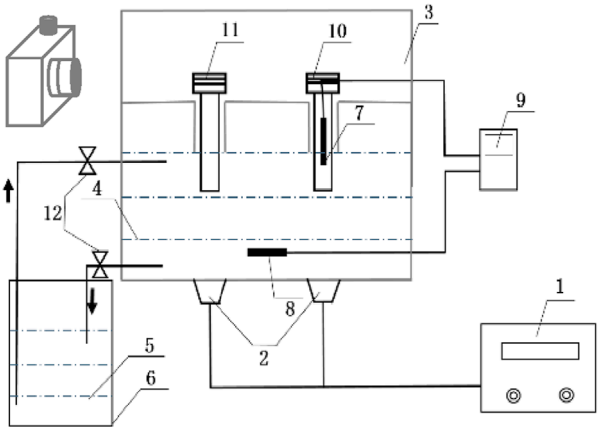

FIGURE 1
The schematic diagram of the ultrasonic ice seeding system. (1) Ultrasonic generator; (2) Ultrasonic vibrator; (3) Ultrasonic inner box; (4,5) Temperature control phase change liquid; (6) low-temperature thermostat; (7) First thermocouple; (8) Second thermocouple; (9) Temperature data acquisition module; (10) Control cryotube; (11) Hepatocyte cells cryotube; (12) Flow control valve.

2.3 Determination of specific heat capacity of hepatocyte solution

The specific heat capacity of different Me_2SO solutions was measured to control the ultrasonic power and ultrasonic intensity dissipated in the hepatocyte's solution more accurately. The DSC three-wire method is used to determine the specific heat capacity of the cell solution (Orozco M. et al., 2021). The experimental principle is shown in Figure 2. First, place an empty crucible on the sample holder and reference holder in the furnace to measure a blank baseline. Second, the DSC curve of the known standard sample sapphire and the DSC curve of the cryopreservation solution were measured under the same conditions. During the test, the high nitrogen purge rate for cleaning was 20 mL/min for liquid nitrogen refrigeration, and the circulating water constant temperature system was set to 30°C. The control program is as follows: the initial temperature is 10°C, continuous time is 5 min, then the temperature is raised to 40°C at 5°C/min and kept at 40°C for 5 min. Before the cell solution test, press the sealer first, weigh the sample mass, and determine the cell solution sample line. The specific heat capacity of the cell solution at the required temperature is calculated by the Formula 1.

$$Cp(s) = \frac{Cp(st) \times Ds \times Wst}{Dst \times Ws} \quad (1)$$

Where $Cp(s)$ (J/(g·°C)) is the specific heat capacity of the cell solution; $Cp(st)$ (J/(g·°C)) is the specific heat capacity of the

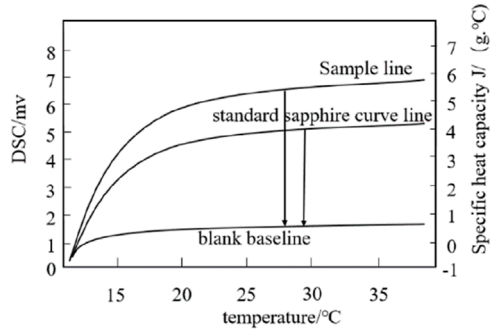

FIGURE 2
Determine the specific heat of the sample line, sapphire line and blank baseline.

standard sample sapphire; *Ds* (mW) is the vertical displacement value between the sample line and the blank baseline of the DSC thermal curve at a specific temperature; *Dst* (mW) is the vertical displacement value between the standard sapphire curve line and the blank baseline of the DSC thermal curve at a particular temperature; *Ws* (mg)is the mass of the hepatocyte cells solution to be tested. *Wst* (mg) is the mass of the standard sapphire curve.

2.4 Determination of parameters of ultrasonic ice seeding system

The ultrasonic power range is 0~150 W and can be adjusted. To reduce the workload, the actual ultrasonic power (P_s) dissipated in the hepatocyte's solution with different Me_2SO concentrations was measured with the electric power of 30 W, 60 W, 75 W, 90 W, 105 W, 120 W, 135 W, and 150 W. This work uses calorimetry to measure the ultrasonic power (P_s) dissipated in the hepatocyte solution. The calorimetry method assumes that the released ultrasonic energy can be absorbed by the liquid sound-transmitting medium and converted into heat energy. The calculation Formula 2 is as follows:

$$P_s = M \times C_P \times (dT/dt)_{t=0} \quad (2)$$

Where M(g) is the mass of the liquid sound transmission medium, as the mass of the hepatocyte cells solution of different Me_2SO; Cp (J/(g·°C) is the specific heat capacity $(dT/dt)_{t=0}$ (°C/min) is the tangent slope of the liquid temperature changing with time at 0 s at the action of ultrasound. First, let the initial temperature of the phase change liquid in the ultrasonic ice seeding system and the cryopreservation tube equal to the room temperature (the temperature in this laboratory is 19°C). The ultrasonic time is 50 s due to the uneven ultrasonic intensity in different directions in the ultrasonic ice seeding instrument (the ultrasonic intensity right above the ultrasonic vibrator is much greater than in other places). The volume and depth of the phase change liquid significantly influence the ultrasonic intensity. Therefore, the experimental samples are all placed in the same position in the ultrasonic container (in this experiment, the samples are placed right above the ultrasonic vibrator). The depth of the phase change liquid is 100 cm higher than the bottom of the ultrasonic ice seeding instrument (the cryopreservation tube is immersed in the phase change liquid at the position of 1.5 cm). Each condition was repeated for three parallel experiments to obtain more accurate results. Sample cryotube and phase change solution were used only once in each experiment. The ultrasonic intensity (I_s) can be calculated by Equation 3.

$$I_s = \frac{P_s}{A_h} \quad (3)$$

Where I_s is ultrasonic intensity; P_s (W) is the actual ultrasonic power dissipated in the sample; P_s is measured by calorimetry. A_h (cm^2) is the cross-street area of the cryotube. The diameter of the cryopreservation tube is 10.20 mm, and the A_h is 0.8171 cm^2.

2.5 Hepatocyte culture

L-02 hepatocyte cells were cultured with RPMI-1640 medium and 10% fetal bovine serum in an incubator at 37°C with an atmosphere of 5% CO_2. Before subculture, observe the number of hepatocyte cells. When hepatocyte reaches 80%~90%, discard the supernatant and add 1 mL PBS buffer. After washing with PBS twice, discard it. Then add 1 mL of trypsin. Put the culture flask in the incubator and enzymolyze the cells for 2 min. When hepatocyte cell morphology has become rounded under the optical microscope, gently tap the side of the T-25 culture flask. The hepatocyte cells can be separated from the surface of the wall. Add a 2 mL RPMI-1640 medium to terminate the digestion, and use a 1 mL pipette to suck the culture solution repeatedly to ensure they are detached from the bottle wall. Then, transfer it to the centrifuge tube and centrifuge it at 1,000 r/min for 4 min. Finally, the hepatocyte cells are resuspended in PBS solution for later use.

2.6 Cryopreservation of hepatocyte cells

Three methods for hepatocyte cell cryopreservation are used: ultrasonic ice seeding freezing, traditional ice seeding freezing, and slow freezing, as shown in Figure 3.

Each method has three parallel experiment groups. (I) The ultrasonic ice seeding freezing method: Prepare 38.5% (v/v) ethylene glycol in advance and lower the temperature to −20°C. After the cell solutions were resuspended, 1,500 μL was sampled into three 2 mL tubes. Solutions without hepatocyte cells were added into control tubes. Then, the control tube and three hepatocyte tubes were put in the ultrasonic ice seeding instrument. First, connect the ultrasonic container with the cryostat. 38.5% (v/v) glycol carrier refrigerant is injected into the ultrasonic inner box and the cryostat. Then, turn on the low-temperature constant tank refrigeration cycle system. When the second thermocouple detects that the temperature of the solution reaches the specified temperature, keep the temperature constant. When the first thermocouple detects that the temperature of the control cryopreservation tube reaches the specified ice planting temperature, turn on the ultrasonic generator. After the ice seeding, turn off the ultrasonic and equilibrate the cell cryopreservation tube in the freezing solution for 5 min to allow the ice crystals to grow. After the equilibration, transfer the cell cryopreservation tube to the cooling box and keep it at −80°C overnight. Then, transfer the cryopreservation tube to liquid

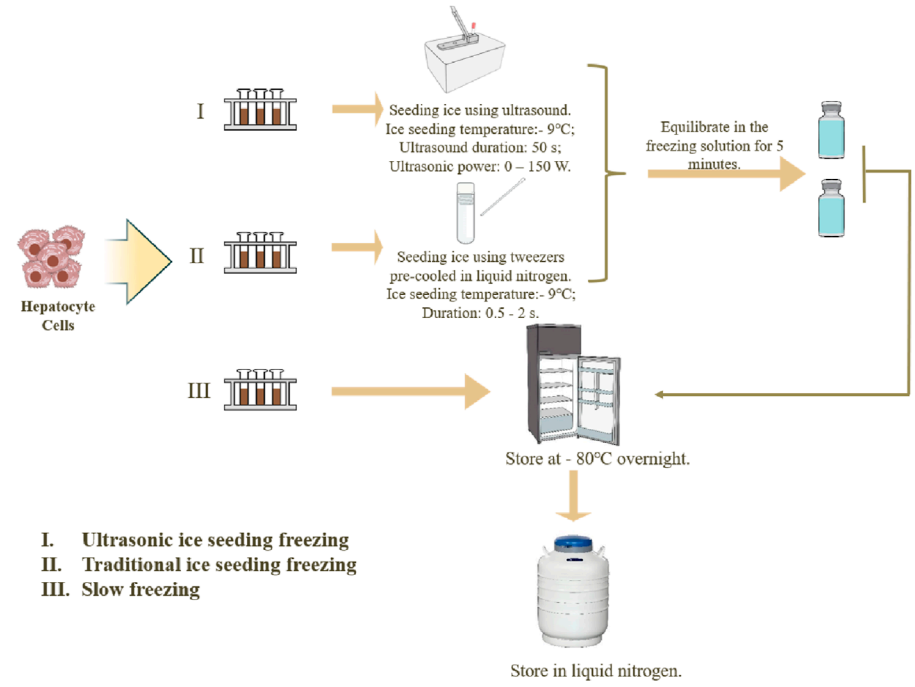

FIGURE 3
Three methods of hepatocyte cryopreservation.

nitrogen for 24 h. (II) The cryopreservation method for traditional ice-seeding freezing: The cell solution is first cooled to the ice-seeding temperature. Tweezers pre-cooled in liquid nitrogen are then used to make direct contact with the outer wall of the cryovial. The tweezers should precisely touch a single point on the cryovial wall for approximately 0.5–2 s to induce nucleation. The contact time should be minimized to prevent excessive sample cooling and ensure controlled ice crystal formation. Following nucleation, the cryovial is equilibrated in the freezing solution for 5 min to allow complete ice crystal growth. After equilibration, the cryovial is transferred to a cooling box and stored at −80°C overnight. Finally, the cryovial is transferred to liquid nitrogen for 24 h (III) The slow freezing method: directly transfer the cell cryopreservation tube to the cooling box and place it at −80°C refrigerator overnight. Then, transfer it to liquid nitrogen for deep cryopreservation the next day.

2.7 Hepatocyte cell number and survival rate determination

After centrifugation, the hepatocyte cells were resuspended with 1 mL of culture medium. Under an optical microscope, 10 μL of resuspension solution was pipetted into the groove on one side of the hemocytometer. To evaluate the survival rate of the hepatocyte cells after cryopreservation, 15 μL of the suspension solution was drawn into a 1.5 mL centrifuge tube by a 15 μL pipette. Since AOPI dye is more accurate than trypan blue dye, 15 μL of the AOPI dye was mixed in the same centrifuge tube and incubated at 4°C in the dark for 10~20 min. After incubation, draw 15 μL of cell staining solution in the center of the slide, cover it with a cover glass and observe through a fluorescent microscope. The wavelength of the excitation light source was 488 nm, and the wavelength of receiving light was 520 nm. The preparation of the AOPI staining solution is as follows: 100 μL reagent C was diluted with 900 μL PBS buffer, 10 μL AO staining solution and 20 μL PI staining solution were added. After the staining, find the cells in the bright field and observe them in the dark room with a fluorescent microscope. Finally, Image Pro Plus 6.0 software was used to count the number of hepatocyte cells.

2.8 Hepatocyte morphology observation and hepatocyte function test

2.8.1 Hepatocyte morphological observation

The morphology changes of different cryopreserved hepatocyte cells were recorded by ordinary optical microscope from the 1st to the 7th day to test the hepatocyte's function.

2.8.1.1 Measurement of urea production

The urea concentration in the culture flask was measured using urease Bourbon colorimetry. Urease hydrolyzed urea, producing ammonia and carbon dioxide. Then, the ammonium ions react with phenol to produce blue indoxyl. The amount of indoxyl produced is directly proportional to the urea content.

Prepared a 5 mmol/L standard solution (standard urea solution (100 mmol/L): ddH_2O = 1:19) and urease solution (urease solution: urea diluent = 1:99). Then added 10 μL ddH_2O, standard urea solution (5 mmol/L) and the sample (culture flask supernatant) into a blank tube, standard tube and measuring tube, separately. Added 200 μL urease solution to each tube and kept in a 37°C water bath for

TABLE 1 Specific heat capacity of Me_2SO (25°C).

Concentration of Me_2SO (v/v) %	Specific heat capacity (J/(g.°C))	Mean ± standard
0	4.008 4.098 4.138	4.081 ± 0.07[a]
3	4.146 4.004 4.004	4.051 ± 0.08 [ab]
5	3.902 3.969 3.978	3.950 ± 0.04 [ab]
10	3.940 3.889 3.866	3.905 ± 0.03[b]

Note: Values with different superscripts (a, b) in the same column are significantly different ($p < 0.05$).

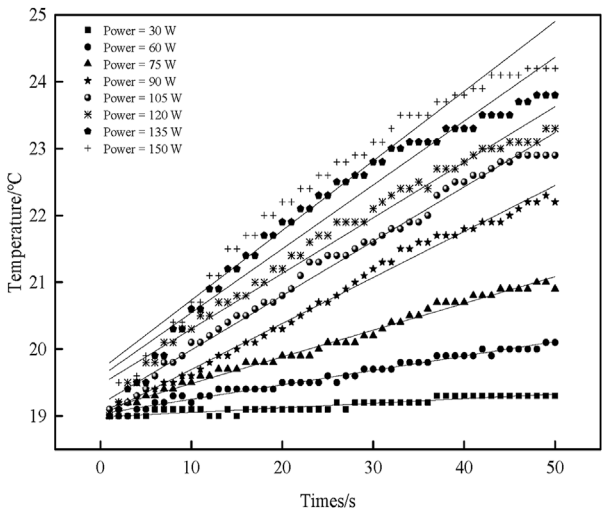

FIGURE 4
The effect of ultrasonic power on sample temperature over time.

15 min. Then, 1 mL of phenol coloring solution and 1 mL urea assay buffer were added to each tube and kept in a water bath at 37°C for 20 min. The absorbance of solutions in each tube was measured at 560 nm by a microplate reader.

2.8.1.2 Measurement of albumin synthesized

Bromocresol green has a high affinity for albumin. Albumin molecules with positive charges react with bromocresol green with negative charges, forming a blue-green complex with strong absorption at 628 nm. The absorbance of the complex is directly proportional to albumin. Thus, bromocresol green colorimetry was used to measure albumin content here.

A 40 mg/mL albumin standard solution was prepared and stored at 20°C. 10 μL albumin standard preparation solution, albumin standard solution (40 mg/mL) and sample (culture flask supernatant) were added to the blank, standard, and measurement tubes separately. Then, 2 mL bromocresol green was added to each tube and kept at room temperature for (30 ± 3) s. A microplate reader was used to measure the absorbance at 628 nm.

2.8.1.3 Measurement of glucose content

Glucose reduces copper ions into cuprous oxide precipitation in a heated alkaline environment. Cuprous oxide reduces phosphomolybdic acid to molybdenum blue. The color depth is proportional to the glucose content. Thus, the Folin-Wu microplate method was used to detect the glucose content.

First, add 300 μL distilled water to the blank tube, 200 μL distilled water and 100 μL Glucose standard (10 mg/mL) to the standard tube, 200 μL distilled water and 100 μL supernatant to the test tube separately. Then, 100 μL Folin alkaline copper solution and 100 μL Wu phosphomolybdic acid solution were added to three tubes separately. After mixing well, boil three tubes in a water bath, take it out, and cool it down in cold water without shaking. A microplate reader was used to measure the absorbance of solutions in each tube at 420 nm.

2.9 Data analysis

The fluorescence images were analyzed using Image-Pro Plus 6.0 software. The data was processed by IBM SPSS Statistics 22.0 software. Each sample was repeated three times, representing all data as mean ± standard deviation. $p < 0.05$ was used as the criterion of significant difference, which was statistically significant.

3 Results and discussion

3.1 The specific heat capacity of different concentrations of Me_2SO cell solution

According to the calculation Formula 2, the specific heat capacity of the cell solutions is obtained (Table 1). There is no significant difference in the specific heat capacity between 0%~10% Me_2SO. For the convenience of subsequent calculations, the average specific heat capacity of the four different concentrations solution of Me_2SO is taken as the specific heat capacity of the cell solution. Therefore, the specific heat capacity of the hepatocyte's solution is 3.997 J/(g.°C).

3.2 The ultrasonic power (P_s) and intensity (I_s) dissipated in the sample

Figure 4 shows the relationship between the sample temperature and the ultrasonic time under different ultrasonic powers.

There is a pronounced linear relationship. The sample temperature increases with the increase in ultrasonic time. Although

TABLE 2 Linear regression equations and related parameters for the relationship between sample temperature and ultrasonic duration under different ultrasonic power.

Ultrasonic power (W)	Linear regression equation	Adj. R-R-square	Mass (g)	$dT/dt_{(t=0)}$ (°C/s)	P_s (W)	I_s (W/cm^2)
30	Y = 0.0068t + 18.99	0.8667	0.991	0.0068	0.0269	0.0329
60	Y = 0.0216t + 19.03	0.9788	0.986	0.0216	0.0851	0.1041
75	Y = 0.0400t + 19.08	0.9884	0.980	0.0436	0.1706	0.2088
90	Y = 0.0688t + 19.01	0.9919	0.984	0.0688	0.2706	0.3312
105	Y = 0.0813t + 19.17	0.9889	0.987	0.0813	0.3207	0.3925
120	Y = 0.0832t + 19.47	0.9770	0.977	0.0903	0.3527	0.4316
135	Y = 0.0956t + 19.59	0.9451	0.985	0.0956	0.3764	0.4607
150	Y = 0.1042t + 19.69	0.9503	0.986	0.1042	0.4107	0.5026

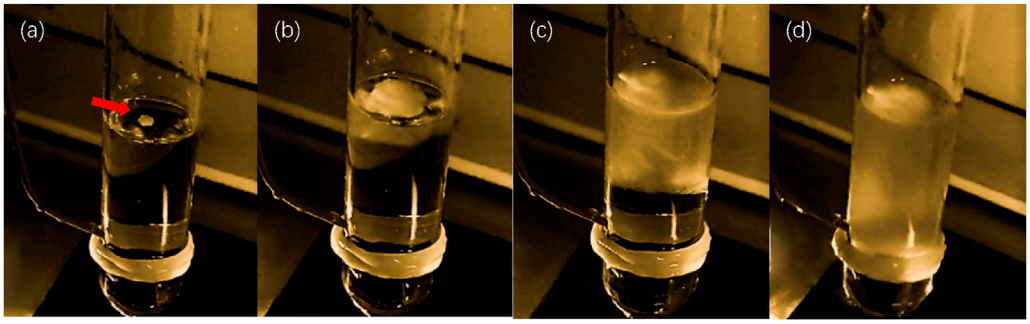

FIGURE 5
The effect of ultrasonic ice planting and nucleation. **(a)** Image of ice crystal growth after ultrasonic ice seeding for 1 s; **(b)** Image of ice crystal growth after ultrasonic ice seeding for 2 s; **(c)** Image of ice crystal growth after ultrasonic ice seeding for 4 s; **(d)** Image of ice crystal growth after ultrasonic ice seeding for 8 s.

a deviation from a strictly linear relationship is observed at higher ultrasonic power levels (120 W, 135 W, 150 W), this is a normal phenomenon caused by the rapid temperature rise, which leads to larger temperature differences and enhanced heat dissipation, ultimately reducing the internal heating rate. Nevertheless, the overall trend remains valid. Origin 8.0 is used to fit the linear equation, and the figure corresponds to the fitted linear equation shown in Table 2. Among them, the correction coefficient of the determination value is close to 1, indicating that the linear regression equation fits better. Therefore, the fitted linear regression equation can approximate the relationship between temperature and ultrasonic time.

According to the fitted linear equation, the slope of the tangent of the temperature versus time can be obtained ($(dT/dt)_{t=0}$). The mass of the sample under different ultrasonic powers is shown in Table 2. The specific heat capacity (C_p) of the sample solution is 3.997 J/(g.°C). According to Formulas (2) and (3), the actual ultrasonic power (P_s) and the ultrasonic intensity (I_s) dissipated in the sample under different ultrasonic electric powers can be obtained, respectively.

3.3 Effect of ultrasonic ice seeding method on inducing nucleation

To test the effect of the ultrasonic ice seeding method on inducing nucleation, the cryopreservation tube was replaced with a glass tube in this experiment. The glass tube has high transparency, which is convenient for observing the nucleation of ice crystals. In the experiment, start the ultrasonic ice seeding when the cell freezing solution in the glass test tube is pre-cooled to a temperature below zero. After the ultrasonic ice seeding, the glass test tube is removed from the ultrasonic container, and the growth of ice crystals is shown in Figure 5.

Notably, upon removal from the ultrasonic container, ice crystals preferentially nucleated at the air-liquid interface, progressively growing downward over time. This phenomenon was consistently observed, demonstrating ultrasonic stimulation's clear and reproducible effect on nucleation. The ultrasonic ice seeding method achieved a nucleation induction success rate exceeding 99% through repeated trials, highlighting its reliability and efficiency. These findings establish a solid foundation for subsequent hepatocyte

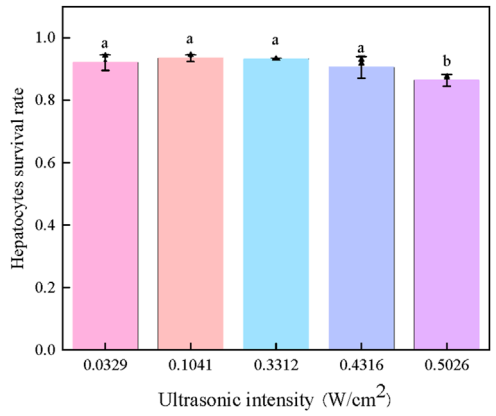

FIGURE 6
Effect of intensities of ultrasonic ice seeding on the survival rate of hepatocyte cells [Bars with a and b are significantly different ($p < 0.05$)].

cryopreservation experiments by providing a controlled and highly effective approach to ice nucleation.

3.4 Effect of ultrasonic intensities on hepatocyte cell cryopreservation

To investigate the effect of ultrasonic intensity on hepatocyte cryopreservation, experiments were conducted under fixed conditions with 5% (v/v) Me_2SO and an ice seeding temperature of −9°C (Figure 6).

As shown in Figure 6, when the ultrasonic intensity remained below 0.4316 W/cm^2, the cell survival rate consistently exceeded 90%, indicating that low-intensity ultrasound had no apparent detrimental effects on cell viability. However, a significant decline in survival rate was observed when the ultrasonic intensity surpassed this threshold, suggesting potential ultrasound-induced cellular damage.

These findings highlight the existence of an optimal ultrasonic intensity range for effective ice seeding while maintaining high cell viability. When applied at an appropriate power level and duration, ultrasound can facilitate controlled nucleation without compromising cell integrity, allowing hepatocyte survival rates to exceed 90%. This result underscores the importance of fine-tuning ultrasonic parameters to maximize cryopreservation efficiency while minimizing potential adverse effects.

3.5 Effect of processing methods on cryopreservation of hepatocyte cells

Figure 7 shows the effect of processing methods on cryopreservation of hepatocyte cells.

As shown in Figure 7, the volume concentration of Me_2SO is 5%, and the pre-cooling temperature is −9°C. Compared with the traditional ice seeding method, the survival rate of ultrasonic ice seeding is greatly improved, and the hepatocyte cell survival rate reaches (93.4 ± 1.1) %, which is not significantly different from the fresh group. The hepatocyte survival rate of the traditional ice seeding method is only (86.71 ± 2.8) %. Ultrasonic ice seeding has more advantages than conventional ice seeding. The hepatocyte cell survival rate of the slow freezing method is (87.2 ± 5.6) %, which is not significantly different from the traditional ice seeding group but is significantly different from the ultrasonic ice seeding group.

The enhanced effectiveness of ultrasonic ice seeding may be attributed to its streamlined operation. The cryotube remains within the container throughout the process, ensuring consistent temperature control and minimizing fluctuations. In contrast, the traditional ice seeding method requires repeated removal of the cryotube, leading to significant temperature variations that may negatively impact cell survival. These findings demonstrate the advantages of ultrasonic ice seeding, including its high success rate, improved preservation efficiency, and superior cell viability compared to conventional methods.

3.6 Effect of treatment methods on hepatocyte cell morphology

To explore the long-term effects of different cryopreservation methods on the metabolic activity of hepatocyte cells, we used three different treatment methods: ultrasonic ice seeding, traditional ice seeding, slow freezing, and fresh group as control. Ultrasound ice seeding, traditional ice seeding and slow-freezing hepatocyte cells developed a characteristic polygonal-shaped monolayer with typical binuclear cells on day 1, as shown in Figure 8.

The number of adherent hepatocyte cells in the fresh group is more than that in the ultrasonic and traditional ice-seeding groups. The slow-freezing group has the largest number of dead cells. Hepatocyte cell numbers began to increase on the first day. Clear and bright intercellular spaces could be seen on the second day. The cells grew wildly from the second to the sixth day, and the hepatocyte cells gradually became denser until no gaps existed. The number of dead hepatocyte cells in the four groups on the sixth day increased. On the seventh day, dead hepatocyte cells increased significantly and appeared in suspension because the hepatocyte cells were adherent. On the sixth day, the culture flask grew to a saturation density, and the hepatocyte cells could not continue to grow and reproduce. After 7 days of cell culture, we found that the hepatocyte cells in the fresh group grew the fastest, and the cells in the ultrasonic ice seeding group grew rapidly. There was no significant difference from the fresh group. The traditional ice seeding group's cell growth rate is slower than that of the fresh and ultrasonic ice seeding groups. The slow-freezing group has slow hepatocyte cell growth and the largest number of dead cells. In short, deep cryopreservation has the most significant impact on preserving slow-frozen cells and the most negligible impact on preserving ultrasonic ice-planted cells.

3.7 Effects of treatment methods on hepatic function

3.7.1 Urea production

Detoxification is a vital function of the liver. Ammonia is a highly toxic base produced during the deamination of amino acids.

10.3389/fcell.2025.1571198

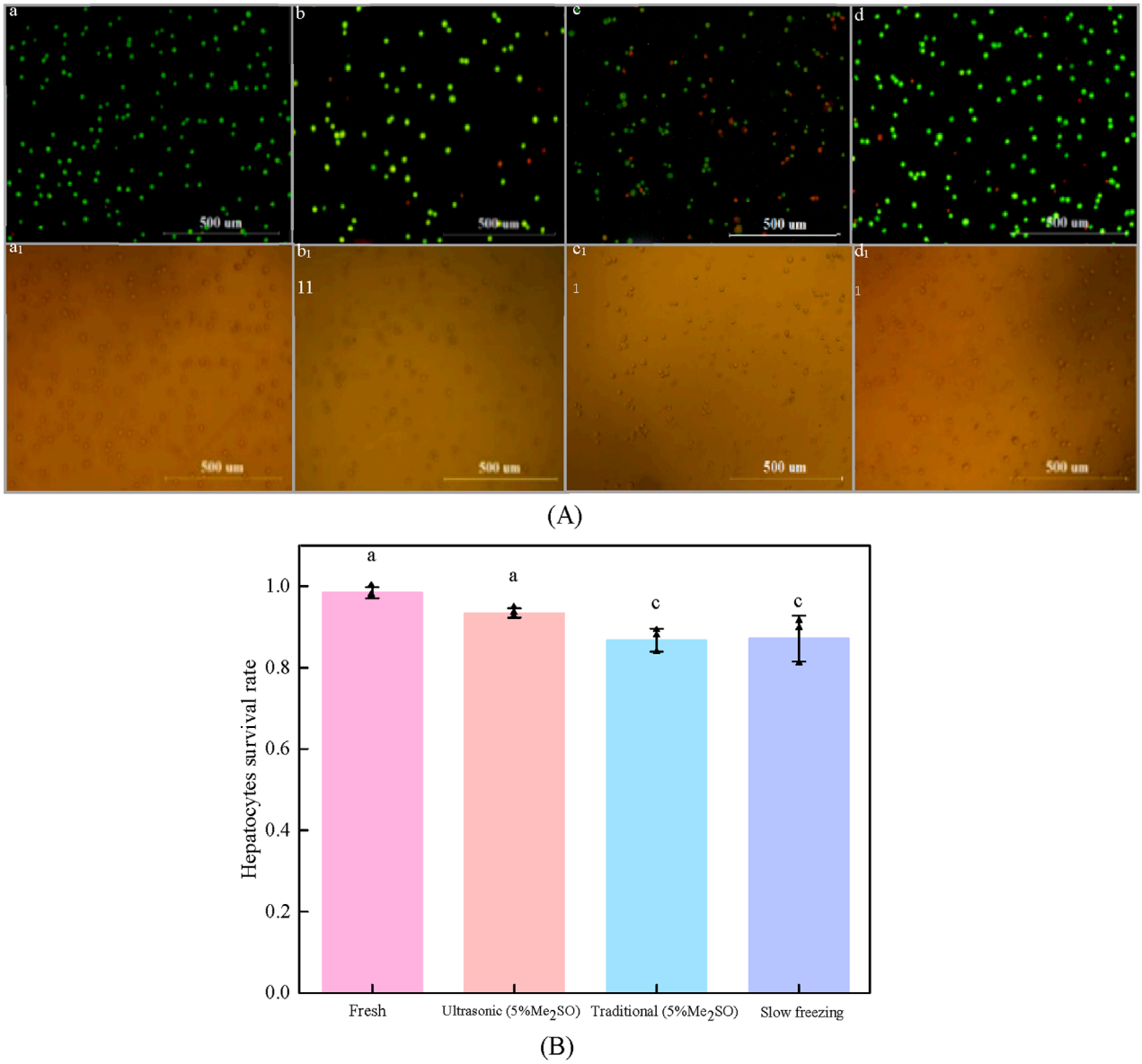

FIGURE 7
The effect of processing methods on cryopreservation of hepatocyte cells. **(A)** Fluorescence images of hepatocyte cells with different processing methods: **(a)** fresh hepatocyte cells; **(b)** Ultrasonic ice seeding method; **(c)** traditional ice seeding method; **(d)** Slow freezing method; **(a1)** ~ **(d1)** Corresponding to the bright field images of **(a–d)** respectively; **(B)** Hepatocyte cells survival rate of different treatment methods [Bars with a and c are significantly different ($p < 0.05$)].

Hepatocyte cells almost exclusively metabolize ammonia into much more poisonous urea. As such, urea production is one of the most common markers of specific hepatic function. The supernatant was sampled to measure the urea production of hepatocyte cells, as shown in Table 3. The urea produced on the first and second days was between 1 and 1.5 mol/L. From the third to the fourth day, the urea secretion increased significantly, and the urea secretion reached the maximum on the sixth day. On the seventh day, urea production decreased. There was no significant difference between the fresh, ultrasonic, and traditional ice seeding groups on the first, fourth, fifth, and seventh days. Still, there was a significant difference from the slow-freezing group.

There was no significant difference between the fresh group, ultrasonic ice seeding, and traditional ice seeding on the second and third days. Still, there was a significant difference from slow freezing. On the sixth day, urea secretion reached its peak. There was no significant difference between ultrasonic ice seeding and the fresh group, and there were significant differences between traditional ice seeding and slow freezing.

These results indicate that ultrasonic ice seeding better preserves hepatocyte metabolic function than traditional ice seeding and slow freezing. The ability of hepatocytes in the ultrasonic ice seeding group to maintain near-native urea production levels suggests that this method offers a superior cryopreservation approach,

10.3389/fcell.2025.1571198

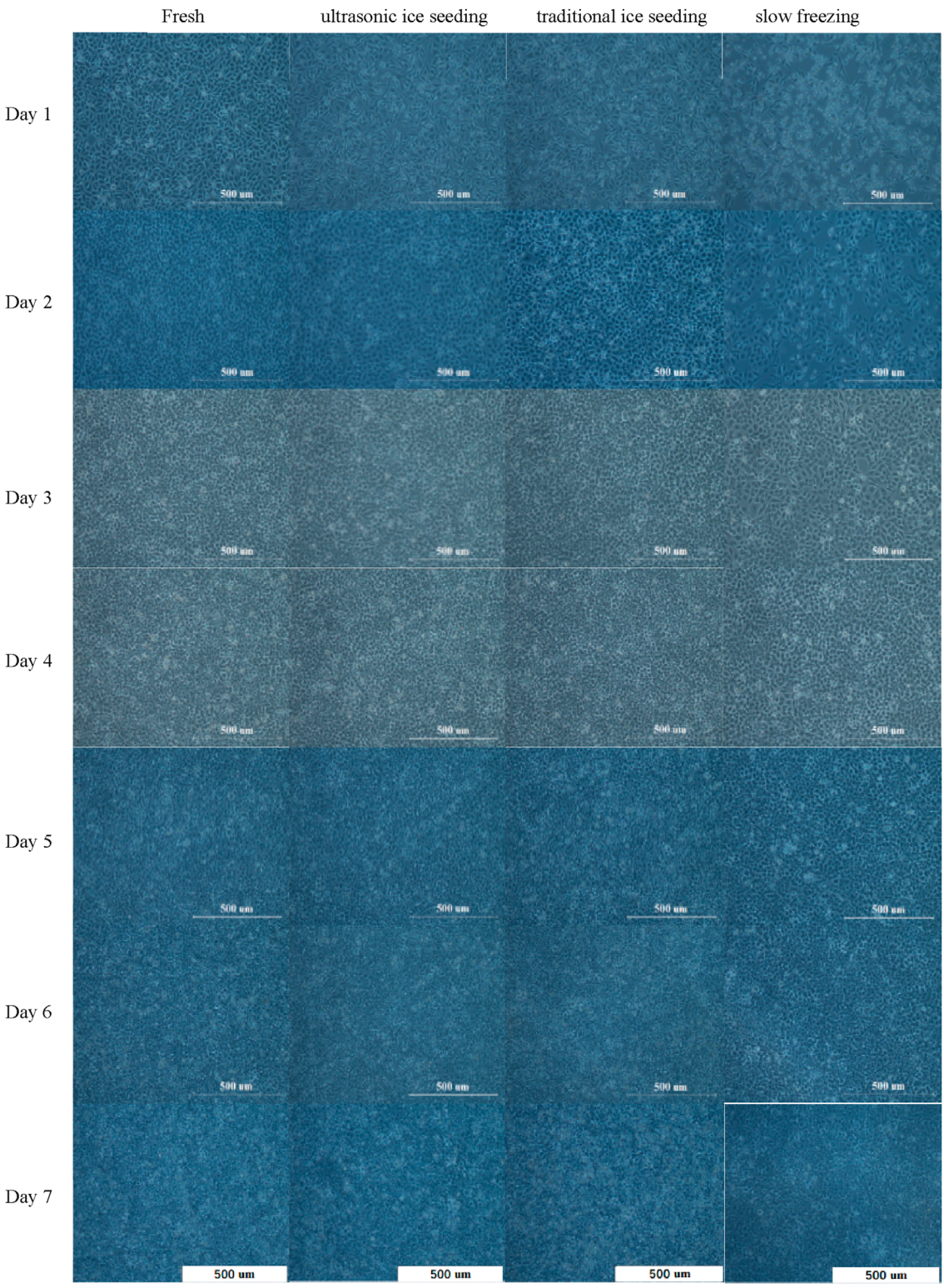

FIGURE 8
The hepatocyte cell morphology cultured for 7 days by different cryopreservation methods.

10.3389/fcell.2025.1571198

TABLE 3 Urea production, albumin synthesis, and glucose secretion of hepatocytes cultured for 7 days under different cryopreservation methods.

Secretion products	Time	Mean ± SD				P values					
		Fresh	Ultrasonic ice seeding	Traditional ice seeding	Slow freezing	Fresh-Ultr	Fresh-Tra	Fresh-Slow	Ultr -Tra	Ultr -Slow	Tra -Slow
Urea (mol/L)	Day 1	1.32 ± 0.04	1.32 ± 0.10	1.21 ± 0.04	1.09 ± 0.02	1.000	0.699	<0.05	0.703	<0.05	<0.05
	Day 2	1.38 ± 0.11	1.32 ± 0.15	1.26 ± 0.12	1.15 ± 0.04	0.919	0.618	0.136	0.924	0.314	0.617
	Day 3	3.44 ± 0.20	3.10 ± 0.26	2.93 ± 0.67	2.36 ± 0.23	0.732	0.442	<0.05	0.948	0.169	0.339
	Day 4	6.49 ± 0.10	6.38 ± 0.08	6.24 ± 0.16	5.17 ± 0.65	0.974	0.793	<0.05	0.955	<0.05	<0.05
	Day 5	7.14 ± 0.11	7.04 ± 0.05	7.01 ± 0.11	6.55 ± 0.19	0.796	0.637	<0.05	0.991	<0.05	<0.05
	Day 6	7.36 ± 0.10	7.24 ± 0.04	7.10 ± 0.09	6.38 ± 0.04	0.276	<0.05	<0.05	0.163	<0.05	<0.05
	Day 7	6.90 ± 0.23	6.72 ± 0.02	6.60 ± 0.23	5.92 ± 0.25	0.737	0.375	<0.05	0.899	<0.05	<0.05
Albumin (g/L)	Day 1	9.30 ± 0.01	9.45 ± 0.46	9.30 ± 0.01	8.37 ± 0.04	1.000	0.848	<0.05	0.856	<0.05	<0.05
	Day 2	10.85 ± 0.10	11.01 ± 0.13	10.85 ± 0.10	9.92 ± 0.06	<0.05	<0.05	<0.05	0.219	<0.05	<0.05
	Day 3	27.41 ± 0.28	27.88 ± 0.19	27.41 ± 0.28	25.43 ± 0.21	0.871	<0.05	<0.05	0.129	<0.05	<0.05
	Day 4	31.01 ± 0.32	33.95 ± 3.17	31.01 ± 0.32	30.87 ± 0.19	0.998	0.146	0.126	0.188	0.162	1.000
	Day 5	32.57 ± 0.45	35.96 ± 0.97	32.57 ± 0.45	33.01 ± 0.01	0.999	<0.05	<0.05	<0.05	<0.05	<0.05
	Day 6	35.86 ± 0.86	38.28 ± 0.16	35.86 ± 0.86	31.16 ± 0.27	0.180	<0.05	<0.05	<0.05	<0.05	<0.05
	Day 7	21.91 ± 0.14	24.82 ± 0.93	21.91 ± 0.14	20.05 ± 0.37	0.8	<0.05	<0.05	<0.05	<0.05	<0.05
Glucose (mol/L)	Day 1	5.61 ± 0.26	5.52 ± 0.27	4.33 ± 0.37	2.32 ± 0.41	0.833	<0.05	<0.05	<0.05	<0.05	<0.05
	Day 2	5.95 ± 0.26	5.82 ± 0.34	4.92 ± 0.35	3.33 ± 0.33	0.635	<0.05	<0.05	<0.05	<0.05	<0.05
	Day 3	6.33 ± 0.27	6.18 ± 0.44	5.28 ± 0.39	4.03 ± 0.39	<0.05	<0.05	<0.05	<0.05	<0.05	<0.05
	Day 4	7.59 ± 0.24	6.93 ± 0.28	6.85 ± 0.34	5.07 ± 0.36	<0.05	<0.05	<0.05	<0.05	<0.05	<0.05
	Day 5	8.10 ± 0.31	7.22 ± 0.36	7.18 ± 0.25	5.21 ± 0.40	<0.05	<0.05	<0.05	0.941	<0.05	<0.05
	Day 6	9.09 ± 0.40	8.21 ± 0.22	7.98 ± 0.35	5.85 ± 0.27	<0.05	<0.05	<0.05	<0.05	<0.05	<0.05
	Day 7	6.78 ± 0.14	6.21 ± 0.20	5.66 ± 0.32	3.89 ± 0.37	<0.05	<0.05	<0.05	<0.05	<0.05	<0.05

minimizing cellular damage and preserving liver-specific functions more effectively.

3.7.2 Albumin secretion

Albumin is the most abundant blood protein, almost entirely produced by the liver, so it is considered the most important sign of hepatocyte anabolism, as shown in Table 3.

From the first day to the sixth day, the albumin secretion increased with time, and it began to decrease after reaching its peak on the sixth day. On day 1, albumin levels were comparable among the fresh, ultrasonic ice seeding, and traditional ice seeding groups, while the slow-freezing group exhibited significantly lower secretion, suggesting that slow freezing may negatively impact hepatocyte function. By day 2, no significant difference was observed between the ultrasonic and traditional ice seeding groups. Still, both displayed significantly higher albumin secretion than the slow-freezing group, further highlighting the detrimental effects of slow-freezing. By day 3, there was no significant difference between the ultrasonic ice seeding and fresh groups. The ultrasonic and traditional ice seeding groups were not significantly different, and there were significant differences between the other groups. On day 4, there was no significant difference between the groups. From days 5 to 7, the ultrasonic ice seeding group consistently maintained albumin secretion levels comparable to the fresh group, while the traditional ice seeding and slow-freezing groups demonstrated significantly lower values. It suggests that ultrasonic ice seeding better preserves hepatocyte function over an extended culture period, ensuring sustained protein synthesis capacity.

3.7.3 Glucose secretion

The liver plays a vital role in the process of glucose metabolism. Glucose secretion increases with time, peaks on the sixth day, and decreases on the seventh day in Table 3. Generally, the glucose content increases first and then decreases. This trend indicates an initial enhancement of metabolic activity, followed by a gradual decline, likely due to cellular density reaching saturation. On the first day, there was no significant difference in glucose secretion between the ultrasonic ice seeding group and the fresh group, and there were significant differences among the other groups. On the second day, there was no significant difference in glucose secretion between the ultrasonic ice seeding group and the fresh group, and there was no significant difference from the traditional ice seeding group. There were significant differences among the other groups. From the third day to the seventh day, there were significant differences among almost all groups, and the glucose secretion of the fresh group was higher than that of the ultrasonic ice seeding group. The ultrasonic ice seeding group is higher than the traditional ice seeding group. The traditional ice-seeding group is higher than the slow-freezing group.

4 Conclusion

The application of ultrasound-induced ice nucleation has been extensively explored in the cryopreservation of valuable food products, vitamins, and nutrients, as well as in the freeze concentration and lyophilization of pharmaceuticals and vaccines (Midya and Bandyopadhyay, 2024; Grover and Negi, 2023; Kazarin et al., 2023; Mokhova et al., 2023; Parale et al., 2024; Song et al., 2024). However, its use in the cryopreservation of cells remains largely unexplored. This study integrates ultrasound-mediated ice nucleation with liver cell cryopreservation to investigate its effects on cell viability and liver function.

In the study of ultrasound-assisted ice crystallization, ultrasound energy dissipation occurs due to heat loss during transmission and energy absorption by the cryovials containing the cells. To quantify this dissipation, the heat balance equation was employed to calculate the ultrasound power and intensity within the cell solution.

The ultrasound-induced ice nucleation system demonstrated a rapid and highly efficient nucleation capability, achieving a success rate exceeding 99%. Moreover, this technique significantly enhanced liver cell survival rates post-cryopreservation, outperforming traditional ice nucleation methods. Ultrasound-mediated ice nucleation effectively reduced supercooling in the cell solution, mitigating large temperature differentials caused by latent heat release and minimizing intracellular stress. This process ultimately facilitated a more controlled cooling rate, reducing intracellular ice formation.

Ultrasound propagates through liquids as alternating positive and negative pressure waves. The negative pressure phase disrupts the liquid's structural integrity at sufficient power and frequency, leading to cavitation bubble formation. These bubbles grow over time as dissolved gases enter them and eventually collapse under positive pressure cycles (Cheng et al., 2015). This cavitation process enhances heat and mass transfer during freezing, reduces interfacial energy, and promotes ice nucleation (Inada et al., 2001; Hu et al., 2013). However, excessively high and low ultrasound intensities were detrimental to liver cell cryopreservation. Experimental results indicate that at ultrasound intensities below 0.4316 W/cm^2, cell survival rates remained above 90%, making this approach suitable for biobanking applications. However, at intensities exceeding this threshold, cell viability declined significantly. Therefore, optimizing ultrasound parameters is crucial.

Over a seven-day culture period, ultrasound-induced ice nucleation had the least impact on liver function compared to traditional ice nucleation, while slow freezing exhibited the most detrimental effects. These findings suggest that ultrasound-mediated ice nucleation can better preserve metabolic activity and functional integrity over extended periods. However, while short-term benefits have been established, further studies evaluating long-term cryopreserved cells are necessary to fully validate the advantages of this technique under optimal ultrasound conditions.

This study provides experimental evidence supporting the application of ultrasound-induced ice nucleation in liver cell cryopreservation and offers new insights into optimizing cryopreservation strategies. Future research should explore the applicability of this method to a broader range of cell types, including embryonic stem cells, immune cells, and other medically significant cell types, to assess its potential in diverse biomedical applications. Additionally, further investigations into the underlying mechanisms of ultrasound-mediated ice nucleation and optimization of ultrasound parameters could facilitate the development of tailored cryopreservation protocols for different cell types. Through these efforts, a more comprehensive understanding of ultrasound-assisted

cryopreservation can be achieved, providing a robust theoretical and experimental foundation for advancing cell preservation technologies.

Data availability statement

The original contributions presented in the study are included in the article/supplementary material, further inquiries can be directed to the corresponding author.

Author contributions

WL: Data curation, Methodology, Supervision, Writing – review and editing. XY: Investigation, Methodology, validation, Software, Writing – review and editing. WB: Writing – original draft, Writing – review and editing. LS: Data curation, Formal Analysis, Investigation, Software, Writing – original draft. BL: Supervision, Validation, Visualization, Writing – original draft.

Funding

The author(s) declare that financial support was received for the research and/or publication of this article. This work was supported by the National Natural Science Foundation of China (No. 51776130), Shanghai Municipal Education Commission (No. 202135), the Medical-engineering Interdisciplinary Project funded by University of Shanghai for Science and Technology (No. 1020308412), and the Special Project of Strategic Emerging Industry funded by Science and Technology Commission of Shanghai Municipality (No. 18441909700).

Conflict of interest

The authors declare that the research was conducted in the absence of any commercial or financial relationships that could be construed as a potential conflict of interest.

Generative AI statement

The author(s) declare that no Generative AI was used in the creation of this manuscript.

Publisher's note

All claims expressed in this article are solely those of the authors and do not necessarily represent those of their affiliated organizations, or those of the publisher, the editors and the reviewers. Any product that may be evaluated in this article, or claim that may be made by its manufacturer, is not guaranteed or endorsed by the publisher.

References

Abir, F. M., and Shin, D. (2024). Specific heat capacity of solar salt-based nanofluids: molecular dynamics simulation and experiment. *Materials* 17, 506. doi:10.3390/ma17020506

Ahmed, S., Miyawaki, O., and Matsumura, K. (2018). Enhanced adsorption of a protein-nanocarrier complex onto cell membranes through a high freeze concentration by a polyampholyte cryoprotectant. *Langmuir* 34, 2352–2362. doi:10.1021/acs.langmuir.7b03622

Altmaier, S., Meiser, I., Lemesre, E., Chanrion, B., Steeg, R., Leonte, L. E., et al. (2022). Human iPSC-derived hepatocytes in 2D and 3D suspension culture for cryopreservation and *in vitro* toxicity studies. *Reprod. Toxicol.* 111, 68–80. doi:10.1016/j.reprotox.2022.05.005

Andres, S., Bartling, B., Stiensmeier, V., Starke, A., and Schmicke, M. (2023). Comparative cryopreservation of bovine and porcine primary hepatocytes. *Front. Veterinary Sci.* 10, 1211135. doi:10.3389/fvets.2023.1211135

Baklanov, A. V., and Kiselev, V. G. (2023). The nature of the enthalpy-entropy compensation and "exotic" arrhenius parameters in the denaturation kinetics of proteins. *Int. J. Mol. Sci.* 24, 10630. doi:10.3390/ijms241310630

Bart, A. N., and Kyaw, H. A. (2003). Survival of zebrafish, Brachydanio rerio (Hamilton-Buchanan), embryo after immersion in methanol and exposure to ultrasound with implications to cryopreservation. *Aquac. Reserch* 34, 609–615. doi:10.1046/j.1365-2109.2003.00852.x

Chen, B., Bao, S., and Zhang, Y. (2024). Effects of key impurities (Al, Fe, P, Si and Na) on the precipitation process of vanadium in the novel ultrasound-assisted precipitation system. *Hydrometallurgy* 224, 106233. doi:10.1016/j.hydromet.2023.106233

Cheng, X., Zhang, M., Xu, B., Adhikari, B., and Sun, J. (2015). The principles of ultrasound and its application in freezing related processes of food materials: a review. *Ultrason. Sonochemistry* 27, 576–585. doi:10.1016/j.ultsonch.2015.04.015

Da Costa, B. B., Lassen, P. G., and Streit, D. P., Jr. (2024). Cryopreservation-induced morphological changes in freshwater fish sperm: a systematic review, biopreservation and biobanking. *Biopreserv Biobank* 5, 416–427. doi:10.1089/bio.2023.0008

D'Adamo, E., Botondi, V., Falconio, L., Giardinelli, G., Di Gregorio, P., Caputi, S., et al. (2023). Effect of temperature on presepsin pre-analytical stability in biological fluids of preterm and term newborns. *Clin. Chem. Laboratory Med.* 62, 1011–1016. doi:10.1515/cclm-2023-1282

Daily, M. I., Whale, T. F., Kilbride, P., Lamb, S., Morris, G. J., Picton, H. M., et al. (2023). A highly active mineral-based ice nucleating agent supports *in situ* cell cryopreservation in a high throughput format. *J. R. Soc. Interface* 20, 20220682. doi:10.1098/rsif.2022.0682

Daily, M. I., Whale, T. F., Partanen, R., Harrison, A. D., Kilbride, P., Lamb, S., et al. (2020). Cryopreservation of primary cultures of mammalian somatic cells in 96-well plates benefits from control of ice nucleation. *Cryobiology* 93, 62–69. doi:10.1016/j.cryobiol.2020.02.008

Dunn, T. H., Skaanvik, S. A., McPherson, I. J., O'Shaughnessy, C., He, X., Kulak, A. N., et al. (2023). Universality of hair as a nucleant: exploring the effects of surface chemistry and topography. *Cryst. Growth and Des.* 23, 8978–8990. doi:10.1021/acs.cgd.3c01035

Eskandari, A., Leow, T. C., Rahman, M. B. A., and Oslan, S. N. (2024). Advanced freezing point insights into regulatory role of antifreeze proteins, their fundamentals, and obstacles in food preservation. *Eur. Food Res. Technol.* 250, 1103–1121. doi:10.1007/s00217-023-04449-w

Grover, Y., and Negi, P. S. (2023). Recent developments in freezing of fruits and vegetables: striving for controlled ice nucleation and crystallization with enhanced freezing rates. *J. Food Sci.* 88, 4799–4826. doi:10.1111/1750-3841.16810

Hamdaoui, O., and Alghyamah, A. (2023). Application of the general rate law model to the sonolytic degradation of nonvolatile organic pollutants in aqueous media. *Ultrason. Sonochemistry* 100, 106606. doi:10.1016/j.ultsonch.2023.106606

Hu, F., Sun, D., Gao, W., Zhang, Z., Zeng, X., Zeng, X., et al. (2013). Effects of pre-existing bubbles on ice nucleation and crystallization during ultrasound-assisted freezing of water and sucrose solution. *Innovative Food Sci. Emerg. Technol.* 20, 161–166. doi:10.1016/j.ifset.2013.08.002

Inada, T., Zhang, X., Yabe, A., and Kozawa, Y. (2001). Active control of phase change from supercooled water to ice by ultrasonic vibration 1. Control of freezing temperature. *Int. J. Heat Mass Transf.* 44, 4523–4531. doi:10.1016/s0017-9310(01)00057-6

Javitt, L. F., Kalita, S., Dubey, K. D., Ehre, D., Shaik, S., Lahav, M., et al. (2023). Electro-freezing of supercooled water is induced by hydrated Al^{3+} and Mg^{2+} ions: experimental and theoretical studies. *J. Am. Chem. Soc.* 145, 18904–18911. doi:10.1021/jacs.3c05004

Jiang, P., Li, Q., Liu, B., and Liang, W. (2023). Effect of cryoprotectant-induced intracellular ice formation and crystallinity on bactria during cryopreservation. *Cryobiology* 113, 104786. doi:10.1016/j.cryobiol.2023.104786

Juckers, A., Knerr, P., Harms, F., and Strube, J. (2024). Digital twin enabled process development, optimization and control in lyophilization for enhanced biopharmaceutical production. *Processes* 12, 211. doi:10.3390/pr12010211

Karasor, O. F., Bucak, M. N., Cenariu, M., Bodu, M., Taspinar, M., and Taspinar, F. (2022). The effects of different doses of ROCK inhibitor, antifreeze protein III, and boron added to semen extender on semen freezeability of ankara bucks. *Molecules* 27, 8070. doi:10.3390/molecules27228070

Kazarin, P., Shivkumar, G., Tharp, T., Alexeenko, A. A., and Shang, S. (2023). Lyophilization scale-up to industrial manufacturing: a modeling framework including probabilistic success prediction. *Chem. Eng. Res. and Des.* 192, 441–455. doi:10.1016/j.cherd.2023.02.044

Lindow, S. (2023). History of discovery and environmental role of ice nucleating bacteria. *Phytopathology* 113, 605–615. doi:10.1094/PHYTO-07-22-0256-IA

Liu, W., Huang, Z., Liu, B., He, X., Xue, S., Yan, X., et al. (2021). Investigating solution effects injury of human T lymphocytes and its prevention during interrupted slow cooling. *Cryobiology* 99, 20–27. doi:10.1016/j.cryobiol.2021.01.018

Maharana, A., Sehrawat, P., Das, A., Kumar, J., and Sarkar, D. (2023). Multi-dimensional population balance modeling of sonocrystallization of pyrazinamide with systematic estimation of kinetic parameters based on uncertainty and sensitivity analyses. *Chem. Eng. Res. and Des.* 200, 356–373. doi:10.1016/j.cherd.2023.10.049

Mehanna, M. M., and Abla, K. K. (2022). Recent advances in freeze-drying: variables, cycle optimization, and innovative techniques. *Pharm. Dev. Technol.* 27, 904–923. doi:10.1080/10837450.2022.2129385

Midya, U. S., and Bandyopadhyay, S. (2024). Ice recrystallization unveils the binding mechanism operating at a diffused interface. *J. Phys. Chem. B* 128, 1170–1178. doi:10.1021/acs.jpcb.3c05934

Mokhova, E., Gordienko, M., Menshutina, N., Gurskiy, I., and Tvorogova, A. (2023). Ultrasonic freezing of polymers of various compositions before freeze drying: effect of ultrasound on freezing kinetics and ice crystal size. *Dry. Technol.* 41, 1663–1685. doi:10.1080/07373937.2023.2173226

Mousazadehkasin, M., Mitchell, N., Asenath-Smith, E., and Tsavalas, J. G. (2023). Ice nucleation promotion impact on the ice recrystallization inhibition activity of polyols. *Biomacromolecules* 24, 678–689. doi:10.1021/acs.biomac.2c01120

Mutsenko, V., Anastassopoulos, E., Zaragotas, D., Simaioforidou, A., Tarusin, D., Lauterboeck, L., et al. (2023). Monitoring of freezing patterns within 3D collagen-hydroxyapatite scaffolds using infrared thermography. *Cryobiology* 111, 57–69. doi:10.1016/j.cryobiol.2023.02.001

Najafi, A., Asadi, E., and Benson, J. D. (2023). Ovarian tissue cryopreservation and transplantation: a review on reactive oxygen species generation and antioxidant therapy. *Cell Tissue Res.* 393, 401–423. doi:10.1007/s00441-023-03794-2

Nogueira, A., Teixeira, A., Geros, H., and Puga, H. (2023). Ultrasound prototype for improving germination and seedling growth in tomato and maize seeds. *J. Plant Growth Regul.* 43, 1216–1229. doi:10.1007/s00344-023-11178-7

O'Kelly Boit, M. (2023). Injectable biomaterials for transplantation of cardiac cell-based therapies

Orozco, M., Vásquez, F., Martínez-Gómez, J., Acurio, K., and Chico-Proano, A. (2021b). Nitrate characterization as phase change materials to evaluate energy storage capacity. 377–389. doi:10.1007/978-3-030-60467-7_31

Orozco, M. A., Acurio, K., Vasquez-Aza, F., Martinez-Gomez, J., and Chico-Proano, A. (2021a). Thermal storage of nitrate salts as phase change materials (PCMs). *Materials* 14, 7223. doi:10.3390/ma14237223

Parale, V. G., Kim, T., Choi, H., Phadtare, V. D., Dhavale, R. P., Kanamori, K., et al. (2024). Mechanically strengthened aerogels through multiscale, multicompositional, and multidimensional approaches: a review. *Adv. Mater.* 36, e2307772. doi:10.1002/adma.202307772

Parihar, A., Kumar, A., Panda, U., Khan, R., Parihar, D. S., and Khan, R. (2023). Cryopreservation: a comprehensive overview, challenges, and future perspectives. *Adv. Biol.* 7, e2200285. doi:10.1002/adbi.202200285

Qin, X., Chen, Z., Shen, L., Liu, H., Ouyang, X., and Zhao, G. (2024). Core-shell microfiber encapsulation enables glycerol-free cryopreservation of RBCs with high hematocrit. *Nano-Micro Lett.* 16, 3. doi:10.1007/s40820-023-01213-3

Rahman, S. M., Strüssmann, C. A., Suzuki, T., Majhi, S. K., Hattori, R. S., and Alam, M. A. (2017). Effects of ultrasound on permeation of cryoprotectants into Japanese whiting Sillago japonica embryos. *Cryobiology* 77, 19–24. doi:10.1016/j.cryobiol.2017.06.003

Rajamma, D. B., Anandan, S., Yusof, N. S. M., Pollet, B. G., and Ashokkumar, M. (2021). Sonochemical dosimetry: a comparative study of Weissler, Fricke and terephthalic acid methods. *Ultrason. Sonochemistry* 72, 105413. doi:10.1016/j.ultsonch.2020.105413

Silva, N. A. O., Denis, S., Vergnaud, J., and Hillaireau, H. (2024). Controlled hydrogel-based encapsulation of macrophages determines cell survival and functionality upon cryopreservation. *Int. J. Pharm.* 650, 123491. doi:10.1016/j.ijpharm.2023.123491

Song, X., Philpott, M. A., Best, S. M., and Cameron, R. E. (2024). Controlling the architecture of freeze-dried collagen scaffolds with ultrasound-induced nucleation. *Polymers* 16, 213. doi:10.3390/polym16020213

Tomas, R. M. F., Dallman, R., Congdon, T. R., and Gibson, M. I. (2023). Cryopreservation of assay-ready hepatocyte monolayers by chemically-induced ice nucleation: preservation of hepatic function and hepatotoxicity screening capabilities. *Biomaterials Sci.* 11, 7639–7654. doi:10.1039/d3bm01046e

Vorobeva, D. E., Majorina, M. A., Marchenko, N. U., and Melnik, B. S. (2023). Investigation of ice nucleation properties of Pseudomonas syringae bacterium and insoluble low molecular weight substances. *bioRxiv*. doi:10.1101/2023.12.09.570762

William, N., and Acker, J. P. (2020). Transient loss of membrane integrity following intracellular ice formation in dimethyl sulfoxide-treated hepatocyte and endothelial cell monolayers. *Cryobiology* 97, 217–221. doi:10.1016/j.cryobiol.2020.10.002

William, N., Mangan, S., Ben, R. N., and Acker, J. P. (2023). Engineered compounds to control ice nucleation and recrystallization. *Annu. Rev. Biomed. Eng.* 25, 333–362. doi:10.1146/annurev-bioeng-082222-015243

Xing, G., Wilkens, V., and Yang, P. (2021). Review of field characterization techniques for high intensity therapeutic ultrasound. *Metrologia* 58, 022001. doi:10.1088/1681-7575/abe02e

Yadegari, F., Pizarro, L. A. G., Marquez-Curtis, L. A., and Elliott, J. A. W. (2024). Temperature dependence of membrane permeability parameters for five cell types using nonideal thermodynamic assumptions to mathematically model cryopreservation protocols. *J. Phys. Chem. B* 128, 1139–1160.

Zhang, Z., Qi, J., Liu, Y., Ji, M., Wang, W., Wu, W., et al. (2024). Anthropogenic impact on airborne bacteria of the Tibetan Plateau. *Environ. Int.* 183, 108370. doi:10.1016/j.envint.2023.108370

Zheng, Y., Zhao, G., Zhang, Y., and Gao, R. (2018). On-chip loading and unloading of cryoprotectants facilitate cell cryopreservation by rapid freezing. *Sensors Actuators B-Chemical* 255, 647–656. doi:10.1016/j.snb.2017.08.084

Zilei, Z., Runfa, Z., Zhenghao, J., Luwen, Q., Shuhong, L., and Yanjun, L. (2023). Effect of Dual-frequency ultrasonic on subcooled water freezing. *Int. J. Refrig.* 154, 1–8. doi:10.1016/j.ijrefrig.2023.07.006

Frontiers in
Cell and Developmental Biology

Explores the fundamental biological processes of life, covering intracellular and extracellular dynamics.

The world's most cited developmental biology journal, advancing our understanding of the fundamental processes of life. It explores a wide spectrum of cell and developmental biology, covering intracellular and extracellular dynamics.

Discover the latest Research Topics

See more →

Frontiers

Avenue du Tribunal-Fédéral 34
1005 Lausanne, Switzerland
frontiersin.org

Contact us

+41 (0)21 510 17 00
frontiersin.org/about/contact